2016

Smart Synthetic Biomaterials for Therapeutic Applications

Tianxin Miao
University of Vermont

SMART SYNTHETIC-BIOMATERIALS FOR THERAPEUTIC APPLICATIONS

A Dissertation Presented

by

Tianxin Miao

to

The Faculty of the Graduate College

of

The University of Vermont

In Partial Fulfillment of the Requirements
for the Degree of Doctor of Philosophy
Specializing in Bioengineering

October, 2016

Defense Date: June 14th, 2016
Dissertation Examination Committee:

Rachael A. Oldinski, Ph.D., Advisor
Christopher C. Landry, Ph.D., Chairperson
Jeffrey L. Spees, Ph.D.
Jason H. Bates, Ph.D.
Dimitry N. Krementsov, Ph.D.
Cynthia J. Forehand, Ph.D., Dean of the Graduate College

ABSTRACT

In the field of biomaterials, naturally-derived and synthetic polymers are utilized individually or in combination with each other, to create bio-inspired or biomimetic materials for various bioengineering applications, including drug delivery and tissue engineering. Natural polymers, such as proteins and polysaccharides, are advantageous due to low or non-toxicity, sustainable resources, innocuous byproducts, and cell-instructive properties. Synthetic polymers offer a variety of controlled chemical and physical characteristics, with enhanced mechanical properties. Together, natural and synthetic polymers provide an almost endless supply of possibilities for the development of novel, smart materials to resolve limitations of current materials, such as limited resources, toxic components and/or harsh chemical reactions. Herein is discussed the synthetic-biological material formation for cell-instructive tissue engineering and controlled drug delivery. We hypothesized that the combination of hydrogel-based scaffold and engineered nanomaterials would assist in the development or regeneration of tissue and disease treatment.

Chemically-modified alginate was formed into alginate-based nanoparticles (ABNs) to direct the intracellular delivery of proteins (e.g., growth factors) and small molecular drugs (e.g., chemotherapeutics). The ABN surface was modified with cell-targeting ligands to control drug delivery to specific cells. The ABN approach to controlled drug delivery provides a platform for studying and implementing non-traditional biological pathways for disease (e.g., osteoporosis, multiple sclerosis) and cancer treatment.

Through traditional organic and polymer chemistry techniques, and materials engineering approaches, a stimuli-responsive alginate-based smart hydrogel (ASH) was developed. Physical crosslinks formed based on supramolecular networks consisting of β-cyclodextrin-alginate and a tri-block amphiphilic polymer, which also provided a reversible thermo-responsiveness to the hydrogel. The hydrogel was shear-thinning, and recovered physical crosslinks, i.e., self-healed, after un-loading. The ASH biomaterials provide a platform for injectable, therapeutics for tissue regeneration and disease treatment. Indeed, various hydrogel constituents and tunable mechanical properties created cell-instructive hydrogels which promoted tissue formation.

CITATIONS

Material from this dissertation has been published in the following form:

Miao, T., Rao, K. S., Spees, J. L., and Oldinski, R. A.. (2014) Osteogenic Differentiation of Human Mesenchymal Stem Cells Through Alginate-graft-poly(ethylene glycol) Microsphere-mediated Intracellular Growth Factor Delivery. Journal of Controlled Release, 192, 57-66.

Miao, T., Fenn, S. L., Charron, P. N., and Oldinski, R. A.. (2015) Self-Healing and Thermoresponsive Dual-Cross-Linked Alginate Hydrogels Based on Supramolecular Inclusion Complexes. Biomacromolecules, 16(12), 3740-3750.

Miao, T., Miller, E. J., McKenzie, C., and Oldinski, R. A.. (2015) Physically Crosslinked Polyvinyl Alcohol and Gelatin Interpenetrating Polymer Network Theta-gels for Cartilage Regeneration. Journal of Materials Chemistry B, 3(48), 9242-9249.

Material from this dissertation has been submitted for publication to ACS Applied Materials & Interfaces on March 16th in the following form:

Fenn, S. L., Miao, T., Scherrer R. M., and Oldinski, R. A.. (2016) Dual Crosslinked Methacrylated Alginate Sub-Microspheres for Intracellular Chemotherapeutic Delivery.

ACKNOWLEDGEMENTS

I dedicate this small contribution to the field of polysaccharide based biomaterials to many people, as I have received a lot of support, advice and encouragement. First, I would love to thank my parents, Yun Song and Weixing Miao, who have been educating, encouraging and supporting me to be a better person and to follow my passion and dream. My mother is a mechanical engineer and my father is a general surgeon. I am honored and proud to be influenced by both their passion about life and career. Being away from home is hard for me and my parents, but I am happy that I have done little contribution to make our life better. I hope to be with them forever for my rest of life.

Second, I would love to thank my boyfriend, Yu Zhang, who is going to be a doctor in 2017. I still remembered the day when we hit each other on the stairway in Perkins building. I could not remember how many times he has been cooking for me while I feed the cells. We built our first home together at Fort Ethan Allen with all our puffy animal friends and toys. He has given me bottomless love and infinite patience.

Third, I would like to thank my PI Dr. Rachael A. Oldinski for hiring me 4 years ago without seeing me in face. She is not only the supervisor in science but a mentor teaching me how to be a nice, delicate and successful woman for my whole life. She has been supporting my ideas and helping me when I face problems. This is why I can finish this thesis and my degree. I would like to thank all members of EBRL (Patrick Charron, Jene Etter, Michael Karasinski, Meredith Koch, Canaan McKenzie, Ryan Scherrer. Sarah Blatt, Alex Poniz, Emily Miller, Samuel Hotaling) who have helped me along the way, especially Spencer Fenn, who started his PhD same time with me and help me get used to American life when I started. I will miss spending time in lab with all of you together.

Fourth, I would like to thank my thesis committee members for their continuing guidance in my PhD study. Thanks to Dr. Jason Bates for continuous mentoring my whole PhD period in America. Thanks to Dr. Christopher Landry for guidance in chemistry. Many thanks to Dr. Jeffrey Spees for supporting and insight mentorship on the microsphere project and lab supplies and Dr. Dimitry Krementsov for mentoring the multiple sclerosis study. I would also love to thank our collaborator Dr. Albert Van der Vliet for supporting in caner project. I am honored to work with all of you and your students, including Krithika S. Rao PhD, Abbas Raza and Andrew Little. I also want to thank UVM Microscopy Center Dr. Douglas Taatijes, Dr. Nicole Bishop, Dr. Nicole Bouffard and Dr. Michele von Turkovich for helping me get beautiful photos about my beads and my cells and UVM Flow Cytometry and Cell Sorting (FCCS) Facility Dr. Roxana del Rio-Guerra for her great help in helping me learn FACS analysis. I would also love to thank my undergraduate advisor Dr. Hua Ai, who introduced me the world of biomaterials and encourage me to pursue my research for the last 8 years.

Finally, I would love to thank all my families and friends around the world for supporting me and putting all their faith in me from the very start.

TABLE OF CONTENTS

Page

CITATIONS ii

ACKNOWLEDGEMENTS iii

LIST OF TABLES xiii

LIST OF FIGURES xiv

CHAPTER 1: CONPREHENSIVE LITERATURE REVIEW 1

1.1. Introduction to Polysaccharides 3

1.2. Structures and Modifications of Polysaccharides 5

1.2.1. Alginate 5

1.2.2. Chitosan/Chitin 8

1.2.3. Hyaluronic Acid 10

1.2.4. Dextran 12

1.3. Preparation of Polysaccharide-Based Particles 13

1.3.1. Crosslinking Reaction 14

1.3.1.1. Physical Crosslinking 14

1.3.1.2. Covalent Crosslinking 15

1.3.2. Methods 16

1.3.2.1. Emulsions 16

1.3.2.2. Microfluidic Device 17

1.4. Preclinical Applications 18

1.4.1. Tissue Engineering and Regeneration 18

1.4.2. Cancer Therapy 21

1.4.2.1. Therapeutic Aspect 21

1.4.2.2. Imaging/Monitoring Aspect 25

1.5. Clinical Translations 28

1.6. Conclusions 30

References 31

CHAPTER 2: OSTEOGENIC DIFFERENTIATIO OF HUMAN MESENCHYMAL STEM CELLS THROUGH ALGINATE-GRAFT-POLY(ETHYLENE GLYCOL) MICROSPHERE-MEDIATED INTRACELLULAR GROWTH FACTOR DELIVERY 39

2.1. Introduction 40

2.2 Materials and Methods 43

2.2.1. Materials 43

2.2.2. Alg-g-PEG-S-S-Pyridine Copolymer Synthesis 44

2.2.3. Microsphere Fabrication 45

2.2.4. Cytotoxicity Assay 47

2.2.5. Dylight 550 Labeling of Human VEGFA 47

2.2.6. VEGFA Encapsulation and Release 48

2.2.7. Human Mesenchymal Stem Cells Intracellular Delivery 49

2.2.8. Human Mesenchymal Stem Cells Differentiation Assay 49

2.2.9. Statistical Methods 51

2.3 Results 51

2.3.1. Synthesis of Alg-g-PEG and Alg-g-PEG-pyridine Copolymers 51

2.3.2. Fabrication of Alg, Alg-g-PEG and Alg-g-RGD Microspheres 53

2.3.3. Alg-g-PEG Microspheres Exhibit no Cytotoxic Effects 56

2.3.4. VEGFA Encapsulation and Release Rates 56

2.3.5. Microsphere Internalization 59

2.3.6. Human MSC Differentiation 61

2.4. Discussion 64

2.5. Conclusion 68

2.6. Supplemental Materials 69

Reference 73

.

CHAPTER 3: DUAL-CROSSLINKED METHARYLATED ALGINATE SUB-MICROSPHERES FOR INTRACELLULAR CHEMOTHERAPEUTIC DELIVERY 76

3.1. Introduction 77

3.2. Materials and Methods 80

3.2.1. Materials and Reagents 80

3.2.2. Synthesis and Characterization of Methacrylated Alginate (Alg-MA) 81

3.2.3. Dual-crosslinked Alg-MA Sub-Microspheres Design and Fabrication 82

3.2.4. Drug Loading and Mechanism of Release 83

3.2.5. Cellular Uptake of Alg-MA Sub-Microspheres 84

3.2.6. Drug Bioactivity and Efficacy of Alg-MA Sub-Microsphere Delivery Vehicles 85

3.2.6.1. Cytotoxicity of Blank and Drug-loaded Alg-MA Sub-Microspheres 85

3.2.6.2. Effective of Intracellular VS. Extracellular Drug Delivery on Cell Proliferation 86

3.2.7. Data Analysis 87

3.3. Results and Discussion 87

3.3.1. Synthesis and Characterization of Alg-MA 87

3.3.2. Fabrication and Characterization of Dual-crosslinked Alg-MA Hydrogel Sub-Microsphere 91

3.3.3. Swelling and Diffusion-based Drug Release 93

3.3.4. Cellular Uptake of Alg-MA Sub-Microsphere 95

3.3.5. Cytotoxicity of Blank and Drug-Loaded Alg-MA Sub-Microspheres 97

3.3.6. Effect of Soluble Drug VS Sub-Microparticle Mediated Delivery on Cell Proliferation 99

3.4. Conclusions 101

3.5. Supplemental Materials 102

References 103

CHAPTER4: NANOPARTICLE-MEDIATED INTRACELLULAR FGF-2 DELIVERY AS A CELL-SELECTIVE, INTRACRINE CANCER THERAPEUTIC 105

4.1. Introduction 106

4.2. Materials and Methods 109

4.2.1. Materials 109

4.2.2. Alginate-g-PEG Sub-microsphere (ABN) Fabrication 110

4.2.3. Cellular uptake of ABNs 111

4.2.4. Bioactivity of Cells after 24 treatment of FGF-2 Intracellularly 114

4.3. Results 116

4.3.1. ABN Fabrication and Characterization 116

4.3.2. ABN Internalization 118

4.3.3. Intracellular Trafficking of ABNs 121

4.3.4. Bioactivity of FGF-2 Intracellular Delivery 125

4.4 Conclusions 128

4.5 Supplemental Materials 129

Reference 131

CHAPTER 5: TARGETED IMMUNOTHERAPY VIA ALGINATE AVIDIN NANOPARTICLES 135

5.1. Introduction 135

5.2. Materials and Methods 137

5.2.1. Materials 137

5.2.2. Alginate Sub-Microsphere (ASM) Fabrication 137

5.5.3. ASM Surface Coating 138

5.2.4. ASM Antibody Conjugation 139

5.2.5. Animals 139

5.2.6. Mixed Mice Spleen Culture 139

5.3. Results and Discussion 140

5.3.1. Alexa 647 Labeled ASMs Uptake by Mixed Culture Splenocytes 140

5.4. Conclusion 142

Reference 144

CHAPTER 6: SELF-HEALING AND THERMO-RESPONSIVE DUAL CROSSLINKED ALGINATE HYDROGELS BASED ON SUPRAMOLECULAR INCLUSION COMPLEXES 145

6.1. Introduction 145

6.2. Experimental Section 148

6.3. Results and Discussion 155

6.3.1. Dual Strategies for Synthesizing Alginate-*graft* Cyclodextrin (Alg-*g*-CD) 155

6.3.2. Hydrogel Formation and Rheological Analysis 158

6.3.3. Strain Responsive Properties and Self-Healing 162

6.3.4. Thermo-Responsive Properties 165

6.3.5. Hydrogel Stability 168

6.3.6. Hydrogel Erosion 169

6.3.7. *In Vitro* BSA Release 170

6.3.8. *In Vitro* Cytotoxicity 171

6.4. Conclusions 173

6.5. Supplemental Materials 174

References 185

CHAPTER 7 CONCLUSIONS AND FUTURE DIRECTIONS 190

.

Reference 194

APPENDIX: PHYSICALLY CROSSLINKED POLYVINYL ALCOHOL AND GELATIN INTERPENETRATING POLYMER NETWORK THETA-GELS FOR CARTILAGE REGENERATION 196

1. Introduction 197

2. Experimental Section 199

2.1. Fabrication of PVA-Gelatin Theta-Gels 199

2.2. Fourier-Transform Infrared (FTIR) Spectroscopy 200

2.3. Rheological Characterization 200

2.4. Scanning Electron Microscopy 201

2.5. Van Geison Staining 201

2.6. Equilibrium Water Content and Weight Loss 202

2.7. Unconfined Compression Testing 203

2.8. Cytotoxicity Assay 203

2.9. Chondrogenic Differentiation 204

2.10. Dimethylmethylene Blue (DMMB) Assay 205

2.11. In Vitro Mechanical Testing 206

2.12. Statistical Analysis 206

3. Results and Discussion 207

3.1. PVA-Gelatin Theta-Gel Formation 207

3.2. Physical Characterization and Mechanical Properties..... 212

3.3. In Vitro Chondrogenic Differentiation 218

4. Conclusions 222

References..... 223

BIBLIOGRAPHY 226

.

LIST OF TABLES

Table **Page**

Table 1-1. A series of examples of different polysaccharides for the delivery of bioactive agents for various applications. 21
Table 1-2. Examples of polysaccharide based drug delivery systems for controlled delivery anticancer agents..... 25
Table 1-3. Examples of clinical trials with polysaccharides. 30

Table 3-1. Dynamic light scattering (DLS) quantitative analysis of hydrodynamic diameters and zeta-potentials of blank (i.e., non-loaded) and DOX-loaded photo-crosslinked and dual-crosslinked Alg-MA sub-microspheres. DOX encapsulation efficiencies were determined using an absorbance assay after sub-microsphere fabrication. 96

.

LIST OF FIGURES

Figure **Page**

Figure 1-1. Structures of repeating units of some of the polysaccharides discussed in this review. Branching is not shown for dextran. The structures of alginate and hyaluronic acid are shown as two linkage types rather than a formal repeating unit. The chitin and chitosan structures represent extremes of a continuum of structures. 5
Figure 1-2. Schematic representation of alginate particulates for surface medication and encapsulated drugs. 8
Figure 1-3. Schematic representation of advantages of HA in drug delivery [44] (Adapted from reference). 11

Figure 2-1. Chemical modification of alginate (Alg) with two different poly(ethylene glycol) (PEG) oligomers with methyl and pyridine end groups, respectively. The synthesis of Alg-g-PEG was conducted using carbodiimide chemistry at pH 5 and room temperature. To synthesize Alg-g-PEG–S-S-Pyridine, NH2-PEG-SH was reacted with 2,2'-dithiodipyridine in degassed acetate buffer at pH 4 and room temperature under N2 flow. Next, the modified NH2-PEG-pyridine was conjugated to alginate using carbodiimide chemistry. 52
Figure 2-2. Schematic representation of microsphere fabrication techniques. Microspheres with or without VEGFA were prepared by premixing alginate or alginate-based copolymer solutions with VEGFA and creating a water/oil emulsion at room temperature in the presence of 1M calcium chloride. An additional surface modification step was performed on Alg-g-PEG-S-S-Pyridine microspheres to chemically conjugate CRGD via disulfide bonds. For Alg-g-RGD microspheres, the conjugation of 2,2'-dithiodipyridine was used to exchange the thiol group on the cysteine-RGD (CRGD) after microsphere fabrication. 54
Figure 2-3. The shape, average diameter, VEGFA encapsulation efficiency and cytotoxicity of alginate-based microspheres were verified using scanning electron microscopy (SEM), an ELISA assay (n = 3), and an MTT-based In Vitro Toxicology assay. SEM micrographs representing (A, D) Alg, (B, E) Alg-g-PEG, and (C,F) Alg-g-RGD microspheres were fabricated without the addition of VEGFA through a water/oil emulsion; micrographs shown in A,B,C have a scale bar = 10 μm while micrographs in D,E,F have a scale bar = 10 μm. In preparation for imaging, microspheres were frozen by immersion in liquid N2 and subsequently lyophilized; samples were sputter-coated with 45 nm of Au-Pb. (G) Microsphere diameters were determined using ImageJ analysis on SEM micrographs. (H) The effect of microsphere concentration (10, 50, 100, and 500 μg/mL) on primary human MSC viability after 24 h culture in standard MSC growth medium at 37°C and 5% CO2 was determined. Experimental groups were normalized to non-modified confluent human MSCs cultured on tissue culture

.

polystyrene. 55
Figure 2-4. Quantitative release of VEGFA was calculated using the encapsulation efficiencies of each sample group and the VEGFA concentration after each time point. Sample aliquots were collected and VEGFA concentration was determined using an ELISA assay (n = 3). (A) Cumulative VEGFA release (ng/mL) from alginate-based microspheres in phosphate buffered saline at pH 7.4 and 37°C over a sampling period of 14 days and (B) 72 hours was determined. 58
Figure 2-5. Confocal light microscopy images of GFP-labeled human MSCs (green) after 24 h of culture with DyLight 550 labeled-VEGFA-encapsulated alginate-based microspheres (red) at a concentration of 500 µg/mL in standard MSC growth medium. The Alg, Alg-g-PEG and Alg-g-RGD images all verify the internalization of microspheres, especially compared to the non-modified empty Alg microsphere control. The red intensity is a qualitative visualization of microspheres internalization rather than a quantitative measurement. 60
Figure 2-6. *In vitro* osteogenic (gray) and adipogenic (black) differentiation assay results of human MSCs after 14 days in culture with differentiation growth medium. (A) and (B) represent the VEGFA-encapsulated microspheres, (C) and (D) represent empty microspheres, and (E) and (F) represent extracellular delivery of pure VEGFA at different concentrations ranging from 0 to 20 ng/ml. A turkey statistical test was performed to compare the experimental groups to the control groups (n = 3). ** shows a significant p-value less than 0.0005 and * shows p-value less than 0.04. For the control group, only standard MSC growth medium was added. The graphs illustrate a significant difference between VEGFA encapsulated Alg, Alg-g-PEG and Alg-g-RGD microsphere groups compared to the control group in the osteogenesis assay as well as for the VEGFA encapsulated Alg microsphere group in the adipogenesis group. No significant differences were seen ($p \leq 0.05$) between control and experimental groups for the osteogenesis and adipogenesis assays when empty microspheres were used or VEGFA was delivered extracellularly. 63
Figure 2-7. ^{1}H-NMR spectra of NH_2-PEG-S-S-pyridine copolymer. The fours peaks between 7-8 ppm, which is amplified on the left, indicated the successful conjugation of pyridine onto PEG. The H2O peak represents the solvent D_2O and the large peaks near 2 ppm and 3.7 ppm represent residual CH_3COOH in the reaction buffer. 70
Figure 2-8. ^{1}H-NMR result of Alg-g-PEG copolymer synthesis. The peak of 3.36 ppm corresponds to the CH_3 moiety of the PEG side chain and 4.31 ppm corresponds to the shift of hydrogen atoms due to the grafting of the PEG side chain. Quantification of Alg-g-PEG conjugation by peak integration of the ^{1}H-NMR was not successful due to extensive broadening and overlapping of the peaks corresponding to the alginate in the Alg-g-PEG. 71
Figure 2-9. ^{13}C-NMR result of Alg–g-PEG-S-S-pyridine synthesis. Peaks at 132.31 ppm, 136.05 ppm, 141.37 ppm, 143.53 ppm, 149.24 ppm correspond to carbon on the pyridine ring, 69.76 ppm corresponds to carbon in the repeat unit of

.

PEG, and 42.84 ppm corresponds to carbon on the alginate repeat unit. 72

Figure 3-1. Schematic of the hydrogel network structure comprising photo-crosslinked and dual-crosslinked Alg-MA sub-microspheres. (I) Photo-crosslinked sub-microspheres exhibit a porous hydrogel network with intermolecular covalent crosslinks, encapsulating DOX. (II) Upon the addition of ionic crosslinking, the hydrogel network tightens, resulting in reduced drug loss and slower diffusion-based drug release; this is the desired product. (III) However, the introduction of aqueous-based calcium chloride ($CaCl_2$) solution may result in drug loss during the ionic crosslinking step. (IV) The non-ideal dual-crosslinked product may exhibit lower drug loading capacity due to the additional steps in the fabrication process. 88

Figure 3-2. (A) Chemical structure of methacrylated alginate (Alg-MA). Alg-MA was covalently crosslinked in the presence of photoinitiators under light activation, to form photo-crosslinked Alg-MA hydrogel networks. Alg-MA hydrogels were ionically crosslinked in the presence of calcium chloride ($CaCl_2$) to form dual-crosslinked Alg-MA hydrogel networks. (B) Schematic representation of microsphere fabrication techniques. Microspheres with or without DOX were prepared by premixing Alg-MA solutions and creating a water/oil emulsion at room temperature. Alg-MA sub-microspheres were photo-crosslinked upon exposure to visible or UV light, respectively, and further dual-crosslinked in the presence of 1 M $CaCl_2$. 90

Figure 3-3 Dynamic light scattering size distribution plots for photo-crosslinked and dual-crosslinked Alg-MA sub-microspheres: green photo-crosslinked (Green), green + Ca2+ dual-crosslinked (Green+C), UV photo-crosslinked (UV), UV + Ca2+ dual-crosslinked (UV+C). H 91

Figure 3-4. Quantitative cumulative release of doxorubicin (DOX) from DOX-loaded Alg-MA sub-microspheres for a period of 11 days (average ± standard deviation, n = 6 hydrogel samples per group). Sample aliquots were collected and the DOX concentration was determined using a standard curve at an absorption wavelength of 485 nm. (A) Cumulative DOX release profile during the first 8 hours; the release profiles for all of the Alg-MA sub-microsphere groups followed a linear trend (trend line $R^2 \geq 0.98$). (B) Cumulative DOX release profile during 11 days; the release profiles for the UV, Green, and Green+C Alg-MA sub-microsphere groups followed a logarithmic trend (trend line $R^2 \geq 0.92$), while the UV+C group continued to follow a linear release profile up to 11 days (trend line $R^2 = 0.98$). 95

Figure 3-5. Flow cytometry analysis of Alg-MA sub-microspheres after 12 hours of co-culture with human lung epithelial carcinoma (A549) cells. (A) Non-treated cell control, (B) cells cultured with non-labeled blank sub-microspheres, (C) cells cultured with green photo-crosslinked sub-microspheres, (D) cells cultured with green photo-crosslinked and calcium crosslinked sub-microspheres, (E) cells cultured with UV photo-crosslinked sub-microspheres, and (F) cells cultured with

.

UV photo-crosslinked and calcium crosslinked sub-microspheres. (G) Flow cytometry histograms were presented to show the different fluorescence intensity between control cells and different Alg-MA groups. 97
Figure 3-6. Human lung epithelial carcinoma (A549) cells were cultured in the presence of hydrogel sub-microspheres for 24 hours in standard growth medium at 37˚C and 5% $C0_2$. Cell viability was determined using an absorbance-based quantitative assay to measure mitochondrial activity (MTT); absorbance data for the groups treated with sub-microspheres were normalized to the non-treated cell control (average ± standard deviation, n = 6 hydrogel samples per group). The cytotoxicity of Alg-MA sub-microspheres was analyzed on (A) blank (non-loaded) sub-microspheres. The bioactivity of doxorubicin (DOX) was verified using (B) DOX-loaded sub-microspheres. Various groups (white diamonds = green photo-crosslinked, white circles = UV photo-crosslinked, black diamonds = green + Ca^{2+} dual crosslinked, black circles = UV + Ca^{2+} dual crosslinked) and sub-microsphere concentrations (10, 50, 100 µg/mL) were characterized. 98
Figure 3-7. The efficacy of doxorubicin (DOX)-loaded Alg-MA sub-microspheres as chemotherapeutic delivery vehicles was assessed using a MTT-based assay, to quantify cell proliferation over a 5-day period. A549 activity was recorded as mitochondrial activity and normalized to non-modified cell controls. Various formulations and concentrations (10-100 µg/mL) of sub-microspheres were assessed: green photo-crosslinked (Green), green + Ca^{2+} dual-crosslinked (Green+C), UV photo-crosslinked (UV), UV + Ca^{2+} dual-crosslinked (UV+C). DOX was added exogenously (Free DOX) to the cell culture medium at various concentrations to test the effect of intracellular versus extracellular DOX delivery. (A) Effect of Alg-MA sub-microsphere concentration for each crosslinking type on A549 mitochondrial activity; (B) Effect of 'free dox' concentration on A549 mitochondrial activity on days 1, 3, and 5; (C) Effect of DOX concentration encapsulated within Alg-MA sub-microspheres on A549 mitochondrial activity on days 1, 3, and 5. 100
Figure 3-8. The ^{1}H-NMR spectra of Alg-MA and alginate are shown here. The peaks at 5.75 and 6.25 ppm indicated that hydrogens on the methylene of the methacrylate groups were present on the alginate backbone after modification. 102

Figure 4-1. Scanning electron micrographs depicting spherical ABNs with (A) scale bar = 1 µm and (B) scale bar = 500 nm. (C) Hydrodynamic diameter distribution of FGF-2-loaded ABNs, measured in PBS, pH 7.4, 37˚C, and reported as number-average mean (84 nm). (D) Hydrodynamic zeta-potential distribution was measured in PBS, pH 7.4, and reported as number-average mean (-8 mV). (E) Cumulative FGF-2 release from 5 mg ABNs over 14 days; FGF-2 concentration (ng/mL) was measured with an ELISA; FGF-2 encapsulation efficiency was 60%. 117
Figure 4-2. Flow cytometry and quantification of the cell population (%) that internalized ABN after 12 hours of co-culture at concentration of 100 µg/ml: A549 cells (top panel) and HBEs (bottom panel). (**A,E**) Non-treated cell controls;

.

(**B,F**) cells treated with non-labeled ABNs; (**C,G**) cells with treated with AlexaFluor 647-labeled ABNs; and (**D,H**) cell count curves plotted on a log scale showing representative mean fluorescent intensities (MFI) for each control and experimental group. 119
Figure 4-3 Endocytosis-dependent ABN uptake by A549s. Results are presented as a percentage of the ABN-positive A549 cell population after treatment with various blockers and normalized to the control. (ANOVA, *p < 0.01 versus ABN control, n=3). Clathrin-inhibitors demonstrated the greatest reduction in ABN-positive cell populations. (**B**) The effect of ABN exposure and inhibition of endocytosis on mitochondrial activity in A549 cells after 30 minutes of culture was not significant. (**C**) CLSM merged images of A549 cells verified ABN internalization (red)..... 121
Figure 4-4. CLSM images of A549 cells cultured with AlexaFluor 647-labeled ABN (red) and rhodamine-labeled dextran (green) after (**A**) 10 minutes and (**B**) 24 hours of incubation. PC = phase contrast. 123
Figure 4-5. TEM images of A549 cells without exposure to ABN (A) or with exposed to ABN for (B) 30 minutes, (C) 4 hours, (D) 8 hours, (E) 24 hours, and (F) 48 hours. Two images at different magnifications are shown for each time point, scale bar = 2 μM. Yellow arrows indicate the location of ABN. 124
Figure 4-6. In vitro MTT test result of different treatments (non-treated control group, empty ASNs, extracellular FGF-2, and FGF-2 loaded ABNs) with HBE cells and A549 cells. (**C, F**) western blot photos of both membrane cytosol ERK1/2 activation and nuclear ERk1/2 activation for HBE cells and A549 cells. (**B, E**) OD reading ratio of pERK/ERK of western blot bands in both membrane/cytosol fraction and nuclear fraction for HBE cells and A549 cells..... 127
Figure 4-7. Schematic representation of proposed internalization and intracellular activity of FGF-2-loaded ABNs..... 128

Figure 5-1. Flow Cytometry result of Alexa 647 labeled ASMs 140
Figure 5-2 Alexa 647 labeled ASMs uptake by mixed culture plenocytes..... 142

Figure 6-1 A) Schematic of Alg-g-CD synthesis using organic solvents or aqueous-based solutions. Alg-C6 was the product of the organic synthesis (top), and Alg-C2 was the product of the aqueous synthesis (bottom). B) Schematic of physical crosslinking between Alg-g-CD macromolecules and Pluronic® F108, and the effect of Pluronic® F108 on the thermo-response of hydrogel network; Pluronic® F108 forms micelles and self-crosslinks at body temperature due to the triblock structure of PEG-b-PPG-b-PEG. β-CD conjugated onto the alginate backbone served as the host (Alg-g-CD), which formed a physically-crosslinked supramolecular inclusion complex with the guest, the PPG component (green) of Pluronic® F108..... 157
Figure 6-2. Rheological experiments were performed at 37 °C to verify formation and physical integrity of the supramolecular alginate network. (A, B) Continuous,

.

increasing shear rates allowed for the determination of viscosity and shear stress of formed hydrogels; A) Alg-C2 and B) Alg-C6. The shear stress increased with an increase in shear rate from 0 to 1 s^{-1}, demonstrating viscoelastic behavior. (C, D) Oscillatory time sweep experiments for hydrogel pre-curser solutions, Alg-g-CD and Pluronic® F108, and formed hydrogels at 1% strain, 10 Hz, 37 °C; C) Alg-C2 and D) Alg-C6. The storage moduli increased from 100 Pa for single polymer constituents to 10 kPa for 4% (w/v) Pluronic® F108:Alg-g-CD hydrogels. (E, F) Oscillatory frequency sweeps were performed at 0.5% radial strain; E) Alg-C2 and F) Alg-C6..... 161
Figure 6-3 (A, B) Oscillatory strain sweeps were performed at 10 Hz and 37 °C using a 40 mm 1°59'47" steel cone geometry on F108:Alg-g-CD hydrogels: A) Alg-C2 and B) Alg-C6 hydrogels. The storage moduli (G') and loss moduli (G") of the hydrogels crossed at higher strains, demonstrating a solid-liquid transition. (C – F) Dynamic shear strain testing of hydrogels was performed to demonstrate a self-healing, physically crosslinked network. Dashed gray lines represent the radial strain (%) input parameters and the solid black lines represent shear storage moduli (G') results. All of the groups tested demonstrated a repeatable ability to deform and re-assemble upon loading and un-loading, resulting in radial shear deformations. Hydrogels consisting of 4% (w/v) Alg-g-CD were analyzed at various ratios of Pluronic® F108:Alg-g-CD; C) Alg-C2 (1:2), D) Alg-C6 (1:2), E) Alg-C2 (1:4), F) Alg-C6 (1:4). The hydrogels exhibited higher storage moduli values at 0.5% strain while exhibiting lower G' values at 250% strain. Compared to alginate supramolecular inclusion complexes formed with β-CD, the novel Pluronic® F108:Alg-g-CD hydrogels presented here are shear-thinning, and amendable to injectable biomaterials applications[25]..... 164
Figure 6-4 (A, B) Oscillatory temperature sweeps were performed at 1 Hz and 1% radial strain on Alg-g-CD hydrogels: A) Alg-C2 and B) Alg-C6. (C, D) Shear storage moduli (G') for Alg-g-CD hydrogels at 25 °C (white bars) and 37 °C (black bars) (n = 3, average ± standard deviation), specifically C) Alg-C2 and D) Alg-C6. The ratio of Alg-g-CD to Pluronic® F108 was critical to the magnitude of the thermo-responsive properties. The greater the ratio of Pluronic® F108, the stiffer the hydrogel and more responsive the thermal behavior. Significant differences, of the same hydrogel sample between 25 and 37 °C, were observed in both Alg-g-CD hydrogel formulations. E) Images of Alg-g-CD and Pluronic® F108 solutions, and Alg-g-CD hydrogels formed after mixing the two pre-cursers and waiting 10 min, 1 day, and 5 days. Images were taken of hydrogels incubated at room temperature (RT) and 37 °C, respectively..... 167
Figure 6-5. (A,B) In vitro BSA release from Pluronic® F108:Alg-g-CD hydrogels. Experiments were performed at 37 °C under mild agitation in PBS, pH 7.4, investigating A) Alg-C2 and B) Alg-C6 hydrogels. Black circles represent 6% (w/v) Alg-g-CD solutions, open circles represent 4% Alg-g-CD solutions. Solid lines represent Pluronic® F108:Alg-g-CD hydrogels with ratios of 1:2; dashed lines represent hydrogels with ratios of 1:4. C) In vitro MTT-based assay

.

results of hydrogels cultured with primary human MSCs indicated no toxic effect for the various hydrogels analyzed along with the non-material treated control group. There were no significant differences between each group. 173
Figure 6-6. ^{1}H-NMR spectrum of β-CD-TsCl in DMSO-d_6. The peaks corresponding to δ = 7.43 ppm (2H) and δ = 7.75 ppm (2H) identify the hydrogens on the benzene ring of the toluenesulfonyl group. The remaining peaks between δ = 7 and 8 ppm refer to non-purified p-tuluenesulfonyl chloride. The peak corresponding to δ = 2.42 ppm (3H) refers to the hydrogens of the methylene group of the toluenesulfonyl group. Peaks between δ = 4.0 and 5.0 ppm refer to the hydrogens on the β-CD ring.[5] [12] 174
Figure 6-7. ^{1}H-NMR spectrum of β-CD-HDA. The disappearance of peaks between δ = 7 and 8 ppm indicates that the toluenesulfonyl group was replaced with hexanediamine. The peaks corresponding to δ = 1.14-1.16 ppm (12H) refer to hydrogens on the hexanediamine group. Peaks between δ = 3 and 5 ppm represent hydrogens on the β-CD ring. Peaks between δ = 1.00 and 1.10 ppm (2H) represent hydrogens on the amine group. [5, 12]..... 175
Figure 6-8. ^{1}H-NMR spectrum of β-CD-EDA. The disappearance of peaks between δ = 7 and 8 ppm indicate that the toluenesulfonyl group was replaced with ethylenediamine. The peak at δ = 2.61 ppm (2H) refers to hydrogens on the amine group. The peak at δ = 2.73 ppm (3H) refers to hydrogens on the methylene chain. Peaks between δ = 3.73 and 3.84 ppm represent hydrogens on the β-CD ring.[65] 176
Figure 6-9. ^{1}H-NMR spectrum of Alg-C6 with integration..... 177
Figure 6-10. ^{1}H-NMR spectra of Alg-C6 with standard procedure (brown), water suppression procedure (green), and diffusion edit procedure at 95% strength (blue). 178
Figure 6-11. ^{1}H-NMR spectrum of Alg-C2 with integration. 179
Figure 6-12. ^{1}H-NMR spectra of Alg-C6 with standard procedure (brown), water suppression procedure (green), and diffusion edit procedure at 95% strength (blue). 180
Figure 6-13. ^{1}H-NMR spectra of alginate with standard procedure (brown), water suppression procedure (green), and diffusion edit procedure at 95% strength (blue). 181
Figure 6-14. ^{1}H-NMR spectra of non-modified alginate (top) compared to Alg-*g*-CD (middle, bottom). Peaks between δ = 7 and 8 ppm represent the hydrogens on the amine group. Peaks between δ = 1 and 2 ppm refer to hydrogens on the methylene chain. 182
Figure 6-15. Optical photographs of hydrogel surface erosion in PBS at 37 ˚C over 14 days. Day 0 images demonstrate that the hydrogels crosslinked in the bottles, taking the shape of the container; hydrogels were not exposed to PBS. Day 0 with PBS images demonstrate how the hydrogels behaved after the addition of PBS. Day 3, 7 and 14 are series photos taken of the same sample at a specific time point. During the 14 day study, hydrogels were incubated at 37 ˚C under

.

gentle agitation. 183

Figure 8-1. Schematic illustrating the formation of a PVA and gelatin theta-gel, through the physical crosslinking of PVA (solid black lines) and gelatin (dashed black lines), respectively, in the presence and subsequent removal of PEG. Areas of hydrogen bonding (i.e., physical crosslinks) between gelatin and PVA are represented by black rectangles. Nucleation of PEG porogens (gray lines) during solidification and subsequent removal through dialysis resulted in a macro-porous network. 208

Figure 8-2. Top: Chemical structure of PVA; physical crosslinking takes place at OH groups between PVA molecules. Bottom: fourier transform infrared spectroscopy (FTIR) spectra of (A) gelatin, (B) PVA-PEG-1Gel, (C) PVA-PEG, (D) PVA-1Gel and (E) PVA hydrogel films, stretching vibrational bands associated with PVA physical crosslinking include C-O and C-O-C. 210

Figure 8-3. SEM images of lyophilized and cryo-fractured surfaces of 18% PVA hydrogel samples, fabricated in the presence of PEG alone (A, B) or with the addition of 5% gelatin (C, D). Magnifications at 250x, scale bar = 100 μm (A, C) and 800x, scale bar = 20 μm (B, D). (E) Van Geison staining qualitatively verified gelatin retention in the hydrogels, which were fabricated using theta-gel techniques. PVA-gelatin hydrogels consisting of 18 and 36% PVA, using low or high molecular weight PVA, were fabricated. Hydrogels also varied in gelatin content; top numbers represent weight percent of gelatin. Samples containing gelatin displayed a higher intensity of the red stain. 211

Figure 8-4. Rheological experiments were performed to examine the effect of PEG porogens on the mechanical response of PVA-gelatin hydrogels. A) Temperature sweep of single macromers, control solutions (PVA-1Gel, PVA-PEG), experimental solutions (PVA-PEG-1Gel); solution from the autoclave was tested from 60 ˚C to 20 ˚C to show the gelation process of each sample. B) Oscillatory time sweep experiments for control hydrogels (gelatin, PVA, PVA-1Gel, PVA-PEG), and experimental hydrogels (PVA-PEG-1Gel) were tested after dialysis at 25 ˚C. C) Oscillatory frequency sweeps were performed on hydrogels at 1% radial strain from 0.1 to 100 Hz at 25 ˚C. 214

Figure 8-5. The physical and mechanical properties of PVA-gelatin hydrogels, developed using theta-gel techniques, are reported. PVA-gelatin hydrogels consisting of 18 and 36% (w/v) PVA, using low (L, 95 kDa) or high (H, 145 kDa) molecular weight PVA, were fabricated. Hydrogels also varied in gelatin content; white = no gelatin, light gray = 1% gelatin, dark gray = 5% gelatin, black = 18% gelatin. (A) To evaluate hydration, the equilibrium water content of PVA-gelatin hydrogels and PVA controls was calculated; lyophilized hydrogel samples were hydrated in phosphate buffered saline (PBS), pH 7.4, for 24 hours at room temperature. (B) Weight loss values were calculated after removal of the hydrogel samples from solution. Measurements were used to determine the loss of soluble low molecular species and hydrolytic degradation. (C) Unconfined compression

.

tests were performed and elastic moduli of PVA-gelatin hydrogels were calculated using a linear regression of the stress-strain curve between 5 – 15% axial compressive strain; average ± standard deviation are reported (n = 4). PVA samples were left out of the study due to high compliance. 217
Figure 8-6. (A) Mitochondrial activity was determined using an MTT-based cytotoxicity assay. The absorbance values for PVA-gelatin and PVA hydrogels were normalized to non-modified cell controls cultured on tissue culture polystyrene; ethanol (EtOH) was used as a negative control. Confluent human MSCs were cultured with PVA-based hydrogels for 24 hours in standard MSC culture medium at 37 ˚C and 5% $C0_2$ (n = 4). (B) Sulfated GAG production was quantified for MSCs cultured in PVA-gelatin scaffolds and in non-modified treated polystyrene culture plates in chondrogenic media. Hydrogel experimental groups consisted of: 18PVA(H)-1Gel (soft), 18PVA(H)-1Gel + type II collagen (soft + T2), and 36PVA(L)-5Gel + type II collagen (stiff +T2); results are reported as average ± standard deviation (n = 4). (* = $p < 0.005$ compared to control samples at day 14; ** = $p < 0.03$ compared to day 4 results within the same sample group.) Unconfined compression tests were performed and the elastic moduli of human MSC-seeded hydrogels and non-seeded hydrogel controls were calculated using a linear regression of the stress-strain curve from 5 – 15% axial compressive strain. Hydrogel experimental groups consisted of: 18PVA(H)-1Gel (soft), 18PVA(H)-1Gel + type II collagen (soft + T2), and 36PVA(L)-5Gel + type II collagen (stiff +T2); results are reported as average ± standard deviation (n = 4). 219
.....

.

CHAPTER 1: CONPREHENSIVE LITERATURE REVIEW

PREFACE

In the field of bioengineering, the essence and motivation for research are ultimately driven by fundamental questions in biology. To provide technical support in the discovery of significant biological (and medical) findings, bioengineers contribute methodologies and tools, to perform research in a safe and controllable manner. In order to do so, bioengineers must have an understanding of, and appreciation for, the work of biologists and doctors. Herein, my thesis has introduced and discussed relevant biology in order to provide context for my work, and the motivation for my research projects.

The contributions of my PhD thesis research are highlighted in detail below, in regards to the collaborative publications in the field of biomaterials and biomedical engineering:

Throughout the 4 years of my PhD research, I designed a natural-based polysaccharide (i.e., alginate) nanoparticle platform for targeted and controlled delivery of a variety of therapeutics, in order to meet treatment requirements for different diseases, including: osteoporosis, lung cancer and multiple sclerosis. Various chemical modifications of the polysaccharide core nanoparticle, and surface conjugation chemistries, were utilized, characterized, and in some respects quantified, to enhance the functionality of the nanoparticles. 1) I synthesized an alginate-graft-poly(ethylene glycol) copolymer in order to form nanoparticles via water/oil emulsions; the side-chain addition of poly(ethylene glycol) (PEG) onto the alginate backbone was designed to partially neutralize the nanoparticle. 2) I performed dithioldipyridine modification of the alginate backbone in order to conjugate a targeting peptide (i.e., arginine-glycine-aspartic acid, RGD) onto the surface of the nanoparticles. 3) I helped design the emulsion of double-crosslinked hydrogel nanoparticles to prolong the release profile of small molecules. In addition, I also performed flow cytometry to verify the nanoparticle cellular uptake, and designed and completed the statistical analysis of the nanoparticle data. The shared nanoparticle fabrication, and cell culture, was performed by Spencer Fenn, a fellow graduate student in the Oldinski Laboratory. 4) I designed and implemented an avidin coating on the nanoparticles, to allow subsequent conjugation of any biotinylated antibody (e.g., a cell surface marker) to target drug delivery to selective cell types. The remainder of the targeting efficacy verification *in vitro* and *in vivo* were done by Abbas, in the Cory Teuscher Ph.D. Laboratory, and Dr. Dimitry Krementostov. 5) I quantified the encapsulation efficiency and drug release profiles over 14 days, for vascular endothelia growth factor A (VEGF-A), fibroblast growth factor 2 (FGF-2), doxorubicin, bovine serum albumin (BSA). I quantified the nanoparticles' size and surface charge with dynamic light scattering, and characterized the surface morphology with scanning electron microscopy. I created an efficient

fluorescent labeling procedure to efficiently tag nanoparticles with Alexa-647, which can be tracked and traced *in vitro* and *in vivo*. I also used these tagged nanoparticles to semi-quantitatively determine how cells are internalized by cells, and how they are transported inside cells. I cultured the nanoparticles with cancer cells, human epithelial cells, and human mesenchymal stem cells. I was able to induce osteogenic differentiation using MSC treated with VEGF-A loaded nanoparticles, and able to slow down lung cancer proliferation using FGF-2 loaded nanoparticles.

The other significant part of my PhD research was to design an injectable thermo-responsive hydrogel, based on alginate, for tissue regeneration and disease treatment, specifically, drug delivery and cell transplantation. I synthesized and characterized the mechanical properties of the hydrogels. I also conjugated RGD, a pro-adhesion peptide, onto the alginate backbone, mixed with cells, injected the material into a tissue culture dish, and verified cell viability.

In the project of poly vinyl alcohol (PVA) /gelatin scaffold, I was able to create porous hydrogels using freeze/thaw methods. I also synthesized theta-gels consisting of PVA, gelatin and PEG. I quantified the mechanical properties of the hydrogels using rheometry and scanning electron microscopy. I also performed a chondrogenesis assay using the PVA/gelatin scaffold to verify the efficacy of using this material to regenerate articular cartilage.

1.1. Introduction to Polysaccharides

Natural-based polysaccharides from different sources attract much attention from various industrial fields, such as the food and feed industries, and medical and pharmaceutical industries[1]. Polysaccharides comprise a groups of molecules known as carbohydrates. Along with oligosaccharides, they are one of the most abundant group of materials in the class of biopolymers to be involved in many biological structural building blocks and processes[2]. The basic structure for polysaccharides consists of a monosaccharide repeating unit with hydroxyl groups, such as cellulose and amylose. Some polysaccharides have other functional groups in addition to basic hydroxyl groups, such as chitosan's amine group, and alginate's carboxyl groups, offering more functionality compared to more basic polysaccharides (**Figure 1-1**). Due to similar biochemical properties compared with human extracellular matrix (ECM), polysaccharides are readily recognized and accepted by the body, and are viewed as biocompatible. In addition, these polymers are susceptible to enzymatic and/or hydrolytic degradation in biological environments, resulting in innocuous byproducts, which can either be reused by the human body or cleared by the immune system[3].

Modern nanotechnology has boosted the development of drug delivery systems to enhance the therapeutic efficacy for different type of diseases. With the tunable small sizes that researchers can achieve, micro/nanoparticles can travel through the smallest capillary vessels while avoiding clearance by phagocytes, resulting in a prolonged blood stream residence time. The small size also facilitates their ability to penetrate

tissue and cell gaps, and to even be internalized by targeted cells for efficient drug delivery. Furthermore, the availability of additional chemical conjugation techniques provides controlled–release drug profiles to target cells with different triggers, such as pH, ion and/or temperature[4].

Compared to other type of polymers, polysaccharides have several advantages for controlled drug delivery. First, the backbone structure of polysaccharides, particularly hydroxyl and amine groups, yield high aqueous solubility, and are better absorbed by the human body, and undergo hydrolysis to degrade into innocuous simple sugar molecules. Second, many polysaccharides possess innate bioactivity, particularly mucoadhesive, antimicrobial, and anti-inflammatory properties[5]. For example, chitosan, which is the only natural positively charged polysaccharide, is capable of attaching to negatively charged mucosal layers via electrostatic interactions[6]. Another example is hyaluronic acid, which binds to CD44 sites in the extracellular domain[7]. Third, polysaccharide-based nanoparticles exhibit biocompatible and biodegradable properties. Finally, polysaccharides are extremely amenable to chemical modification. For example pegylation, peptide conjugation, and antibody coatings provide various physiological behaviors and bioactivities for different applications[8].

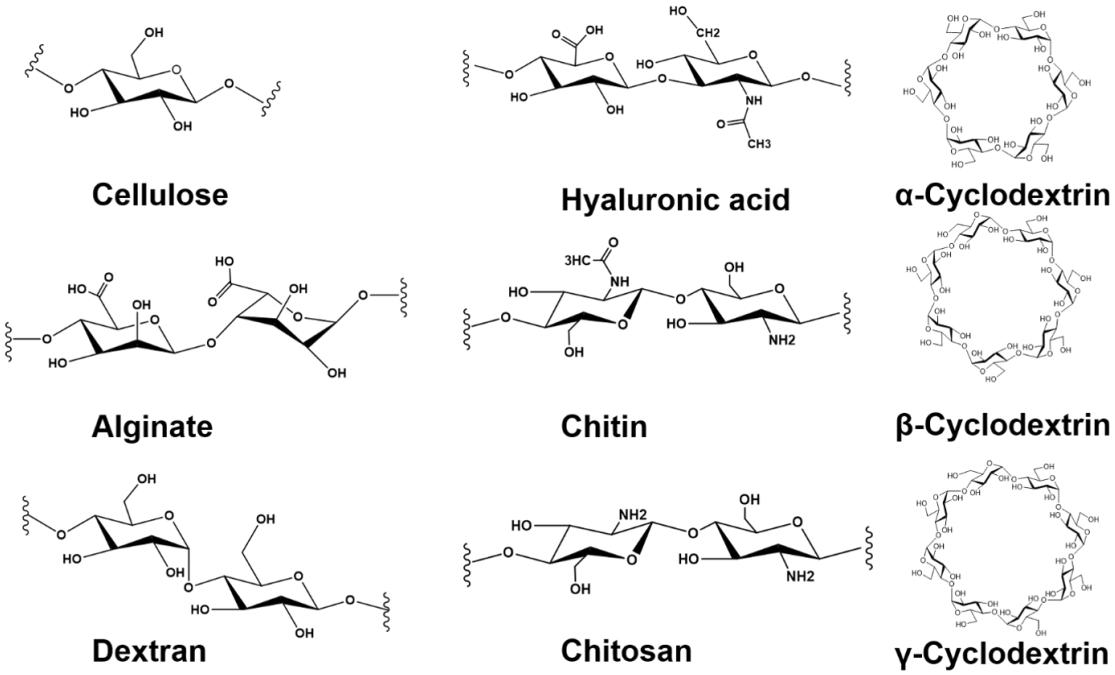

Figure 1-1. Structures of repeating units of some of the polysaccharides discussed in this review. Branching is not shown for dextran. The structures of alginate and hyaluronic acid are shown as two linkage types rather than a formal repeating unit. The chitin and chitosan structures represent extremes of a continuum of structures.

1.2. Structures and Modifications of Polysaccharides

1.2.1. Alginate

Alginates are non-branched polysaccharides consisting of 1→4 linked β-D-mannuronic acid (M) and its C-5 epimer α-L-guluronic acid (G), extracted from algae (such as kelp), or an exopolysaccharide of bacterial origin including Pseudomanas aeruginosa. Commercially available alginates are most often derived from brown

.

algae[9]. With the widely found extrusion source as well as the low cost of purifying techniques, alginate has been applied in the food, biochemical, and biomedical industries. The U.S. Food and Drug Administration (US-FDA) recognizes alginate as a "Generally Referred As Safe (GRAS)" material[10].

Referring to the backbone structure of alginate, two functional groups have been used for chemical conjugation. One is the common hydroxyl group from polysaccharides and the other is the carboxyl group. The hydroxyl group can be reacted with methacrylic anhydride via esterification, which can then be crosslinked upon exposure to long-wave UV light in the presence of a photoinitiator[11]. Jeon *et al.* have also developed a protocol using 2-aminoethyl methacrylate to react with the carboxyl groups on alginates, providing alternatives for designing alginate-based photo-sensitive materials[12].

Hydroxyl groups can also be oxidized to create more reactive groups and increase the rate of degradation[13-15]. The periodate oxidation of alginate, which chemically breaks the carbon-carbon bond of the cis-diol group in the urinate residue and changes the chain conformation, results in promotion of hydrolysis of alginate in aqueous solutions[13]. Jeon *et al.* also suggested that photo-crosslinked oxidized methacrylated alginate hydrogels can promote enhanced cell adhesion and spreading compared to those prepared with alginate that had not been oxidized[16], due to the free aldehyde groups on photo-crosslinked oxidized methacrylated alginate hydrogels forming bonds with amines present on cell surface or ECM proteins[16, 17].

The carboxyl group also offers potential variations of alginate-based materials. The most common strategy is to react the carboxyl group with an amine group to form peptide bond using water-based reaction, which is catalyzed by 1-ethyl-3-(3-dimethylaminopropyl)-carbodiimide (EDC) and N-hydroxysulfosuccinimide (sulfo-NHS)[18-20]. While the water-based reaction is capable of directing bioconjugation without prior organic solvent dissolution, excess reagent and byproducts can be easily removed by dialysis or gel-filtration. The high reaction efficiency allows researchers to conjugate polymers[20-22], peptides[23, 24] and proteins[25] onto alginate. In addition to aqueous reactions, carbodiimide chemistry can also be performed in organic solvent, rendering alginate soluble in organic solvent. The organic-based carbodiimide chemistry was performed with (benzotriazol-1-yloxy)tris(dimethylamino) phophonium hexa-fluorophosphate (BOP)[26]. To render alginate soluble in organic solvent, Pawar *et al.* dissolved tetrabutylammonium (TBA) salts of alginic acid in polar aprotic solvents containing tetrabutylammonium fluoride (TBAF)[27], which react with alginates homogeneously in organic solvents, including dimethyl sulfoxide (DMSO) and dimethylformamide (DMF).

Alginate particles have the ability to deliver proteins such as growth factors[9] and cytokines[28], chemotherapeutics such as doxorubicin[29] and paclitaxel[30], small molecules drugs[28] and nucleic acids including DNA[31] and RNA[32] (**Figure 1-2**). Thus, alginate shows great potential for the development of innovative drug delivery systems.

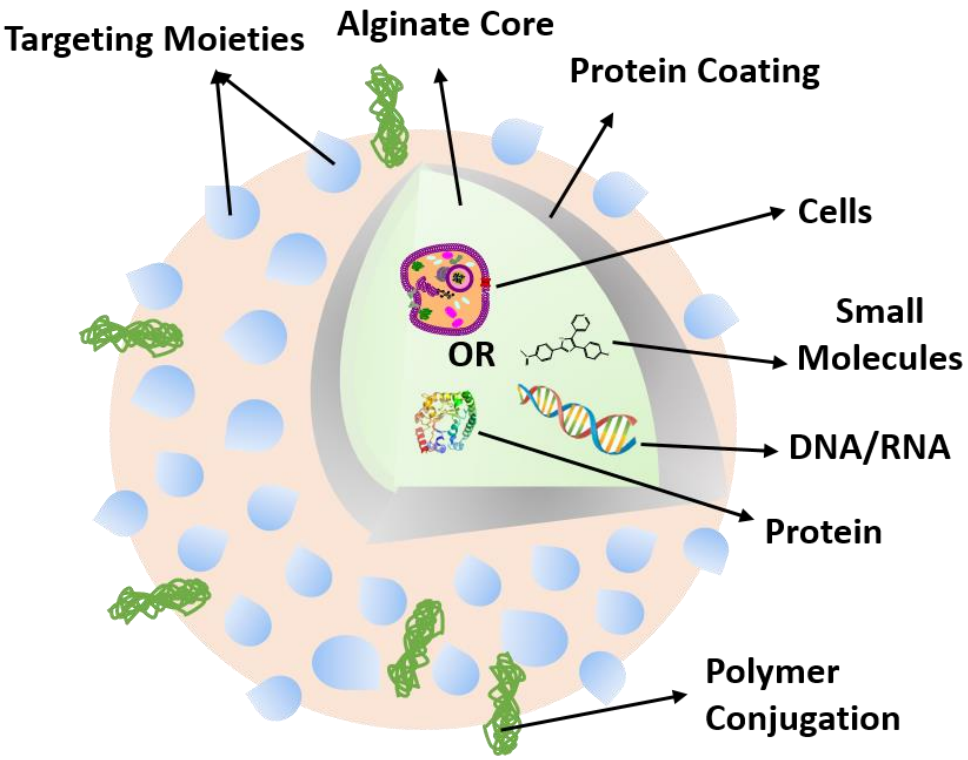

Figure 1-2. Schematic representation of alginate particulates for surface medication and encapsulated drugs.

1.2.2. Chitosan/Chitin

Chitin is one of the most abundant polysaccharides in the natural world, and is the supporting material for crustaceans, insects, etc., where it represents the major component of their exoskeleton. The structure of chitin consists of 2-acetamido-2-deoxy-β-D-glucose through a β (1→4) linkage[33]. Chitosan is the *N*-deacetylated derivative of chitin, which consists of β(1-4)-linked D-glucosamine and *N*-acetyl-D-glucosamine, though this N-deacetylation is almost never complete[33, 34].Chitosan has been used in the pharmaceutical industry for almost three decades, inspiring both

academic and industrial researchers to create various therapeutic systems. In contrast to all biodegradable polysaccharides, chitosan is cationic, based on its primary amino groups. The polycations can be used to promote mucoadhesion, because the mucus gel layer contains anionic sub-structures including sialic acid and sulfonic acid. Based on the ionic interactions between the cationic primary amino groups of chitosan and the anionic sub-structures of mucus, mucoadhesion can be achieved. In addition, hydrophobic interactions may also contribute to the mucoadhesive properties [34, 35]. The solubility of chitosan in water is relatively poor, which limits its application in the pharmaceutical industry. To facilitate dissolution, researchers have utilized acidic solution with pH below 6.5 to increase the repulsion between different polymer chains[36]. The backbone of chitosan contains multiple hydroxyl groups, capable of supporting many reactions including methacylation[37]. Chitosan also contains amine groups, which can react with carboxylate groups via carbodiimide chemistry catalyzed by NHS/EDC. Rafat *et al.* reported using poly(ethylene glycol) dibutylaldehyde (PEG-DBA) and short-range amide-type cross-linkers (EDC and NHS) to crosslink collagen and chitosan molecules, which enhanced the mechanical strength and elasticity[38].

The unique properties of chitosan make it useful for developing drug delivery systems for various applications. Studies have shown that chitosan can assist oral drug delivery, ocular drug delivery, nasal drug delivery, vaginal drug delivery, buccal drug delivery, parenteral drug delivery, intravesical drug delivery and vaccine delivery[34]. The commercially available chitosan derivative “Ciclopoli®” has been registered and

we foresee more commercially available chitosan derivative products boosting the pharmaceutical industry[34].

1.2.3. Hyaluronic Acid

Hyaluronic acid (HA) is a naturally occurring linear polysaccharide with repeating units of D-glucuronic acid and *N*-acetyl-D-glucosamine disaccharide (**Figure 1-1**). It was first isolated from the vitreous humor of bovine eyes by Meyer and Palmer[39, 40]. Due to the presence of carboxyl group on each of the repeat units, HA is usually associated with cations at pH=7. As with other polysaccharides, HA is highly hydrophilic, capable of absorbing large amounts of water and swelling up to 1000 times [39, 41]. The unique character of HA that is different from other polysaccharides is that it is capable of interacting with cell receptors, i.e. hyaluronan binding proteins, such as CD44, RHAMM, LYVE-1, IVd4 and LEC receptors, since it is a major constituent of skin and ECM[7, 42]. The inherent bioactivity of HA makes it a desirable biomaterial for tissue engineering and drug delivery (**Figure 1-3**)[39, 43, 44].

Figure 1-3. Schematic representation of advantages of HA in drug delivery [44] (Adapted from reference).

HA contains a carboxyl group on each repeat unit, making it an anionic polymer at neutral pH. Similar to alginate, the available hydroxyl and carboxyl groups on HA are subject to a series of modifications including methacrylation[45] and carbodiimide conjugation[46]. Methacrylated HA can be photo-crosslinked with either ultraviolet (UV) light[46] or visible light[46]. The -$NHCOCH_3$ group, which is distinctive in HA, is available for deacetylation and amidation activated by hydrazine sulfate[47]. There is

.

a trend of conjugating other polysaccharides onto hyaluronic acid for tissue regeneration. Rodell *et al.* reported a shear-thinning hydrogel based on the guest-host interactions of adamantine modified HA and β-cyclodextrin modified HA. The physical crosslinked hydrogels show potential as a minimally invasive injectable hydrogel for biomedical applications [48]. Owing to the unique and valuable physico-chemical property of HA, researchers have designed and synthesized innovative HA derivatives for various biomedical applications.

1.2.4. Dextran

Dextran consists of repeat units of branched glucans of varying lengths, which is medically applied as an antithrombotic to reduce blood viscosity, or as a volume expander for hypovolaemia. Dextran is produced by numerous types of bacteria, including *Leuconostocmesenteroids*. Similar to other type of polysaccharides, the properties of dextrans are strongly dependent on their structure including molecular weight and degree of branching. Dextran is soluble in water, formamide and DMSO, and insoluble in alcohol and acetone[49]. Only normal hydroxyl groups from the sugar repeat unit are present on the dextran backbone; therefore, reactions which modify hydroxyl groups are applicable to dextran. Maia *et al.* have investigated the degree of oxidation of dextran using sodium periodate[50].

Cyclodextrin is one type of dextran obtained from the enzymatic degradation of starch, belonging to the family of cage molecules (**Figure 1-1**). Supramolecular

hydrogels utilizing interactions between macrocyclic host and guest polymers to form inclusion complexes have drawn attention in the biomedical field[51]. The most common host polymer is cyclodextrin, of which there are three types with different numbers of sugar units on the ring[52]. The 3-dimensional structure of cyclodextrin (CD) reveals an inner hydrophobic cavity, The core of cyclodextrin is composed of a dimensionally stable hydrophobic cavity, able to trap and encapsulate other molecules, making it a valuable material for drug delivery[53]. However, the smaller size of CD limits its application. Therefore, there is a great need to conjugate CDs onto other polysaccharides, such as alginate. Rodell *et al.* conjugated β-CD onto HA to form supramolecular hydrogels. Alginate is also a popular polysaccharide to react with CD. Pluemsab *et al.* reported a coupling reaction between α-CD and alginate at the hydroxyl groups of alginate via the Cyanogen bromide (CNBr) method. After ionically crosslinking with $CaCl_2$, alginate-CD microparticles were generated approximately 500 μm in diameter[54]. Researchers have also reported using carbodiimide chemistry to synthesize alginate-CD, providing alternatives for similar formulations[55]. Dextran modification yielded other polymers with different molecular weights, shapes, structures and various coupling groups, which is helpful in achieving controlled drug delivery and release[56].

1.3. Preparation of Polysaccharide-Based Particles

To maintain the network of polysaccharide particles while avoiding dissolution

of the hydrophilic polymer chains/segments into the aqueous phase, crosslinking is performed. In general, labile bonds are introduced to form the crosslinked network. However, these bonds are subjected to degradation either enzymatically or chemically. Both chemical and physical crosslinking methods have been applied in forming polysaccharide particulates[57].

1.3.1. Crosslinking Reaction

1.3.1.1. Physical Crosslinking

The advantage of physical crosslinking is that it can avoid using toxic crosslinkers, which need to be extracted from particles before application *in vivo*. The most common physical interactions are ionic. Alginate is a well-established material that has been extensively studied to form nanoparticles. As stated above, the mannuronic and guluronic repeat units on an alginate backbone contain carboxyl groups, which can be crosslinked by calcium ions. The reaction is simple and fast, and can be performed at room temperature. It occurs through the exchange of sodium ions from the guluronic acid blocks with multivalent cations, such as Ca^{2+}, forming a characteristic “egg-box” structure [58]. The higher the percentage of guluronic acid, the tighter the ionically crosslinked network, resulting in a prolonged drug release profile[58]. The mild gelation method has enabled particle-based delivery of pDNAs, growth factors or even live cells[28]. The formation of ionic crosslinks is reversible, and the addition of a chelating agent will destabilize the crosslinked network, causing

particle degradation.

An example of Ca^{2+} crosslinked alginate microspheres was generated from a microfluidic device by Chen *et al.* They reported on a versatile droplet microfluidics method to fabricate alginate microspheres while simultaneously immobilizing anti-Mycobacterium tuberculosis complex IgY and anti-Escherichia coli IgG antibodies on the porous alginate microspheres for specific binding and binding affinity tests[59].They showed that calcium crosslinked alginate microspheres were generally round with undulating membranes.

1.3.1.2. Covalent Crosslinking

The water solubility of polysaccharides comes from the presence of functional groups, including hydroxyl groups, carboxyl groups and amine groups, which can also react to form new bonds in order form crosslinked networks. Yoon *et al.* developed photo-crosslinked HA nanoparticles (c-HANPs) with improved stability for tumor-targeted drug delivery[60]. The photo-crosslinking reaction was triggered by UV-Vis activation of acrylate groups in the polymer backbone. c-HANPs showed significantly higher stability in a physiological buffer and prolonged the release profile of a chemotherapeutic, paclitaxel, enabling long circulation in the body with enhanced tumor targeting ability. Researchers compared the near infrared fluorescence (NIRF) imaging of SCC7 tumor-bearing mice treated with FPR675-labeled HANP and c-HANP. C-HANP showed longer body circulation and higher tumor accumulation

compared to NHNP without crosslinking, with lower excretion within 24 h post-injection of PR674-labeled nanoparticles[60].

1.3.2. Methods

1.3.2.1. Emulsions

Emulsions have been widely applied in the design of drug delivery particles and pharmacotherapy. Emulsions provide a number of attributes, such as optical clarity, ease of preparation, thermodynamic stability, and increased surface area. Phase behavior studies have shown that the size of the droplets is determined by the surfactant phase structure (bicontinuousmicroemulsion or lamellar) at the inversion point induced, by either material composition or temperature[61]. Since polysaccharides are usually water soluble, water/oil emulsions are most applicable in the fabrication of polysaccharide nanoparticles. Machado *et al.* prepared calcium alginate nanoparticles using w/o nano-emulsions. The emulsions were produced from mixtures of nonionic surfactant tetraethylene glycol monododecyl ether ($C_{12}E_4$), decane, and aqueous solutions of up to 2 wt % sodium alginate by means of the phase inversion temperature (PIT) emulsification method. This method produced finely dispersed emulsions without a large input of mechanical energy[62].

To ensure evenly sized nanoparticles, a homogenizer is often used in the emulsion process to reduce the size of droplets in liquid-liquid dispersions, thus generating stable homogenized particles. However, the inherent random emulsion

process is not ideal for industry. Microfluidics have shown unparalleled advantages for the synthesis of polymer particles and have been utilized to produce hydrogel particles with a well-defined size, shape and morphology. Most importantly, during the cell encapsulation process, microfluidics can control the number of cells per particle and the overall encapsulation efficiency. Therefore, microfluidics is becoming a powerful approach for cell microencapsulation and construction of cell-based drug delivery systems[63].

1.3.2.2. Microfluidic Device

Microfluidic devices utilize the science of manipulating and controlling fluids and particles at micron or sub-micron dimensions to exploit a wide range of biological applications such as high-throughput drug screening, single cell or molecular analysis and manipulation, drug delivery and advanced therapeutics, biosensing, and point of care diagnostics, among others[64]. Fluid flow in microchannels is diffusion-based laminar flow due to low Reynolds numbers[65]. Several materials have been cast to make microfluidic devices, including polymer polydimethylsiloxane (PDMS), polymethylmethacrylate (PMMA), polystyrene (PS), polycarbonate (PC), cyclic olefin copolymer (COC)[66], silicon[67] and metal[68].Typically syringe pumps or microfabricated pumps provide pressure-driven flow in the microchannels; electrokinetic devices provide additional options for pumping liquids. Reagent solutions are manipulated inside microfluidic devices. A T-junction is usually designed

to generate droplets alternatively and fuse droplets in a tapered chamber[69]. Indeed, in the Oldinski Laboratory, a microfluidic flow focusing device was developed, which is consistently reproducible, readily characterized, and easy to test and use, to produce homogeneous alginate microparticles[70]. Microfluidic devices allow researchers to control the physical conditions and behavior of fluids in a micro/nano scaled domain to fabricate polysaccharide biomaterials, offering versatile solutions for fabrication, manufacturing and research in the field of cell biology, pharmacology and tissue engineering.

1.4. Preclinical Applications

1.4.1. Tissue Engineering and Regeneration

Polysaccharides form hydrogels and micro/nanoparticles through various reactions, and are able to encapsulate drug for therapeutic applications. Polysaccharide based micro/nanoparticles also provide protection to encapsulated growth factors, offering versatile release profiles in a controlled manner, while reducing the risk of adverse events[71]. Tissue engineering is an emerging biomedical field aiming to assist and enhance the regeneration of tissue as well as to substitute for the biological functions of damaged organs. To promote tissue regeneration or wound healing, growth factors are required to induce angiogenesis, which supplies oxygen and nutrients to cells transplanted for organ substitution, to maintain their biological functions[72]. Some growth factors stimulate the proliferation and differentiation of stem cells via certain cellular signaling pathway[73]. Various growth factors enhance the proliferation

and survival of multipotential stromal cells, including transforming growth factor beta (TGF-β), fibroblast growth factor (FGF), vascular endothelial growth factor (VEGF), platelet-derived growth factor (PDGF), epidermal growth factor (EGF), hepatocyte growth factor (HGF) and Wnt[74]. Almubarak *et al.* summarized the role of common growth factors in angiogenesis and osteogenesis, with the current status of preclinical and clinical trials[75]. **Table 1-1** lists a series of examples of different polysaccharides for the delivery of bioactive agents for various applications.

Polysaccharide type	Bioactive Agents	Application	Role in Tissue Engineering	Reference
Alginate	Amidated pectin hosting doxycycline (Antibiotics)	Wound healing	Inhibit bacterial-infection-caused necrosis in wound healing process	[76]
Alginate	human fibroblast growth factor 1 (FGF-1) human bone morphogenetic protein 4 (BMP-4)	Cartilage defects	Promote the in vitro development of mature adipocytes	[77]
Alginate	human fibroblast growth factor 1 (FGF-2)	Peripheral artery disease and coronary artery disease	Promote neovascularization and restore blood flow and tissue function of heart muscle	[78]
Alginate	FGF-1	Hypoxia	Enhancement of graft neovascularization in a retrievable rat omentum pouch	[79]

.

Alginate	Transforming growth factor-beta (TGF-β)	Articular cartilage defects	Controlled delivery of TGF-β selectively to the injury site and improve the repair of articular cartilage defects in rabbit model	[80]
Alginate	Insulin-like growth factor-1 (IGF-1)	Nervous system disorders such as stroke	Enhanced the proliferation of the encapsulated NSCs	[81]
Hyaluronic acid	None	atherosclerosis	Reach the atherosclerotic lesion after systemic administration with high potential as carrier for diagnosis and therapy of atherosclerosis	[82]
Hyaluronic acid Chitosan	VEGF	Wound healing	Promote angiogenesis and accelerate healing	[83]
Hyaluronic acid Chitosan	VEGF PGDF-BB	Development of vascular network during implantation	Promote angiogenesis	[84]
Poly(L-lactide-co-glycolide) (PLGA)-grafted hyaluronic acid	bone morphogenetic protein-2 (BMP-2) and IGF-1	Bone regeneration	Promote the attachment, proliferation, spreading, and alkaline phosphatase (ALP) activity of human adipose-derived stem cells (hADSCs).	[85]

.

Alginate microspheres within hyaluronic acid hydrogels	TGF-β3 Parathyroid hormone related protein (PTHrP)	Cartilage repair	Promote neo cartilage formation	[86]
Hyaluronic acid/Chitosan nanoparticles embedded in porous chitosan scaffold	DNA encoding TGF-β1	Cartilage tissue engineering	Promotion of chondrocyte proliferation	[87]
Glycidyl methacrylated dextran	BMP-2	Wound Healing	Periodontium Drug Delivery	[88]
Acetalated Dextran	Hepatocyte growth factor fragment	Myocardial Infarction (MI)	Largest arterioles, fewest apoptotic cardiomyocytes bordering the infarct, and the smallest infarcts	[89]
Methacrylated dextran	VEGF	Ischemia	Increase blood perfusion and angiogenesis	[90]
Chitosan–polyethylenimine	BMP-2 gene	Repair of bone defect	Affect cell differentiation through a BMP-2 signal pathway and promote new bone formation at the defect area	[91]

Table 1-1. A series of examples of different polysaccharides for the delivery of bioactive agents for various applications.

1.4.2. Cancer Therapy

1.4.2.1. Therapeutic Aspect

Cancer remains one of the worlds' major causes of death[92] and the

.

improvement of effective therapies continues to challenge researchers. With optimal size and surface properties, polysaccharide nanoparticles can be designed and engineered to increase bloodstream circulation time. Due to the enhanced permeability and retention effect, and ligand conjugation, nanoparticles can accumulate in the tumor site while delivering anticancer therapeutics, providing a higher targeting efficacy comparing to traditional drug delivery methods. Surface conjugation of cell targeting moieties also facilitates precise delivery of chemotherapeutics, resulting in higher treatment efficiency and fewer adverse events[93]. **Table 1-2** list a serious of examples of polysaccharide based drug delivery systems for cancer therapy.

Polysaccharide Type	Anticancer agents	Imaging Agents	Cancer Type	Result and Application	Reference
Hyaluronic Acid (HA)	None	Cy5.5	Xenograft subcutaneous dorsa of athymic nude mice	To visualize the biodistribution of HA nanoparticles accumulating into the tumor with a combination of passible and active targeting mechanism	[94]

.

Liposome-protamine-hyaluronic acid	TGF-β siRNA	None	Melanoma	Induction of antigen-specific immune response and target modification of tumor microenvironment; powerful tool for immunotherapy	[95]
Chitosan	siRNA for VEGRA, VEGFR1 and VEGFR2	None	Breast Cancer	Suppressive effect on VEGF expression and tumor volume	[96]
Chitosan/Alginate	Doxorubicin	None	HepG2 hepatoma cells xenografts	Induce the apoptosis of HepG2 tumor cells both in vitro and in vivo	[97]
Alginate	Doxorubicin	None	Liver tumor	Tumor necrosis; heart cells and healthy liver cells surrounding the tumor were not affected	[98]
Glycyrrhetinic acid-modified alginate	Doxorubicin	None	Hepatoma Carcinoma	Tumor inhabitation rate reach 79.3%	[99]

.

Alginate-g- Poly (N-isopropylacrylamide) (PNIPAAm)	Doxorubicin	FCR-675	Squamous cell carcinoma	DOX-loaded alginate-g-PNIPAAm micelles showed excellent anti-cancer therapeutic efficacy in a mouse model without any significant side effects	[100]
Alginate	Cisplatin	Cy5.5	Human caucasian ovary adenocarcinoma	Enhance delivery of CDDP into ovarian tumor tissues and improved the antitumor efficacy of CDDP, while reducing nephrotoxicity and body weight loss in mice	[101]
N-trimethyl chitosan	Cisplatin–alginate complex	None	Human ovarian and lung Carcinoma	Induce apoptosis	[102]
Hyaluronic acid	Cisplatin	None	Human malignant gliomas	Induce apoptosis	[103]
Chitosan	Destran-doxorubicin	None	Various Cancer type	Induce apoptosis and shrink tumor size	[104]

.

Hyaluronic acid	Cisplatin siRNA that downregulate anti-apopotic genes overexpressed in cisplatin resistant tumor	Indocyanine green	Lung cancer	Overcome the Multidrug resistance effect of lung cancer in xenograft model and induce apopotosis	[105]

Table 1-2. Examples of polysaccharide based drug delivery systems for controlled delivery anticancer agents.

Zhang *et al.* used glycyrrhetinic acid (GA) modified alginate nanoparticles to target the delivery of doxorubicin (DOX) to mice for treating liver cancer. After single tail-vein injections of 7mg/kg body weight, the concentration of DOX in the liver reached 67.8 ± 4.9 μg/g, which was 2.8-fold and 4.7-fold higher compared to non-GA modified alginate nanoparticles and free DOX HCl. Histological examination showed tumor necrosis in both experimental groups. Most importantly, the heart cells and the liver cells surrounding the tumor were not affected by administration of DOX/GA-ALG NPs, whereas myocardial necrosis and apparent liver cell swelling were observed after DOX·HCl administration[106].

1.4.2.2. Imaging/Monitoring Aspect

The rapid developing field of cancer treatment requires an appealing and versatile strategy for selective drug delivery, diagnostic and therapy purpose. Molecular

.

imaging technology has gained tremendous attention in cancer therapy, driven by nanoparticle mediated theranostics[107-111]. The nanotheranostics-based imaging platform holds great potential to provide invaluable insights into both cancer diagnosis and therapeutic response monitoring. Polysaccharide particulates can encapsulate multiple imaging contrasts into one single system for systematic administration. Chan et al. reported of using gadolinium-chelating crosslinkers to crosslink self-assembled pullulan nanogels to both impact magnetic properties and to stabilize the materials for tumor magnetic response imaging (MRI). The polysaccharide coating provides high signal enhancement lasting 7 days in long imaging time scales while causing no damage or toxicity in major organs over three months' monitoring, highlighting the potential clinical application of this Gd-chelating pullulan nanogels as a tumor-imaging MRI contrast agent, permitting tumor identification and assessment with a high signal-to-background ratio[112].

Another application of polysaccharides in assisting cancer imaging is through surface coating of nanoparticles, especially magnetic nanoparticles. The polysaccharide coatings of magnetic particles increased their biocompatibility, stability and concentration in the in vivo circulation[113, 114]. Thomas et al. reported developing hyaluronic acid (HA) coated superparamagnetic iron oxide nanoparticles (SPIONs) primarily for use in a hyperthermia application with an MR diagnostic feature. As stated in the previous session, HA is able to target CD44 over expressed cancer cells, providing more functionality to the imaging contrast agent. HA-SPION-injected mice

tumors showed nearly 40% MR T2 contrast compared to the 20% MR T2 contrast of the HA-PEG10-SPION group over a 3 h time period[115].

The RNA interference (RNAi) technique has been a new route for cancer therapy and several candidates are being tested clinically. In the development of RNAi-based techniques, imaging methods provide a visible and quantitative solution to investigate the therapeutic effect at anatomical, cellular and molecular level, able to noninvasively trace the distribution and study the biological processes in preclinical and clinical stages[116]. Nanocarrier-mediated delivery of RNAi therapeutics usually encounters different biological barriers including reaching the circulation, crossing the vascular barrier, cellular uptake, and endosomal escape. With the advancements in chemical modification and nanotechnology, polysaccharide nanoparticles are diverse in size and charge, being widely applied as platforms for simultaneous gene/drug delivery and imaging[117]. Yoon et al. reported a novel type of biodegradable hyaluronic acid-*graft*-poly(dimethylaminoethyl methacrylate) (HPD) conjugate that can form complexes with siRNA and be chemically crosslinked via the formation of the disulfide bonds under facile conditions, exhibiting high stability in 5-% serum solution compere to uncrosslinked ones.The in vivo study, which was performed using FPR675labeled HPDwith siRNAcomplexes, showed the efficacy of selective accumulation of the complexes at the tumor site after intravenous injection into tumor-bearing mice, achieving successful gene silencing effect while being able to be monitored with whole body NIRF imager[118].

While the application of polysaccharide-coated particles show promising results in research, there are limitations. One problem is to target sites located farther from the magnetic source. Future research should focus on designing multimodality imaging probes with polysaccharide coatings to upgrade the use of particle based imaging based contrasts, offering versatile solutions for early cancer detection and monitoring[113].

1.5. Clinical Translations

Despite the potential for polysaccharide-based nanoparticles, they remain elusive to the market and only a few products have continued to a clinical trial. As natural biomaterials, polysaccharides have been applied in different industries, including food and medical. **Table 1-3** includes a list of ongoing and completed clinical trials with polysaccharide-based drug delivery systems; many of the clinical trials involving alginate focus on dietary supplements, such as iron[119]. DIABECELL is one of the most promising products available, in Phase III clinical trial, for the encapsulation of porcine islets for the treatment of type 1 diabetes[79]. In addition, there are a wide variety of applications using polysaccharide coatings on other nanoparticles to reduce cytotoxicity and immunogenicity[120, 121].

Indications	***Name***	***Delivery Route***	***Bioactive Components***	***Delivery System***	***Development Phase***	***Country***	***Reference***
Iron deficiency anemia	Alginate beads	Dietary Supplement	ferrous gluconate	Alginate beads	Complete Phase I trial	United Kingdom	[119]
Gastroesophageal Reflux Disease Systemic Sclerosis Scleroderma	Alginic acid	Dietary Supplement	Domperidone Omeprazole Alginic acid	N/A	Ongoing Phase III	Thailand	N/A
Type 1 diabetes	DIABECELL	Xenotransplantation	Porcine islets	Alginate	Ongoing Phase III	New Zealand	[122]
Myocardial Infarction	IK-5001	Intracoronary slow bolus injection	Calcium Gluconate	Sodium Alginate	Phase I	United States, Australia, Belgium, Canada, France, Germany, Israel, Poland, Spain	[123]
Cystic Fibrosis	OligoG CF-5/20	Inhalation	OligoG CF-5/20 G-block Oligosaccharide Derived From Alginate Polysaccharide	N/A	Phase I	Merthyr Tydfil, United Kingdom	[124]
Breast Cancer	RadiaPlex Aquaphor	Injection to the medial half or the lateral half of the irritated breast.	Radiation	Hyaluronic acid	Phase III	United States	[125]
Immune related Disease	Chitin Micro-Particles	Intranasal dosing	N/A	Chitin	Phase I	Denmark	[126]
non-muscle invasive bladder cancer	Immucist®	Intravesical administration	Bacillus Calmette-Guérin	Hyaluronic acid	Phase I	Italy	[127]

.

Table 1-3. Examples of clinical trials with polysaccharides.

1.6. Conclusions

The biocompatibility, accessibility, and versatile options for chemical modifications make polysaccharides desired materials for applications in biomedical engineering. I have selected alginate as the focus of my research to make different systems for tissue engineering and drug delivery applications.

.

References

[1] Liu J, Willför S, Xu C. A review of bioactive plant polysaccharides: Biological activities, functionalization, and biomedical applications. Bioactive Carbohydrates and Dietary Fibre 2015;5:31-61.

[2] Lin N, Huang J, Dufresne A. Preparation, properties and applications of polysaccharide nanocrystals in advanced functional nanomaterials: a review. Nanoscale 2012;4:3274-94.

[3] Shelke NB, James R, Laurencin CT, Kumbar SG. Polysaccharide biomaterials for drug delivery and regenerative engineering. Polymers for Advanced Technologies 2014;25:448-60.

[4] Liu Z, Jiao Y, Wang Y, Zhou C, Zhang Z. Polysaccharides-based nanoparticles as drug delivery systems. Advanced Drug Delivery Reviews 2008;60:1650-62.

[5] Zhang N, Wardwell PR, Bader RA. Polysaccharide-Based Micelles for Drug Delivery. Pharmaceutics 2013;5:329-52.

[6] Sogias IA, Williams AC, Khutoryanskiy VV. Why is chitosan mucoadhesive? Biomacromolecules 2008;9:1837-42.

[7] Peach RJ, Hollenbaugh D, Stamenkovic I, Aruffo A. Identification of hyaluronic acid binding sites in the extracellular domain of CD44. The Journal of cell biology 1993;122:257-64.

[8] Cumpstey I. Chemical Modification of Polysaccharides. ISRN Organic Chemistry 2013;2013:27.

[9] Pawar SN, Edgar KJ. Alginate derivatization: A review of chemistry, properties and applications. Biomaterials 2012;33:3279-305.

[10] Sosnik A. Alginate Particles as Platform for Drug Delivery by the Oral Route: State-of-the-Art. ISRN Pharmaceutics 2014;2014:17.

[11] Chou AI, Akintoye SO, Nicoll SB. Photo-crosslinked Alginate Hydrogels Support Enhanced Matrix Accumulation by Nucleus Pulposus Cells In Vivo. Osteoarthritis and cartilage / OARS, Osteoarthritis Research Society 2009;17:1377-84.

[12] Jeon O, Bouhadir KH, Mansour JM, Alsberg E. Photocrosslinked alginate hydrogels with tunable biodegradation rates and mechanical properties. Biomaterials 2009;30:2724-34.

[13] Bouhadir KH, Lee KY, Alsberg E, Damm KL, Anderson KW, Mooney DJ. Degradation of partially oxidized alginate and its potential application for tissue engineering. Biotechnology progress 2001;17:945-50.

[14] Priddy LB, Chaudhuri O, Stevens HY, Krishnan L, Uhrig BA, Willett NJ, et al. Oxidized alginate hydrogels for bone morphogenetic protein-2 delivery in long bone defects. Acta Biomater 2014;10:4390-9.

[15] Balakrishnan B, Joshi N, Jayakrishnan A, Banerjee R. Self-crosslinked oxidized alginate/gelatin hydrogel as injectable, adhesive biomimetic scaffolds for cartilage regeneration. Acta Biomater 2014;10:3650-63.

[16] Jeon O, Alt DS, Ahmed SM, Alsberg E. The effect of oxidation on the degradation of photocrosslinkable alginate hydrogels. Biomaterials 2012;33:3503-14.

[17] Shazly TM, Baker AB, Naber JR, Bon A, Van Vliet KJ, Edelman ER. Augmentation of postswelling surgical sealant potential of adhesive hydrogels. Journal of biomedical materials research Part A 2010;95:1159-69.

[18] Rowley JA, Madlambayan G, Mooney DJ. Alginate hydrogels as synthetic extracellular matrix materials. Biomaterials 1999;20:45-53.

[19] Polyak B, Geresh S, Marks RS. Synthesis and Characterization of a Biotin-Alginate Conjugate and Its Application in a Biosensor Construction. Biomacromolecules 2004;5:389-96.

.

[20] Miao T, Rao KS, Spees JL, Oldinski RA. Osteogenic differentiation of human mesenchymal stem cells through alginate-graft-poly(ethylene glycol) microsphere-mediated intracellular growth factor delivery. Journal of Controlled Release 2014;192:57-66.
[21] Devi DA, Smitha B, Sridhar S, Jawalkar SS, Aminabhavi TM. Novel sodium alginate/polyethyleneimine polyion complex membranes for pervaporation dehydration at the azeotropic composition of various alcohols. Journal of Chemical Technology & Biotechnology 2007;82:993-1003.
[22] Yang J-S, Xie Y-J, He W. Research progress on chemical modification of alginate: A review. Carbohydrate Polymers 2011;84:33-9.
[23] Shachar M, Tsur-Gang O, Dvir T, Leor J, Cohen S. The effect of immobilized RGD peptide in alginate scaffolds on cardiac tissue engineering. Acta Biomaterialia 2011;7:152-62.
[24] Kang S-W, Cha B-H, Park H, Park K-S, Lee KY, Lee S-H. The Effect of Conjugating RGD into 3D Alginate Hydrogels on Adipogenic Differentiation of Human Adipose-Derived Stromal Cells. Macromolecular Bioscience 2011;11:673-9.
[25] Levy MC, Edwards-Levy F. Coating alginate beads with cross-linked biopolymers: a novel method based on a transacylation reaction. Journal of microencapsulation 1996;13:169-83.
[26] Miao T, Fenn SL, Charron PN, Oldinski RA. Self-Healing and Thermoresponsive Dual-Cross-Linked Alginate Hydrogels Based on Supramolecular Inclusion Complexes. Biomacromolecules 2015;16:3740-50.
[27] Pawar SN, Edgar KJ. Chemical Modification of Alginates in Organic Solvent Systems. Biomacromolecules 2011;12:4095-103.
[28] Lee KY, Mooney DJ. Alginate: properties and biomedical applications. Progress in polymer science 2012;37:106-26.
[29] Guo H, Lai Q, Wang W, Wu Y, Zhang C, Liu Y, et al. Functional alginate nanoparticles for efficient intracellular release of doxorubicin and hepatoma carcinoma cell targeting therapy. Int J Pharm 2013;451:1-11.
[30] Wu JL, Wang CQ, Zhuo RX, Cheng SX. Multi-drug delivery system based on alginate/calcium carbonate hybrid nanoparticles for combination chemotherapy. Colloids Surf B Biointerfaces 2014;123:498-505.
[31] Jain S, Amiji M. Tuftsin-Modified Alginate Nanoparticles as a Noncondensing Macrophage-Targeted DNA Delivery System. Biomacromolecules 2012;13:1074-85.
[32] Krebs MD, Jeon O, Alsberg E. Localized and sustained delivery of silencing RNA from macroscopic biopolymer hydrogels. J Am Chem Soc 2009;131:9204-6.
[33] Ravi Kumar MNV. A review of chitin and chitosan applications. Reactive and Functional Polymers 2000;46:1-27.
[34] Bernkop-Schnürch A, Dünnhaupt S. Chitosan-based drug delivery systems. European Journal of Pharmaceutics and Biopharmaceutics 2012;81:463-9.
[35] Grabovac V, Guggi D, Bernkop-Schnurch A. Comparison of the mucoadhesive properties of various polymers. Adv Drug Deliv Rev 2005;57:1713-23.
[36] Riva R, Ragelle H, Rieux A, Duhem N, Jérôme C, Préat V. Chitosan and Chitosan Derivatives in Drug Delivery and Tissue Engineering. In: Jayakumar R, Prabaharan M, Muzzarelli ARA, editors. Chitosan for Biomaterials II. Berlin, Heidelberg: Springer Berlin Heidelberg; 2011. p. 19-44.
[37] Diolosà M, Donati I, Turco G, Cadenaro M, Di Lenarda R, Breschi L, et al. Use of Methacrylate-Modified Chitosan to Increase the Durability of Dentine Bonding Systems. Biomacromolecules 2014;15:4606-13.

.

[38] Rafat M, Li F, Fagerholm P, Lagali NS, Watsky MA, Munger R, et al. PEG-stabilized carbodiimide crosslinked collagen–chitosan hydrogels for corneal tissue engineering. Biomaterials 2008;29:3960-72.
[39] Mero A, Campisi M. Hyaluronic Acid Bioconjugates for the Delivery of Bioactive Molecules. Polymers 2014;6:346.
[40] Meyer K, Palmer JW. THE POLYSACCHARIDE OF THE VITREOUS HUMOR. Journal of Biological Chemistry 1934;107:629-34.
[41] Serra L, Doménech J, Peppas NA. Drug transport mechanisms and release kinetics from molecularly designed poly (acrylic acid-g-ethylene glycol) hydrogels. Biomaterials 2006;27:5440-51.
[42] Lesley J, He Q, Miyake K, Hamann A, Hyman R, Kincade PW. Requirements for hyaluronic acid binding by CD44: a role for the cytoplasmic domain and activation by antibody. J Exp Med 1992;175:257-66.
[43] Collins MN, Birkinshaw C. Hyaluronic acid based scaffolds for tissue engineering—A review. Carbohydrate Polymers 2013;92:1262-79.
[44] Chen B, Miller RJ, Dhal PK. Hyaluronic Acid-Based Drug Conjugates: State-of-the-Art and Perspectives. Journal of Biomedical Nanotechnology 2014;10:4-16.
[45] Khetan S, Guvendiren M, Legant WR, Cohen DM, Chen CS, Burdick JA. Degradation-mediated cellular traction directs stem cell fate in covalently crosslinked three-dimensional hydrogels. Nature materials 2013;12:458-65.
[46] Han HS, Thambi T, Choi KY, Son S, Ko H, Lee MC, et al. Bioreducible Shell-Cross-Linked Hyaluronic Acid Nanoparticles for Tumor-Targeted Drug Delivery. Biomacromolecules 2015;16:447-56.
[47] Oerther S, Maurin AC, Payan E, Hubert P, Lapicque F, Presle N, et al. High interaction alginate-hyaluronate associations by hyaluronate deacetylation for the preparation of efficient biomaterials. Biopolymers 2000;54:273-81.
[48] Rodell CB, Kaminski AL, Burdick JA. Rational Design of Network Properties in Guest–Host Assembled and Shear-Thinning Hyaluronic Acid Hydrogels. Biomacromolecules 2013;14:4125-34.
[49] Dhaneshwar SS, Kandpal M, Gairola N, Kadam S. Dextran: A promising macromolecular drug carrier. Indian journal of pharmaceutical sciences 2006;68:705.
[50] Maia J, Carvalho RA, Coelho JFJ, Simões PN, Gil MH. Insight on the periodate oxidation of dextran and its structural vicissitudes. Polymer 2011;52:258-65.
[51] Dong R, Pang Y, Su Y, Zhu X. Supramolecular hydrogels: synthesis, properties and their biomedical applications. Biomaterials Science 2015;3:937-54.
[52] Crini G. Review: A History of Cyclodextrins. Chemical Reviews 2014;114:10940-75.
[53] Tiwari G, Tiwari R, Rai AK. Cyclodextrins in delivery systems: Applications. Journal of Pharmacy and Bioallied Sciences 2010;2:72-9.
[54] Pluemsab W, Sakairi N, Furuike T. Synthesis and inclusion property of α-cyclodextrin-linked alginate. Polymer 2005;46:9778-83.
[55] Lin N, Dufresne A. Supramolecular hydrogels from in situ host-guest inclusion between chemically modified cellulose nanocrystals and cyclodextrin. Biomacromolecules 2013;14:871-80.
[56] Varshosaz J. Dextran conjugates in drug delivery. Expert opinion on drug delivery 2012;9:509-23.
[57] Hennink WE, van Nostrum CF. Novel crosslinking methods to design hydrogels. Advanced

.

Drug Delivery Reviews 2012;64, Supplement:223-36.
[58] Paques JP, van der Linden E, van Rijn CJM, Sagis LMC. Preparation methods of alginate nanoparticles. Advances in Colloid and Interface Science 2014;209:163-71.
[59] Chen W, Kim JH, Zhang D, Lee KH, Cangelosi GA, Soelberg SD, et al. Microfluidic one-step synthesis of alginate microspheres immobilized with antibodies. Journal of the Royal Society, Interface / the Royal Society 2013;10:20130566.
[60] Yoon HY, Koo H, Choi KY, Chan Kwon I, Choi K, Park JH, et al. Photo-crosslinked hyaluronic acid nanoparticles with improved stability for in vivo tumor-targeted drug delivery. Biomaterials 2013;34:5273-80.
[61] Lovelyn C, Attama AA. Current state of nanoemulsions in drug delivery. Journal of Biomaterials and Nanobiotechnology 2011;2:626.
[62] Machado AHE, Lundberg D, Ribeiro AJ, Veiga FJ, Lindman B, Miguel MG, et al. Preparation of Calcium Alginate Nanoparticles Using Water-in-Oil (W/O) Nanoemulsions. Langmuir 2012;28:4131-41.
[63] Wan J. Microfluidic-Based Synthesis of Hydrogel Particles for Cell Microencapsulation and Cell-Based Drug Delivery. Polymers 2012;4:1084.
[64] Yeo LY, Chang HC, Chan PP, Friend JR. Microfluidic devices for bioapplications. Small 2011;7:12-48.
[65] Freemantle M. DOWNSIZING CHEMISTRY. Chemical & Engineering News Archive 1999;77:27-36.
[66] Alrifaiy A, Lindahl OA, Ramser K. Polymer-based microfluidic devices for pharmacy, biology and tissue engineering. Polymers 2012;4:1349-98.
[67] Iliescu C, Taylor H, Avram M, Miao J, Franssila S. A practical guide for the fabrication of microfluidic devices using glass and silicon. Biomicrofluidics 2012;6:016505--16.
[68] Li G, Parmar M, Lee D-W. An oxidized liquid metal-based microfluidic platform for tunable electronic device applications. Lab on a Chip 2015;15:766-75.
[69] Hung L-H, Lee AP. Microfluidic devices for the synthesis of nanoparticles and biomaterials. Journal of Medical and Biological Engineering 2007;27:1.
[70] Hotaling SO. Design and Fabrication of Flow-Focusing Devices for Tissue Engineering Applications [Honors College Thesis]. UVM Honors College Senior Theses: University of Vermont; 2015.
[71] Monteiro N, Martins A, Reis RL, Neves NM. Nanoparticle-based bioactive agent release systems for bone and cartilage tissue engineering. Regenerative Therapy 2015;1:109-18.
[72] Tabata Y. Tissue regeneration based on growth factor release. Tissue Engineering 2003;9:5-15.
[73] Oda K, Matsuoka Y, Funahashi A, Kitano H. A comprehensive pathway map of epidermal growth factor receptor signaling. Molecular Systems Biology 2005;1:2005.0010-2005.0010.
[74] Rodrigues M, Griffith LG, Wells A. Growth factor regulation of proliferation and survival of multipotential stromal cells. Stem Cell Research & Therapy 2010;1:1-12.
[75] Almubarak S, Nethercott H, Freeberg M, Beaudon C, Jha A, Jackson W, et al. Tissue engineering strategies for promoting vascularized bone regeneration. Bone 2016;83:197-209.
[76] De Cicco F, Russo P, Reverchon E, García-González CA, Aquino RP, Del Gaudio P. Prilling and Supercritical Drying: a Successful Duo to Produce Core-Shell Polysaccharide Aerogel Beads for wound healing. Carbohydrate Polymers.
[77] Greenwood-Goodwin M, Teasley ES, Heilshorn SC. Dual-stage growth factor release within

.

3D protein-engineered hydrogel niches promotes adipogenesis. Biomaterials Science 2014;2:1627-39.
[78] Kuraitis D, Arzhangi Z, Hyatt A, Vulesevica B, Merrett K, Zhang J. Tertiary biomaterial encapsulation controls the release of FGF-2 without impacting bioactivity. Open Tissue Eng Regen Med J 2012;5:4.
[79] McQuilling JP, Arenas-Herrera J, Childers C, Pareta RA, Khanna O, Jiang B, et al. New alginate microcapsule system for angiogenic protein delivery and immunoisolation of islets for transplantation in the rat omentum pouch. Transplantation proceedings 2011;43:3262-4.
[80] Mierisch CM, Cohen SB, Jordan LC, Robertson PG, Balian G, Diduch DR. Transforming growth factor-beta in calcium alginate beads for the treatment of articular cartilage defects in the rabbit. Arthroscopy : the journal of arthroscopic & related surgery : official publication of the Arthroscopy Association of North America and the International Arthroscopy Association 2002;18:892-900.
[81] Li W, Guan T, Zhang X, Wang Z, Wang M, Zhong W, et al. The Effect of Layer-by-Layer Assembly Coating on the Proliferation and Differentiation of Neural Stem Cells. ACS Applied Materials & Interfaces 2015;7:3018-29.
[82] Lee GY, Kim J-H, Choi KY, Yoon HY, Kim K, Kwon IC, et al. Hyaluronic acid nanoparticles for active targeting atherosclerosis. Biomaterials 2015;53:341-8.
[83] Mohandas A, Anisha BS, Chennazhi KP, Jayakumar R. Chitosan–hyaluronic acid/VEGF loaded fibrin nanoparticles composite sponges for enhancing angiogenesis in wounds. Colloids and Surfaces B: Biointerfaces 2015;127:105-13.
[84] Parajó Y, d'Angelo I, Welle A, Garcia-Fuentes M, Alonso MJ. Hyaluronic acid/Chitosan nanoparticles as delivery vehicles for VEGF and PDGF-BB. Drug Delivery 2010;17:596-604.
[85] Choi GH, Lee HJ, Lee SC. Titanium-adhesive polymer nanoparticles as a surface-releasing system of dual osteogenic growth factors. Macromol Biosci 2014;14:496-507.
[86] Bian L, Zhai DY, Tous E, Rai R, Mauck RL, Burdick JA. Enhanced MSC chondrogenesis following delivery of TGF-beta3 from alginate microspheres within hyaluronic acid hydrogels in vitro and in vivo. Biomaterials 2011;32:6425-34.
[87] Lu H, Lv L, Dai Y, Wu G, Zhao H, Zhang F. Porous Chitosan Scaffolds with Embedded Hyaluronic Acid/Chitosan/Plasmid-DNA Nanoparticles Encoding TGF-β1 Induce DNA Controlled Release, Transfected Chondrocytes, and Promoted Cell Proliferation. PLoS ONE 2013;8:e69950.
[88] Chen F-m, Ma Z-w, Dong G-y, Wu Z-f. Composite glycidyl methacrylated dextran (Dex-GMA)/gelatin nanoparticles for localized protein delivery. Acta Pharmacologica Sinica 2009;30:485-93.
[89] Suarez S, Grover GN, Braden RL, Christman KL, Almutairi A. Tunable Protein Release from Acetalated Dextran Microparticles: A Platform for Delivery of Protein Therapeutics to the Heart Post-MI. Biomacromolecules 2013;14:3927-35.
[90] Xie J, Wang H, Wang Y, Ren F, Yi W, Zhao K, et al. Induction of Angiogenesis by Controlled Delivery of Vascular Endothelial Growth Factor Using Nanoparticles. Cardiovascular Therapeutics 2013;31:e12-e8.
[91] Zhao L, Zhang K, Bu W, Xu X, Jin H, Chang B, et al. Effective delivery of bone morphogenetic protein 2 gene using chitosan-polyethylenimine nanoparticle to promote bone formation. RSC Advances 2016;6:34081-9.
[92] Siegel RL, Miller KD, Jemal A. Cancer statistics, 2016. CA: A Cancer Journal for Clinicians 2016;66:7-30.

.

[93] Gomes B, Moreira I, Rocha S, Coelho M, Pereira MdC. Polysaccharide-Based Nanoparticles for Cancer Therapy. Journal of Nanopharmaceutics and Drug Delivery 2013;1:335-54.
[94] Choi KY, Chung H, Min KH, Yoon HY, Kim K, Park JH, et al. Self-assembled hyaluronic acid nanoparticles for active tumor targeting. Biomaterials 2010;31:106-14.
[95] Xu Z, Wang Y, Zhang L, Huang L. Nanoparticle-delivered transforming growth factor-beta siRNA enhances vaccination against advanced melanoma by modifying tumor microenvironment. ACS nano 2014;8:3636-45.
[96] Salva E, Kabasakal L, Eren F, Ozkan N, Cakalagaoglu F, Akbuga J. Local delivery of chitosan/VEGF siRNA nanoplexes reduces angiogenesis and growth of breast cancer in vivo. Nucleic acid therapeutics 2012;22:40-8.
[97] Zhao Q, Han B, Wang Z, Gao C, Peng C, Shen J. Hollow chitosan-alginate multilayer microcapsules as drug delivery vehicle: doxorubicin loading and in vitro and in vivo studies. Nanomedicine: Nanotechnology, Biology and Medicine 2007;3:63-74.
[98] Zhang C, Wang W, Liu T, Wu Y, Guo H, Wang P, et al. Doxorubicin-loaded glycyrrhetinic acid-modified alginate nanoparticles for liver tumor chemotherapy. Biomaterials 2012;33:2187-96.
[99] Guo H, Lai Q, Wang W, Wu Y, Zhang C, Liu Y, et al. Functional alginate nanoparticles for efficient intracellular release of doxorubicin and hepatoma carcinoma cell targeting therapy. International Journal of Pharmaceutics 2013;451:1-11.
[100] Ahn DG, Lee J, Park SY, Kwark YJ, Lee KY. Doxorubicin-loaded alginate-g-poly(N-isopropylacrylamide) micelles for cancer imaging and therapy. ACS Appl Mater Interfaces 2014;6:22069-77.
[101] Wang Y, Zhou J, Qiu L, Wang X, Chen L, Liu T, et al. Cisplatin–alginate conjugate liposomes for targeted delivery to EGFR-positive ovarian cancer cells. Biomaterials 2014;35:4297-309.
[102] Cafaggi S, Russo E, Stefani R, Leardi R, Caviglioli G, Parodi B, et al. Preparation and evaluation of nanoparticles made of chitosan or N-trimethyl chitosan and a cisplatin–alginate complex. Journal of Controlled Release 2007;121:110-23.
[103] Jeong YI, Kim ST, Jin SG, Ryu HH, Jin YH, Jung TY, et al. Cisplatin-incorporated hyaluronic acid nanoparticles based on ion-complex formation. Journal of pharmaceutical sciences 2008;97:1268-76.
[104] Bisht S, Maitra A. Dextran-doxorubicin/chitosan nanoparticles for solid tumor therapy. Wiley interdisciplinary reviews Nanomedicine and nanobiotechnology 2009;1:415-25.
[105] Ganesh S, Iyer AK, Gattacceca F, Morrissey DV, Amiji MM. In vivo biodistribution of siRNA and cisplatin administered using CD44-targeted hyaluronic acid nanoparticles. Journal of Controlled Release 2013;172:699-706.
[106] Zhang C, Wang W, Liu T, Wu Y, Guo H, Wang P, et al. Doxorubicin-loaded glycyrrhetinic acid-modified alginate nanoparticles for liver tumor chemotherapy. Biomaterials 2012;33:2187-96.
[107] Su H, Wu C, Zhu J, Miao T, Wang D, Xia C, et al. Rigid Mn(ii) chelate as efficient MRI contrast agent for vascular imaging. Dalton Transactions 2012;41:14480-3.
[108] Luo K, Tian J, Liu G, Sun J, Xia C, Tang H, et al. Self-assembly of SiO2/Gd-DTPA-polyethylenimine nanocomposites as magnetic resonance imaging probes. Journal of nanoscience and nanotechnology 2010;10:540-8.
[109] Miao T, Zhang Y, Zeng Y, Tian R, Liu G. Functional Nanoparticles for Molecular Imaging-Guided Gene Delivery and Therapy. In: Dai Z, editor. Advances in Nanotheranostics II: Cancer Theranostic Nanomedicine. Singapore: Springer Singapore; 2016. p. 273-305.

.

[110] Liu G, Swierczewska M, Lee S, Chen X. FUNCTIONAL NANOPARTICLES FOR MOLECULAR IMAGING GUIDED GENE DELIVERY. Nano today 2010;5:524-39.
[111] Zheng J, Lin Z, Zhang L, Yang H. Polydopamine-mediated immobilization of phenylboronic acid on magnetic microspheres for selective enrichment of glycoproteins and glycopeptides. Science China Chemistry 2015;58:1056-64.
[112] Chan M, Lux J, Nishimura T, Akiyoshi K, Almutairi A. Long-Lasting and Efficient Tumor Imaging Using a High Relaxivity Polysaccharide Nanogel Magnetic Resonance Imaging Contrast Agent. Biomacromolecules 2015;16:2964-71.
[113] Mokhtarzadeh A, Alibakhshi A, Yaghoobi H, Hashemi M, Hejazi M, Ramezani M. Recent advances on biocompatible and biodegradable nanoparticles as gene carriers. Expert Opinion on Biological Therapy 2016.
[114] Liu H, Zhang J, Chen X, Du X-S, Zhang J-L, Liu G, et al. Application of iron oxide nanoparticles in glioma imaging and therapy: from bench to bedside. Nanoscale 2016;8:7808-26.
[115] Thomas RG, Moon MJ, Lee H, Sasikala ARK, Kim CS, Park I-K, et al. Hyaluronic acid conjugated superparamagnetic iron oxide nanoparticle for cancer diagnosis and hyperthermia therapy. Carbohydrate Polymers 2015;131:439-46.
[116] Wang J, Mi P, Lin G, Wang YX, Liu G, Chen X. Imaging-guided delivery of RNAi for anticancer treatment. Adv Drug Deliv Rev 2016.
[117] Swierczewska M, Han HS, Kim K, Park JH, Lee S. Polysaccharide-based nanoparticles for theranostic nanomedicine. Advanced Drug Delivery Reviews 2016;99, Part A:70-84.
[118] Yoon HY, Kim HR, Saravanakumar G, Heo R, Chae SY, Um W, et al. Bioreducible hyaluronic acid conjugates as siRNA carrier for tumor targeting. Journal of Controlled Release 2013;172:653-61.
[119] Wawer AA, Harvey LJ, Dainty JR, Perez-Moral N, Sharp P, Fairweather-Tait SJ. Alginate inhibits iron absorption from ferrous gluconate in a randomized controlled trial and reduces iron uptake into Caco-2 cells. PLoS One 2014;9:e112144.
[120] Leung K. Ferumoxides. Molecular Imaging and Contrast Agent Database (MICAD). Bethesda (MD): National Center for Biotechnology Information (US); 2004.
[121] Leung K. Ferumoxtran. Molecular Imaging and Contrast Agent Database (MICAD). Bethesda (MD): National Center for Biotechnology Information (US); 2004.
[122] Bayes M, Rabasseda X, Prous J. Gateways to clinical trials. Methods and findings in experimental and clinical pharmacology 2007;29:697-735.
[123] Frey N, Linke A, Suselbeck T, Muller-Ehmsen J, Vermeersch P, Schoors D, et al. Intracoronary delivery of injectable bioabsorbable scaffold (IK-5001) to treat left ventricular remodeling after ST-elevation myocardial infarction: a first-in-man study. Circulation Cardiovascular interventions 2014;7:806-12.
[124] Pritchard MF, Powell LC, Menzies GE, Lewis PD, Hawkins K, Wright C, et al. A New Class of Safe Oligosaccharide Polymer Therapy To Modify the Mucus Barrier of Chronic Respiratory Disease. Molecular Pharmaceutics 2016;13:863-72.
[125] Pinnix C, Perkins GH, Strom EA, Tereffe W, Woodward W, Oh JL, et al. Topical Hyaluronic acid vs. Standard of Care for the Prevention of Radiation Dermatitis after Adjuvant Radiotherapy for Breast Cancer: Single-Blind Randomized Phase III Clinical Trial. International journal of radiation oncology, biology, physics 2012;83:1089-94.
[126] Sigsgaard T, Thorne PS, Schlünssen V, Bønløkke J, Riddervold IS, Hoppe KA, et al. The change in nasal inflammatory markers after intranasal challenges with particulate chitin and

.

lipopolysaccharide: a randomized, double-blind, placebo-controlled, crossover study with a positive control. International Forum of Allergy & Rhinology 2015;5:716-23.
[127] Topazio L, Miano R, Maurelli V, Gaziev G, Gacci M, Iacovelli V, et al. Could hyaluronic acid (HA) reduce Bacillus Calmette-Guerin (BCG) local side effects? Results of a pilot study. BMC urology 2014;14:64.

.

CHAPTER 2: OSTEOGENIC DIFFERENTIATIO OF HUMAN MESENCHYMAL STEM CELLS THROUGH ALGINATE-GRAFT-POLY(ETHYLENE GLYCOL) MICROSPHERE-MEDIATED INTRACELLULAR GROWTH FACTOR DELIVERY

The intracellular delivery of growth factors increases opportunities for controlling cell behavior and maintaining tissue homeostasis. Recently, VEGFA was reported to enhance osteogenic differentiation of mesenchymal stem cells (MSCs) through an intracrine mechanism, suggesting a new strategy to promote bone tissue formation in osteoporotic patients. The goal of this study was to design and fabricate ligand-conjugated alginate-graft-poly(ethylene glycol) microspheres for intracellular delivery and release of VEGFA in primary human MSCs to enhance osteogenic differentiation as a potential therapeutic. Three types of microspheres were synthesized and characterized by scanning electron microscopy, in vitro drug release kinetics, MSC uptake and internalization: alginate alone (Alg), alginate-graft-poly(ethylene glycol) (Alg-g-PEG) and alginategraft-poly(ethylene glycol)-S-S-arginine-glycine-aspartic acid (Alg-g-RGD). Each of the different microsphere formulations successfully transported bioactive VEGFA into primary human MSCs within 48 h of culture, and significantly enhanced osteogenic differentiation compared to control treatments with empty microspheres (intracellular control) or non-encapsulated VEGFA (extracellular control). Adipogenic differentiation was not affected by the presence of VEGFA intracellularly or extracellularly. These results demonstrating the internalization of

.

alginate-based microspheres and intracellular delivery of VEGFA support the efficacy of using this drug delivery and intracrine mechanism to control the fate of human MSCs and enhance osteogenic differentiation.

2.1. Introduction

Osteoporosis is defined by a reduction in the quantity and quality of bone that results in skeletal fragility [1]. As people age, bone resorption rates become unbalanced and bone resorption dominates over bone formation, which leads to reduced bone mass and altered bone architecture. Human bone marrow progenitor cells known as multipotent stromal cells or mesenchymal stem cells (MSCs) can differentiate into osteoblasts, chondrocytes and adipocytes and show promise for clinical bone repair [2]. A notable recent study with murine MSCs showed that intracellular as opposed to extracellular signaling of vascular endothelial growth factor A (VEGFA) had the ability to distinctly regulate MSC lineage commitment toward osteoblasts or adipocytes [3]. Liu *et al.* (2012) demonstrated that murine bone marrow stromal cells were more likely to differentiate into osteoblasts when MSC expressed VEGFA and possessed intracellular VEGFA, compared with no change in osteoblastic differentiation following exposure of MSCs to extracellular VEGFA. The investigators proposed that VEGFA regulated differentiation through an intracrine mechanism unique to the intracellular form of VEGFA and different from the typical mechanism for secreted, extracellular VEGFA and signaling through cell surface receptors. For patients, the

intracellular delivery of VEGFA into MSCs prior to cell therapy could be a potential approach to speed the repair of large or complex bone fractures or perhaps even to treat chronic skeletal diseases such as osteoporosis [4]. In this work, we developed and functionally tested a specialized drug delivery system designed to accomplish the controlled, intracellular delivery of VEGFA in MSCs.

Modern drug delivery systems are designed to maintain the structure and bioactivity of biomolecules and to release therapeutics in a controlled and predictable manner. Micro-encapsulation is one of the core technologies used in polymer drug delivery systems [5]. Polymeric particles or microspheres for controlled drug delivery applications are designed to provide uniform particle dimensions, shield the drug from the extracellular environment, and be biocompatible [6]. Alginate microspheres have attracted much attention for the development of controlled- and sustained-release drug delivery systems for proteins [7], cytokines [8] and cells [9, 10]. Alginate is a naturally occurring polysaccharide extracted from brown seaweed that is generally regarded as non-toxic. The fabrication of alginate microspheres is favorable for drug delivery due to the relatively mild yet rapid gelation process that omits the use of harsh chemicals to ensure stability of encapsulated biomolecules [11-14]. However, the application of alginate microspheres has been limited due to their relatively large diameters (10 – 100 μm) and rapid drug-release rates (< 24 h) [15]. In addition, the anionic nature of alginate interferes with the encapsulation and release of charged molecules such as polyelectrolytes. To overcome these limitations, alginate microspheres have been

refined by varying molecular weight and concentration, stirring conditions, degree of crosslinking, and chemical modification of the alginate polymer to achieve sustained drug release [16, 17].

Poly(ethylene glycol) (PEG) is the most widely applied synthetic polymer in the emerging field of biomaterials for drug delivery. Recently, alginate has been modified with PEG for the fabrication of microcapsule coatings [18], mucoadhesive polymers [19, 20], self-assembling nanospheres [21, 22] and hybrid microspheres [23, 24]. The ability of PEG to influence the pharmacokinetic properties of drugs and drug carriers has been used to modify many different pharmaceutical compounds and components [25]. Biocompatibility and stealth behavior make PEG an ideal material to avoid opsonization and subsequent elimination by the reticuloendothelial system [26]. In addition, PEG-modified products are less immunogenic and antigenic; hemolysis and aggregation of erythrocytes may also decrease, as can the risk of embolism. However, the lack of a cell adhesion ligand limits its application in targeted drug delivery systems. To address this issue, we developed novel PEG-modified alginate copolymer microspheres with and without the surface conjugation of a bioactive cell adhesion ligand.

Proteins containing tri-peptide arginine-glycine-aspartate (RGD) attachment sites, along with the integrins serving as receptors for them, constitute a major recognition system for cell adhesion to the extracellular matrix (ECM) [27]. Consequently, researchers continue to utilize RGD in order to mimic cell adhesion

proteins and bind to integrins [28], inhibit apoptosis, angiogenesis, and tumor formation [29], coat surfaces for use as biomaterials [30], and enhance drug delivery systems [31, 32], including microspheres [33]. In this study RGD was utilized as a model cell-recognition molecule to demonstrate the efficacy of immobilizing ligands onto microsphere surfaces. Our results demonstrate that the incorporation of an adhesion ligand onto the surface of alginate-graft-PEG (Alg-g-PEG) microspheres containing VEGFA provides a promising strategy to regulate osteoprogenitor cell differentiation and bone tissue homeostasis, in addition to providing efficacy for the use of surface ligands for cell-targeted therapeutic applications *in vivo*.

2.2 Materials and Methods

2.2.1. Materials

Sodium alginate (M_W = 65–75 kg/mol, 60-70% guluronic acid residues) was generously donated by FMC BioPolymer. Cysteine-L-arginyl-glycyl-L-aspartic acid (CRGD) was purchased from Genscript. Amine-poly(ethylene glycol)-thiol (NH_2-PEG-SH, M_W = 1000 g/mol) and methyl-poly(ethylene glycol)-amine (mPEG-NH_2, M_w = 500 g/mol) were purchased from Laysan Bio. N-ethyl-N'(3-dimethylaminopropyl) carbodiimide hydrochloric acid (EDC), N-hydroxysuccinimide (NHS), 2,2'-dithiodipyridine, methanol (MeOH, anhydrous, 99.8%), biology-grade mineral oil, Span 80, Tween 80, ethylenediaminetetraacetic acid (EDTA), dexamethasone, ascorbic acid, β-glycerol phosphate, hydrocortisone, isobutylmethylxanthine, indomethacin,

deuterium oxide (D_2O), the *In Vitro* Toxicology Assay Kit (MTT-based), Hoechst 33342 and Alizarin red were purchased from Sigma-Aldrich. One molar hydrochloric acid (HCl) and 1 M sodium hydroxide were purchased from BDH ARISTAR®PLUS. Dichloromethane (DCM, 99.9%), sodium citrate, isopropanol, sodium chloride (NaCl), sodium acetate (NaAc), alpha-modified eagle medium (α-MEM, Hyclone), DyLight 550 Microscale Antibody Labeling Kit, and 20X phosphate buffered saline (PBS) were purchased from Fisher Scientific. Penicillin, streptomycin and Trypsin EDTA were purchased from Corning Cellgro. AdipoRed™ was purchased from Lonza Inc. Human VEGF DuoSet ELISA Kit was purchased from R&D Systems. Fetal bovine serum (FBS) was purchased from Atlanta Biologics and screened for a lot that best supported growth of human MSCs. Green fluorescent protein (GFP)-labeled human MSCs were generated by lentiviral transduction for stable integration of the gene and enriched by selecting for GFP-positive cells by fluorescence activated cell sorting (FACS).

2.2.2. Alg-g-PEG-S-S-Pyridine Copolymer Synthesis

First, NH_2-PEG-SH (0.1 mg, 0.1 mM) was dissolved in 5 mL of de-gassed acetate buffer (0.1 N sodium acetate adjusted to pH 4.6 with acetic acid, 0.3 M sodium chloride, and 1 mM EDTA) into which a solution of 2,2'-dithiodipyridine (88.124 mg, 0.4 mM) dissolved in 10 mL of MeOH was added; the mixture was stirred at room temperature under a flowing N_2 atmosphere for 4 h. The MeOH was extracted three times with DCM and the sample was prepared for ^{1}H-NMR analysis [34].

Alginate was modified with the newly formed NH_2-PEG-S-S-pyridine using EDC and NHS chemistry. The COOH:EDC:NHS molar ratio remained consistent at 1:8:3.2 during the carbodiimide reactions, where COOH refers to the moles of alginate carboxyl groups. A 1% (w/v) alginate solution was adjusted to pH 5 with 1 N HCl. EDC was then added followed by NHS and the solution was mixed at room temperature for 30 min. NH_2-PEG-S-S-pyridine and mPEG-NH_2 (the control PEG graft chain) were added to separate alginate solutions, respectively; the target degrees of PEG modification of the alginate was 10 %. After 12 h of reacting at room temperature, the various alginate and PEG polymer solutions were placed into dialysis cassettes (MWCO 20 kDa, Pierce Biotechnology) and dialyzed against deionized (DI) water for 4 d; dialysis solution was changed every 12 h. The Alg-g-PEG-S-S-pyridine copolymer product was lyophilized and the powder was stored in a desiccator until use. PEG retention post-fabrication was verified using ^{13}C-NMR (Bruker AVANCE III 500 MHz high-field NMR spectrometer) in D_2O [34]. As a control, Alg-g-PEG copolymers were synthesized with this approach using mPEG-NH_2. The polymer was dissolved in D_2O and the result was verified via ^{1}H-NMR (Bruker AVANCE III 500 MHz high-field NMR spectrometer).

2.2.3. Microsphere Fabrication

To fabricate microspheres containing VEGFA, Alg-g-PEG-S-S-pyridine was dissolved in phosphate buffered saline (PBS) with pH pre-adjusted to 5.0 with 1 N HCl.

Non-modified alginate (Alg) and Alg-g-PEG microspheres were fabricated using a 1% (w/v) polymer solution. VEGFA was added to the copolymer solution at a ratio of 10^6:1 (copolymer:VEGFA). Microspheres without VEGFA were fabricated as blank controls. One mL of polymer/VEGFA solution was slowly added to 6.72 mL of biological-grade mineral oil containing 5% (v/v) Spam 80 while mixing at 1200 rpm for 5 min at room temperature. Next, 400 µL of 30% (v/v) Tween 80 was added and the emulsion was mixed for an additional 5 min. Then, 5 mL of 1 M calcium chloride ($CaCl_2$) solution was added slowly. After 30 min of mixing, 3 mL of isopropanol was added to the emulsion and allowed to mix for 5 min, then was centrifuged at 400 rpm for 5 min to precipitate microspheres. The microspheres were washed sequentially with isopropanol (x2) and DI water (x2), respectively, and centrifuged after each wash. The Alg-g-PEG-S-S-pyridine microspheres were formed in a similar fashion, however, the DI water wash was replaced with a 1% (w/v) CRGD solution (x2); the corresponding microspheres are here-after identified as Alg-g-RGD. Microspheres were flash frozen in liquid N_2.

After lyophilization Alg, Alg-g-PEG and Alg-g-RGD microspheres were characterized by scanning electronic microscopy (SEM, JEOL 600; samples were sputter coated with 45 nm of gold). SEM micrographs of various magnifications were used to quantify microsphere diameters; images were analyzed using ImageJ (3 images per group).

2.2.4. Cytotoxicity Assay

Human MSCs were isolated from bone marrow aspirates with an IRB-approved protocol. Human MSCs (passage 7) were seeded in 24 well tissue culture polystyrene (TCPS) plates at a density of 20,000 cells/well in 500 µL/well of standard MSC growth medium (α-MEM, 10% fetal bovine serum (FBS), 100 U/mL penicillin, 100 µg/mL streptomycin) and allowed to adhere for 24 h. Cells were incubated in the presence of Alg, Alg-g-PEG, and Alg-g-RGD microspheres encapsulating VEGFA (n = 3 per group) at concentrations of 10, 50, 100, 500 µg/mL at 37°C and 5% CO_2. After 24 h of incubation, medium containing the microspheres was removed, and cells were rinsed two times in sterile PBS then analyzed using a MTT-based *In Vitro* Toxicology Assay Kit following the manufacturer's protocol. The optical density was measured at 570 nm using a BioTek plate reader. Background absorbance at 690 nm was subtracted from the measured absorbance. Absorbance values for the experimental and control samples were normalized to non-modified TCPS controls [35].

2.2.5. Dylight 550 Labeling of Human VEGFA

Recombinant human VEGFA was cloned, expressed in HEK 293 cells, and purified in the Spees laboratory [36]. 1 mg/mL of purified VEGFA in PBS was used for labeling. The DyLight Microscale Antibody Labeling Kit was used according to the manufacturer's instructions. Briefly, 100 µL of 1 mg/mL protein was mixed with a commercial vial of DyLight 550 reagent and incubated for 60 min in the dark after

gentle vortexing and a quick centrifugation step to mix the sample and dye. Spin columns provided by the kit were then placed into microfuge collection tubes and used for purification of protein from unbound dye. The labeling solution was mixed with purification resin and centrifuged in the spin column to purify labeled protein. The dye: protein ratio was determined based on methods described in the labeling kit.

2.2.6. VEGFA Encapsulation and Release

A known amount of lyophilized VEGFA-loaded Alg, Alg-g-PEG and Alg-g-RGD microspheres was dissolved by immersion in 3% (w/v) sodium citrate solution to dissolve the microspheres by displacing calcium ions [37]. The VEGFA concentration was measured with a DuoSet ELISA Development Kit. Briefly, standard series and sample solutions were added to a culture plate (100 µL/well) pre-coated with capture antibody after washing in mild detergent (0.05% Tween 20 in PBS). After 2 h of blocking and incubation at room temperature, the biotin-conjugated detection antibody was added and incubated for another 2 h. Then 100 µL poly HRp conjugated streptavidin substrate was incubated in each well for 20 min after washing the detection antibody, followed by incubation with 100 µL substrate (ABTS, Thermo Scientific.) in the dark at room temperature. The absorbance was measured at 450 nm with a BioRad microplate reader. The VEGFA concentration was determined with a standard curve, and the VEGFA encapsulation efficiency (mass of VEGFA encapsulated in the microspheres / mass of VEGFA added when forming the microspheres) was calculated.

A VEGFA release test was performed in a 48 well plate at 37°C. Six mg lyophilized VEGFA-loaded Alg, Alg-g-PEG and Alg-g-RGD microspheres was dissolved in 500 µL of PBS (pH 7.4). At each time point (1, 2, 4, 8, 12, and 24 h, followed by collection each day for a total of 14 d) 100 µL of the PBS was removed and another 100 µL was added to maintain the total volume. The released VEGFA concentration was determined with the DuoSet ELISA Development Kit as above.

2.2.7. Human Mesenchymal Stem Cells Intracellular Delivery

DyLight 550-labeled VEGFA (red fluorescence) was incorporated within Alg, Alg-g-PEG and Alg-g-RGD microspheres using the same above approach except the ratio of polymer to VEGFA was increased from 10^6:1 to 10^5:1 to increase the intensity of the visualized signal. Microspheres (500 µg/mL) were cultured with GFP-labeled human MSCs (100,000 cells, passage 4, green fluorescence) for 24 h in glass bottom culture dishes pre-coated with poly-d-lysine (MatTek Corporation). Confocal laser scanning (CLS) microscopy (Zeiss LSM 510 META) was used to visualize the microspheres by detecting directly through the plate. Z-stack images were formed with the use of AimImage Software.

2.2.8. Human Mesenchymal Stem Cells Differentiation Assay

Human MSCs (passage 4) were seeded in 12 well TCPS plates at a seeding density of 50,000 cells/well. Cells were cultured at 37°C and 5% CO_2 in standard MSC

growth medium containing 100 μg/mL of VEGFA-encapsulated microspheres (Alg, Alg-g-PEG or Alg-g-RGD) or pure microspheres not containing VEGFA. The experiments were done in triplicate. After 48 h, old medium was aspirated off and one plate was given osteogenic differentiation medium (growth medium including dexamethasone, ascorbic acid, β-glycerol phosphate) and the other plate received adipogenic differentiation medium (growth medium including hydrocortisone, isobutylmethylxanthine, indomethacine). Cells that served as controls were cultured without the addition of microspheres (either with VEGFA or without VEGFA). Differentiation medium was changed every 3 d. After 14 d of culture in differentiation medium, cells were rinsed with sterile PBS and analyzed via an Alizarin Red osteogenic differentiation assay [38, 39] or an AdipoRed™ adipogenesis assay (Sigma). In addition, six different concentrations of VEGFA ranging from 0 to 20 ng/ml (0, 0.01, 0.025, 0.05, 0.5, 20 ng/ml) were incubated with human MSCs for the control assay (extracellular VEGFA). The extracellular VEGFA differentiation experiment was conducted in 24 well TCPS plates with a seeding density of 30,000 cells/well. After 48 h, medium containing VEGFA was aspirated off and the plates were given either osteogenic or adipogenic differentiation medium. Differentiation medium was changed every 3 d. After 7 d of culture in differentiation medium, cells were rinsed with sterile PBS and analyzed via an Alizarin Red osteogenic differentiation assay [38, 39] or an AdipoRed™ adipogenic differentiation assay (Sigma).

2.2.9. Statistical Methods

All experiments were performed in triplicate; results are reported as mean ± standard deviation. Statistical analysis was performed using one-way ANOVA with Tukey multiple comparisons ($\alpha = 0.05$) via the SAS statistics program in the GLM procedure as the post-test to compare all of the groups. A $p < 0.05$ is considered significantly different.

2.3 Results

2.3.1. Synthesis of Alg-g-PEG and Alg-g-PEG-pyridine Copolymers

The copolymer reactions for the chemical modification of alginate are shown in **Figure 2-1**. To synthesize Alg-g-PEG-pyridine, the oligomer NH_2-PEG-S-S-pyridine was synthesized first. ^{1}H-NMR spectral analysis confirmed the presence of both PEG and pyridine in the final product (7.1 ppm, 7.5 ppm, 7.7 ppm, 7.9 ppm corresponding to the hydrogen on pyridine ring and 3.6 ppm corresponding to the hydrogen within the repeat group in PEG) when compared to the alginate and PEG controls (**Figure 2-7**). The large peak at 1.8 ppm corresponds to the excess acetate in the reaction system; this by-product does not interfere with the carbodiimide chemistry and can be removed through dialysis in the proceeding step of the copolymer reaction. Quantification of the reaction yield by peak integration determined approximately 70% reaction efficiency.

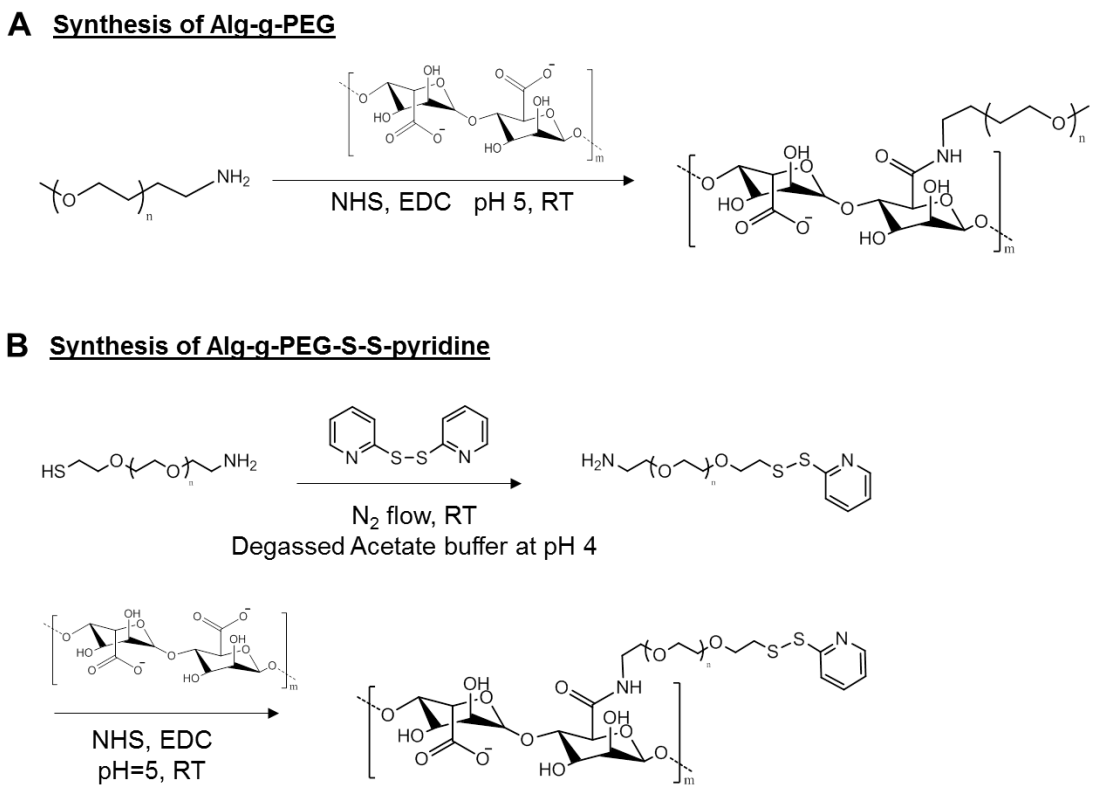

Figure 2-1. Chemical modification of alginate (Alg) with two different poly(ethylene glycol) (PEG) oligomers with methyl and pyridine end groups, respectively. The synthesis of Alg-g-PEG was conducted using carbodiimide chemistry at pH 5 and room temperature. To synthesize Alg-g-PEG–S-S-Pyridine, NH2-PEG-SH was reacted with 2,2'-dithiodipyridine in degassed acetate buffer at pH 4 and room temperature under N2 flow. Next, the modified NH2-PEG-pyridine was conjugated to alginate using carbodiimide chemistry.

The natural polysaccharide alginate was grafted with a short chain PEG decorated with either pyridine or methyl end groups resulting in the copolymers Alg-g-

.

PEG or Alg-g-PEG-pyridine. For the synthesis of Alg-g-PEG, ^{1}H-NMR spectral analysis confirmed the presence of both alginate and PEG functional groups in the final purified graft copolymers through the appearance of new peaks and peak shifts in the Alg-g-PEG spectrum (**Figure 2-8**); 3.36 ppm corresponds to the -CH_3 moiety of the PEG side chain and 4.31 ppm corresponds to the shift of hydrogen atoms due to the grafting of the PEG side chain when compared to the alginate and PEG controls. As stated in the methods, the theoretical degree of PEG modification was 10 molar % of alginate backbone. Quantification of PEG conjugation by peak integration of the ^{1}H-NMR spectra was not successful due to extensive broadening and overlapping of peaks corresponding to alginate in the Alg-g-PEG spectra. The synthesis of Alg-g-PEG-pyridine was confirmed by ^{13}C-NMR (**Figure 2-9**); 132.31 ppm, 136.05 ppm, 141.37 ppm, 143.53 ppm, 149.24 ppm correspond to carbon on the pyridine ring, 69.76 ppm corresponds to the carbon within the repeat unit of PEG, and 42.84 ppm corresponds to the carbon on the alginate. Verification of NH_2-PEG-S-S-pyridine by ^{13}C-NMR confirmed that the reaction was successful.

2.3.2. Fabrication of Alg, Alg-g-PEG and Alg-g-RGD Microspheres

Complete microsphere fabrication strategies are shown in **Fig. 2**. Alg, Alg-g-PEG and Alg-g-RGD microspheres were designed to encapsulate VEGFA without interfering with the bioactivity and electrostatically-condensed structure of VEGFA. The mild gelation method by the addition of $CaCl_2$ during an emulsion was successful

in creating microspheres encapsulating VEGFA. The surface functionalization of microspheres through CRGD conjugation did not appear to affect the shape or yield of the microspheres. SEM photomicrographs demonstrate that the microspheres (Alg, Alg-g-PEG and Alg-g-RGD) were spherical in shape with an average diameters and standard deviations of approximately 1.9 ± 1.0 µm, 0.5 ± 0.1 µm, and 1.1 ± 0.4 µm, respectively (**Figure 2-2**).

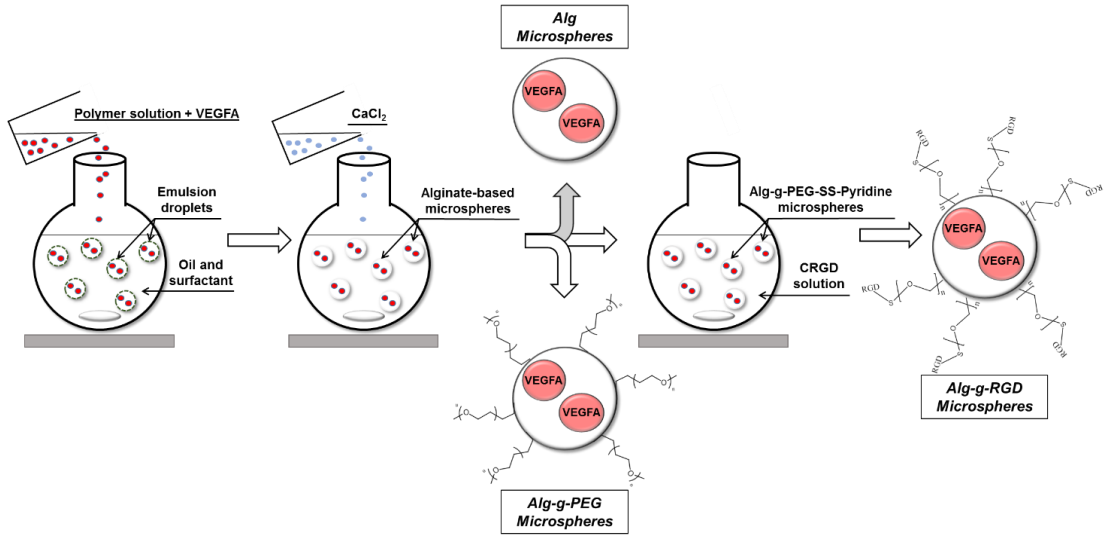

Figure 2-2. Schematic representation of microsphere fabrication techniques. Microspheres with or without VEGFA were prepared by premixing alginate or alginate-based copolymer solutions with VEGFA and creating a water/oil emulsion at room temperature in the presence of 1M calcium chloride. An additional surface modification step was performed on Alg-g-PEG-S-S-Pyridine microspheres to chemically conjugate CRGD via disulfide bonds. For Alg-g-RGD microspheres, the conjugation of 2,2'-dithiodipyridine was used to exchange the thiol group on the cysteine-RGD (CRGD) after

.

microsphere fabrication.

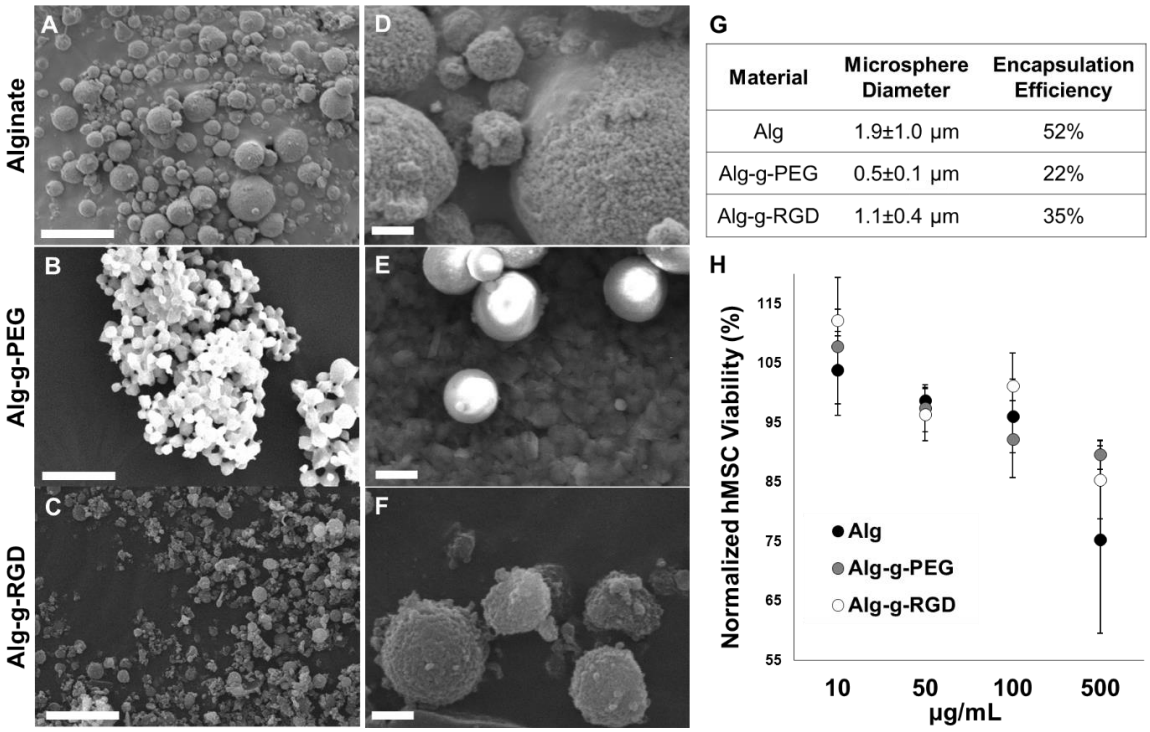

Figure 2-3. The shape, average diameter, VEGFA encapsulation efficiency and cytotoxicity of alginate-based microspheres were verified using scanning electron microscopy (SEM), an ELISA assay (n = 3), and an MTT-based In Vitro Toxicology assay. SEM micrographs representing (A, D) Alg, (B, E) Alg-g-PEG, and (C,F) Alg-g-RGD microspheres were fabricated without the addition of VEGFA through a water/oil emulsion; micrographs shown in A,B,C have a scale bar = 10 μm while micrographs in D,E,F have a scale bar = 10 μm. In preparation for imaging, microspheres were frozen by immersion in liquid N2 and subsequently lyophilized; samples were sputter-coated with 45 nm of Au-Pb. (G) Microsphere diameters were determined using ImageJ analysis on SEM micrographs. (H) The effect of microsphere concentration (10, 50, 100, and 500

.

μg/mL) on primary human MSC viability after 24 h culture in standard MSC growth medium at 37°C and 5% CO2 was determined. Experimental groups were normalized to non-modified confluent human MSCs cultured on tissue culture polystyrene.

2.3.3. Alg-g-PEG Microspheres Exhibit no Cytotoxic Effects

The viability of human MSCs in the presence of Alg, Alg-g-PEG and Alg-g-RGD microspheres containing no VEGFA was determined at increasing concentrations (10, 50, 100 and 500 μg/mL, **Fig. 3H**). These results demonstrated that Alg, Alg-g-PEG and Alg-g-RGD microspheres were non-toxic (cell viability > 90%) at concentrations up to 100 μg/mL. and cell viability > 75% at a concentration as high as 500 μg/mL. RGD-modified and PEG-modified alginate microspheres showed increased viability in higher concentrations compared to Alg microspheres.

2.3.4. VEGFA Encapsulation and Release Rates

VEGFA release rates from Alg, Alg-g-PEG and Alg-g-RGD microspheres are shown in **Fig. 4**. VEGFA encapsulation efficiency values were 52, 22 and 35% respectively for the different microsphere groups (see **Fig. 3G**). All of the microsphere groups sustained VEGFA release for 14 d; almost 100% of the encapsulated VEGFA was released within the 14 d sudy. Alg-g-RGD microspheres released more drug overall when compared to the other microsphere groups (shown in **Fig. 4A**). More importantly, within the first 72 h the VEGFA release profile demonstrated that the microspheres released a substantial amount correlating to the 48 h incubation time used

.

during for the differentiation assays. Alg and Alg-g-RGD microspheres released nearly twice that of Alg-g-PEG microspheres (shown in **Fig. 4B**). When comparing the 72 h release profile with the longer 14 d release profile, it is evident that a burst release within the first 12 h was followed by a gradual sustained release until the termination of the study.

.

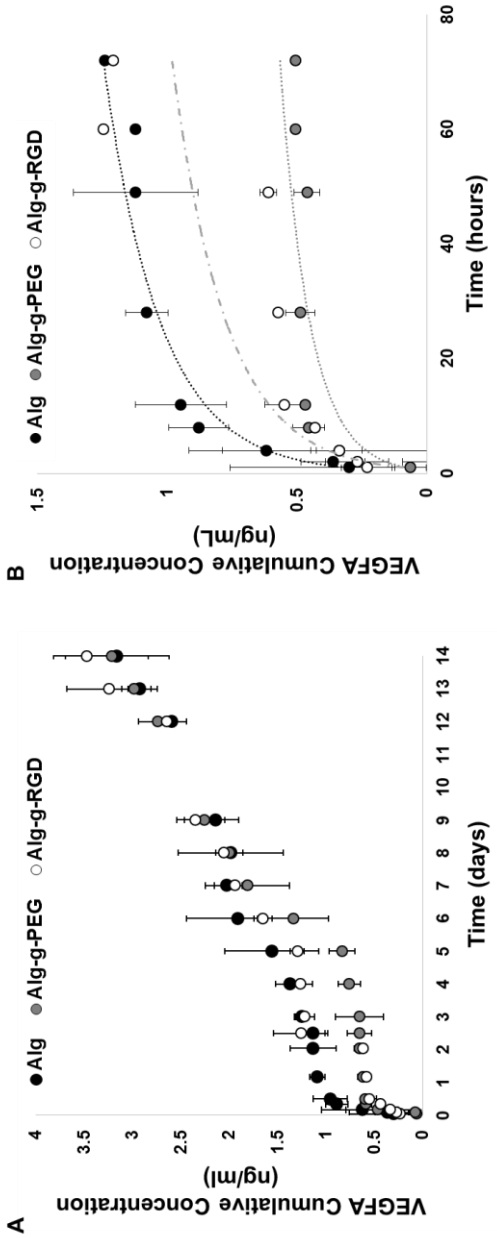

Figure 2-4. Quantitative release of VEGFA was calculated using the encapsulation efficiencies of each sample group and the VEGFA concentration after each time point. Sample aliquots were collected and VEGFA concentration was determined using an ELISA assay (n = 3). (A) Cumulative VEGFA release (ng/mL) from alginate-based

.

microspheres in phosphate buffered saline at pH 7.4 and 37°C over a sampling period of 14 days and (B) 72 hours was determined.

2.3.5. Microsphere Internalization

Internalized Alg, Alg-g-PEG and Alg-g-RGD microspheres encapsulated with DyLight 550 (red fluorescent) labeled VEGFA was verified after examination of CLS micrographs. GFP human MSCs (green) were successfully delivered DyLight-labeled VEGFA (red) using the Alg, Alg-g-PEG and Alg-g-RGD microsphere delivery systems (**Figure 2-5**). The red microspheres were spread throughout the cytoplasm and appeared to surround the nucleus. The intensity of red is a qualitative visualization of microsphere internalization rather than a quantitative measurement.

.

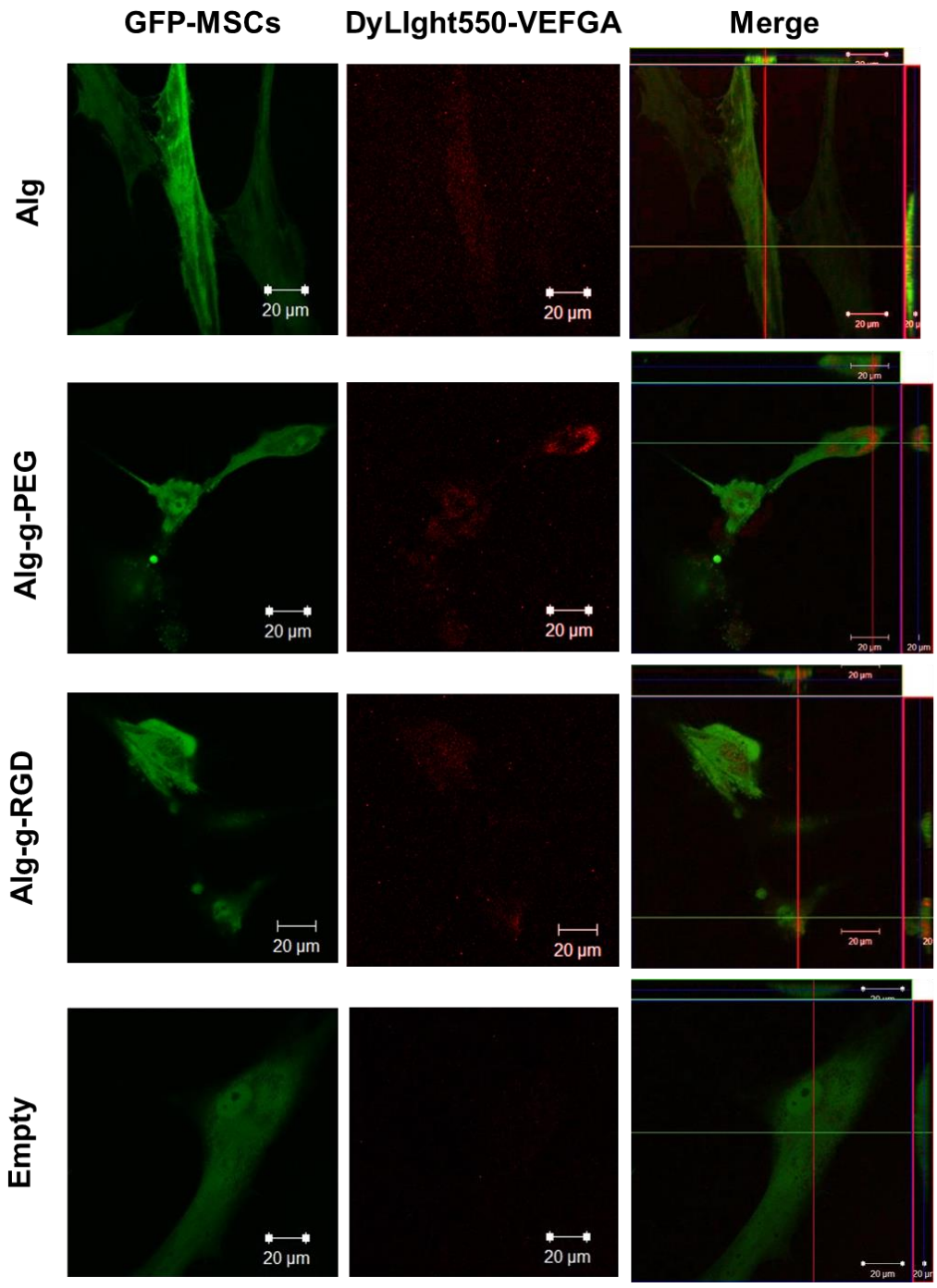

Figure 2-5. Confocal light microscopy images of GFP-labeled human MSCs (green) after 24 h of culture with DyLight 550 labeled-VEGFA-encapsulated alginate-based

microspheres (red) at a concentration of 500 µg/mL in standard MSC growth medium. The Alg, Alg-g-PEG and Alg-g-RGD images all verify the internalization of microspheres, especially compared to the non-modified empty Alg microsphere control. The red intensity is a qualitative visualization of microspheres internalization rather than a quantitative measurement.

2.3.6. Human MSC Differentiation

The UV absorbance of Alizarin red and fluorescent AdipoRed™ assays were used to quantify the osteogenic and adipogenic differentiation of human MSCs, respectively. The extent of differentiation was normalized to cell number by measuring the fluorescence intensity of Hoechst nuclear staining. As shown in **Figure 2-6**, incubation of human MSCs with microspheres containing VEGFA resulted in a significant increase in osteogenic differentiation when compared with non-modified TCPS controls. Statistical analysis of the data indicated a significant difference ($p < 0.04$) between the experimental groups (Alg, Alg-g-PEG and Alg-g-RGD) and the control group (cells cultured without the addition of VEGFA-encapsulated microspheres). The p-values for Alg, Alg-g-PEG and Alg-g-RGD microsphere groups compared to the control group were 0.0001, 0.0005 and 0.0330, respectively. For the adipogenesis differentiation assay, the Alg microsphere group showed a significant enhancement compared to the control group ($p = 0.02$). For the other two groups (Alg-g-PEG and Alg-g-RGD), there were no significant differences for the adipogenesis

assay with p-value of 0.28 and 0.57 respectively (**Figure 2-6**). The empty microspheres and pure VEGFA experimental groups did not exhibit any trends or significant differences for either adipogenic or osteogenic differentiation ($p > 0.06$) as shown in **Figure 2-6**. The significant differences between the experimental and control groups demonstrate that the VEGFA-encapsulated microspheres (Alg, Alg-g-PEG, Alg-g-RGD) were internalized by hMSCs and that VEGFA was delivered intracellularly, resulting in a functional output (osteogenic differentiation).

.

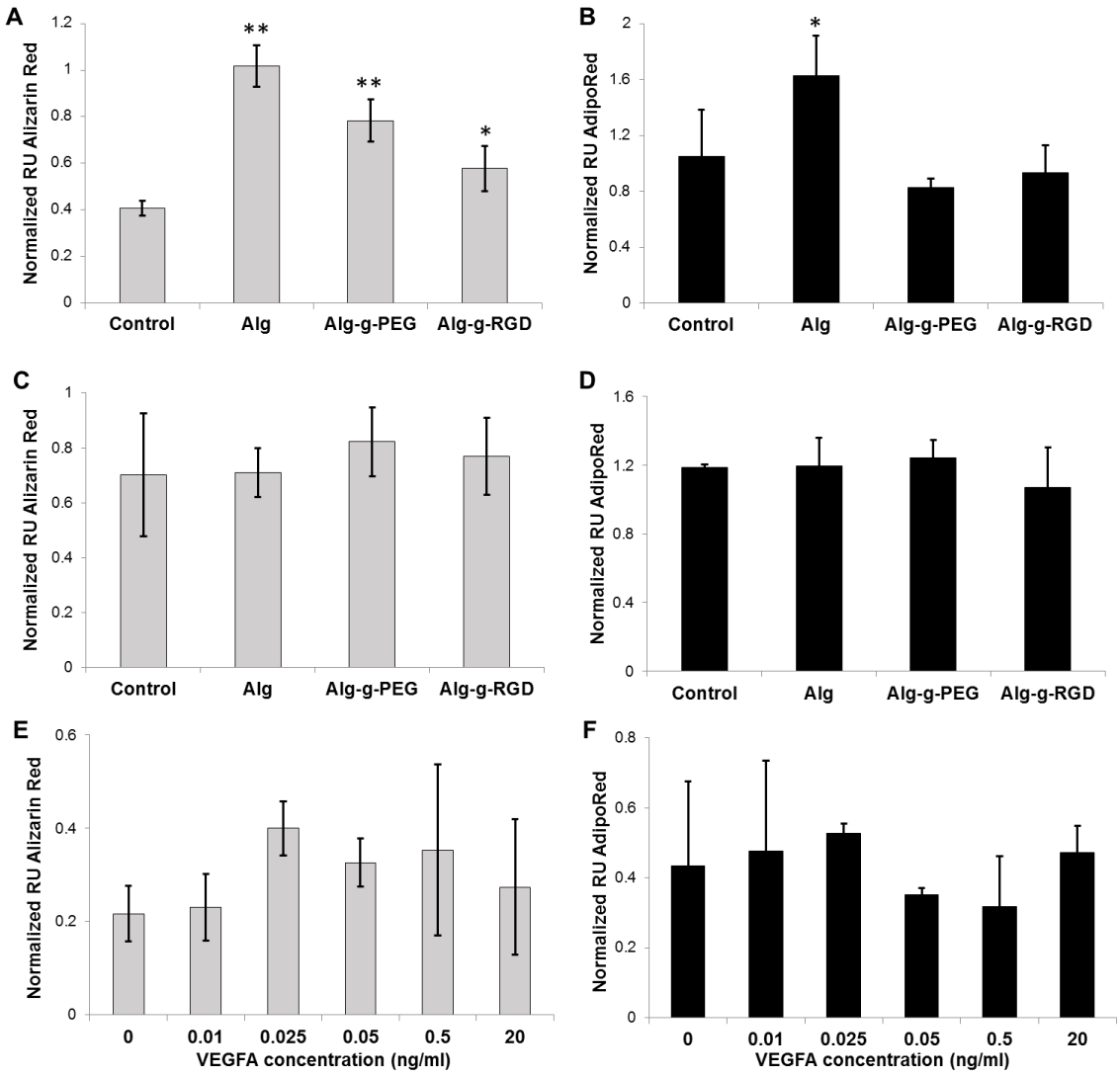

Figure 2-6. *In vitro* osteogenic (gray) and adipogenic (black) differentiation assay results of human MSCs after 14 days in culture with differentiation growth medium. (A) and (B) represent the VEGFA-encapsulated microspheres, (C) and (D) represent empty microspheres, and (E) and (F) represent extracellular delivery of pure VEGFA at different concentrations ranging from 0 to 20 ng/ml. A turkey statistical test was performed to compare the experimental groups to the control groups (n = 3). ** shows

a significant p-value less than 0.0005 and * shows p-value less than 0.04. For the control group, only standard MSC growth medium was added. The graphs illustrate a significant difference between VEGFA encapsulated Alg, Alg-g-PEG and Alg-g-RGD microsphere groups compared to the control group in the osteogenesis assay as well as for the VEGFA encapsulated Alg microsphere group in the adipogenesis group. No significant differences were seen ($p \leq 0.05$) between control and experimental groups for the osteogenesis and adipogenesis assays when empty microspheres were used or VEGFA was delivered extracellularly.

2.4. Discussion

There is a growing demand for injectable acellular therapeutics for the enhanced mineralization of osteoporotic bone. This study provides the first evidence that Alg, Alg-g-PEG and Alg-g-RGD microspheres, fabricated from graft copolymers of alginate and amine-terminated PEG or alginate and pyridine-conjugated PEG, may be used for the controlled intracellular delivery of VEGFA into living human stem/progenitor cells for enhanced osteogenic differentiation. Through the use of a biodegradable natural polymer, mild gelation methods, chemical conjugation of PEG, and immobilization of the adhesion ligand RGD, the applicability of controlled drug delivery by means of microspheres increases. The Alg, Alg-g-PEG and Alg-g-RGD microspheres were uniform in shape, of a moderate size to allow for internalization into human MSCs, and proved adaptable to surface-modification [34, 35]. The fabrication was easy to perform

and translate to engineering applications compared to other approaches which require higher spinning speeds and double emulsion processes.

VEGFA release from alginate-based microspheres was sustained over a period of 14 d, which is promising for targeted intracellular delivery. However, the main interest of this paper was the intracellular delivery of VEGFA into human MSCs, which took place over a shorter time-span of 48 h during culture. The non-selectivity of the microspheres in culture with MSCs allowed uptake to occur quickly, and this is also believed to be the case for the internalization of microspheres during the differentiation assay; the microsphere concentration and duration of co-culture were consistent among the internalization and differentiation studies. The short time frame allowed for delivery also suggests that the VEGFA content of the internalized microspheres was high enough to significantly affect human MSC differentiation. Indeed, alginate modification with bulky side groups can hinder drug diffusion; an effect that has been reported for Alg-g-PEG chains of moderate to high molecular weights [19]. Modification of alginate through PEG conjugation at the carboxyl groups decreases the electrostatic repulsion within the hydrogel, thus decreasing the degree of swelling and decreasing the rate of drug diffusion. The varying release kinetics with time suggest that the microsphere structure may be optimized further for controlled release applications [40].

Multiple uptake pathways have been targeted as a means of delivering material intracellularly, namely endocytosis, in the case of cationic nanoparticles [41] or for

larger micron-scale particles [42]. Due to the mild and quick gelation used to fabricate Alg, Alg-g-PEG and Alg-g-RGD microspheres, encapsulated drugs and proteins are better protected. Chemical conjugation of RGD onto PEG utilized disulfide bonds, which are covalent linkages arising from the oxidation of two sulfhydryl (SH) groups of cysteine connected to RGD (CRGD) and the SH terminal group on PEG (SH-PEG-NH_2). Disulfide bonds exist commonly in eukaryotic cell proteins with the function of fortifying the protein tertiary structure. Due to the reversibility and relative stability in plasma, the disulfide bond linkage becomes attractive in designing drug delivery systems. In addition, the physical properties and network structure of the calcium crosslinked alginate-based microspheres are readily changed after alterations in pH (such as in an endosome) or in the presence of calcium chelators. For the system described herein, it is hypothesized that the microspheres rapidly released VEGFA into the cytoplasm once inside the human MSCs [43, 44] due to the disassembly of the microspheres.

RGD is widely utilized in tissue engineering studies and has been used in studies with alginate [45, 46]. In the current study RGD was used a model ligand which may be replaced with more relevant cell-recognition molecules for targeting MSCs *in vivo*. However, RGD has been shown to increase uptake of surface modified DNA complexes for intracellular delivery [47]. Although a limitation of the current study was in the collection of qualitative internalization results, future work will investigate RGD modified microspheres for enhanced MSC uptake and it may be combined with other

cell-recognition motifs to control drug delivery for target cell populations. Results of the differentiation assays did not exhibit significant enhancement of the RGD or PEG modification between alginate microsphere groups in promoting osteoblast differentiation. Although Alg-g-PEG microspheres resulted in the highest Alizarin red absorbance, several reasons may account for this. The cells in the current study were only directed to differentiate for 14 d, meaning that the human MSCs cultured with Alg-g-RGD microspheres might still result in enhanced osteogenesis but more time is needed to demonstrate that result. Another possible explanation is RGD's influence on differentiation signaling. The research of Garcia *et al.* (2005) and Park *et al.* (2010) indicate a promotion effect of RGD in stem cell differentiation [33, 48]. In addition, it could also enhance chondrogenic differentiation [49]. However, other studies present findings in disagreement with the aforementioned work [50, 51]. The potential for Alg, Alg-g-PEG and Alg-g-RGD microspheres to deliver VEGFA intracellularly may be applied to investigate a wide array of differentiation lineages for MSCs and perhaps other progenitor cells.

Of special interest, our functional tests with VEGFA-bearing microspheres support an intracrine mechanism for VEGFA in human MSCs and are consistent with results reported by Liu *et al.* (2012) with retroviral expression of VEGFA in murine MSCs. We found that intracellular delivery of VEGFA via alginate-based microspheres resulted in up-regulated osteogenic differentiation by human MSCs, suggesting the effectiveness of our drug delivery system to control the intracrine mechanism that

balances osteoblast and adipocyte activity. Extracellular VEGFA did not alter differentiation of human MSCs. To carefully evaluate the function of intracellular VEGFA in regard to specificity for bone formation, we used adipogenesis as an alternative differentiation out-put. MSCs from osteoporotic bones exhibit a higher adipogenic capacity compared to healthy MSC donors, which is why adipogenic differentiation was chosen as the alternative lineage [52]. Except for the Alg microsphere group, in which adipogenesis by MSCs was enhanced, there was not a significant difference in adipogenesis for MSCs incubated with the VEGFA-encapsulated Alg-g-PEG and Alg-g-RGD microspheres. Based on the enhanced adipogenesis we observed in the VEGFA-encapsulated Alg microspheres group, Alg-g-PEG and Alg-g-RGD microspheres may be better suited for controlled intracellular delivery to enhance osteogenesis *in vivo*. The investigation of various cell-recognition molecules (*i.e.* ligands, antibodies, *etc.*) may provide a viable option for targeting a specific cell population *in vivo* for enhanced mineralization of osteoporotic bone.

2.5. Conclusion

This study is the first to report the fabrication and surface-functionalization of Alg, Alg-g-PEG and Alg-g-RGD microspheres for the encapsulation and intracellular delivery of a bioactive growth factor, VEGFA. Alg, Alg-g-PEG and Alg-g-RGD microspheres containing VEGFA promoted osteogenic differentiation of human MSCs upon intracellular delivery after 48 h of incubation time. These results provide

encouraging evidence for development of a systemic growth factor delivery system with potential to treat many debilitating diseases. Future work will involve manipulation of the surface ligand to enhance cell-targeted internalization of microspheres for intracellular growth factor delivery.

2.6. Supplemental Materials

NH_2-S-S-pyridine was verified via ^{1}H-NMR spectra (500 MHz, D_2O) as shown in **Figure 2-7**. The peaks within the range of 7-8 ppm confirmed the success of the chemistry. ^{1}H-NMR analysis of Alg-g-PEG was performed to verify the retention of PEG after the grafting reaction. Alg-g-PEG was synthesized using mPEG-NH_2 and sodium alginate via carbodiimide chemistry (**Figure 2-8**). ^{1}H-NMR spectra (500 MHz, D_2O) are shown, comparing the graft copolymer Alg-g-PEG to the homopolymer constituents: mPEG-NH_2 and sodium alginate. The inset image is the chemical structure of the Alg-g-PEG copolymer. The alginate conjugation onto NH_2-S-S-pyridine which forms the Alg-g-pyridine was confirmed by ^{13}C-NMR (500 MHz, D_2O) (**Figure 2-9**).

.

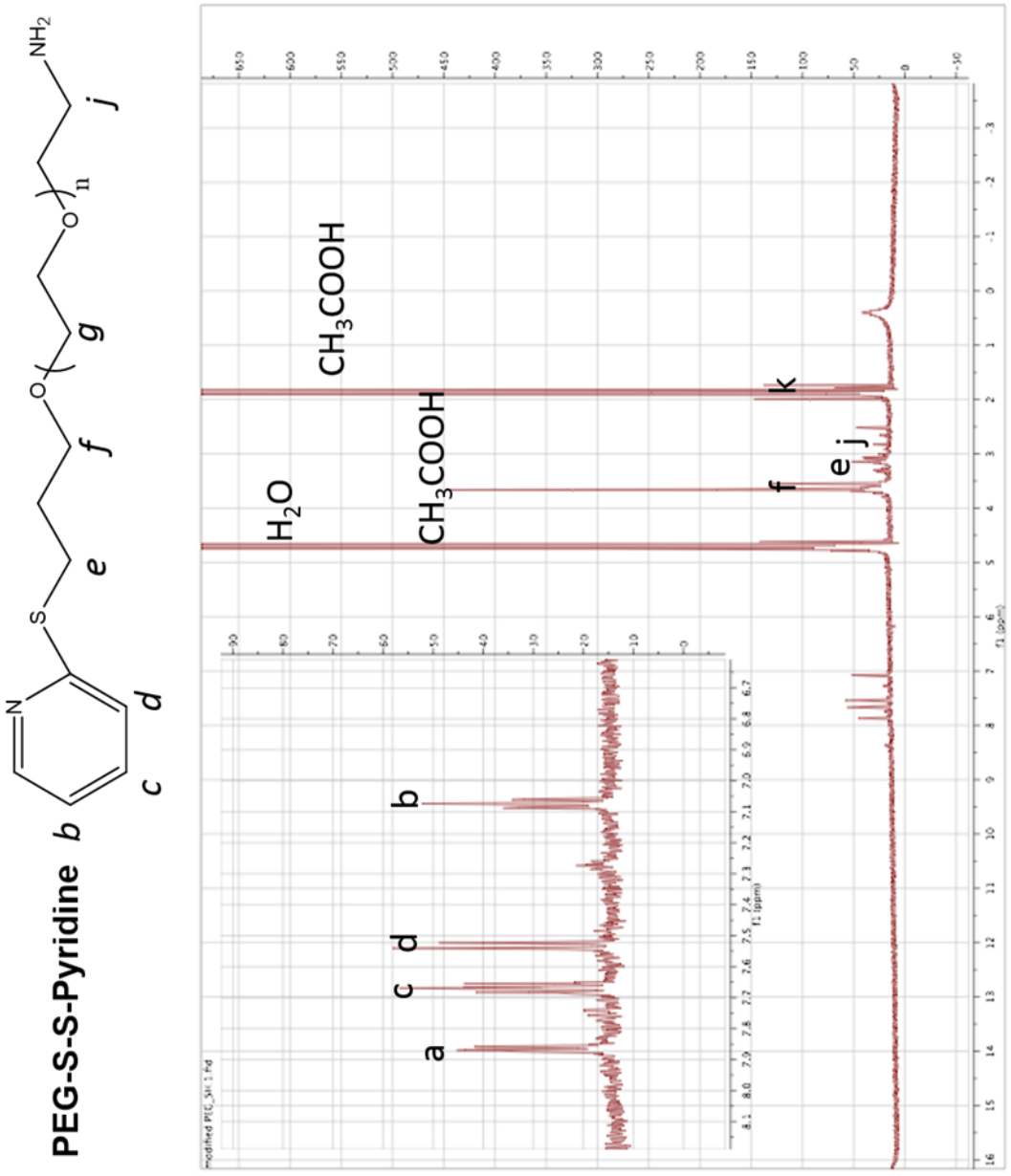

Figure 2-7. ^{1}H-NMR spectra of NH_2-PEG-S-S-pyridine copolymer. The fours peaks between 7-8 ppm, which is amplified on the left, indicated the successful conjugation of pyridine onto PEG. The H2O peak represents the solvent D_2O and the large peaks near 2 ppm and 3.7 ppm represent residual CH_3COOH in the reaction buffer.

.

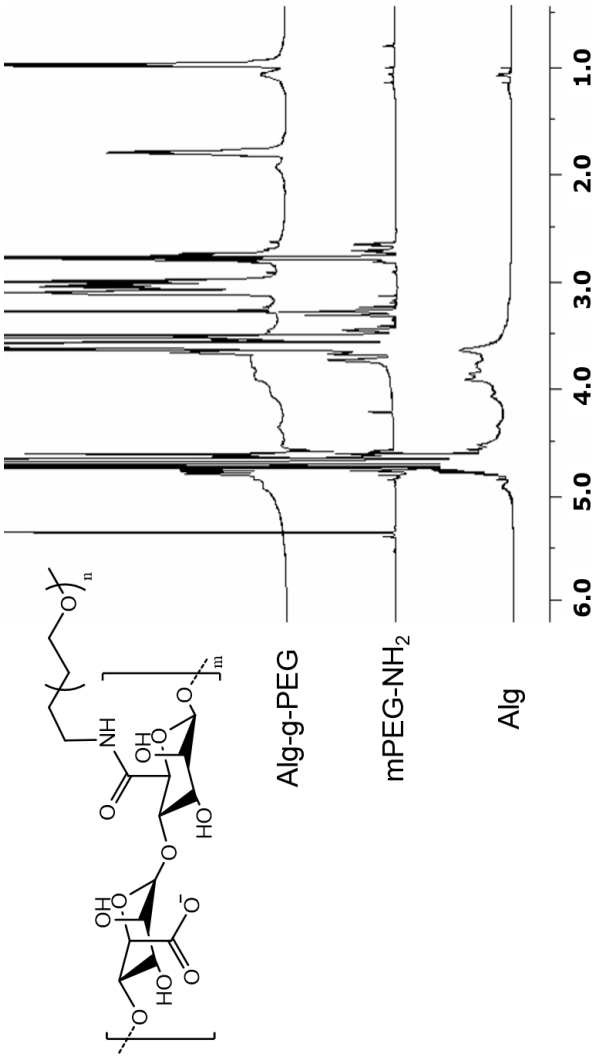

Figure 2-8. ^{1}H-NMR result of Alg-g-PEG copolymer synthesis. The peak of 3.36 ppm corresponds to the CH_3 moiety of the PEG side chain and 4.31 ppm corresponds to the shift of hydrogen atoms due to the grafting of the PEG side chain. Quantification of Alg-g-PEG conjugation by peak integration of the ^{1}H-NMR was not successful due to extensive broadening and overlapping of the peaks corresponding to the alginate in the Alg-g-PEG.

.

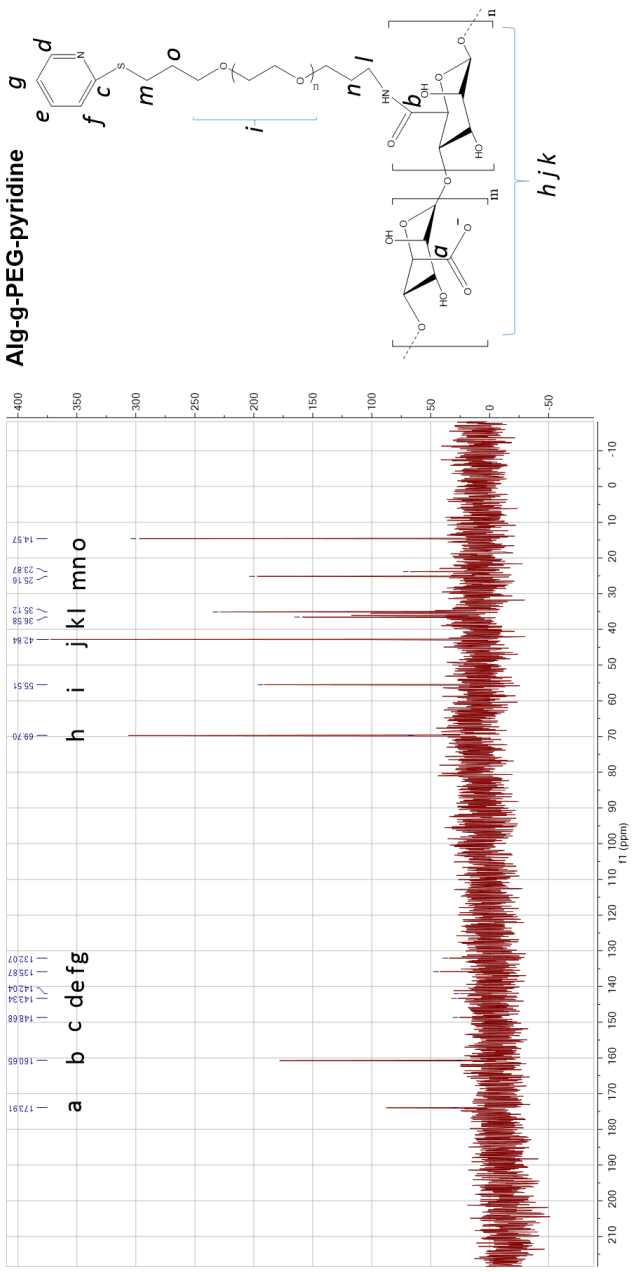

Figure 2-9. ^{13}C-NMR result of Alg–g-PEG-S-S-pyridine synthesis. Peaks at 132.31 ppm, 136.05 ppm, 141.37 ppm, 143.53 ppm, 149.24 ppm correspond to carbon on the pyridine ring, 69.76 ppm corresponds to carbon in the repeat unit of PEG, and 42.84 ppm corresponds to carbon on the alginate repeat unit.

.

Reference

[1] Harvey N, Dennison E, Cooper C. Osteoporosis: impact on health and economics. Nat Rev Rheumatol 2010;6:99-105.
[2] Prockop DJ. Marrow Stromal Cells as Stem Cells for Nonhematopoietic Tissues. Science 1997;276:71-4.
[3] Ferrara N, Gerber HP, LeCouter J. The biology of VEGF and its receptors. Nature medicine 2003;9:669-76.
[4] Liu Y, Berendsen AD, Jia S, Lotinun S, Baron R, Ferrara N, et al. Intracellular VEGF regulates the balance between osteoblast and adipocyte differentiation. J Clin Invest 2012;122:3101-13.
[5] Sinha VR, Trehan A. Biodegradable microspheres for protein delivery. Journal of Controlled Release 2003;90:261-80.
[6] Wu YQ, MacKay JA, McDaniel JR, Chilkoti A, Clark RL. Fabrication of Elastin-Like polypeptide Nanoparticles for Drug Delivery by Electrospraying. Biomacromolecules 2009;10:19-24.
[7] Wheatley MA, Chang M, Park E, Langer R. Coated alginate microspheres: factors influencing the controlled delivery of macromolecules. Journal of Applied Polymer Science 1991;43:2123-35.
[8] Wang Y, Irvine DJ. Engineering chemoattractant gradients using chemokine-releasing polysaccharide microspheres. Biomaterials 2011;32:4903-13.
[9] Mittal SK, Aggarwal N, Sailaja G, van Olphen A, HogenEsch H, North A, et al. Immunization with DNA, adenovirus or both in biodegradable alginate microspheres: effect of route of inoculation on immune response. Vaccine 2000;19:253-63.
[10] Lee KY, Mooney DJ. Alginate: Properties and biomedical applications. Progress in Polymer Science 2012;37:106-26.
[11] Ciofani G, Raffa V, Menciassi A, Dario P. Alginate and chitosan particles as drug delivery system for cell therapy. Biomedical Microdevices 2008;10:131-40.
[12] Jay SM, Saltzman WM. Controlled delivery of VEGF via modulation of alginate microparticle ionic crosslinking. Journal of Controlled Release 2009;134:26-34.
[13] Jay SM, Shepherd BR, Bertram JP, Pober JS, Saltzman WM. Engineering of multifunctional gels integrating highly efficient growth factor delivery with endothelial cell transplantation. The Federation of American Societies for Experimental Biology 2008;22:2949-56.
[14] Lemoine D, Wauters F, Bouchend'homme S, Preat ς. Preparation and characterization of alginate microspheres containing a model antigen. International Journal of Pharmaceutics 1998;176:9-19.
[15] Tonnesen HH, Karlsen J. Alginate in drug delivery systems. Drug Development and Industrial Pharmacy 2002;28:621-30.
[16] Lin N, Huang J, Chang PR, Feng L, Yu J. Effect of polysaccharide nanocrystals on structure, properties, and drug release kinetics of alginate-based microspheres. Colloids and Surfaces B: Biointerfaces 2011;85:270-9.
[17] Pawar SN, Edgar KJ. Alginate derivatization: A review of chemistry, properties and applications. Biomaterials 2012;33:3279-305.
[18] Chang SJ, Lee CH, Hsu CY, Wang YJ. Biocompatible microcapsules with enhanced mechanical strength. Journal of Biomedical Materials Research 2002;59:118-26.
[19] Davidovich-Pinhas M, Bianco-Peled H. Alginate-PEGAc: A new mucoadhesive polymer. Acta Biomaterialia 2011;7:625-33.

.

[20] Davidovich-Pinhas M, Bianco-Peled H. Physical and structural characteristics of acrylated poly(ethylene glycol)-alginate conjugates. Acta Biomaterialia 2011;7:2817-25.
[21] Meng X-W, Qin J, Liu Y, Fan M-M, Li B-J, Zhang S, et al. Degradable hollow spheres based on self-assembly inclusion. Chemical Communications 2010;46:643-5.
[22] Meng X-W, Ha W, Cheng C, Dong Z-Q, Ding L-S, Li B-J, et al. Hollow nanospheres based on the self-assembly of alginate-graft-poly(ethylene glycol) and α-cyclodextrin. Langmuir 2011;27:14401-7.
[23] Mahou R, Wandrey C. Alginate-Poly(ethylene glycol) Hybrid Microspheres with Adjustable Physical Properties. Macromolecules (Washington, DC, U S) 2010;43:1371-8.
[24] Mahou R, Tran NM, Dufresne M, Legallais C, Wandrey C. Encapsulation of Huh-7 cells within alginate-poly(ethylene glycol) hybrid microspheres. J Mater Sci-Mater M 2012;23:171-9.
[25] Knop K, Hoogenboom R, Fischer D, Schubert US. Poly(ethylene glycol) in Drug Delivery: Pros and Cons as Well as Potential Alternatives. Angewandte Chemie International Edition 2010;49:6288-308.
[26] Bassyouni F, ElHalwany N, Abdel Rehim M, Neyfeh M. Advances and new technologies applied in controlled drug delivery system. Res Chem Intermed 2013:1-36.
[27] Leahy DJ, Aukhil I, Erickson HP. 2.0 ≈ Crystal Structure of a Four-Domain Segment of Human Fibronectin Encompassing the RGD Loop and Synergy Region. Cell 1996;84:155-64.
[28] Ruoslahti E. RGD and Other Reconition Sequencies for Intrgrins. Annual Review of Cell and Developmental Biology 1996;12:697-715.
[29] Colombo R, Mingozzi M, Belvisi L, Arosio D, Piarulli U, Carenini N, et al. Synthesis and Biological Evaluation (in Vitro and in Vivo) of Cyclic Arginine-Glycine-Aspartate (RGD) Peptidomimetic-Paclitaxel Conjugates Targeting Integrin alpha(v)beta(3). Journal of Medicinal Chemistry 2012;55:10460-74.
[30] Hersel U, Dahmen C, Kessler H. RGD modified polymers: biomaterials for stimulated cell adhesion and beyond. Biomaterials 2003;24:4385-415.
[31] Chung HJ, Park TG. Surface engineered and drug releasing pre-fabricated scaffolds for tissue engineering. Advanced Drug Delivery Reviews 2007;59:249-62.
[32] Temming K, Schiffelers RM, Molema G, Kok RJ. RGD-based strategies for selective delivery of therapeutics and imaging agents to the tumour vasculature. Drug Resist Update 2005;8:381-402.
[33] Park JS, Yang HN, Jeon SY, Woo DG, Na K, Park K-H. Osteogenic differentiation of human mesenchymal stem cells using RGD-modified BMP-2 coated microspheres. Biomaterials 2010;31:6239-48.
[34] Huang S-Y, Pooyan S, Wang J, Choudhury I, Leibowitz MJ, Stein S. A Polyethylene Glycol Copolymer for Carrying and Releasing Multiple Copies of Cysteine-Containing Peptides. Bioconjugate Chem 1998;9:612-7.
[35] Mosmann T. Rapid colorimetric assay for cellular growth and survival: Application to proliferation and cytotoxicity assays. Journal of Immunological Methods 1983;65:55-63.
[36] Iso Y, Rao KS, Poole CN, Zaman AK, Curril I, Sobel BE, et al. Priming with ligands secreted by human stromal progenitor cells promotes grafts of cardiac stem/progenitor cells after myocardial infarction. Stem Cells 2014;32:674-83.
[37] Gåserød O, Sannes A, Skjåk-Bræk G. Microcapsules of alginate–chitosan. II. A study of capsule stability and permeability. Biomaterials 1999;20:773-83.
[38] Gregory CA, Gunn WG, Peister A, Prockop DJ. An Alizarin red-based assay of mineralization

.

by adherent cells in culture: comparison with cetylpyridinium chloride extraction. Anal Biochem 2004;329:77-84.
[39] Aldridge A, Kouroupis D, Churchman S, English A, Ingham E, Jones E. Assay validation for the assessment of adipogenesis of multipotential stromal cells—a direct comparison of four different methods. Cytotherapy 2013;15:89-101.
[40] Kim S, Kim J-H, Jeon O, Kwon IC, Park K. Engineered polymers for advanced drug delivery. European Journal of Pharmaceutics and Biopharmaceutics 2009;71:420-30.
[41] Midoux P, Breuzard G, Gomez JP, Pichon C. Polymer-based gene delivery: A current review on the uptake and intracellular trafficking of polyplexes. Current Gene Therapy 2008;8:335-52.
[42] Khalil IA, Kogure K, Akita H, Harashima H. Uptake pathways and subsequent intracellular trafficking in nonviral gene delivery. Pharmacological Reviews 2006;58:32-45.
[43] Akinc A, Thomas M, Klibanov AM, Langer R. Exploring polyethylenimine-mediated DNA transfection and the proton sponge hypothesis. The Journal of Gene Medicine 2005;7:657-63.
[44] Jain S, Amiji M. Tuftsin-modified alginate nanoparticles as a noncondensing macrophage-targeted DNA delivery system. Biomacromolecules 2012;13:1074-85.
[45] Liu J, Zhou HZ, Weir MD, Xu HHK, Chen QM, Trotman CA. Fast-Degradable Microbeads Encapsulating Human Umbilical Cord Stem Cells in Alginate for Muscle Tissue Engineering. Tissue Eng Pt A 2012;18:2303-14.
[46] Moshaverinia A, Chen C, Xu X, Akiyama K, Ansari S, Zadeh HH, et al. Bone Regeneration Potential of Stem Cells Derived from Periodontal Ligament or Gingival Tissue Sources Encapsulated in RGD-Modified Alginate Scaffold. Tissue engineering Part A 2013.
[47] Majzoub RN, Chan C-L, Ewert KK, Silva BFB, Liang KS, Jacovetty EL, et al. Uptake and transfection efficiency of PEGylated cationic liposome–DNA complexes with and without RGD-tagging. Biomaterials.
[48] Garcia AJ, Reyes CD. Bio-adhesive surfaces to promote osteoblast differentiation and bone formation. J Dent Res 2005;84:407-13.
[49] Salinas CN, Anseth KS. The enhancement of chondrogenic differentiation of human mesenchymal stem cells by enzymatically regulated RGD functionalities. Biomaterials 2008;29:2370-7.
[50] Lee KY, Alsberg E, Hsiong S, Comisar W, Linderman J, Ziff R, et al. Nanoscale Adhesion Ligand Organization Regulates Osteoblast Proliferation and Differentiation. Nano letters 2004;4:1501-6.
[51] Petrie TA, Raynor JE, Reyes CD, Burns KL, Collard DM, García AJ. The effect of integrin-specific bioactive coatings on tissue healing and implant osseointegration. Biomaterials 2008;29:2849-57.
[52] Rodriguez JP, Montecinos L, Rios S, Reyes P, Martinez J. Mesenchymal stem cells from osteoporotic patients produce a type I collagen-deficient extracellular matrix favoring adipogenic differentiation. Journal of Cellular Biochemistry 2000;79:557-65.

.

CHAPTER 3: DUAL-CROSSLINKED METHARYLATED ALGINATE SUB-MICROSPHERES FOR INTRACELLULAR CHEMOTHERAPEUTIC DELIVERY

Intracellular delivery vehicles comprised of methacrylated alginate (Alg-MA) were developed for the internalization and release of doxorubicin hydrochloride (DOX). Alg-MA was synthesized via an anhydrous reaction, and a mixture of Alg-MA and DOX was formed into sub-microspheres using a water/oil emulsion. Covalently crosslinked sub-microspheres were formed via exposure to green light, in order to investigate effects of crosslinking on drug release and cell internalization, compared to traditional techniques such as ultra violet (UV) light. Crosslinking was performed using light exposure alone, or in combination with ionic crosslinking using calcium chloride ($CaCl_2$). Alg-MA sub-microsphere diameters were between 88 – 617 nm, and zeta-potentials were between -20 and -37 mV. Using human lung epithelial carcinoma cells (A549s) as a model, cellular internalization was confirmed using flow cytometry; different sub-microsphere formulations varied the efficiency of internalization, with UV-crosslinked sub-microspheres achieving the highest internalization percentages. While blank (non-loaded) Alg-MA sub-microspheres were non-cytotoxic to A549s, DOX-loaded sub-microspheres significantly reduced mitochondrial activity after five days of culture. Photo-crosslinked Alg-MA sub-microspheres may be a potential chemotherapeutic delivery system for cancer treatment.

3.1. Introduction

Lung cancer is one of the most widespread type of carcinoma, resulting in the largest number of cancer-related deaths around the world.[1-3] Greater than 85% of lung cancer cases are currently classified as non-small-cell lung cancer (NSCLC), including adenocarcinoma, squamous-cell carcinoma and large-cell carcinoma. Despite the recent advances in early detection and cancer treatment, NSCLC is often diagnosed at an advanced stage and has a poor prognosis.[1] Chemotherapy is one of the current recommended treatments to prevent or reduce tumor-induced symptoms, prolong patient survival, and maintain patient quality of life.[4] Chemotherapy treatments can last as long as 6 months at high parenteral dosages, and are frequently associated with systemic toxicity.[5, 6]

Doxorubicin hydrochloride (DOX) is one of the most widely used chemotherapeutic drugs, and is known as an anthracycline antibiotic.[7] The main anti-cancer mechanisms that have been suggested for DOX fall into the following categories: 1) DOX intercalation into DNA, shutting down protein synthesis and DNA replication; 2) DOX-induced production of reactive oxygen species (ROS), inducing DNA damage and/or lipid membrane peroxidation; 3) DNA crosslinking, binding and alkylation; 4) DOX interference with DNA unwinding, strand separation and helicase activity; 5) damage to the bilayer structure of cell membranes; 6) DNA inhibition of topoisomerase II, initiating DNA damage pathways. All the above activities require that

DOX be presented inside the cytoplasm,[8-10] which requires intracellular delivery of DOX to cancer cells. DOX treatment induces several side effects including nausea, vomiting, and fever in patients.[11] A significant incidence of cardiovascular side effects – hypotension, tachycardia, arrhythmias, and ultimately congestive heart failure – are also reported.[8, 12] Therefore, there is a need for drug delivery systems which efficiently encapsulate and deliver chemotherapeutics while reducing adverse events. As a small molecule, concerns of low encapsulation efficiency, drug leakage, and aggregation limit the therapeutic efficacy of DOX, and complications associated with sterilization have not been resolved.[5]

Modern drug delivery systems are designed to maintain the structure and bioactivity of biomolecules and to release therapeutics in a controlled and predictable manner. Micro-encapsulation is one of the core technologies used in polymer drug delivery systems.[13] However, the relatively large micron-size (> 10 μm) of the drug delivery particles limits cellular internalization. Therefore, the association of DOX to sub-micron carriers has drawn greater interest,[14] including liposomes,[15] nanospheres and sub-microspheres,[16] and micelles.[17]

Alginate is an unbranched polysaccharide consisting of 1→4 linked β-D-mannuronic acid (M) and its C-5 epimer α-L-guluronic acid (G). Alginate is extracted from brown seaweed, and has been investigated for biomedical and pharmaceutical

applications due to its relatively low cost, low toxicity, biocompatibility, and biodegradability.[18-21] Alginate particles have increasingly been shown to offer controllable drug encapsulation efficiencies and release profiles, while maintaining the bioactivity of various drugs, including proteins,[22] cytokines,[23] and small molecules.[24] Through the formation of a water/oil emulsion and subsequent exposure to calcium ions, alginate particles within the micrometer – nanometer size scale can be generated, and are often referred to as ionically crosslinked alginate particles.[20, 22, 25]

The fabrication of alginate microspheres and sub-microspheres is favorable for drug delivery due to the relatively mild ionic gelation process.[22, 26] However, limitations associated with the relatively weak ionic bonds include low drug encapsulation efficiency and rapid drug-release rates (< 24 h).[27] To overcome these limitations, methacrylated alginate (Alg-MA) was synthesized [28] and sub-microspheres were generated utilizing a water/oil emulsion [22] and subsequent crosslinking. Alg-MA sub-microspheres were covalently crosslinked using photoinitiators and visible (i.e., green) or UV light irradiation.[28] Dual-crosslinked sub-microspheres were generated with the subsequent addition of calcium chloride.[22] To evaluate the efficiency of internalization and the bioactivity of DOX-loaded Alg-MA sub-microspheres, human lung epithelial carcinoma cells (A549s) were utilized as a model system. We hypothesized the dual-crosslinking would result in a tighter

hydrogel network for more efficient intracellular DOX delivery (Figure 1). DOX encapsulation efficiency and *in vitro* release were quantified using an absorbance assay. While blank (non-loaded) Alg-MA sub-microspheres were non-cytotoxic to A549s, DOX-loaded sub-microspheres significantly reduced mitochondrial activity after five days of *in vitro* culture.

3.2. Materials and Methods

3.2.1. Materials and Reagents

Sodium alginate (M_W = 65–75 kg/mol, 60-70% guluronic acid residues) was generously donated by FMC BioPolymer. Irgacure D2959 was generously donated by Ciba Inc. Biology-grade mineral oil, Span 80, Tween 80, ethylenediaminetetriacetic acid (EDTA), deuterium oxide (D_2O), dimethyl sulfoxide (DMSO, 99% anhydrous), dodecyltrimethylammonium bromide salt (DTAB), methacrylic anhydride (MA), 4-(dimethylamino)pyridine (DMAP), doxorubicin hydrochloride (DOX), N-ethyl-N'(3-dimethylaminopropyl) carbodiimide hydrochloric acid (EDC), N-hydroxysuccinimide (NHS), and the *in vitro* toxicology assay kit (3-(4,5-dimethylthiazol-2-yl)-2,5-diphenyltetrazolium bromide (MTT)-based) were purchased from Sigma-Aldrich. One molar hydrochloric acid (HCl) and 1 M sodium hydroxide (NaOH) were purchased from BDH ARISTAR®PLUS. Dichloromethane (DCM, 99.9%), sodium citrate, isopropanol, sodium chloride (NaCl), sodium citrate, DMEM/F-12 mammalian cell

culture medium, Alexa Fluor® 647 cadaverine and 20X phosphate buffered saline (PBS) were purchased from Fisher Scientific. Fetal bovine serum (FBS) was purchased from Atlanta Biologics. Penicillin, streptomycin, and 0.25% trypsin EDTA were purchased from Corning Cellgro. A549 (CCL-185™) human lung epithelial carcinoma cells were purchased from ATCC®.

3.2.2. Synthesis and Characterization of Methacrylated Alginate (Alg-MA)

Alg-MA was synthesized utilizing an anhydrous reaction to control the degree of methacrylation (DOM).[28, 29] Sodium alginate was rendered soluble in anhydrous DMSO through an ion exchange with DTAB. Aqueous solutions of sodium alginate (1%, w/v) and DTAB (2%, w/v) were prepared and slowly mixed while stirring at 1000 rotations per minute (rpm). The precipitate was washed in DI water and lyophilized. A 1% (w/v) alginate-DTA/DMSO solution was reacted with MA in the presence of a catalyst, DMAP, for 24 hours at room temperature. The solution was hydrolyzed through extensive dialysis in 0.2 M sodium phosphate dibasic salt solution followed by further dialysis in DI water. Alginate methacrylation was confirmed using ^{1}H-NMR spectroscopy, (Bruker AVANCE III 500 MHz high-field NMR spectrometer) by the presence of methacrylate (6.25, 5.75 ppm) and alginate methyl resonances (2.0 ppm). A 1% (w/v) polymer solution in D_2O was analyzed at room temperature, spinning at 20 Hz for 16 scans.[28, 30] The DOM was quantified by peak integration and calculation of the ratio between of the methyl protons at 2.0 ppm and the newly formed methylene

protons of methacrylate at 5.75 ppm and 6.25 ppm.[30, 31]

3.2.3. Dual-crosslinked Alg-MA Sub-Microspheres Design and Fabrication

Aqueous Alg-MA solutions were mixed with photoinitiators for UV (0.05%, w/v, Irgacure D2959) or visible green light activation [1 mM eosin Y (photosensitizer), 125 mM triethanolamine (initiator) and 20 mM 1-vinylpyrrolidone (catalyst)], respectively. Two percent (w/v) Alg-MA solutions were mixed with 0.1% (w/v) DOX and formed into sub-microspheres using a water/oil emulsion and subsequent crosslinking (Figure 2). Alg-MA sub-microspheres without DOX were fabricated as blank (i.e., non-loaded) controls.22 One milliliter of polymer/DOX solution was slowly added to 6.72 mL of biological-grade mineral oil containing 5% (v/v) Span 80, while mixing at 1200 rpm for 5 minutes at room temperature. Subsequently, 400 μL of 30% (v/v) Tween 80 (in biological-grade mineral oil) was added and mixed for an additional 5 minutes. Crosslinking was performed four different ways: 1) green light exposure for 10 minutes (Green, using 525 nm wavelength, NFLS-G30 3-WHT, SuperBrightLEDs); 2) UV light exposure for 10 minutes (UV, using 320–390 nm wavelength, Uvitron Intelliray 400); 3) green light plus 5 mL of 0.5 M CaCl2, mixing for 15 minutes (Green+C); and 4) UV light plus 5 mL of 0.5 M CaCl2, mixing for 15 minutes (UV+C).28 After crosslinking, 3 mL of isopropanol was added to the emulsion and mixed for 5 minutes, then centrifuged at 400 rpm for 5 minutes to precipitate sub-microspheres. Alg-MA sub-microspheres were washed sequentially with isopropanol

(x2) and DI water (x2), respectively, and centrifuged after each wash.

The diameters and zeta-potentials (i.e., surface charge) for hydrated, blank and DOX-loaded Alg-MA sub-microspheres were quantified using dynamic light scattering (DLS, Zetasizer Nano ZSP, Malvern). Sub-microspheres were suspended in PBS, pH = 7.4, at room temperature. Hydrodynamic diameters were determined based on number averages, and the size distribution was plotted for each sub-microsphere group. After lyophilization, Alg-MA sub-microspheres were characterized by scanning electronic microscopy (SEM, JEOL 600); samples were sputter coated with 45 nm of Au-Pb prior to imaging. SEM micrographs of various magnifications were used to visualize or attempt to visualize Alg-MA sub-microspheres.

3.2.4. Drug Loading and Mechanism of Release

Covalently and/or dual-crosslinked Alg-MA sub-microspheres were evaluated for use as chemotherapeutic delivery vehicles. DOX was utilized as a model drug for its intrinsic UV absorbance and ease of quantification, for drug encapsulation, drug release and effectiveness assays. To determine whether or not UV or green light exposure changed the chemical structure or bioactivity of DOX, aqueous DOX solutions were exposed to UV and green light for 10 minutes, and then characterized by 1H-NMR, using non-modified DOX as a control. DOX encapsulation efficiency, i.e., drug retention during sub-microsphere fabrication, was calculated as a percentage of the initial loading concentration. Covalent crosslinking of the sub-microspheres prevents

dissolution; therefore, an extended diffusion process was utilized to quantify encapsulated drug. Briefly, 1 mg of sub-microspheres was suspended in 1 mL of PBS, incubated at 37°C and agitated for three weeks. The solution was centrifuged, and the supernatant was analyzed on a microplate reader (Synergy HT microplate reader, BioTek) at 485 nm absorbance, and compared to standard curve (EE = Actual Drug Encapsulated ÷ Theoretical Drug Loaded). Detection of drug lost during washing procedures was not possible due to presence of multiple phases of emulsion additives and the absorbance detection limit of DOX on the equipment utilized.

To characterize in vitro release profiles, released DOX concentration was quantified using the intrinsic absorbance at 485 nm in a 48-well tissue culture polystyrene (TCPS) plate at 37°C (Synergy HT microplate reader, BioTek). One milligram of lyophilized DOX-loaded Alg-MA sub-microspheres was dissolved in 500 µL of PBS, pH 7.4 (n = 3). At 1, 2, 4, 8, 12, and 24 hours, and daily up to 11 days, 100 µL of PBS was removed for analysis, and replaced with 100 µL of fresh PBS to maintain the total volume. DOX concentration was determined using an absorbance assay and generating a standard curve. Cumulative DOX (µg) released over time was calculated by adding the mass of DOX released at each time point per mass of sub-microspheres.

3.2.5. Cellular Uptake of Alg-MA Sub-Microspheres

Four different formulations of blank (i.e., non-loaded) Alg-MA sub-microspheres were reacted with Alexa Fluor® 647 cadaverine dye to form fluorescent

sub-microspheres (Alexa 647-Alg-MA); the surface reaction chemistry was performed according to the manufacturers protocol through carbodiimide chemistry at room temperature catalyzed by NHS/EDC. Alg-MA sub-microspheres without DOX were used in order to avoid cell death during internalization and analysis. A549s were seeded in 48-well TCPS plates at 25,000 cells/well in 500 µL/well of standard growth culture medium (DMEM/F-12, 10% FBS, 100 U/mL penicillin, 100 µg/mL streptomycin), and allowed to adhere for 24 hours at 37°C and 5% CO_2. Cells were then incubated with blank Alexa 647-Alg-MA sub-microspheres (n = 6 per group) at 100 µg/mL, 37°C and 5% CO_2. After 12 hours, culture medium containing Alexa 647-Alg-MA sub-microspheres was removed, and adherent cells were thoroughly rinsed with PBS three times to remove non-internalized and cell-surface-bound sub-microspheres. Cells were trypsinized and re-suspended in PBS at $1x10^6$ cells/mL, and analyzed by flow cytometry (BD LSRII Flow Cytometer) to quantify the percentage of A549s that internalized the sub-microspheres. A549s cultured with no sub-microspheres, and cells cultured with non-fluorescent sub-microspheres, were prepared and analyzed as controls.[22]

3.2.6. Drug Bioactivity and Efficacy of Alg-MA Sub-Microsphere Delivery Vehicles

3.2.6.1. Cytotoxicity of Blank and Drug-loaded Alg-MA Sub-Microspheres

The cytotoxicity of blank (i.e., non-loaded) and DOX-loaded sub-microspheres was evaluated using a toxicology, MTT-based assay. A549s were seeded in 48-well TCPS plates at 25,000 cells/well in 500 µL/well of standard growth culture medium, and allowed to adhere for 24 hours at 37°C and 5% CO_2. Cells were then incubated in the presence of blank Alg-MA sub-microspheres or DOX-loaded Alg-MA sub-microspheres (n = 6 per group, per fabrication type) at sub-microsphere concentrations of 10, 50, 100 µg/mL. After 24 hours, medium containing sub-microspheres (blank groups and DOX-loaded groups) was removed, cells were rinsed two times in sterile PBS, and then analyzed using a MTT-based assay according to the manufacturer's protocol. The optical density was measured at 570 nm; background absorbance at 690 nm was subtracted from the measured absorbance at 570 nm (Synergy HT microplate reader, BioTek). Absorbance values for the experimental samples were normalized to controls and reported as normalized mitochondrial activity.[22]

3.2.6.2. Effective of Intracellular VS. Extracellular Drug Delivery on Cell Proliferation

The bioactivity of the DOX-loaded sub-microspheres was evaluated using a similar method discussed in section 2.6.1. A549s were seeded in 48-well TCPS plates at 10,000 cells/well in 500 µL/well of standard growth culture medium, and allowed to adhere for 24 hours. Cells were incubated in the presence of DOX-loaded Alg-MA sub-microspheres (n = 6 per fabrication type) at sub-microsphere concentrations of 10, 50,

and 100 µg/mL. A549s and Alg-MA sub-microspheres were co-cultured for 5 days with media exchanges. Free DOX (i.e., DOX contained within the cell culture medium) was added to A549s at different concentrations (5, 4, 3, 2, 1, 0.5, 0.25, 0.125, 0.06, 0.03, 0.015 and 0 µg/mL) to compare the effect of intracellular versus extracellular DOX delivery. After 1, 3 and 5 days of culture, a MTT-based assay was performed according to the manufacturer's protocol, to quantify the effects of DOX-loaded Alg-MA sub-microspheres and free DOX on *in vitro* cancer cell proliferation. Absorbance values for the experimental samples were normalized to controls and reported as normalized mitochondrial activity.[22]

3.2.7. Data Analysis

The quantitative results for all experiments are reported as mean ± standard deviation. Statistical analysis was performed on Alg-MA sub-microsphere co-cultured cell assays, using one-way ANOVA with Tukey multiple comparisons ($\alpha = 0.05$) via the SAS statistics program in the GLM procedure, as the post-test to compare all of the groups. A $p < 0.05$ was considered significantly different.

3.3. Results and Discussion

3.3.1. Synthesis and Characterization of Alg-MA

The chemical modification of alginate rendered it hydrophobic and soluble in

organic solvents. An anhydrous methacrylation of alginate resulted in a functionalized biomacromolecule with a controllable DOM.[28] ^{1}H-NMR spectra for Alg-MA and non-modified alginate are shown in Supplemental Figure S1. The DOM for the Alg-MA used as the base material in the sub-microspheres was approximately 64%.[31-34] Peaks between 3.0 and 3.5 ppm indicate methyl groups at the end of alginate chains resulting from degradation during the methacrylation chemistry.

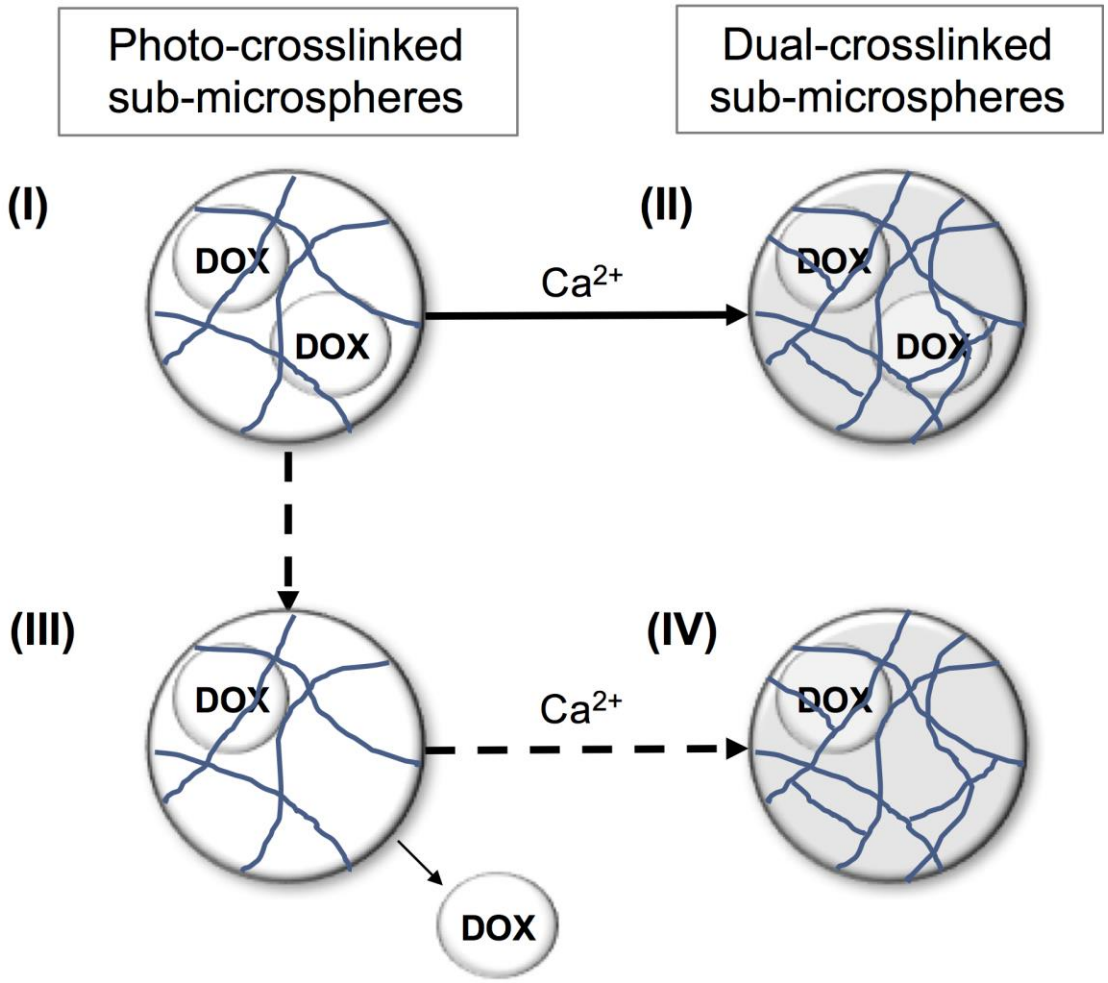

Figure 3-1. Schematic of the hydrogel network structure comprising photo-crosslinked and dual-crosslinked Alg-MA sub-microspheres. (I) Photo-crosslinked sub-microspheres

.

exhibit a porous hydrogel network with intermolecular covalent crosslinks, encapsulating DOX. (II) Upon the addition of ionic crosslinking, the hydrogel network tightens, resulting in reduced drug loss and slower diffusion-based drug release; this is the desired product. (III) However, the introduction of aqueous-based calcium chloride ($CaCl_2$) solution may result in drug loss during the ionic crosslinking step. (IV) The non-ideal dual-crosslinked product may exhibit lower drug loading capacity due to the additional steps in the fabrication process.

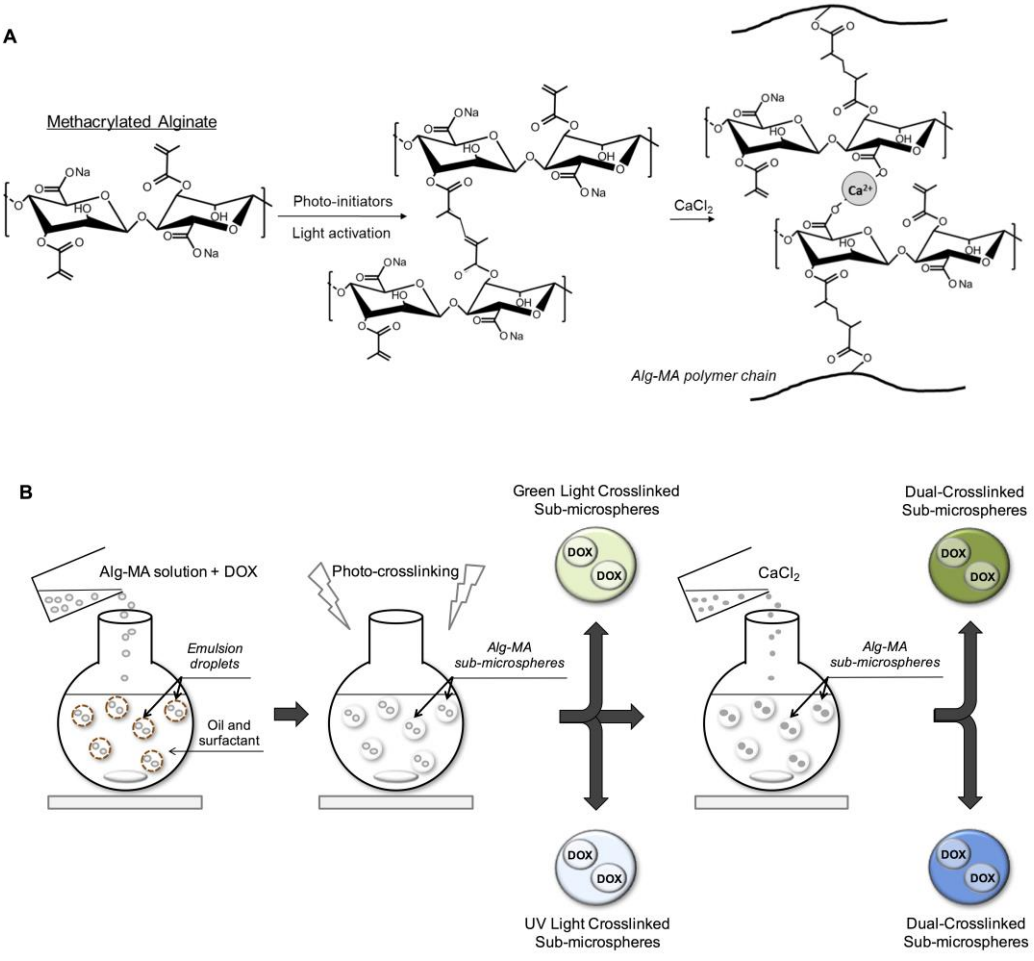

.

Figure 3-2. (A) Chemical structure of methacrylated alginate (Alg-MA). Alg-MA was covalently crosslinked in the presence of photoinitiators under light activation, to form photo-crosslinked Alg-MA hydrogel networks. Alg-MA hydrogels were ionically crosslinked in the presence of calcium chloride ($CaCl_2$) to form dual-crosslinked Alg-MA hydrogel networks. (B) Schematic representation of microsphere fabrication techniques. Microspheres with or without DOX were prepared by premixing Alg-MA solutions and creating a water/oil emulsion at room temperature. Alg-MA sub-microspheres were photo-crosslinked upon exposure to visible or UV light, respectively, and further dual-crosslinked in the presence of 1 M $CaCl_2$.

.

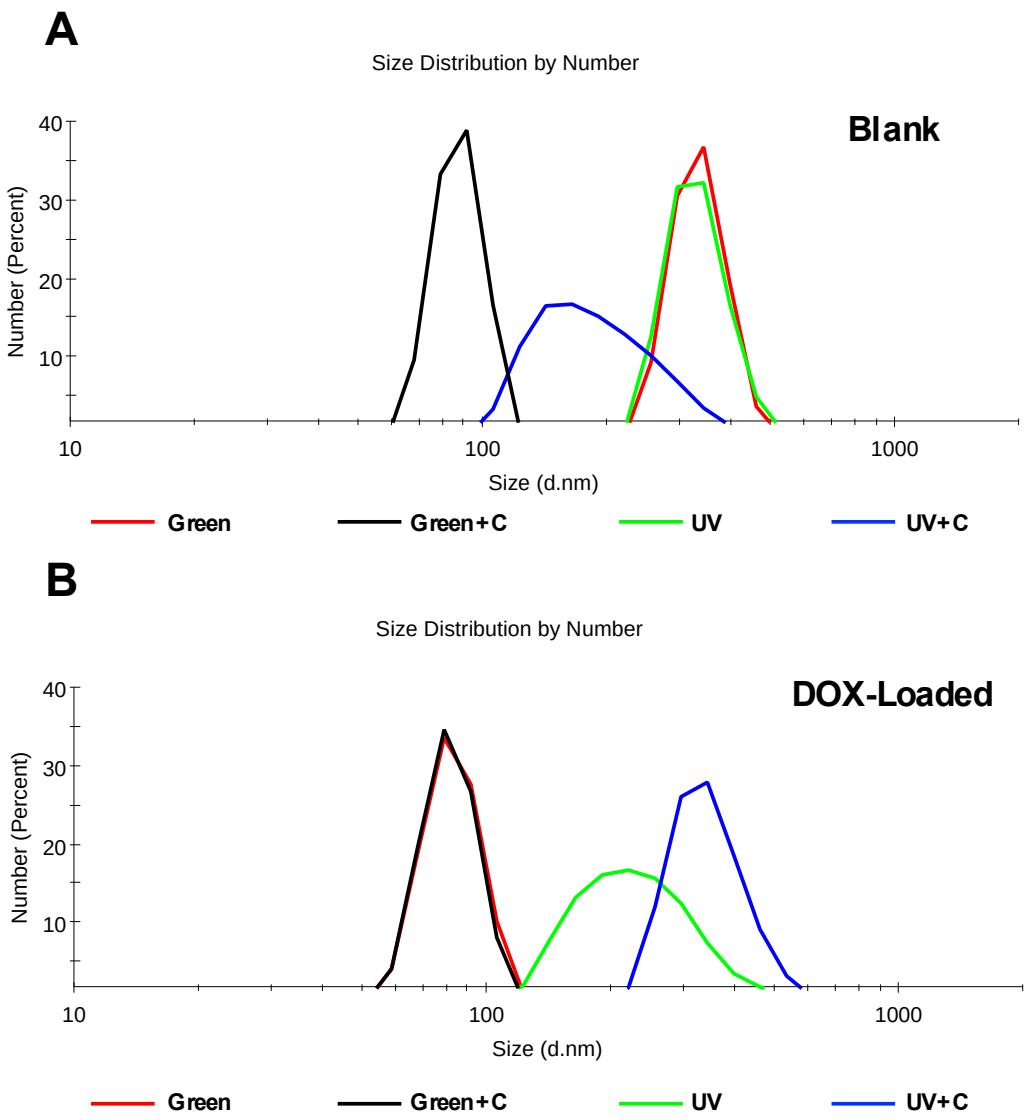

Figure 3-3 Dynamic light scattering size distribution plots for photo-crosslinked and dual-crosslinked Alg-MA sub-microspheres: green photo-crosslinked (Green), green + Ca2+ dual-crosslinked (Green+C), UV photo-crosslinked (UV), UV + Ca2+ dual-crosslinked (UV+C). H

3.3.2. Fabrication and Characterization of Dual-crosslinked Alg-MA Hydrogel

.

Sub-Microsphere

The formation of Alg-MA sub-microspheres was indicative of a crosslinked hydrogel network, obtained through either covalent crosslinking[35] (e.g., via photo-crosslinking) alone, or in combination with ionic crosslinking (e.g., by the addition of $CaCl_2$), as illustrated in Figure 2.[27, 35, 36] The DOM for the Alg-MA base material was 64%, and this moderate-DOM sustained both covalent and ionic crosslinking. Photo-crosslinking occurred upon UV or green light activation between adjacent acrylate groups, while the subsequent presence of $CaCl_2$ induced ionic crosslinking between adjacent carboxyl groups. While methacrylation took place at available hydroxyl groups, ionic crosslinks formed between adjacent carboxyl side-groups on neighboring alginate chains, thus allowing Alg-MA to sustain dual-crosslinking.

DOX-loaded sub-microsphere hydrodynamic diameters were quantified using DLS analysis (Table 1). The largest populations of DOX-loaded sub-microspheres were sized between 243 – 391 nm: UV = 243 nm, Green = 391 nm, UV+C = 346 nm, Green+C = 358 nm. The variability of the sub-microsphere diameters, plotted as size distributions in Figure 3A+B, is an almost unavoidable result of the emulsion process, and is indeed a limitation of the fabrication method; however, the linear size distribution plots indicate the following: Alg-MA sub-microspheres exhibited size populations within the same size scale, thus demonstrating consistency in fabrication method. SEM images (see Supplemental Figure S2) also indicated that Alg-MA sub-microspheres were spherical in shape, however heterogeneous in size. The zeta-

potentials ranged between -20 mV and -37 mV, and none of the groups demonstrated any significant outlying data.

3.3.3. Swelling and Diffusion-based Drug Release

The efficacy of Alg-MA sub-microspheres as chemotherapeutic delivery vehicles was investigated. DOX was utilized as a model drug for its intrinsic UV absorbance and ease of quantification for subsequent drug encapsulation, drug release and effectiveness assays. Alg-MA sub-microspheres were designed to encapsulate DOX without interfering with the detectability or bioactivity of DOX. Both photo-crosslinking alone or dual-crosslinking were successful in fabricating DOX-loaded sub-microspheres. The low level of UV or green light exposure required for sub-microsphere fabrication did not change the chemical structure of DOX, verified by 1H-NMR spectroscopy (see Supplemental Figure S3), and the toxic effects of DOX were still active.37 The mild-gelation techniques used to form Alg-MA sub-microspheres may retain the functionality and bioactivity of other therapeutics. Indeed, it was hypothesized that secondary, ionic crosslinking may show no beneficial effect on DOX encapsulation efficiency, however, the effect of ionic crosslinking may result in sustained drug release due to a tighter hydrogel network structure.

The cumulative mass of DOX released over time was calculated from four different types of Alg-MA sub-microspheres, and release profiles are shown in Figure 4. The DOX release profiles followed two different trends – a linear release profile was

seen during the first 8 hours of release, consistent with hydrogel-swelling induced drug release (see Figure 4A). Cumulative DOX release profiles through 11 days are shown in Figure 4B. The release profiles for UV, Green, and Green+C groups followed a logarithmic trend (trend line $R2 \geq 0.92$), while the UV+C group followed a linear release profile up to 11 days (trend line $R2 = 0.98$); however, these trends were not analyzed further. The amount of DOX released did show a similar trend with encapsulation efficiencies: dual-crosslinked sub-microspheres encapsulated less drug and released less drug over an 11 day period.38-39 The introduction of aqueous-based $CaCl2$ solution to the emulsion resulted in drug loss due to DOX solubility in aqueous solutions.40 The varying release kinetics with time suggest that the sub-microsphere structure may be optimized further for controlled release applications, by varying the degree of crosslinking to extend or delay the drug release rate.35 It is hypothesized that increasing the drug-loading concentration, increased efficacy over longer time periods could be achieved. Decreasing the variability in the diameter of the sub-microspheres and varying the Alg-MA DOM may also result in varied release rates due to changes in the network microstructure. However, sub-microsphere size homogeneity and drug release profile optimization were outside the scope of this study and may be addressed through further investigations.

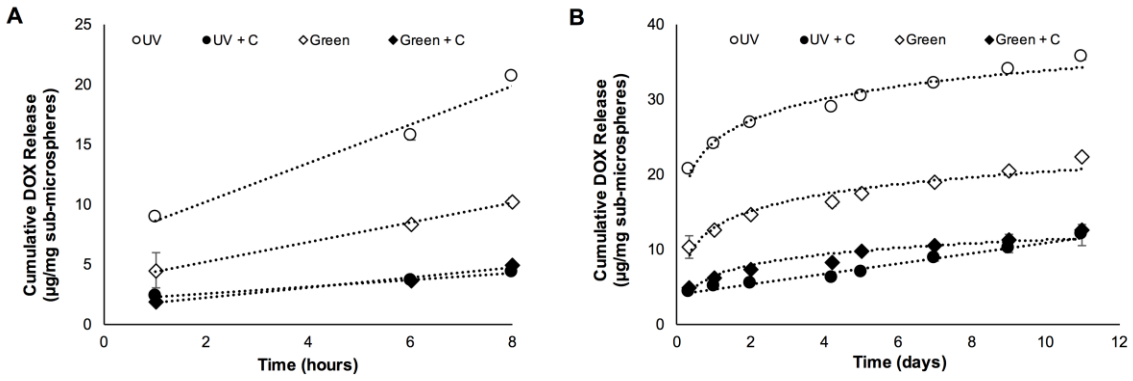

Figure 3-4. Quantitative cumulative release of doxorubicin (DOX) from DOX-loaded Alg-MA sub-microspheres for a period of 11 days (average ± standard deviation, n = 6 hydrogel samples per group). Sample aliquots were collected and the DOX concentration was determined using a standard curve at an absorption wavelength of 485 nm. (A) Cumulative DOX release profile during the first 8 hours; the release profiles for all of the Alg-MA sub-microsphere groups followed a linear trend (trend line $R^2 \geq 0.98$). (B) Cumulative DOX release profile during 11 days; the release profiles for the UV, Green, and Green+C Alg-MA sub-microsphere groups followed a logarithmic trend (trend line $R^2 \geq 0.92$), while the UV+C group continued to follow a linear release profile up to 11 days (trend line $R^2 = 0.98$).

3.3.4. Cellular Uptake of Alg-MA Sub-Microsphere

Uptake of Alg-MA sub-microspheres into A549s was quantitatively determined via flow cytometry to detect the fluorescent signal of Alexa-647-labeled sub-microspheres. Non-treated A549s and cells cultured with non-fluorescently labeled sub-microspheres were used as controls. Utilizing gate settings based on the fluorescent

.

intensity level of the probe, negative and positive populations were established, and it was found that all four types of Alg-MA sub-microspheres were readily internalized by A549s.[22] The positive population was > 80% in all four treatment groups (Figure 5A-F). UV crosslinked Alg-MA sub-microspheres (single and dual-crosslinked) exhibited higher internalization rates compared to green light crosslinked groups (Figure 5G), which may be related to sub-microsphere diameter; however, statistics were not performed on the internalization data.

Sub-Microsphere Group	**Hydrodynamic Diameter by Number (nm)**		**Zeta-Potential (mV)**		**Encapsulation Efficiency (%)**
	Blank	***DOX Loaded***	***Blank***	***DOX Loaded***	***DOX Loaded***
Green Light	334	391	-37	-27	28
UV Light	331	243	-21	-21	84
Green Light + Calcium	88	358	-29	-33	26
UV Light + Calcium	197	346	-27	-25	3

Table 3-1. Dynamic light scattering (DLS) quantitative analysis of hydrodynamic diameters and zeta-potentials of blank (i.e., non-loaded) and DOX-loaded photo-crosslinked and dual-crosslinked Alg-MA sub-microspheres. DOX encapsulation efficiencies were determined using an absorbance assay after sub-microsphere fabrication.

.

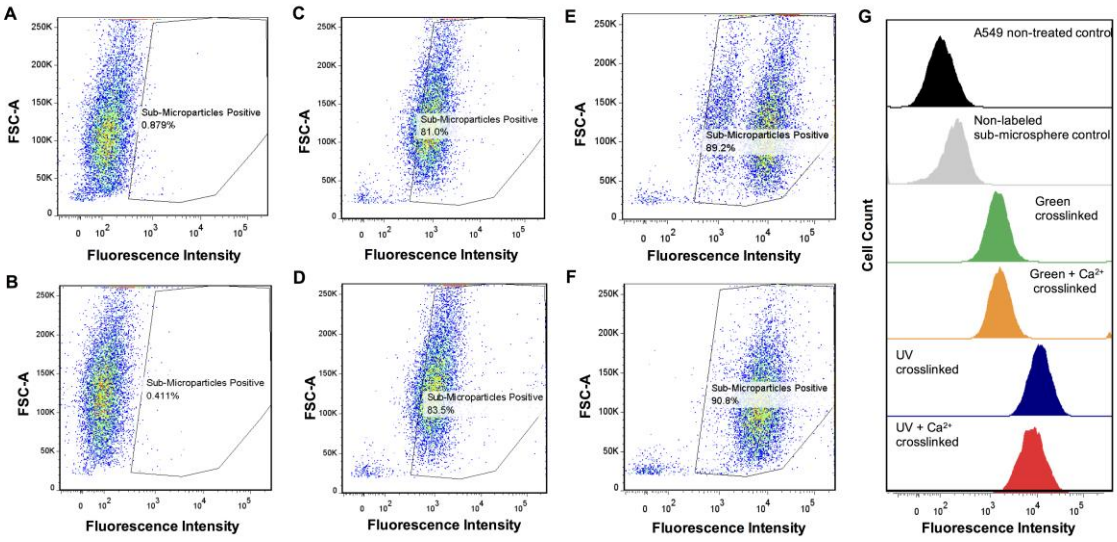

Figure 3-5. Flow cytometry analysis of Alg-MA sub-microspheres after 12 hours of co-culture with human lung epithelial carcinoma (A549) cells. (A) Non-treated cell control, (B) cells cultured with non-labeled blank sub-microspheres, (C) cells cultured with green photo-crosslinked sub-microspheres, (D) cells cultured with green photo-crosslinked and calcium crosslinked sub-microspheres, (E) cells cultured with UV photo-crosslinked sub-microspheres, and (F) cells cultured with UV photo-crosslinked and calcium crosslinked sub-microspheres. (G) Flow cytometry histograms were presented to show the different fluorescence intensity between control cells and different Alg-MA groups.

3.3.5. Cytotoxicity of Blank and Drug-Loaded Alg-MA Sub-Microspheres

To verify the non-toxicity and retention of DOX bioactivity after sub-microsphere encapsulation, MTT assays were performed on blank Alg-MA sub-microspheres and DOX-loaded Alg-MA sub-microspheres after 24 hours of culture

.

with A549s to quantify mitochondrial activity. A549 viability was assessed in the presence of Alg-MA sub-microspheres at increasing concentrations (10, 50, 100 µg/mL, Figure 6). Blank Alg-MA sub-microspheres (with no drug content) were minimally cytotoxic to A549s (mitochondrial activity > 80%) at concentrations up to 100 µg/mL (Figure 6A). Increased mitochondrial activity may be attributed to low molecular weight soluble alginate (i.e., sugar) in the culture media. Additionally, we hypothesize the reduced cytotoxicity seen in the UV+C group may be due to enhanced clearance of residual UV photoinitiator upon secondary crosslinking with an aqueous calcium chloride solution.[37] DOX-encapsulated sub-microspheres delivered bioactive drug, significantly reducing mitochondrial activity within 24 hours (Figure 6B).

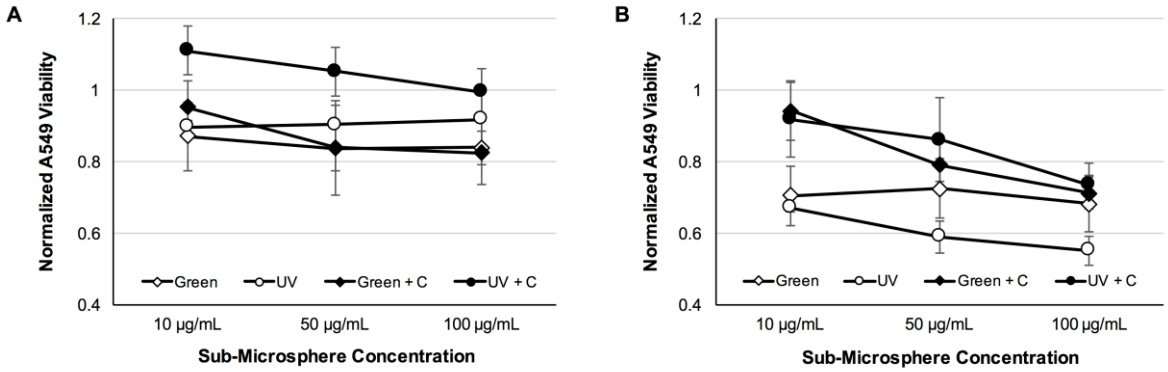

Figure 3-6. Human lung epithelial carcinoma (A549) cells were cultured in the presence of hydrogel sub-microspheres for 24 hours in standard growth medium at 37˚C and 5% $C0_2$. Cell viability was determined using an absorbance-based quantitative assay to measure mitochondrial activity (MTT); absorbance data for the groups treated with sub-microspheres were normalized to the non-treated cell control (average ± standard

.

deviation, n = 6 hydrogel samples per group). The cytotoxicity of Alg-MA sub-microspheres was analyzed on (A) blank (non-loaded) sub-microspheres. The bioactivity of doxorubicin (DOX) was verified using (B) DOX-loaded sub-microspheres. Various groups (white diamonds = green photo-crosslinked, white circles = UV photo-crosslinked, black diamonds = green + Ca^{2+} dual crosslinked, black circles = UV + Ca^{2+} dual crosslinked) and sub-microsphere concentrations (10, 50, 100 μg/mL) were characterized.

3.3.6. Effect of Soluble Drug VS Sub-Microparticle Mediated Delivery on Cell Proliferation

Four different types of DOX-loaded Alg-MA sub-microspheres were cultured with A549s at concentrations of 10, 50 and 100 μg/mL. In addition, different concentrations of free DOX was added to the culture media and served a control. A short-term cell proliferation study (utilizing an MTT assay) was performed for 5 days. On day 1, all of the Alg-MA sub-microsphere groups reduced A549 proliferation, regardless of the crosslinking type or concentration (Figure 7A). On days 3 and 5, the UV crosslinked Alg-MA sub-microspheres showed the greatest reduction in the A549 proliferation. For comparison, normalized mitochondrial activity was plotted versus free DOX, Figure 7B, or DOX-loaded sub-microspheres calculated, Figure 7C. Compared to the free DOX control, Alg-MA sub-microsphere-mediated delivery shows a similar decreasing trend as drug concentration increases, though remains less

.

effective. Also, it is likely that drug remains within the sub-microspheres and is not released intracellularly. Another consideration is that due to the extended drug release profile of DOX from sub-microspheres (Figure 4B), improved efficacy beyond 5 days may be achieved. Indeed, photo-crosslinked microspheres alone are advantageous for delivering a chemotherapeutic to cancer cells, at clinically-relevant dosages, and decreased lung cancer cell mitochondrial activity.

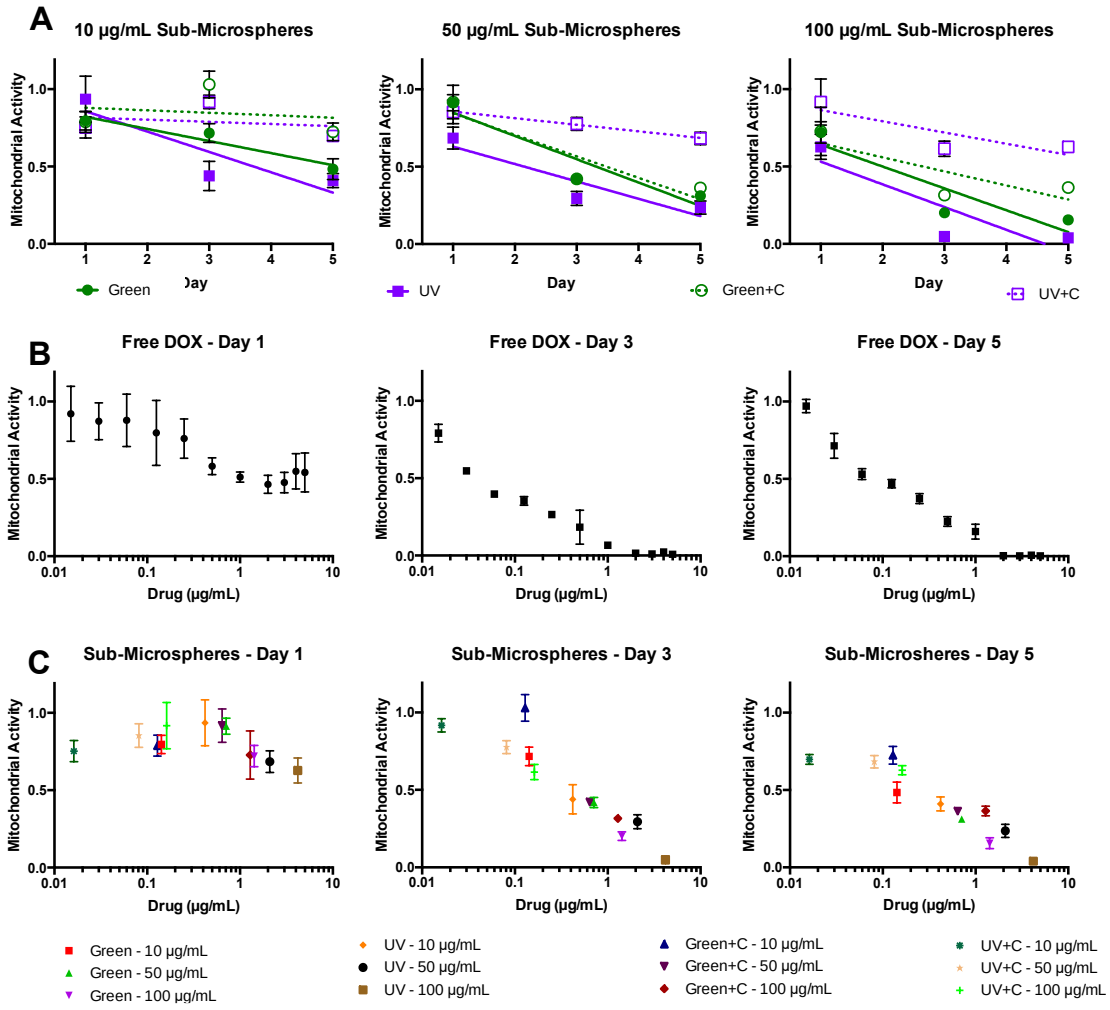

Figure 3-7. The efficacy of doxorubicin (DOX)-loaded Alg-MA sub-microspheres as

chemotherapeutic delivery vehicles was assessed using a MTT-based assay, to quantify cell proliferation over a 5-day period. A549 activity was recorded as mitochondrial activity and normalized to non-modified cell controls. Various formulations and concentrations (10-100 μg/mL) of sub-microspheres were assessed: green photo-crosslinked (Green), green + Ca^{2+} dual-crosslinked (Green+C), UV photo-crosslinked (UV), UV + Ca^{2+} dual-crosslinked (UV+C). DOX was added exogenously (Free DOX) to the cell culture medium at various concentrations to test the effect of intracellular versus extracellular DOX delivery. (A) Effect of Alg-MA sub-microsphere concentration for each crosslinking type on A549 mitochondrial activity; (B) Effect of 'free dox' concentration on A549 mitochondrial activity on days 1, 3, and 5; (C) Effect of DOX concentration encapsulated within Alg-MA sub-microspheres on A549 mitochondrial activity on days 1, 3, and 5.

3.4. Conclusions

The study reported here-in focused on the efficacy of utilizing crosslinked Alg-MA sub-microspheres to intracellularly deliver a chemotherapeutic. Photo-crosslinked and dual-crosslinked Alg-MA sub-microspheres successfully encapsulated DOX, were internalized by A549s, and delivered DOX to A549s, reducing mitochondrial activity compared to non-modified cell controls. The outcome of this study suggests that photo-crosslinking alone, and in particular green light activation, is an effective means of producing drug delivery vehicles, and perhaps additional crosslinking steps or procedures are not beneficial, perhaps even detrimental, to drug encapsulation

.

efficiencies. Based on drug encapsulation predictions and calculations, effective clinical drug dosages were achieved, as compared to free DOX delivery, and were controllable. While the efficacy for using photo-crosslinking Alg-MA sub-microspheres was shown during a short time frame (5 days) *in vitro*, future *in vivo* work may show enhanced drug efficacy using microsphere-mediated delivery compared to exogenous intravenous chemotherapy over extended periods of time.

3.5. Supplemental Materials

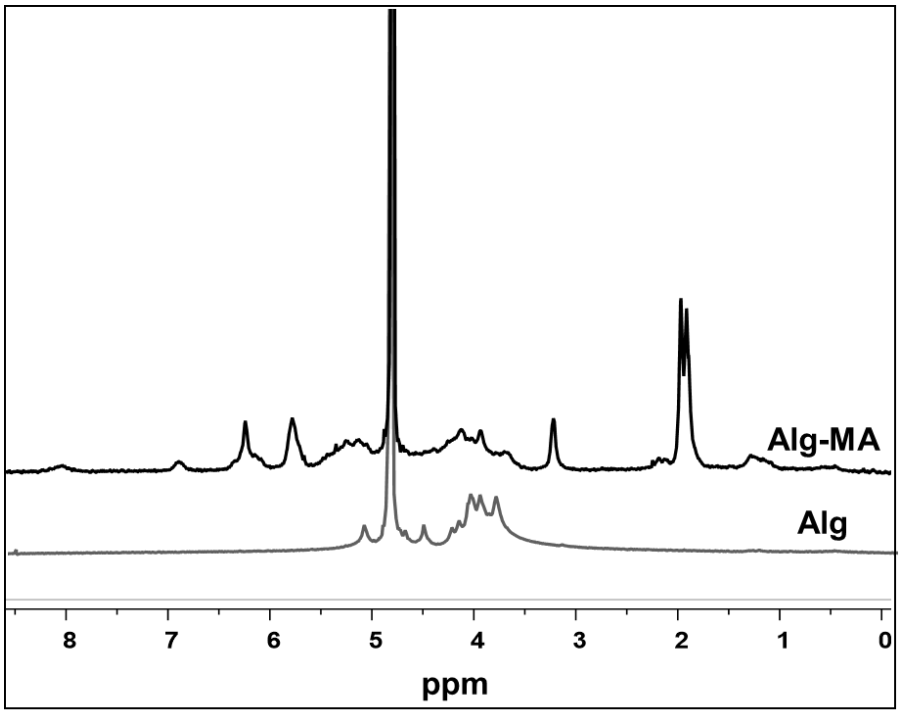

Figure 3-8. The ^{1}H-NMR spectra of Alg-MA and alginate are shown here. The peaks at 5.75 and 6.25 ppm indicated that hydrogens on the methylene of the methacrylate groups were present on the alginate backbone after modification.

.

References

[1] Chen Z, Fillmore CM, Hammerman PS, Kim CF, Wong K-K. Non-small-cell lung cancers: a heterogeneous set of diseases. Nat Rev Cancer 2014;14:535-46.
[2] Jemal A, Bray F, Center MM, Ferlay J, Ward E, Forman D. Global cancer statistics. Ca-Cancer J Clin 2011;61:69-90.
[3] Siegel RL, Miller KD, Jemal A. Cancer statistics, 2015. Ca-Cancer J Clin 2015;65:5-29.
[4] Manegold C. Chemotherapy for advanced non-small cell lung cancer: standards. Lung Cancer 2001;34 Suppl 2:S165-70.
[5] Lee WL, Guo WM, Ho VHB, Saha A, Chong HC, Tan NS, et al. Delivery of doxorubicin and paclitaxel from double-layered microparticles: The effects of layer thickness and dual-drug vs. single-drug loading. Acta Biomater 2015;27:53-65.
[6] Wong HL, Bendayan R, Rauth AM, Li Y, Wu XY. Chemotherapy with anticancer drugs encapsulated in solid lipid nanoparticles. Adv Drug Delivery Rev 2007;59:491-504.
[7] Marchal S, Hor AE, Millard M, Gillon V, Bezdetnaya L. Anticancer Drug Delivery: An Update on Clinically Applied Nanotherapeutics. Drugs 2015;75:1601-11.
[8] Carvalho FS, Burgeiro A, Garcia R, Moreno AJ, Carvalho RA, Oliveira PJ. Doxorubicin-induced cardiotoxicity: from bioenergetic failure and cell death to cardiomyopathy. Med Res Rev 2014;34:106-35.
[9] Hortobagyi GN. Anthracyclines in the treatment of cancer. An overview. Drugs 1997;54 Suppl 4:1-7.
[10] Aubel-Sadron G, Londos-Gagliardi D. Daunorubicin and doxorubicin, anthracycline antibiotics, a physicochemical and biological review. Biochimie 1984;66:333-52.
[11] Bonadonna G, Monfardini S, De Lena M, Fossati-Bellani F, Beretta G. Phase I and preliminary phase II evaluation of adriamycin (NSC 123127). Cancer Res 1970;30:2572-82.
[12] Rochette L, Guenancia C, Gudjoncik A, Hachet O, Zeller M, Cottin Y, et al. Anthracyclines/trastuzumab: new aspects of cardiotoxicity and molecular mechanisms. Trends Pharmacol Sci 2015;36:326-48.
[13] Singh MN, Hemant KSY, Ram M, Shivakumar HG. Microencapsulation: A promising technique for controlled drug delivery. Res Pharm Sci 2010;5:65-77.
[14] Janes KA, Fresneau MP, Marazuela A, Fabra A, Alonso MaJ. Chitosan nanoparticles as delivery systems for doxorubicin. J Controlled Release 2001;73:255-67.
[15] Li X, Ding L, Xu Y, Wang Y, Ping Q. Targeted delivery of doxorubicin using stealth liposomes modified with transferrin. Int J Pharm (Amsterdam, Neth) 2009;373:116-23.
[16] Couvreur P, Roblot-Treupel L, Poupon MF, Brasseur F, Puisieux F. Nanoparticulate Systems for Drug Delivery Nanoparticles as microcarriers for anticancer drugs. Adv Drug Delivery Rev 1990;5:209-30.
[17] Hrubý M, Koňák Č, Ulbrich K. Polymeric micellar pH-sensitive drug delivery system for doxorubicin. J Controlled Release 2005;103:137-48.
[18] Lee KY, Mooney DJ. Alginate: properties and biomedical applications. Progress in polymer science 2012;37:106-26.
[19] Wu H, Liao C, Jiao Q, Wang Z, Cheng W, Wan Y. Fabrication of core–shell microspheres using alginate and chitosan–polycaprolactone for controlled release of vascular endothelial growth factor. React Funct Polym 2012;72:427-37.
[20] Baimark Y, Srisuwan Y. Preparation of alginate microspheres by water-in-oil emulsion

.

method for drug delivery: Effect of Ca2+ post-cross-linking. Adv Powder Technol 2014;25:1541-6.
[21] Miao T, Fenn SL, Charron PN, Oldinski RA. Self-Healing and Thermoresponsive Dual-Cross-Linked Alginate Hydrogels Based on Supramolecular Inclusion Complexes. Biomacromolecules 2015;16:3740-50.
[22] Miao T, Rao KS, Spees JL, Oldinski RA. Osteogenic differentiation of human mesenchymal stem cells through alginate-graft-poly(ethylene glycol) microsphere-mediated intracellular growth factor delivery. J Controlled Release 2014;192:57-66.
[23] Jiang T, Kim YK, Singh B, Kang SK, Choi YJ, Cho CS. Effect of microencapsulation of Lactobacillus plantarum 25 into alginate/chitosan/alginate microcapsules on viability and cytokine induction. J Nanosci Nanotechnol 2013;13:5291-5.
[24] Sosnik A. Alginate Particles as Platform for Drug Delivery by the Oral Route: State-of-the-Art. ISRN Pharm 2014;2014:17.
[25] Machado AHE, Lundberg D, Ribeiro AJ, Veiga FJ, Lindman B, Miguel MG, et al. Preparation of Calcium Alginate Nanoparticles Using Water-in-Oil (W/O) Nanoemulsions. Langmuir 2012;28:4131-41.
[26] Jay SM, Saltzman WM. Controlled delivery of VEGF via modulation of alginate microparticle ionic crosslinking. J Controlled Release 2009;134:26-34.
[27] Tonnesen HH, Karlsen J. Alginate in drug delivery systems. Drug Dev Ind Pharm 2002;28:621-30.
[28] Fenn SL, Oldinski RA. Visible light crosslinking of methacrylated hyaluronan hydrogels for injectable tissue repair. J Biomed Mater Res, Part B 2015.
[29] Wagner DE, Fenn SL, Bonenfant NR, Marks ER, Borg Z, Saunders P, et al. Design and Synthesis of an Artificial Pulmonary Pleura for High Throughput Studies in Acellular Human Lungs. Cell Mol Bioeng 2014;7:184-95.
[30] Charron PN, Fenn SL, Poniz A, Oldinski RA. Mechanical properties and failure analysis of visible light crosslinked alginate-based tissue sealants. J Mech Behav Biomed Mater 2016;59:314-21.
[31] Jeon O, Bouhadir KH, Mansour JM, Alsberg E. Photocrosslinked alginate hydrogels with tunable biodegradation rates and mechanical properties. Biomaterials 2009;30:2724-34.
[32] Jeon O, Alsberg E. Photofunctionalization of alginate hydrogels to promote adhesion and proliferation of human mesenchymal stem cells. Tissue Eng, Part A 2013;19:1424-32.
[33] Jeon O, Alt DS, Ahmed SM, Alsberg E. The effect of oxidation on the degradation of photocrosslinkable alginate hydrogels. Biomaterials 2012;33:3503-14.
[34] Jeon O, Samorezov JE, Alsberg E. Single and dual crosslinked oxidized methacrylated alginate/PEG hydrogels for bioadhesive applications. Acta Biomater 2014;10:47-55.
[35] Nguyen AH, McKinney J, Miller T, Bongiorno T, McDevitt TC. Gelatin methacrylate microspheres for controlled growth factor release. Acta Biomater 2015;13:101-10.
[36] Hamidi M, Azadi A, Rafiei P. Hydrogel nanoparticles in drug delivery. Adv Drug Delivery Rev 2008;60:1638-49.
[37] Williams CG, Malik AN, Kim TK, Manson PN, Elisseeff JH. Variable cytocompatibility of six cell lines with photoinitiators used for polymerizing hydrogels and cell encapsulation. Biomaterials 2005;26:1211-8.

.

CHAPTER4: NANOPARTICLE-MEDIATED INTRACELLULAR FGF-2 DELIVERY AS A CELL-SELECTIVE, INTRACRINE CANCER THERAPEUTIC

Systemic toxicity and adverse events (AEs) are often unavoidable drawbacks of conventional chemotherapy. Therefore, it is highly desirable to develop more specific treatments to target cancer cells that avoid use of broad-spectrum toxins. Previous reports have shown that cytosolic fibroblast growth factor 2 (FGF-2) promotes chromatin compaction and death of cancer cells through intracrine-mediated activation of Extracellular signal Regulated Kinase (ERK1/2) and engagement of mitochondria. The goal of our study was to provide controlled, intracellular delivery of FGF-2 using alginate-graft-poly(ethylene glycol) nanoparticles (ABN) to activate the FGF-2 intracrine signaling mechanism(s) and reduce cancer cell proliferation. We observed that both adenocarcinomic human alveolar basal epithelial cells (A549 cells) and healthy bronchial epithelial cells (HBE) readily internalized ABN by means of non-selective endocytosis, and displayed intracellular trafficking within 24 hours. Compared with extracellular exposure to FGF-2, intracellular delivery of FGF-2 via ABN significantly reduced mitochondrial activity and significantly increased the nuclear content of activated-ERK1/2 in A549 cells. In contrast, HBE were not affected by ABN-mediated intracellular FGF-2 treatment. Our results demonstrate that FGF-2-loaded ABN hold promise as an effective cancer therapeutic that selectively targets cancer cells through the intracrine FGF-2 signaling pathway.

.

4.1. Introduction

Lung cancer is one of the most prevalent types of carcinoma, resulting in the largest number of cancer-related deaths worldwide.[1-3] Greater than 85% of lung cancer cases are classified as non-small-cell lung cancer (NSCLC), including adenocarcinoma, squamous-cell carcinoma, and large-cell carcinoma. Despite recent advances in early detection and cancer treatment, NSCLC is often diagnosed at a late stage in the disease and bears a poor prognosis.[1] Standard of Care treatment for NSCLC includes surgical resection of pulmonary lesions, combined with radiotherapy[4] or chemotherapy to prevent or reduce tumor-induced symptoms, prolong patient survival, and maintain quality of life.[5] Chemotherapy can last up to 6 months at high parenteral dosages, and is frequently associated with systemic toxicity[6, 7] and long-term adverse effects (AEs) for patients that include hearing loss, cardiomyopathy, sterility, and hypomagnesaemia.[8] Accordingly, cancer treatments that are selectively-cytotoxic and that prevent recurrence are highly sought after by clinicians and the biomedical research community.

Among the family of receptor tyrosine kinases (RTKs), fibroblast growth factor receptors (FGFRs) transmit signals from the extracellular space to the cytoplasm, and are commonly altered in cancer. FGFs are secreted glycoproteins that are readily sequestered by the extracellular matrix and cell surface. FGF-FGFR binding leads to receptor dimerization and trans-phosphorylation of tyrosine kinase domains,[9, 10] extracellular signal-regulated kinase 1 and 2 (ERK1/2) activation and nuclear transport;

these signals commonly result in cell proliferation, drug resistance, and neoangiogenesis.[11] FGFR signaling also plays significant roles in the invasion and survival of several types of tumor cells.[12-14] Notably, the ERK pathway is reported as a master regulator of cell proliferation, survival, transformation, and programmed death.[15-18]

Low and high molecular weight FGF-2 (lo-FGF-2 and hi-FGF-2) isoforms can have similar, as well as isoform-specific, effects on cell proliferation, differentiation, migration, and survival, and accumulate in varying proportions in different cell types.[19] Lo-FGF-2 is associated with paracrine/autocrine signaling – it is smaller and can be secreted from cells.[20] In contrast, hi-FGF-2 is a larger protein that is generally not secreted by cells.[21] The hi-FGF-2 isoform, specifically, has activity independent of cell surface FGFR activation and that instead involves an intracrine signaling pathway which activates ERK1/2. This, in turn, can activate a Death Associated Protein Kinase (DAPK) that promotes nuclear transport of ERK1/2, chromatin compaction and cell death.[22] Notably, several reports suggest the FGF-2 isoform can negatively impact cell division,[23-25] and endocytosis of FGF-2 bound latex microspheres by cultured avian cochleovestibular ganglion cells was shown to deplete cell surface FGFR.[26] Furthermore, hi-FGF-2 was shown to reduce glioma cell proliferation *in vivo* by inhibiting cell-cycle progression and protein translation.[27] Thus, intracellular delivery of FGF-2 has exciting potential to target proliferating cancer cells and may led to novel intracrine-based therapeutics for cancer patients.

Particle encapsulation is a core technology used in drug delivery systems,[28] and provides the following benefits: (a) uniform particle size and shape; (b) protective barrier from the extracellular environment; and (c) controlled temporal and drug release.[29] Nanoparticles encompass an assortment of colloidal nano-systems (<1 μm), capable of passing through biological barriers (i.e., passive targeting), and encapsulating drugs at relatively high densities. Compared with systemic or exogenous drug delivery methods, nanoparticles that deliver chemotherapeutics through intracellular means exhibit enhanced drug efficacy.[30]

Alginate, a naturally occurring biopolymer, has been formed into microspheres and used to deliver proteins, cytokines, cells, and small molecules.[31-33] However, the relatively large diameter, rapid drug-release,[34] and anionic properties of alginate particles impede efficient cellular uptake and drug encapsulation, limiting its clinical application. To overcome these limitations, we conjugated poly(ethylene glycol) onto alginate to form a slightly-neutralized alginate-*graft*-poly(ethylene glycol) (Alg-*g*-PEG), which was then used to form nanoparticles.[35] The Alg-*g*-PEG-based nanoparticles (ABN) improved cellular uptake compared with that of non-modified alginate nanoparticles.

Using an engineered ABN, here we investigate the direct, controlled intracellular delivery of FGF-2 as a potential intracrine-mediated cancer treatment. Unlike typical FGF-2 signaling, which requires cell surface FGF-2/FGFR dimerization, we delivered FGF-2 by non-FGFR-mediated endocytosis, via ABN, to determine

whether we could effectively activate an FGF-2-mediated intracrine signaling pathway. We hypothesized that non-FGFR-mediated internalization of FGF-2-loaded ABN would generate intracrine signals that are: 1) Selectively-toxic to proliferating cancer cells and 2) Relatively non-toxic for normal, healthy, non-cycling primary cells. Herein, for both diseased (transformed) and healthy (non-transformed) primary cells treated with FGF-2-loaded ABN, we report the routes of cellular uptake, internalization, and intracellular trafficking for FGF-2-loaded ABN. Furthermore, we demonstrate dramatic, specific effects of internalized, FGF-2-loaded ABN on the cytosolic and nuclear protein pools that correlate to decreased proliferation of cancer cells, but not of healthy primary cells.

4.2. Materials and Methods

4.2.1. Materials

Sodium alginate (M_w=65–75 kg/mol, 60–70% guluronic acid residues) was generously donated by FMC BioPolymer. Amine-poly(ethylene glycol)-thiol (NH_2-PEG-SH, M_w=1000 g/mol) and methyl-poly(ethylene glycol)-amine (mPEG-NH_2, M_w=500 g/mol) were purchased from Laysan Bio. N-ethyl-N′(3-dimethylaminopropyl) carbodiimide hydrochloric acid (EDC), N-hydroxysuccinimide (NHS), 2,2′-dithiodipyridine, methanol (MeOH, anhydrous, 99.8%), biology-grade mineral oil, Span 80, 3-(4,5-dimethylthiazol-2-yl)-2,5-diphenyltetrazolium bromide (MTT)-based *In Vitro* Toxicology Assay Kit, cholera toxin, bovine serum albumin (BSA) and dexamethasone were purchased from Sigma-Aldrich. One molar

hydrochloric acid (HCl) and 1 M sodium hydroxide were purchased from BDH ARISTAR®PLUS. Sodium citrate, isopropanol, calcium chloride ($CaCl_2$), sodium chloride (NaCl), magnesium chloride ($MgCl_2$), Alexa Fluor® 647 Cadaverine, 20x phosphate buffered saline (PBS), 4% paraformaldehyde (PFA) in PBS, Triton® X-100, 4-(2-hydroxyethyl)-1-piperazineethanesulfonic acid (HEPES), glycerol, phenylmethylsulfonyl fluoride (PMSF), sodium orthovanadate (Na_3VO_4), aprotinin, leupeptin, a bicinchoninic acid assay (BCA) kit, a subcellular protein fractionation kit for cultured cells, and BupH™ MES Buffered Saline Packs were purchased from Fisher Scientific. Fetal bovine serum (FBS) was purchased from Atlanta Biologics. Dulbecco's Modification of Eagle's Medium (DMEM, glutaGRO™)/F-12 media, penicillin, streptomycin and trypsin EDTA were purchased from Corning Cellgro. A human FGF ELISA Kit was purchased from BioLegend. Human anti-FGF-2 antibody and immunoglobulin G (IgG) (rabbit) were purchased from Abcam. Human epidermal growth factor (EGF), insulin, transferrin, and bovine pituitary extract (BPE) were purchased from Lonza. A549 (CCL-185™) adenocarcinomic human alveolar basal epithelial cells (A549 cells) and healthy bronchial epithelial cells (HBEs), were isolated and cultured in Dr. Van der Vliet's laboratory.[36]

4.2.2. Alginate-g-PEG Sub-microsphere (ABN) Fabrication

FGF-2-loaded ABN Fabrication

ABN fabrication was based on our previous work, including Alg-g-PEG synthesis.[35] FGF-2 was added to a 1% (w/v) Alg-g-PEG solution at a weight ratio of

1:10^5 (FGF-2:polymer). ABNs without FGF-2 were fabricated as blank controls. At room temperature, 1 mL of Alg-g-PEG/FGF-2 solution was added to 6.72 mL of 5% (v/v) Span 80 in mineral oil and mixed at 1200 rpm for 5 minutes. Next, 400 µL of 30% (v/v) Tween 80 in mineral oil was added followed by the slow addition of 5 mL of 2 M calcium chloride ($CaCl_2$) solution. The emulsion was mixed for 30 minutes, 3 mL of isopropanol was added, and then the emulsion was centrifuged at 4000 rpm for 5 minutes. ABNs were washed sequentially with isopropanol (x2) and DI water (x2). The size and zeta-potential of ABNs were determined using dynamic light scattering (DLS, Zetasizer Nano ZSP, Malvern) in PBS at pH = 7.4, room temperature. ABNs were flash frozen in liquid N_2, lyophilized, and characterized by scanning electronic microscopy (SEM, JEOL 600); samples were sputter coated with 45 nm of gold/palladium (Au/Pd).

FGF-2 Encapsulation and In Vitro FGF-2 Release Assay

Lyophilized FGF-2-loaded ABNs were dissolved in 3% (w/v) sodium citrate solution.[37] The FGF-2 concentration was measured using a BioLegend ELISA Development Kit as per manufacturer's instructions.

4.2.3. Cellular uptake of ABNs

Cellular Uptake

A549 cells and HBEs were seeded in 6 well plates at $3x10^5$ per well and cultured until they reached 80% confluence.[6,38] A549 cell culture medium contained DMEM/F12, 10% FBS, and 1% penicillin/streptomycin. HBE culture medium

contained DMEM/F12, cholera toxin (10 ng/mL), epidermal growth factor (10 ng/mL), transferrin (5 μg/mL), BPE (15 μg/mL) and BSA (0.5 mg/mL). ABN were labeled with AlexaFluor 647 via carbodiimide chemistry and added to cells at 100 μg/mL (n=3). After 24 hours of co-culture, medium was removed and the adherent cells were thoroughly rinsed with PBS. Cells were trypsinized and centrifuged at 200 x g for 10 minutes, and then re-suspended and fixed in 1 mL of 4% PFA in PBS for 10 minutes. After fixation, cells were centrifuged to remove excess PFA, and thoroughly rinsed with 1 x PBS. Cells were re-suspended in sterile PBS and transferred to 5 mL polystyrene round-bottom tubes for flow cytometry to determine the percentage of the cell population that internalized ABN (BD LSRII Flow Cytometer). Alexa 647-positive cell population percentages were gated with non-treated cells and those treated with non-labeled ABN.

Route of Internalization and Intracellular Transportation

Blank ABN were labeled with AlexaFluor 647 via carbodiimide chemistry, and suspended in medium with various blockers of endocytosis– 1) chlorpromazine hydrochloride (CH) to inhibit clathrin-mediated endocytosis[38] (10 mg/mL); 2) nyastin (NY) to inhibit caveolar-mediated endocytosis[39] (25 μg/mL); 3) colchicine (CO) to inhibit macropinocytosis[40] (40 μg/mL); and 4) dynasore (DY) to inhibit dynamin[41, 42] (80 μM).[43] A549 cells were seeded in 6-well plates at $3x10^5$ per well and cultured until they reached 80% confluence. Cells were incubated in the presence of blank AlexaFluor 647-labeled ABN (n=3) at 100 μg/mL, 37°C and 5%

CO_2. After 30 minutes, culture medium was removed and adherent cells were thoroughly rinsed with sterile PBS to remove non-internalized ABN. Cell samples were prepared for flow cytometry (*vida supra*). A Tukey test was performed to compare the difference of the percentage of cells with ABN between non-blocked groups and blocked groups. To verify that fluorescent signals were coming from internalized ABN, and not membrane-bound ABN, the same cell samples were imaged using confocal laser scanning microscopy (CLSM, Zeiss LSM 510 META). Z-stack images were obtained with AimImage Software.

To track ABN internalization, A549 cells were incubated with AlexaFluor 647-labeled ABN (100 µg/mL) and rhodamine-labeled dextran (12.5 mg/mL) for 10 and 30 minutes, and 3 and 24 hours.[44, 45] Cells with non-labeled dextran, and without any treatments, were prepared as controls. At different time points, medium was removed and adherent cells were thoroughly-rinsed with PBS. Cells were prepared for CLSM (*vida supra*) and z-stack images were obtained.

A549 cells were seeded on sterile Nunc™ Thermanox™ Coverslips in 6-well plates overnight in preparation for transmission electron microscopy (TEM). ABN (100 µg/mL) were added to the medium and co-cultured for 10 and 30 minutes, and 1, 4, 8, 12, 24 and 48 hours. At each time point, medium was removed and cells were thoroughly-rinsed with PBS. Cells were fixed for 30 minutes in Karnovsky's fixative (2.5% glutaraldehyde, 1% PFA in 0.1 M PBS) at 4°C, rinsed with Millonig's phosphate buffer, and post-fixed in 1% osmium tetroxide (OsO4) in 0.1 M cacodylate buffer at

4°C for 30 minutes. Samples were dehydrated in a graded series of ethanol, through propylene oxide, and infiltrated and embedded in Spurr's resin. Ultra-thin sections were cut with a diamond knife, placed onto 200 mesh nickel thin-bar grids, and contrasted with alcoholic uranyl acetate and lead citrate. Grids were viewed with a TEM (JEOL 1400 USA, Inc.) operating at 60 or 80 kV, and digital images were acquired with an AMT-XR611 11 megapixel ccd camera.[46, 47] A customized Matlab code was written to measure particle diameters using TEM images, providing an image-based average size of internalized ABNs.[48, 49]

4.2.4. Bioactivity of Cells after 24 treatment of FGF-2 Intracellularly

Mitochondrial Activity Assay

A549 cells and HBE cells were seeded in 24 well plates at $5*10^4$ per well and cultured until reaching 80% confluent. ABNs with or without FGF were added to cell seeded plates at concentration of 100 μg/ml were added to each well and co-culturing for 24h with n=3 replicates. Extracellular FGF-2 (20 ng/ml) and ABNs with BSE (100 μg/ml) were also added to cells serving as controls. After 24h co-culturing, medium with ABNs were removed and fresh full medium without ABNs was added to culture for another 24h. Finally, fresh medium was washed with PBS for three times. then analyzed using a MTT-based In Vitro Toxicology Assay Kit following the manufacturer's protocol. The optical density was measured at 570 nm using a BioTek plate reader. Background absorbance at 690 nm was subtracted from the measured

absorbance. Absorbance values for the experimental and control samples were normalized to non-modified TCPS controls[50].

Western Blot

The production of ERK1/2 proteins in A549 cells and HBEs, after treatment with ABN, was determined by immunoblotting.[23] Six control and experimental groups were prepared – 1) cells without any treatment; 2) cells with FGF-2-loaded ABNs; 3) cells with extracellular FGF-2 (20 ng/ml); 4) cells with blank ABNs; 5) cells treated with 2 μg/mL anti-FGF for 30 minutes, and FGF-2-loaded ABNs; and 6) cells treated with 2 μg/mL IgG for 30 minutes, and with FGF-2-loaded ABNs. Cells were plated and cultured until 80% confluence, and the different treatments were added to the cultures for 24 hours. For whole cell protein analysis, cells were lysed using 200 μL of 1x western solubilization lysis buffer (1% Triton X-100, 50 mM HEPES, 250 mM NaCl, 10% glycerol, 1.5 mM MgCl, 1 mM PMSF, 1 mM EGTA, 2 mM Na3VO4, 10 μg/mL aprotinin, 10 μg/mL leupeptin), pH 7.4, per well. For cellular fraction protein analysis, protein samples from membrane/cytosol and nuclei fractions were obtained using a subcellular protein fractionation kit based on the manufacturer's protocols. Equal amounts of protein (20-25 μg; determined using BCA protein assay) were separated on Novex 10% Tris-Glycine gels, transferred to nitrocellulose membranes, and blotted using antibodies against pERK-1/2 (#4370; 1:1000; Cell Signaling) and Erk1/2 (#4695; 1:1000; Cell Signaling).[43, 51]

4.3. Results

4.3.1. ABN Fabrication and Characterization

Blank and FGF-2-loaded ABNs were fabricated using a water/oil emulsion based on our previous reports.[52] SEM images of lyophilized ABNs depicted a textured surface and spherical morphology (**Fig.4-1A,B**). To quantify ABN properties, we used dynamic light scattering (DLS) on suspended ABNs at physiological conditions. Indeed, the greatest population of particles were <100 nm and the average hydrodynamic diameter of FGF-2-loaded ABN was 84 nm (**Fig.4-1C)**. ABN were slightly negative and the average surface charge of ABN was -8 mV (**Fig.4-1D**). This was expected, since alginate is an anionic molecule.[33] Furthermore, with only 10% PEGylation, ABN should retain some electronegativity.[35] The encapsulation efficiency (i.e. amount of drug retained) of FGF-2 after loading and ABN fabrication was 60%, an appreciably high value; however, in the future, it may be possible to optimize the ABN fabrication to improve upon this value. Using the encapsulation efficiency, FGF-2 release in buffered saline at 37˚C was quantified over the course of 2 weeks. FGF-2 diffusion occurred for 14 days, although the rate of release leveled -off after 8 days, and a FGF-2 concentration around 10 ng/mL was maintained (**Fig.4-1E**). While the data demonstrate that FGF-2 was loaded and subsequently released from the ABNs, it is critical that FGF-2 remain within ABN until cellular uptake occurs. Although only ~30% of the drug was released within the first day, our data suggest that further optimization could help to limit the extracellular release of FGF-2 from ABNs.

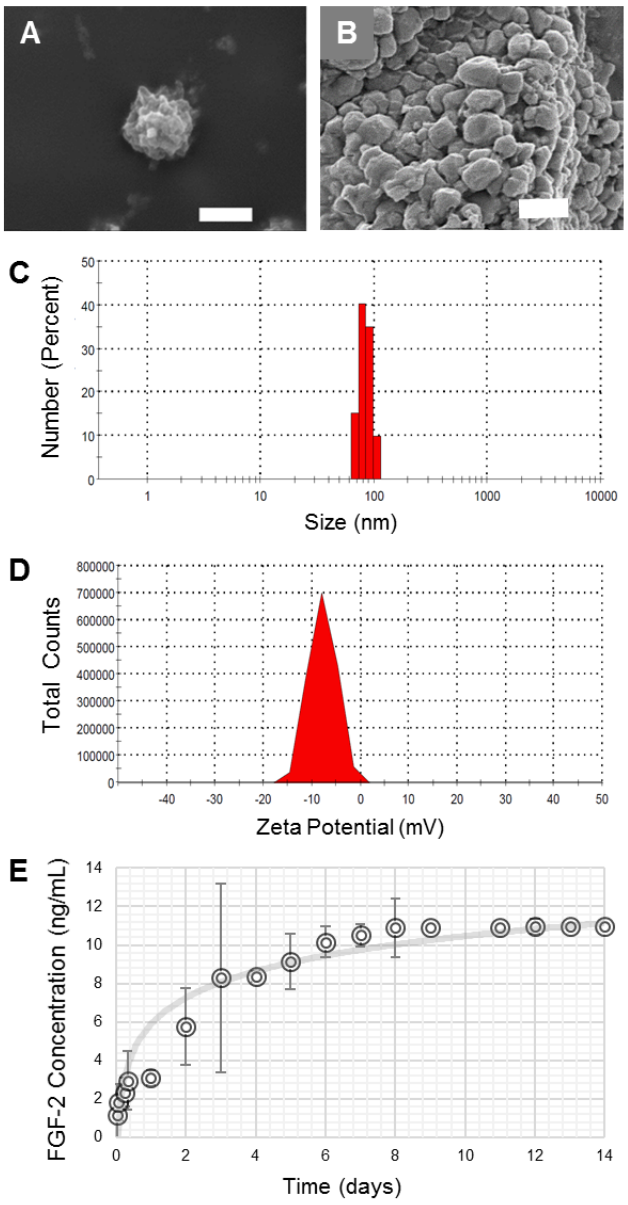

Figure 4-1. Scanning electron micrographs depicting spherical ABNs with (A) scale bar = 1 µm and (B) scale bar = 500 nm. (C) Hydrodynamic diameter distribution of FGF-2-loaded ABNs, measured in PBS, pH 7.4, 37˚C, and reported as number-average mean (84 nm). (D) Hydrodynamic zeta-potential distribution was measured in PBS, pH 7.4, and reported as number-average mean (-8 mV). (E) Cumulative FGF-2 release from 5 mg

.

ABNs over 14 days; FGF-2 concentration (ng/mL) was measured with an ELISA; FGF-2 encapsulation efficiency was 60%.

4.3.2. ABN Internalization

Logarithmic plots of non-treated cells (**Fig.4-2A,E**), and cells treated with non-labeled ABNs (**Fig.4-2B,F**), were prepared as controls (with positive cell populations <1.3%) and used to establish gates for AlexaFluor 647-labeled ABN experimental groups. Further flow cytometry analysis demonstrated that >40% of A549 cells (**Fig.4-2C**) and >15% of HBEs (**Fig.4-2G**) internalized AlexaFluor 647-labeled ABNs after 24 hours of culture. Histograms (**Fig.4-2D,H**) demonstrate clear shifts in fluorescent intensities between control and experimental groups for each cell type, demonstrating successful internalization and more efficient uptake of ABNs cultured with cancer cells compared to healthy cells. The median fluorescence intensity (MFI) for non-treated A549 cells and for A549 cells treated with non-labeled ABN were 355 and 375, respectively, whereas the MFI for AlexaFluor 647-labeled ABNs notably increased to 1155 (**Fig.4-2D**). The MFI for non-treated HBEs and HBEs treated with non-labeled ABN were only 361 and 328, respectively, whereas the MFI for AlexaFluor 647-labeled ABNs increased to 838 (**Fig.4-2H**).

.

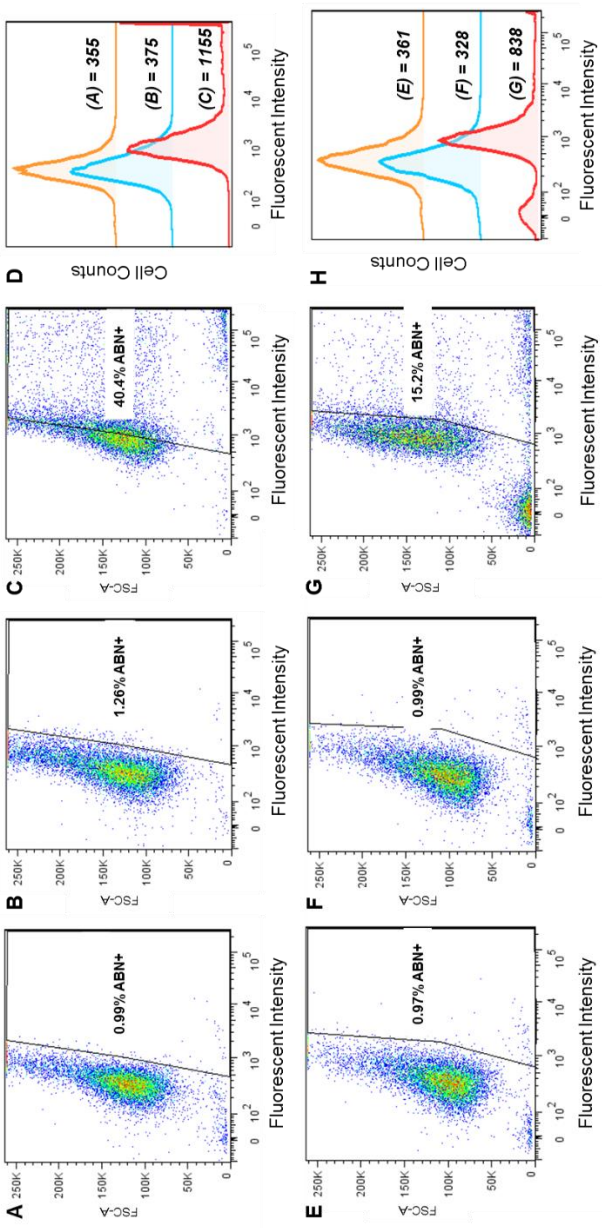

Figure 4-2. Flow cytometry and quantification of the cell population (%) that internalized ABN after 12 hours of co-culture at concentration of 100 µg/ml: A549 cells (top panel) and HBEs (bottom panel). (**A,E**) Non-treated cell controls; (**B,F**) cells treated with non-labeled ABNs; (**C,G**) cells with treated with AlexaFluor 647-labeled ABNs; and (**D,H**)

.

cell count curves plotted on a log scale showing representative mean fluorescent intensities (MFI) for each control and experimental group.

Endocytosis Assay

We explored the endocytic pathways used by A549 cells to internalize ABN in order to further understand the cellular mechanism mediating the process. The inhibition of clathrin-mediated endocytosis significantly reduced the ABN-positive cell population more than other blockers and decreased ABN uptake by 41% (**Fig.4-3A**), suggesting that endocytosis played a key role in transport of ABN across the cell membrane. The inhibition of macropinocytosis had the least effect on ABN uptake, reducing internalization by 24%. Indeed, compared with the control group (without any blockers), all four blockers significantly decreased ABN uptake, suggesting that a combination of multiple pathways may be involved.[53, 54] In addition, viability of A549 cells was not significantly affected by the inhibition of endocytosis during the 30 minutes of culture (**Fig.4-3B**). To verify that ABN were indeed inside cells, CLSM was performed following flow cytometry. Z-stack merged images confirmed AlexaFluor 647-labeled ABN (red) were located inside the cytoplasm rather than adhered to the cell surface (**Fig.4-3C, D, E, F**).

.

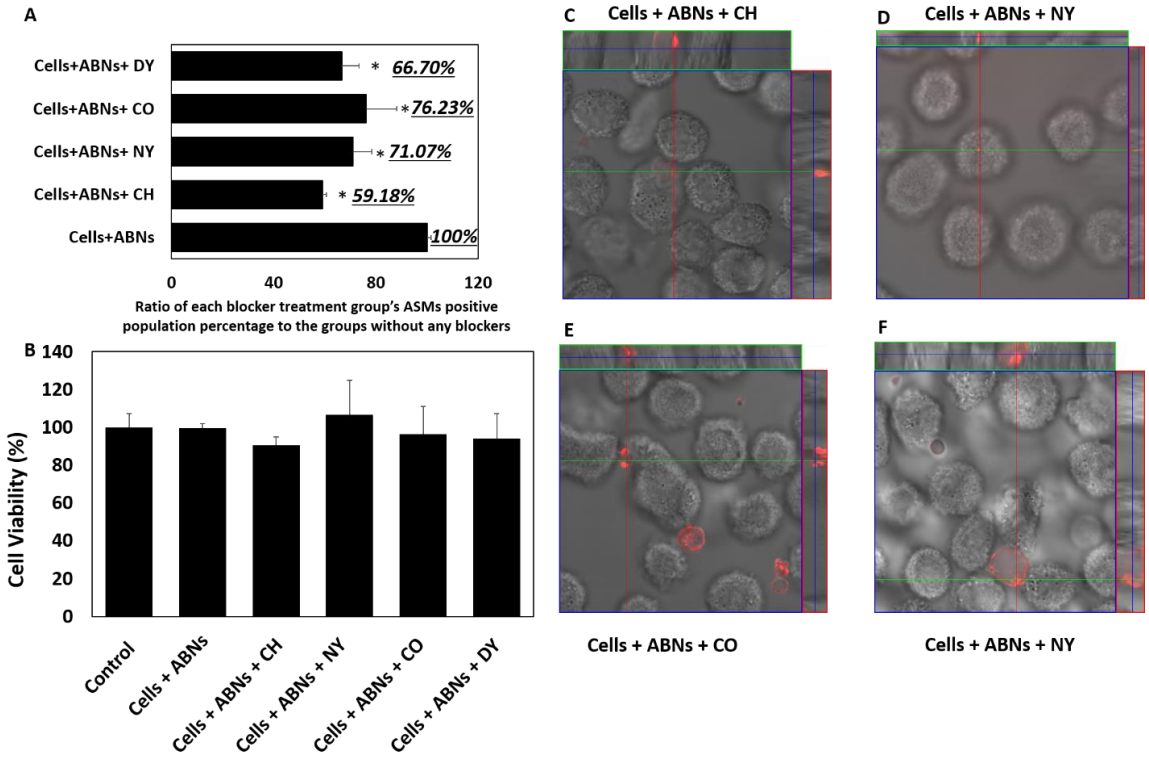

Figure 4-3 Endocytosis-dependent ABN uptake by A549s. Results are presented as a percentage of the ABN-positive A549 cell population after treatment with various blockers and normalized to the control. (ANOVA, *p < 0.01 versus ABN control, n=3). Clathrin-inhibitors demonstrated the greatest reduction in ABN-positive cell populations. (**B**) The effect of ABN exposure and inhibition of endocytosis on mitochondrial activity in A549 cells after 30 minutes of culture was not significant. (**C**) CLSM merged images of A549 cells verified ABN internalization (red).

4.3.3. Intracellular Trafficking of ABNs

Internalization by A549 cells and vesicle-mediated intracellular transport of

.

AlexaFluor 647-labeled ABN (red) was confirmed by culturing with rhodamine-labeled dextran (green), which is enclosed in membrane-bound vesicles during intracellular transport (e.g., endosomes and lysosomes). After culturing for 10 minutes, fluorescent signals for both ABN (red) and dextran (green) were visible, and merged images verified co-localization (yellow) of ABN within dextran-labeled vesicles (**Fig.4-4A**). Thus, the CLSM data complemented our previous flow cytometry data, demonstrating that ABN are internalized in membrane-bound vesicles. Next, we examined cultures after 24 hours to determine if ABN were escaping endo/lysosomes. Indeed, there appeared to be less overlay between dextran-labeled lysosomes and ABN, indicating that ABN were escaping lysosomes (**Fig.4-4B**). We hypothesize that the mechanism is via ABN swelling , or the proton sponge effect in the relatively low-pH lysosomes, thereby causing vesicles to burst and release their contents within the cytoplasm.[55] Notably, however, this concept will need to be investigated further.

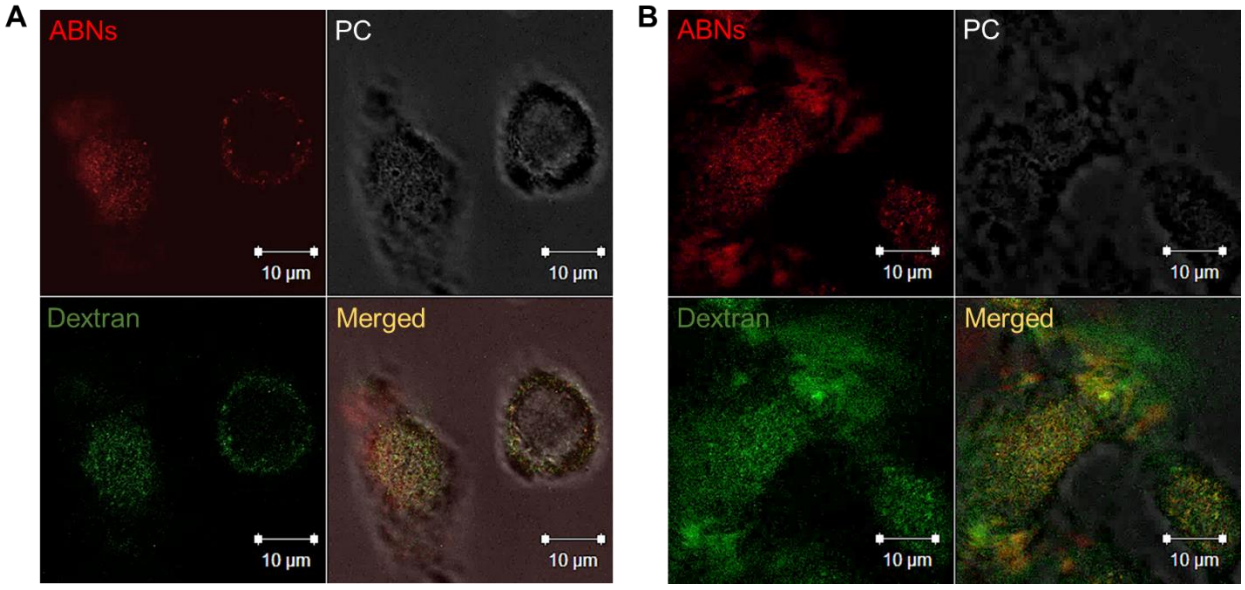

Figure 4-4. CLSM images of A549 cells cultured with AlexaFluor 647-labeled ABN (red) and rhodamine-labeled dextran (green) after (**A**) 10 minutes and (**B**) 24 hours of incubation. PC = phase contrast.

CLSM was followed by transmission electron microscopy (TEM). Compared to images of non-treated (control) cells, in images of treated cells, the ABN were clearly distinguishable from intracellular compartments and organelles due to their dark contrast and spherical shape (**Fig.4-5A**). In TEM images of A549 cells exposed to ABN, extension of the cell membrane and endocytosis were seen within 30 minutes' post-incubation (**Fig.4-5B**). At 4 hours' post-incubation, higher concentrations of ABNs were seen within the cell, close to the cell membrane (**Fig.4-5C**). ABN located at the edge of the cell membrane were still detectable at later time points, and we hypothesized that cellular endocytosis and exocytosis were occurring continuously. At 8 hours' post-incubation, the density of ABN decreased in the cytoplasm, however, the ABN that remained in the cell localized closer to the nucleus (**Fig.4-5D**). At later time points, ABN located at the edge of the cell membrane were still detectable, indicating that cellular endocytosis and exocytosis had continued. At 24 and 48 hours post-incubation, ABNs localized to the nucleus and appeared to interact with the nuclear membrane (**Fig.4-5E,F**). Using a custom-written MATLAB code, we performed a numerical analysis of the internalized ABN in the TEM micrographs, and determined the average size of ABN internalized by the cells was 297 nm (diameter). This value differed from that detected by DLS since it could only measure ABN inside cells. Both

.

the CLS and TEM photos confirmed the destination/fate of endocytosed nanoparticles, namely that they surrounded cell nuclei while releasing bioactive ABN contents. Of interest, our analysis indicated that intracellular trafficking of nanoparticles should likely be considered as important as particulate design and characterized whenever new particulate types are being developed.

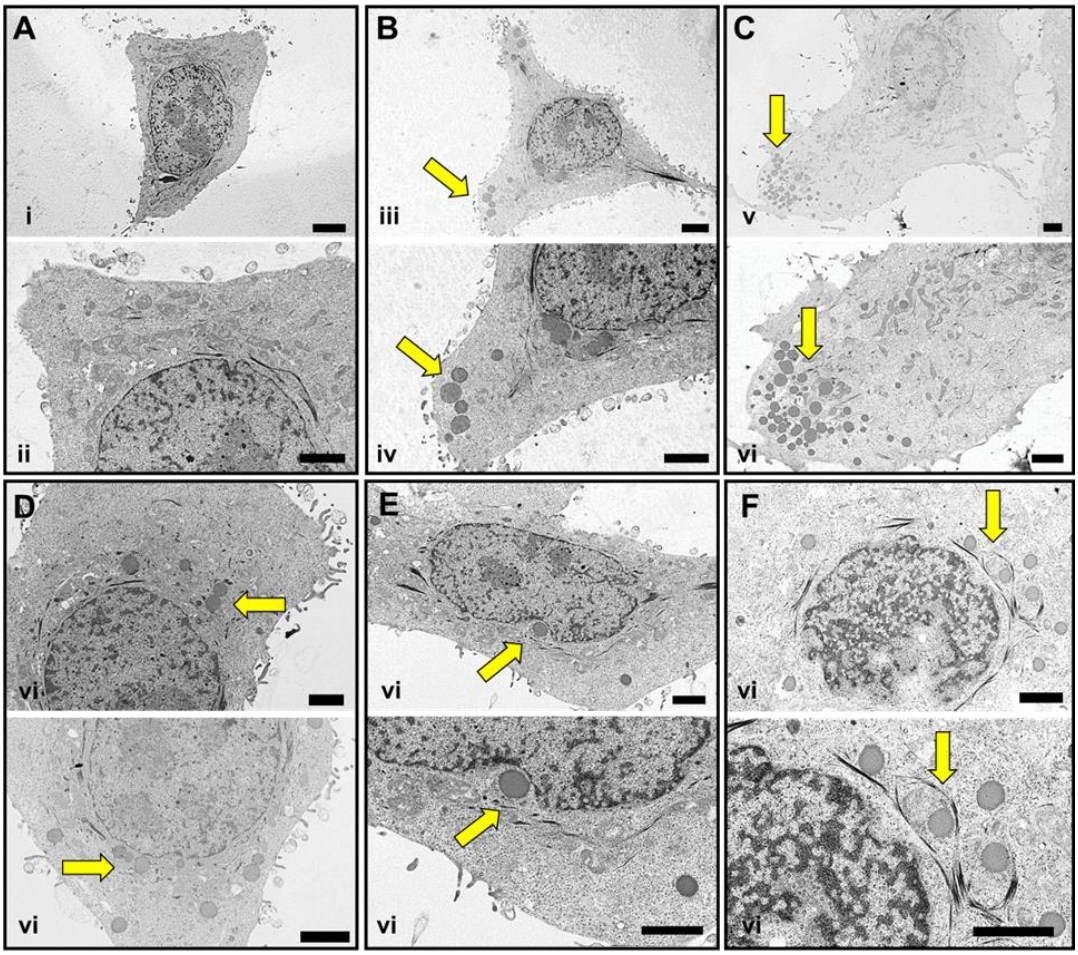

Figure 4-5. TEM images of A549 cells without exposure to ABN (A) or with exposed to ABN for (B) 30 minutes, (C) 4 hours, (D) 8 hours, (E) 24 hours, and (F) 48 hours. Two images at different magnifications are shown for each time point, scale bar = 2 μM.

.

Yellow arrows indicate the location of ABN.

4.3.4. Bioactivity of FGF-2 Intracellular Delivery

ABN (e.g. blank and FGF-2-loaded) cytotoxicity and the effects on healthy and diseased cell ERK1/2 activation were used to determine the bioactivity of FGF-2 and the effectiveness of our delivery system. After 24 hours of exposure, our results indicated that FGF-2-loaded ABN significantly decreased MTT activity in A549 cells, while the exogenous (i.e. free) FGF-2 significantly increased MTT activity (**Fig.4-6A**). Notably, no significant effect was seen in HBEs after exposure to FGF-2 loaded ABN indicating these effects may be selective for cancer cells; however, mitochondrial activity slightly increased due to exposure to exogenous FGF-2 (**Fig.4-6B**). As expected, blank ABN had no significant effect on either cell type.

To determine further whether or not the cytotoxic effects correlated with changes in ERK1/2 activation, we first examined whole cellular protein lysates and observed no significant difference between treatment groups, in either cell type (**Supplemental Information**). Therefore, we quantified ERK1/2 activation in different cellular fractions (membrane/cytosol and nucleus). Immunoblotted protein bands for phosphorylated ERK (pERK1/2) and total ERK (tERK1/2) are shown in **Fig.4-6C,D**. Nuclear ERK1/2 activation in A549 cells treated with FGF-2-loaded ABN was the highest compared with that of control or other treatment groups (**Fig.4-6E**). The second highest amount of activated nuclear ERK1/2 was associated with exogenous FGF-2, however, values were approximately 50% that of the FGF-2-loaded ABN treatment

.

group. Most notably, compared with levels in control cells and those for the other treatment groups, the level of nuclear ERK1/2 activation in HBEs decreased (**Fig.4-6F**). Thus, we found that the distribution of ERK1/2 was governed by the stimulus concentration, the route of stimulation (paracrine vs. intracrine), and the duration of stimulation.

Reports in the literature suggest that upregulation of nuclear ERK1/2 may lead to apoptosis and cell death,[56] which supports the cumulative bioactivity data for FGF-2-loaded ABNs (summarized in **Fig.4-7)**. Nuclear activation of ERK1/2 upregulates p53 expression, which is a pro-apoptotic protein known to induce chromatin compaction and cell death.[57, 58] Conversely, cytosolic ERK1/2 activation can inhibit nuclear ERK1/2 activation, inducing cell proliferation.[57] In addition, the ERK/p53 signal transduction pathway is also involved in various chemotherapeutic-induced cell apoptotic events.[56, 57, 59] In agreement with our observations, Ma *et al.* suggested that mitochondrial engagement plays an important role in inducing chromatin compaction and cell death.[22]

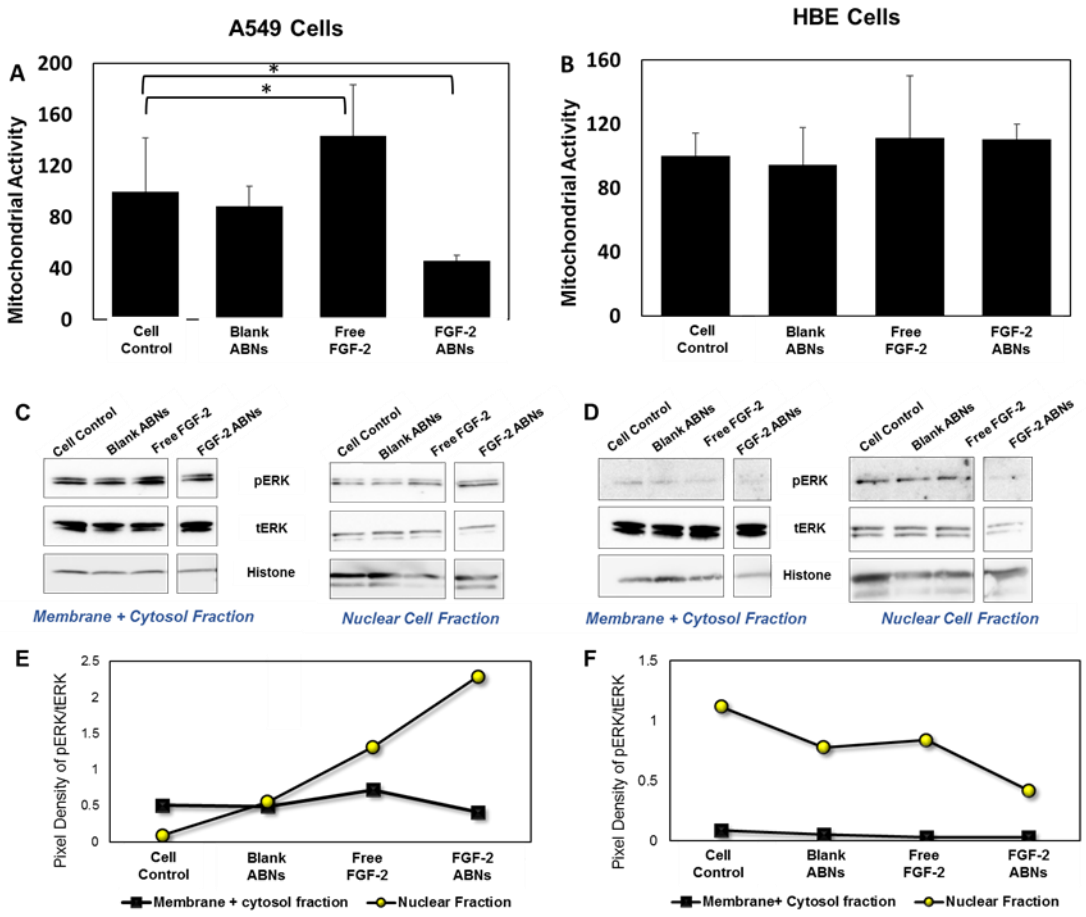

Figure 4-6. In vitro MTT test result of different treatments (non-treated control group, empty ASNs, extracellular FGF-2, and FGF-2 loaded ABNs) with HBE cells and A549 cells. (**C, F**) western blot photos of both membrane cytosol ERK1/2 activation and nuclear ERk1/2 activation for HBE cells and A549 cells. (**B, E**) OD reading ratio of pERK/ERK of western blot bands in both membrane/cytosol fraction and nuclear fraction for HBE cells and A549 cells.

.

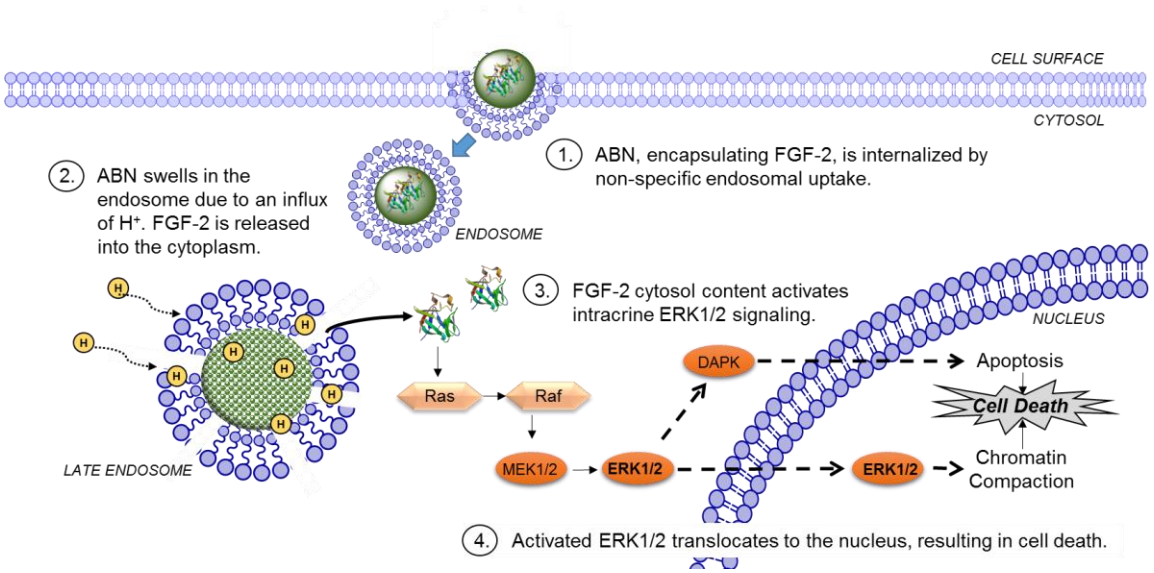

Figure 4-7. Schematic representation of proposed internalization and intracellular activity of FGF-2-loaded ABNs.

4.4 Conclusions

This study is the first to report on the toxic effects of ABN-mediated FGF-2 delivery on cancer cells. We demonstrated successful cellular uptake using flow cytometry and electron microscopy, and our data suggest ABN are internalized through non-specific endocytosis. Healthy cells did not respond significantly when dosed with FGF-2 loaded ABNs. However, when delivered to cancer cells, intracellular delivery of FGF-2 via ABN produced significantly higher cytotoxic effects that correlated to significantly higher activated-ERK1/2 nuclear content. Notably, the growth-inhibitory effects of intracellular FGF-2 may be broadly applicable to various cancers of the lung transformed epithelial cells in general, and perhaps those of other tissues/organs. Moving forward, we are excited to now determine the efficacy of FGF-2 loaded ABNs to treat animal models of tumorigenesis and metastasis.

.

4.5 Supplemental Materials

DLS Result for ABNs

Size distribution by number

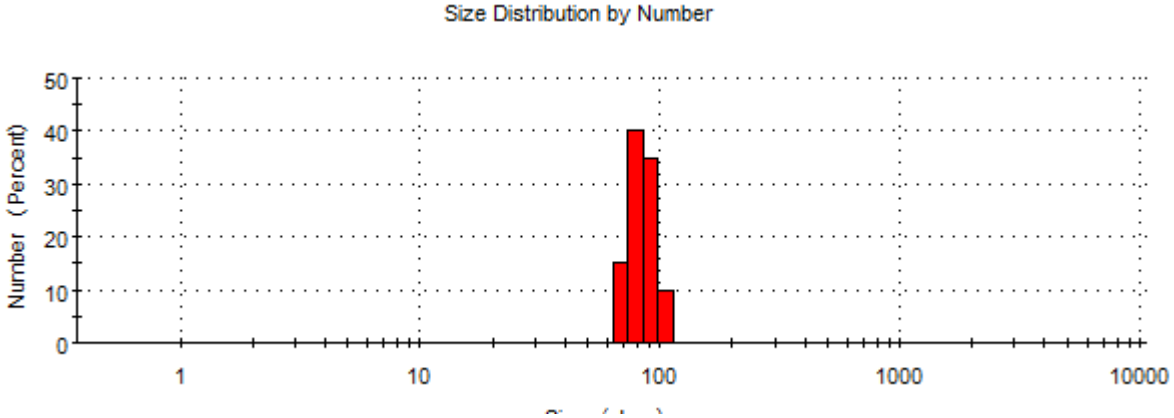

Size distribution by intensity

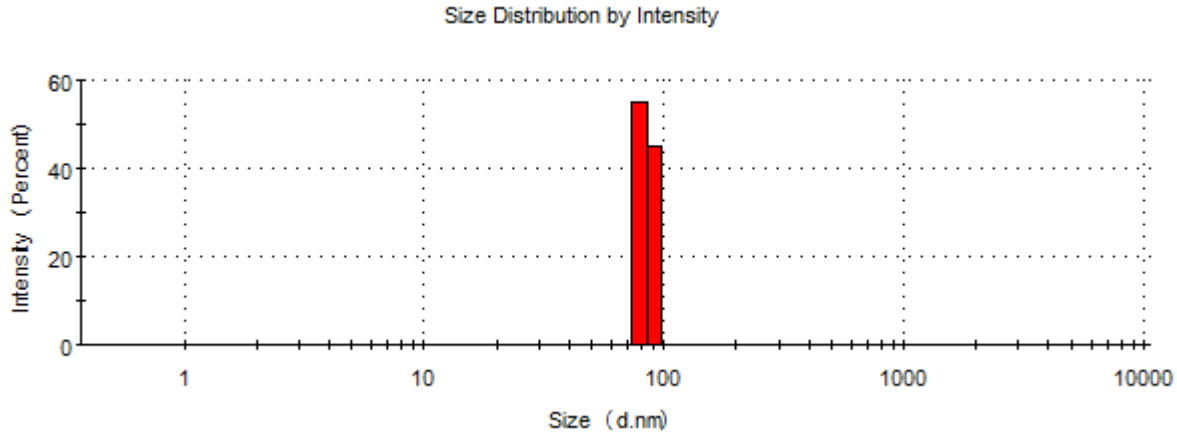

Size distribution by Volume

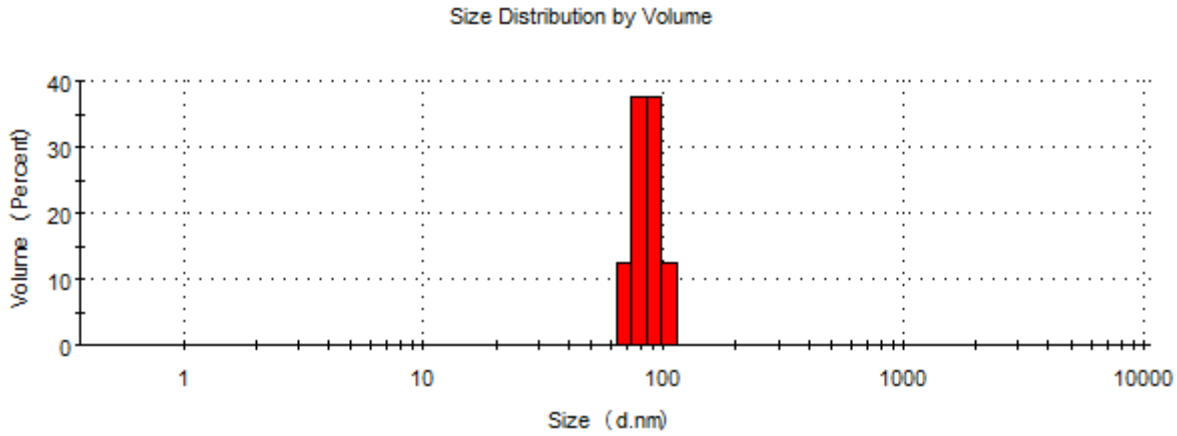

Zeta potential by number

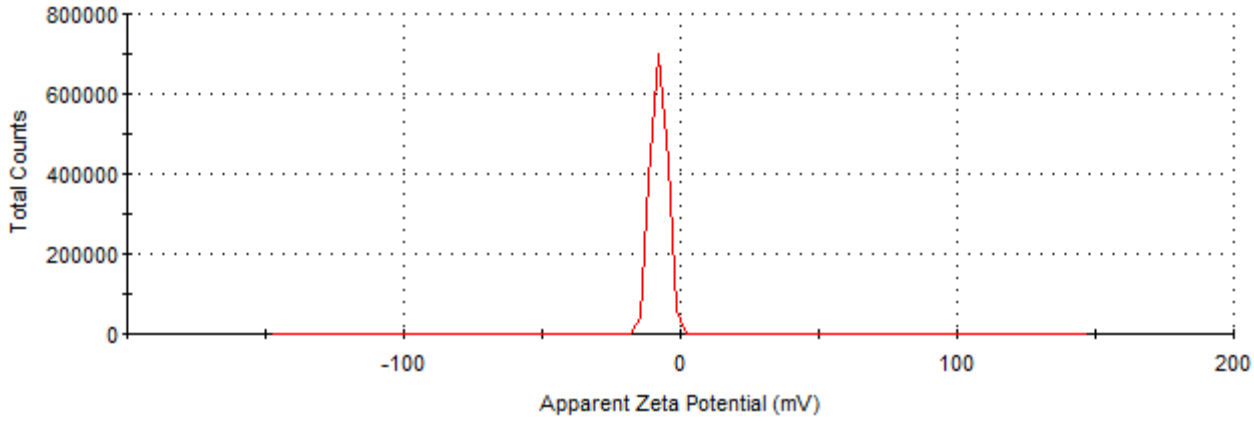

Total Protein ERK1/2 western blot

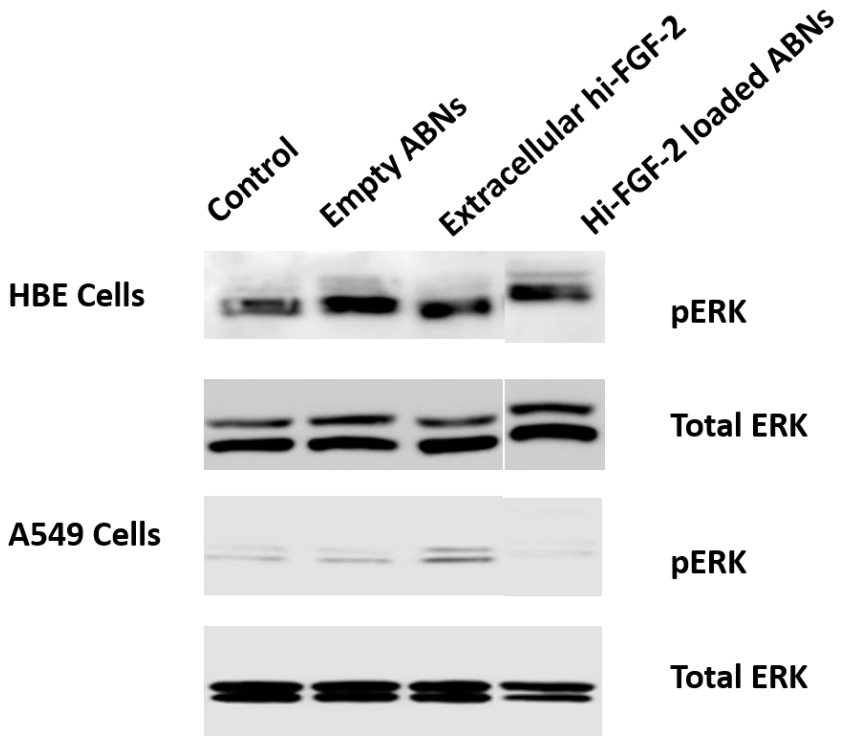

.

Reference

[1] Chen Z, Fillmore CM, Hammerman PS, Kim CF, Wong K-K. Non-small-cell lung cancers: a heterogeneous set of diseases. Nat Rev Cancer 2014;14:535-46.
[2] Jemal A, Bray F, Center MM, Ferlay J, Ward E, Forman D. Global cancer statistics. CA Cancer J Clin 2011;61:69-90.
[3] Siegel RL, Miller KD, Jemal A. Cancer statistics, 2015. CA: A Cancer Journal for Clinicians 2015;65:5-29.
[4] Marina N, Gebhardt M, Teot L, Gorlick R. Biology and therapeutic advances for pediatric osteosarcoma. The oncologist 2004;9:422-41.
[5] Manegold C. Chemotherapy for advanced non-small cell lung cancer: standards. Lung cancer (Amsterdam, Netherlands) 2001;34 Suppl 2:S165-70.
[6] Lee WL, Guo WM, Ho VHB, Saha A, Chong HC, Tan NS, et al. Delivery of doxorubicin and paclitaxel from double-layered microparticles: The effects of layer thickness and dual-drug vs. single-drug loading. Acta Biomaterialia 2015;27:53-65.
[7] Wong HL, Bendayan R, Rauth AM, Li Y, Wu XY. Chemotherapy with anticancer drugs encapsulated in solid lipid nanoparticles. Advanced Drug Delivery Reviews 2007;59:491-504.
[8] Wagner ER, Luther G, Zhu G, Luo Q, Shi Q, Kim SH, et al. Defective osteogenic differentiation in the development of osteosarcoma. Sarcoma 2011;2011.
[9] Dieci MV, Arnedos M, Andre F, Soria JC. Fibroblast Growth Factor Receptor Inhibitors as a Cancer Treatment: From a Biologic Rationale to Medical Perspectives. Cancer Discov 2013;3:264-79.
[10] Korc M, Friesel RE. The role of fibroblast growth factors in tumor growth. Curr Cancer Drug Targets 2009;9:639-51.
[11] Touat M, Ileana E, Postel-Vinay S, Andre F, Soria JC. Targeting FGFR Signaling in Cancer. Clin Cancer Res 2015;21:2684-94.
[12] Turner N, Grose R. Fibroblast growth factor signalling: from development to cancer. Nat Rev Cancer 2010;10:116-29.
[13] Brooks AN, Kilgour E, Smith PD. Molecular pathways: fibroblast growth factor signaling: a new therapeutic opportunity in cancer. Clin Cancer Res 2012;18:1855-62.
[14] Dienstmann R, Rodon J, Prat A, Perez-Garcia J, Adamo B, Felip E, et al. Genomic aberrations in the FGFR pathway: opportunities for targeted therapies in solid tumors. Ann Oncol 2014;25:552-63.
[15] Shindo Y, Iwamoto K, Mouri K, Hibino K, Tomita M, Kosako H, et al. Conversion of graded phosphorylation into switch-like nuclear translocation via autoregulatory mechanisms in ERK signalling. Nat Commun 2016;7:10485.
[16] Yoon S, Seger R. The extracellular signal-regulated kinase: Multiple substrates regulate diverse cellular functions. Growth Factors 2006;24:21-44.
[17] Kamata T, Hattori Y, Hamada H, Kizaki M, Terada M, Ikeda Y. Keratinocyte growth factor regulates proliferation and differentiation of hematopoietic cells expressing the receptor gene K-sam. Exp Hematol 2002;30:297-305.
[18] Caunt CJ, McArdle CA. ERK phosphorylation and nuclear accumulation: insights from single-cell imaging. Biochem Soc Trans 2012;40:224-9.
[19] Delrieu I. The high molecular weight isoforms of basic fibroblast growth factor (FGF-2): an insight into an intracrine mechanism. FEBS Letters 2000;468:6-10.

.

[20] Liao S, Bodmer J, Pietras D, Azhar M, Doetschman T, Schultz JEJ. Biological Functions of the Low and High Molecular Weight Protein Isoforms of Fibroblast Growth Factor-2 in Cardiovascular Development and Disease. Developmental dynamics : an official publication of the American Association of Anatomists 2009;238:249-64.
[21] Chlebova K, Bryja V, Dvorak P, Kozubik A, Wilcox WR, Krejci P. High molecular weight FGF2: the biology of a nuclear growth factor. Cellular and molecular life sciences : CMLS 2009;66:225-35.
[22] Ma X, Dang X, Claus P, Hirst C, Fandrich RR, Jin Y, et al. Chromatin compaction and cell death by high molecular weight FGF-2 depend on its nuclear localization, intracrine ERK activation, and engagement of mitochondria. J Cell Physiol 2007;213:690-8.
[23] Gaubert F, Escaffit F, Bertrand C, Korc M, Pradayrol L, Clemente F, et al. Expression of the high molecular weight fibroblast growth factor-2 isoform of 210 amino acids is associated with modulation of protein kinases C delta and epsilon and ERK activation. J Biol Chem 2001;276:1545-54.
[24] Stachowiak EK, Maher PA, Tucholski J, Mordechai E, Joy A, Moffett J, et al. Nuclear accumulation of fibroblast growth factor receptors in human glial cells--association with cell proliferation. Oncogene 1997;14:2201-11.
[25] Moffett J, Kratz E, Myers J, Stachowiak EK, Florkiewicz RZ, Stachowiak MK. Transcriptional regulation of fibroblast growth factor-2 expression in human astrocytes: implications for cell plasticity. Mol Biol Cell 1998;9:2269-85.
[26] Bilak MM, Hossain WA, Morest DK. Intracellular fibroblast growth factor produces effects different from those of extracellular application on development of avian cochleovestibular ganglion cells in vitro. J Neurosci Res 2003;71:629-47.
[27] Lemiere S, Azar R, Belloc F, Gursel D, Pyronnet S, Bikfalvi A, et al. Overexpression of high molecular weight FGF-2 forms inhibits glioma growth by acting on cell-cycle progression and protein translation. Exp Cell Res 2008;314:3701-11.
[28] Sinha VR, Trehan A. Biodegradable microspheres for protein delivery. Journal of Controlled Release 2003;90:261-80.
[29] Wu YQ, MacKay JA, McDaniel JR, Chilkoti A, Clark RL. Fabrication of Elastin-Like polypeptide Nanoparticles for Drug Delivery by Electrospraying. Biomacromolecules 2009;10:19-24.
[30] Cheng J, Pun SH. Polymeric biomaterials for cancer nanotechnology. Biomater Sci 2015;3:891-3.
[31] Lemoine D, Wauters F, Bouchend'homme S, Preat V. Preparation and characterization of alginate microspheres containing a model antigen. Int J Pharmaceut 1998;176:9-19.
[32] Pawar SN, Edgar KJ. Alginate derivatization: A review of chemistry, properties and applications. Biomaterials 2012;33:3279-305.
[33] Lee KY, Mooney DJ. Alginate: properties and biomedical applications. Progress in polymer science 2012;37:106-26.
[34] Tonnesen HH, Karlsen J. Alginate in drug delivery systems. Drug Development and Industrial Pharmacy 2002;28:621-30.
[35] Miao T, Rao KS, Spees JL, Oldinski RA. Osteogenic differentiation of human mesenchymal stem cells through alginate-graft-poly(ethylene glycol) microsphere-mediated intracellular growth factor delivery. Journal of Controlled Release 2014;192:57-66.
[36] Hristova M, Habibovic A, Veith C, Janssen-Heininger YMW, Dixon AE, Geiszt M, et al. Airway epithelial dual oxidase 1 mediates allergen-induced IL-33 secretion and activation of type 2

.

immune responses. Journal of Allergy and Clinical Immunology.
[37] Gåserød O, Sannes A, Skjåk-Bræk G. Microcapsules of alginate–chitosan. II. A study of capsule stability and permeability. Biomaterials 1999;20:773-83.
[38] Shimoda A, Sawada Si, Akiyoshi K. Cell Specific Peptide‐Conjugated Polysaccharide Nanogels for Protein Delivery. Macromolecular bioscience 2011;11:882-8.
[39] Lee RJ, Wang S, Low PS. Measurement of endosome pH following folate receptor-mediated endocytosis. Biochimica et Biophysica Acta (BBA)-Molecular Cell Research 1996;1312:237-42.
[40] Huang R, Ke W, Han L, Liu Y, Shao K, Ye L, et al. Brain-targeting mechanisms of lactoferrin-modified DNA-loaded nanoparticles. Journal of Cerebral Blood Flow & Metabolism 2009;29:1914-23.
[41] Preta G, Cronin JG, Sheldon IM. Dynasore - not just a dynamin inhibitor. Cell Communication and Signaling : CCS 2015;13:24.
[42] Kirchhausen T, Macia E, Pelish HE. Use of dynasore, the small molecule inhibitor of dynamin, in the regulation of endocytosis. Methods Enzymol 2008;438:77-93.
[43] Yin S, Huai J, Chen X, Yang Y, Zhang X, Gan Y, et al. Intracellular delivery and antitumor effects of a redox-responsive polymeric paclitaxel conjugate based on hyaluronic acid. Acta Biomater 2015;26:274-85.
[44] Baravalle G, Schober D, Huber M, Bayer N, Murphy RF, Fuchs R. Transferrin recycling and dextran transport to lysosomes is differentially affected by bafilomycin, nocodazole, and low temperature. Cell and tissue research 2005;320:99-113.
[45] Mundy DI, Li WP, Luby-Phelps K, Anderson RGW. Caveolin targeting to late endosome/lysosomal membranes is induced by perturbations of lysosomal pH and cholesterol content. Molecular Biology of the Cell 2012;23:864-80.
[46] Hou X, Lewis KT, Wu Q, Wang S, Chen X, Flack A, et al. Proteome of the porosome complex in human airway epithelia: Interaction with the cystic fibrosis transmembrane conductance regulator (CFTR). Journal of Proteomics 2014;96:82-91.
[47] Wang S, Lee JS, Bishop N, Jeremic A, Cho WJ, Chen X, et al. 3D organization and function of the cell: Golgi budding and vesicle biogenesis to docking at the porosome complex. Histochemistry and cell biology 2012;137:703-18.
[48] Zhang Y, Xu DQ. Improved Watershed Algorithm for Cell Image Segmentation. Advanced Materials Research 2012;546:464-8.
[49] Zhang Y, Duanquan X. Improvement on watershed algorithm of OpenCV and its application in cell image segmentation. Journal of Computer Applications 2012;32:134-6.
[50] Mosmann T. Rapid colorimetric assay for cellular growth and survival: Application to proliferation and cytotoxicity assays. Journal of Immunological Methods 1983;65:55-63.
[51] Sham D, Wesley UV, Hristova M, van der Vliet A. ATP-mediated transactivation of the epidermal growth factor receptor in airway epithelial cells involves DUOX1-dependent oxidation of Src and ADAM17. PloS one 2013;8:e54391.
[52] Miao T, Rao KS, Spees JL, Oldinski RA. Osteogenic differentiation of human mesenchymal stem cells through alginate-graft-poly(ethylene glycol) microsphere-mediated intracellular growth factor delivery. J Control Release 2014;192:57-66.
[53] Nam HY, Kwon SM, Chung H, Lee S-Y, Kwon S-H, Jeon H, et al. Cellular uptake mechanism and intracellular fate of hydrophobically modified glycol chitosan nanoparticles. Journal of Controlled Release 2009;135:259-67.
[54] Kou L, Sun J, Zhai Y, He Z. The endocytosis and intracellular fate of nanomedicines:

.

Implication for rational design. Asian Journal of Pharmaceutical Sciences 2013;8:1-10.
[55] Boussif O, Lezoualc'h F, Zanta MA, Mergny MD, Scherman D, Demeneix B, et al. A versatile vector for gene and oligonucleotide transfer into cells in culture and in vivo: polyethylenimine. Proc Natl Acad Sci U S A 1995;92:7297-301.
[56] Cagnol S, Chambard JC. ERK and cell death: mechanisms of ERK-induced cell death--apoptosis, autophagy and senescence. FEBS J 2010;277:2-21.
[57] Catalgol B, Batirel S, Taga Y, Ozer NK. Resveratrol: French Paradox Revisited. Frontiers in Pharmacology 2012;3.
[58] Lee JH, Kim KT. Regulation of cyclin-dependent kinase 5 and p53 by ERK1/2 pathway in the DNA damage-induced neuronal death. J Cell Physiol 2007;210:784-97.
[59] Liu J, Mao W, Ding B, Liang CS. ERKs/p53 signal transduction pathway is involved in doxorubicin-induced apoptosis in H9c2 cells and cardiomyocytes. American journal of physiology Heart and circulatory physiology 2008;295:H1956-65.

.

CHAPTER 5: TARGETED IMMUNOTHERAPY VIA ALGINATE AVIDIN NANOPARTICLES

The goal of this study was to design and fabricate an alginate-graft-avidin nanoparticles, which are able to conjugate with any biotinylated antibody of cell surface marker (i.e. anti-CD 11b or anti-CD8) to target interacts with desire cell types.

5.1. Introduction

Targeted drug delivery is an innovative method of delivering medications to patients in a manner that increases the concentration of the medication in desired disease locations relative to other body parts. Recent research focused on three fronts: finding the proper target for a particular disease state; finding a drug that effectively treats this disease; and finding a means of carrying the drug in a stable form to specific sites while avoiding the immunogenic and nonspecific interactions that efficiently clear foreign material from the body[1]. Nanoparticles encompass a variety of submicron (<1 μm) colloidal nanosystems, able to pass through certain biological barriers and encapsulate high density of therapeutic agents. With a large variety of chemical and preparation methods, nanoparticles can be engineered to yield different properties and release characteristics for the entrapped agent with different surface functionalities, such as targeting ligands for interaction with specific cells or tissue[1], which is required in p38 inhibitor delivery for MS treatment. Targeting moieties are classified as proteins (antibodies and fragments), peptides, nucleic acids (aptamers), small

molecules, or others molecules (vitamins or carbohydrates)[2]. Monoclonal antibodies are clinically and commercially-established therapeutics[3-5]. The full sequence of an antibody provides an accurate and efficient targeting effect compared to other types of moieties.

Alginate, a naturally occurring non-toxic biopolymer, has been used as a matrix for the entrapment and/or delivery of a variety of biological agents [18-20]. Alginate sub-microspheres have attracted much attention for the development of controlled and sustained-release drug delivery for proteins[6], cytokines[7, 8], and cells[9]. Our group has previously reported on utilizing alginate sub-microspheres for promoting osteogenic differentiation of human mesenchymal stem cells. However, the reported targeting moieties was only a tri-peptide arginine-glycine-aspartic acid (RGD). To increase the targeting efficiency, we herein report on utilizing the streptavidin (SA)/biotin interaction to conjugate biotinylated antibodies, specific to macrophages (anti-CD11b) or CD 8+ T cells, onto the SA surface modified alginate nanoparticles. The high affinity of the noncovalent interaction between biotin and avidin has been widely applied in research, which relies on the formation of an irreversible and specific linkage between biological macromolecules[10]. The capture of the small molecule biotin (vitamin H/vitamin B_7) by the bacterial protein SA is both a powerful tool in biology and a model system for the study of high-affinity protein–ligand interactions[11]. Therefore, our SA surface modified alginate sub-microparticles will serve as a general drug delivery platform for targeting drug delivery.

5.2. Materials and Methods

5.2.1. Materials

Sodium alginate (MW = 65–75 kg/mol, 60–70% guluronic acid residues) was generously donated by FMC BioPolymer. N-ethyl-N′(3-dimethylaminopropyl) carbodiimide hydrochloric acid (EDC), N-hydroxysuccinimide (NHS), 2,2′-dithiodipyridine, methanol (MeOH, anhydrous, 99.8%), biology-grade mineral oil, Span 80, bovine serum albumin (BSA) were purchased from Sigma-Aldrich. Sodium citrate, isopropanol, calcium chloride ($CaCl_2$), Alexa Fluor® 647 Cadaverine, 4% Formaldehyde (PFA) Solution in PBS, BupH™ MES Buffered Saline Packs and 20 × phosphate buffered saline (PBS), Alexa 647 Cadaverine, FTIC avidin, alexa 647 avidin were purchased from Fisher Scientific. Fetal bovine serum (FBS) was purchased from Atlanta Biologics and screened for a lot that best supported growth of human cells. Dulbecco's Modification of Eagle's Medium/Ham's F-12 Mix and 1X DMEM medium, penicillin, streptomycin and Trypsin EDTA were purchased from Corning Cellgro. Rat anti-CD11b antibody and anti-CD8+ were purchased from BioLegend.

5.2.2. Alginate Sub-Microsphere (ASM) Fabrication

ASMs were fabricated using a 1% (w/v) polymer solution. One milliliter of alginate-graft-poly(ethylene glycol) solution was slowly added to 6.72 mL of biological-grade mineral oil containing 5% (v/v) Spam 80 while mixing at 1200 rpm for 5 min at room temperature. Next, 400 µL of 30% (v/v) Tween 80 was added and the

emulsion will be mixed for an additional 5 min. Then, 5 mL of 2 M calcium chloride ($CaCl_2$) solution was added slowly. After 30 min of mixing, 3 mL of isopropanol was added to the emulsion and allowed to mix for 5 min, then was centrifuged at 400 rpm for 5 min to precipitate ASMs. ASMs were washed sequentially with isopropanol (x2) and DI water (x2), respectively, and centrifuged after each wash. Microspheres were flash frozen in liquid N_2 and lyophilized into powder for long term storage. The size and zeta-potential of the sub-microspheres were determined using dynamic light scattering (DLS, Zetasizer Nano ZSP, Malvern) in PBS at pH = 7.4 at room temperature.

5.5.3. ASM Surface Coating

The surface modification of ASMs with FTIC/Alexa 647 labeled avidin was achieved via carbodiimide chemistry catalyzed with EDC and NHS. Twenty milligrams of lyophilized ASMs were added to 3 mL of 0.1M MES buffer at pH 5 with the addition of EDC and NHS, and stirred at room temperature to activate the carboxyl groups on alginate. The COOH:EDC:NHS molar remained consistent at 1:8:3.2 during the reaction, where COOH refers to the moles of alginate carboxyl groups. After 1 h of vigorous stirring, 200 µg FTIC or Alexa 647 labeled avidin or Alexa 647®Cadaverine (labeling control group) in 200 µL DI water were added to the reaction system and reacted for 48 h at room temperature protected from light. The reaction suspensions were centrifuged for 3 min at 4000 rpm to precipitate ASMs. ASMs were washed sequentially with DI water (X2) respectively, and centrifuged after each wash. ASMs

were flash-frozen in liquid N_2 and lyophilized for long term storage. The size and zeta-potential of ASMs were determined using dynamic light scattering (DLS, Zetasizer Nano ZSP, Malvern) in PBS at pH = 7.4 at room temperature.

5.2.4. ASM Antibody Conjugation

Two milligrams of ASMs were mixed with 50 µg anti-CD11b, anti-CD8 or isotype control IgG (BioLegend Cat# 101204, 100704 and 400604 respectively) in a total volume of 100 µL PBS with 10% FBS and allowed to conjugate for 60 min at room temperature. A separate reaction with no antibody served as an additional control. After the reaction, ASMs were centrifuged for 5 min at maximum speed to pellet antibody-coated ASMs. ASMs were washed sequentially with PBS (X2) respectively, and re-suspended in 100 µL PBS.

5.2.5. Animals

C57BL/6J mice were purchased from The Jackson Laboratory and were maintained in the animal facility at the University of Vermont. The experimental procedures used in this study were approved by the Animal Care and Use Committee of the University of Vermont.

5.2.6. Mixed Mice Spleen Culture

Single-cell suspensions of splenocytes were prepared and the red blood cells were lysed with ammonium chloride. Total numbers of cells were counted using the Trypan blue live dead staining. These cultures typically consist of a mixture B cells

(CD19+), T cells (CD3+), macrophages (CD11b+, CD3-, CD19-), and other cells (negative for all 4 markers). The cells were incubated overnight with 100, 10, 1, 0.1 and 0.01 µg/mL of ASM particles labeled with FITC or A647 and conjugated with CD11b, CD8 or IgG isotype control. Labeled beads with no antibody conjugation served as an additional control. For flow cytometric analysis, the cells were washed twice and incubated for 30 min on ice with the desired fluorochrome-conjugated mAbs or isotype control immunoglobulin at 0.5 µg/10^6 cells. The antibodies being used in the experimental design includes anti-CD19 for B cells, anti-TCR for T cells, anti-CD4 and anti-CD8 for individual T cell populations, anti-CD11b and anti F4/80 for macrophages. All antibodies were purchased from BioLegend. As a parallel approach, we will conjugate specific antibodies to ABNs that will direct them to our cells of interest. There are many commercially available antibodies that will bind to surface markers of macrophages (CD11b) and conventional DCs (CD11c).

5.3. Results and Discussion

5.3.1. Alexa 647 Labeled ASMs Uptake by Mixed Culture Splenocytes

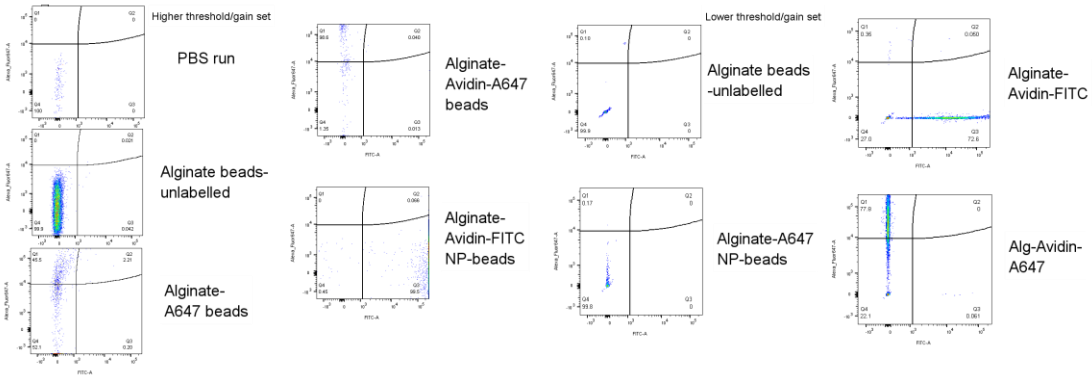

Figure 5-1. Flow Cytometry result of Alexa 647 labeled ASMs

.

The surface coating of avidin-Alexa 647 was verified through flow cytometry. ASMs were coated with Avidin-Alexa 647 and then conjugated with anti-CD11b (target to macrophages) and anti-CD8. IgG was also conjugated to ASMs avidin-Alexa 647 as control group. ASMs without avidin coating were labeled with Alexa Fluor ®647 cadaverine to obtain fluorescent labeled ASMs in order to be detected through flow cytometry. ASMs without avidin or antibody coating were not internalized until concentrations reached 10 μg/mL. At higher doses (100 μg/mL), >70% of the B cells and >40% of the macrophages contained ASMs whereas <10% of CD8+ T cells and CD4+ T cells internalized the ASMs. Similar results were also evident in isotype controls (IgG), where 40% of B cells and 10% of macrophages were ASM positive and all other type of cells were less than 5% positive at 100 μg/mL. Both non-avidin coated groups and IgG coated groups presented nearly no uptake at concentrations less than 1 μg/mL; however, non-specific uptake occurred at concentrations equal to 100 μg/mL. Using both groups as standard gates, we hereby analyzed antiCD11b groups, which were hypothesized to target macrophages. The results indicated a nearly 100% of uptake of macrophages at 10 μg/mL, whereas other types of cells' uptake activity were almost zero, indicating the successful targeting effect to macrophages. To back up our targeting efficacy, we also coated anti-CD8 to ASMs. In our control experiments, T Cells did not internalize ASMs at a concentration of 10 μg/mL. With the anti-CD8 coating, 80% of CD8+ cells were ASM positive at 1 μg/mL, while other cells did not internalize ASMs.

The above *in vitro* mixed culture proved the efficacy of using antibody-coated avidin-ASMs for targeting specific cell populations. Avidin-Alexa647 ASMs are an efficient drug delivery platform with multiple advantages: 1) they can be stored at -20 ºC long term after lyophilization; 2) they are traceable with Alexa 647 dye and can be used to semi-quantitatively track cell specific uptake *in vitro*; 3) the targeting efficiency was significantly effective at concentrations as low as 1 µg/mL[12].

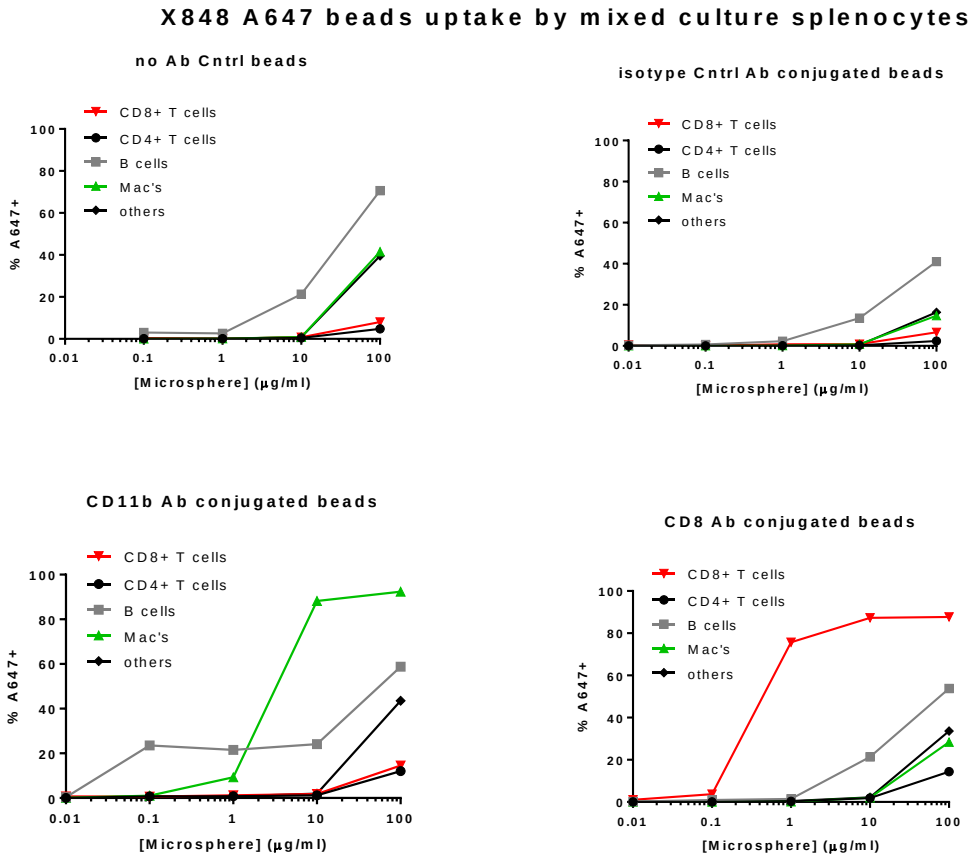

Figure 5-2 Alexa 647 labeled ASMs uptake by mixed culture plenocytes.

5.4. Conclusion

SA surface modified ASMs will serve as a general drug delivery platform for targeting drug delivery with different antibodies.

.

Reference

[1] Fahmy TM, Fong PM, Goyal A, Saltzman WM. Targeted for drug delivery. Materials Today 2005;8:18-26.
[2] Yu MK, Park J, Jon S. Targeting Strategies for Multifunctional Nanoparticles in Cancer Imaging and Therapy. Theranostics 2012;2:3-44.
[3] Deonarain MP, Kousparou CA, Epenetos AA. Antibodies targeting cancer stem cells: A new paradigm in immunotherapy? mAbs 2009;1:12-25.
[4] Carter PJ. Potent antibody therapeutics by design. Nat Rev Immunol 2006;6:343-57.
[5] Deonarain MP. Recombinant antibodies for cancer therapy. Expert Opin Biol Ther 2008;8:1123-41.
[6] Li T, Shi XW, Du YM, Tang YF. Quaternized chitosan/alginate nanoparticles for protein delivery. Journal of Biomedical Materials Research Part A 2007;83:383-90.
[7] Jain S, Amiji M. Tuftsin-modified alginate nanoparticles as a noncondensing macrophage-targeted DNA delivery system. Biomacromolecules 2012;13:1074-85.
[8] Sarmento B, Ribeiro A, Veiga F, Sampaio P, Neufeld R, Ferreira D. Alginate/chitosan nanoparticles are effective for oral insulin delivery. Pharmaceutical research 2007;24:2198-206.
[9] Liu Z, Jiao Y, Wang Y, Zhou C, Zhang Z. Polysaccharides-based nanoparticles as drug delivery systems. Advanced drug delivery reviews 2008;60:1650-62.
[10] Weber P, Ohlendorf D, Wendoloski J, Salemme F. Structural origins of high-affinity biotin binding to streptavidin. Science 1989;243:85-8.
[11] Chivers Claire E, Koner Apurba L, Lowe Edward D, Howarth M. How the biotin–streptavidin interaction was made even stronger: investigation via crystallography and a chimaeric tetramer. Biochemical Journal 2011;435:55-63.
[12] Miao T, Rao KS, Spees JL, Oldinski RA. Osteogenic differentiation of human mesenchymal stem cells through alginate-graft-poly(ethylene glycol) microsphere-mediated intracellular growth factor delivery. Journal of Controlled Release 2014;192:57-66.

.

CHAPTER 6: SELF-HEALING AND THERMO-RESPONSIVE DUAL CROSSLINKED ALGINATE HYDROGELS BASED ON SUPRAMOLECULAR INCLUSION COMPLEXES

β-cyclodextrin (β-CD), with a lipophilic inner cavity and hydrophilic outer surface, interacts with a large variety of non-polar guest molecules to form non-covalent inclusion complexes. Conjugation of β-CD onto biomacromolecules can form stiff, physically-crosslinked hydrogel networks upon mixing with a guest molecule. Herein describes the development and characterization of self-healing, thermo-responsive hydrogels, based on host-guest inclusion complexes between alginate-*graft*-β-CD and Pluronic® F108 (poly(ethylene glycol)-*b*-poly(propylene glycol)-*b*-poly(ethylene glycol)). The mechanics, flow characteristics, and thermal response were contingent on the polymer concentration, and the host-guest molar ratio. Transient and reversible physical crosslinking between host and guest polymers governed self-assembly, allowing flow under shear stress, and facilitating complete recovery of the material properties within a few seconds of unloading. The mechanical properties of the dual-crosslinked, multi-stimuli responsive hydrogels were tuned as high as 30 kPa at body temperature, which make it a potential candidate for biomedical applications such as drug delivery and cell transplantation.

6.1. Introduction

Polymeric hydrogels are porous, 3-D networks of crosslinked macromolecules, able to retain large amounts of water.[1] Injectable polymeric hydrogels, which are

crosslinked and solidify *in situ*,[2] are advantageous for drug and cell delivery, and tissue engineering applications.[2-4] Many existing injectable hydrogel systems polymerize to form covalent crosslinks, through the use of photo-initiated systems, autonomous redox reactions, or Michael Addition chemistries,[5] which can affect cytocompatibility[6] and protein bioactivity.[7] Furthermore, covalently crosslinked hydrogels are unable to undergo reversible solid-liquid transitions.[8] In contrast, the dynamic and reversible nature of non-covalent interactions, such as physical crosslinks, demonstrate variable mechanical properties and stimuli responses which lead to unique and programmable modifications in the network structure.[9]

Indeed, physically-crosslinked hydrogels avoid the limitations associated with permanently crosslinked hydrogel networks.[10] Gelation conditions are relatively mild, and reversible physical crosslinks allow hydrogels to re-assemble, or self-heal, after deformation or a disruption in the network.[11-13] In addition, physically-crosslinked hydrogels offer a new route toward innocuous, stable materials and components *in vivo*.[14] Recently, the utilization of supramolecular polymer chemistry, specifically host-guest chemistry, has enabled the design of more sophisticated multi-functional materials.[15-18],[5, 10, 19, 20] Such hydrogels, which mimic strain and stress-responsive tissues, are now being considered for biomedical applications.[21]

Several macrocyclic host-guest inclusion complexes are reported in the literature, including crown ethers, cyclophanes, ctananes, and cavitands (such as cyclodextrins, calix[n]arenes and cucurbit[n]urils).[1] Of particular interest is β-

cyclodextrin (β-CD), which is easily grafted onto polymer chains, exhibits negligible cytotoxic effects, and is an important attribute in the pharmaceutical and food industries.[22] The covalent conjugation of β-CD onto large biomacromolecules, such as alginate, increases the functionality of the large polymer.[23-25] Alginate is a plant-derived polysaccharide, and alginate hydrogels have served as scaffolds for tissue engineering, drug delivery vehicles, and models of extracellular matrices for biological studies.[26-29] Alginate hydrogel properties, including stiffness, swelling, degradation, cell attachment, and binding or release of bioactive molecules, can be optimized through the chemical or physical modification of the polysaccharide itself or the inclusion of alginate into a hydrogel network.[30, 31]

β-CD, with a lipophilic inner cavity and hydrophilic outer surface, interacts with a large variety of non-polar guest molecules to form physical inclusion complexes.[22, 32] The hydrophobic guest molecule is held within the cavity of β-CD and the main driving force of complex formation is the release of enthalpy-rich water molecules from the cavity.[22, 32] The binding activities between host and guest molecules are not fixed, but rather self-assemble in a dynamic manner.[22] Several guest molecules are reported for β-CD, including adamantine,[5, 33, 34] cholesterol,[35] and other custom-designed molecular recognition compounds.[36] Macromolecules such as poly(propylene glycol), PPG, have also been investigated as guest molecules for β-CD.[15, 37-40] Difunctional block copolymers, such as PEG-*b*-PPG-*b*-PEG (i.e., Pluronic® F108), are utilized in drug delivery systems and cell culture due to low

cytotoxicity and innate thermo-responsive propoerties.[41-48] The inclusion of hydrophobic PPG chain segments into the inner cavity of β-CD affords a high binding affinity to form a hydrogel network, while mobile PEG end-blocks entrap water molecules and provide an innocuous environment for cells.[49-52] In addition, the thermo-responsive property of Pluronic® F108 is advantageous for *in vivo* applications due to the presence of PPG in the block copolymer - PPG is water-soluble at low temperatures and reverts into an insoluble form at higher temperatures.[45, 53, 54] This behavior is similar to poly(N-isopropyl acrylamide) (PNIPAAm), a commonly synthesized thermo-responsive polymer.[16, 53, 55] However, the non-biodegradability and relatively weak mechanical properties limit the wide application of PNIPAAm.[56]

The goal of this study was to create a host biomacromolecule, alginate-*graft*-β-CD, and incorporate a difunctional guest molecule, Pluronic® F108, to create physically-crosslinked, moderately stiff hydrogels. We hypothesized that the supra The hydrophobic guest molecule is held within the cavity of β-CD and the main driving force of complex formation is the release of enthalpy-rich water molecules from the cavity.[22, 32] molecular inclusion complex formation between alginate-*graft*-β-CD and Pluronic® F108 would generate non-cytotoxic, dual-crosslinked, multi-stimuli responsive hydrogels with physiologically relevant mechanical properties for biomedical applications.[56]

6.2. Experimental Section

Materials: Sodium alginate (PROTANAL® LF200 FTS, M_v 67-142 kg/mol was generously donated by FMC BioPolymer. Beta-cyclodextrin (β-CD), *ρ*-toluenesulfonyl chloride (TosCl), acetonitrile, acetone, 1,6-hexanediamine (HDA), diethyl ether, dimethylformamide (DMF), (benzotriazol-1-yloxy)tris-(dimethylamino) phophonium hexafluorophosphate (BOP), dimethyl sulfoxide (DMSO), ethylenediamine (EDA), and deuterium oxide (D_2O) were purchased from Acros Organics. Sodium hydroxide, ammonium chloride, hydrogen chloride (HCl), ethanol, tetrabuylammonium fluoride (TBAF), phosphate buffered saline (PBS), 2-morpholinoethanesulfonic acid (MES) buffer, alpha-modified eagle medium (α-MEM, Hyclone), and bovine serum albumin (BSA) were purchased from Thermo Fisher Scientific. Human mesenchymal stem cell-screened fetal bovine serum (FBS) was purchased from Atlanta Biologics. Penicillin, streptomycin, and trypsin ethylenediaminetetraacetic acid (EDTA) were purchased from Corning Cellgro. Tetrabutylammonium hydroxide (TBAOH), N-ethyl-N'(3-dimethylaminopropyl) carbodiimide hydrochloric acid (EDC), N-hydroxysuccinimide (NHS), Pluronic® F108 ($M_n \approx 14{,}600$ g/mol), and an *In Vitro* Toxicology Assay Kit (3-(4,5-dimethylthiazol-2-yl)-2,5-diphenyltetrazolium bromide, i.e., MTT-based) were purchased from Sigma Aldrich. BCA® Protein Assay Kit was purchased from Life Technologies Inc.

Alginate-Tetrabutylammonium (Alg-TBA) Synthesis: Sodium alginate (Na-Alg, 2 g) was added to a mixture of HCl (0.6 N, 30 mL) and ethanol (30 mL) and stirred overnight at 4 ºC. After filtering under vacuum with filter paper and washing with

ethanol and acetone, pure alginic acid was obtained and dried overnight. The dried powder was dispersed in DI water (100 mL). Aqueous TBAOH was added slowly under continuous stirring and the pH was adjusted to between 7.0 and 10.0. The solution was dialyzed and lyophilized to yield white Alg-TBA powder.[57-61]

β-CD-TosCl Synthesis: β-CD (20 g, 17.62 mM, 1 molar equivalent) was suspended in 125 mL ice DI water, and TosCl (4.2 g) was dissolved in minimum acetonitrile (~10 mL) and added drop wise to the aqueous phase. The reaction was stirred vigorously for 2 h at room temperature. Sodium hydroxide (2.18 g) was dissolved in DI water (~10 mL) and added drop wise. After 30 min of stirring at room temperature, solid ammonium chloride was added to adjust the pH to 8.5 and the solution was cooled on ice to collect precipitants. The product was washed with cold DI water and acetone 3 times respectively and dried under vacuum; 6-*o*-monotosyl-6-deoxy-β-CD was obtained (~25%).[5, 62, 63]

β-CD-HDA Synthesis: β-CD-TosCl (5 g) was dissolved in DMF (25 mL) with 1,6-hexanediamine (20 g) and stirred under nitrogen at 80 ºC for 24 h using a condenser. The product was precipitated out of solution using cold acetone (5 x 500 mL), washed with cold diethyl ether (2 x 100 mL), and dried under vacuum to afford the final product mono-6-deoxy-6-aminohexaneamino-β-CD).[5, 64]

β-CD-EDA Synthesis: 6-(6-aminohyxyl)amino-6-deoxy-*β*-cyclodextrin (1.5 g) was added to EDA (5 mL). The reaction was performed at 60 ºC for 24 h and cooled to room temperature. The precipitant was collected from a large amount of ethanol and

dried under vacuum to afford the final product (mono-6-deoxy-6-aminoethylamino-β-CD).[65]

Alginate-graft-C_6-Cyclodextrin (Alg-C6) Synthesis: TBAF (10 g) was dissolved in DMSO (100 mL) to afford a 10% (w/v) solution. Alg-TBA (2 g, 1 molar equivalent) and β-CD-HDA (2.96 g, 0.5 molar equivalent) were added to the mixture and stirred at room temperature under nitrogen flow until a clear solution was obtained.[58] BOP (1.06 g, 0.5 molar equivalent) was dissolved in minimal DMSO (5 mL) and added via syringe. The reaction was carried out at room temperature under vigorous mixing for 24 h and then dialyzed against DI water (x 3), followed by 0.05 M sodium phosphate dibasic solution until fully dissolved in water, and finally DI water (x 2). The final product was frozen and lyophilized. The theoretical modification was 50%.[5]

Alginate-graft-C_2-Cyclodextrin (Alg-C2) Synthesis: Sodium alginate (2.73 g) was dissolved in 0.1 M MES buffer (pH 5.6, 150 mL) to which EDC (2 g) and NHS (1.2 g) were added. After mixing for 30 min at room temperature, β-CD-EDA (4.5 g) was added under vigorous mixing at room temperature for 1 day. The alginate solution was dialyzed against DI water for 3 days, frozen, and lyophilized to afford dry polymer.[65]

^{1}H-NMR Spectroscopy: To qualitatively verify the successful synthesis of Alg-C6 and Alg-C2, lyophilized polymer was dissolved in D_2O and the result was confirmed via ^{1}H-NMR (Bruker AVANCE III 500 MHz high-field NMR spectrometer). In addition to standard ^{1}H-NMR, solvent (water) suppression ^{1}H-NMR,

as well as diffusion edited ^{1}H-NMR at 95% strength (programmed in Bruker NMR spectrometer), were also performed for alginate, Alg-C2, and Alg-C6, to confirm the covalent conjugation of β-CD onto alginate. The detailed ^{1}H-NMR spectra are provided in the supplemental data.

Alginate Hydrogel Formation and Erosion: Alg-C2 and Alg-C6 hydrogels were prepared from solutions of the individual polymers in PBS at desired concentrations. 4 and 6% (w/v) Alg-C2 and Alg-C6 solutions were prepared in 10 mL syringes. Pluronic® F108 crystals were dissolved in DI water (10% w/v), frozen at -80 ºC, and lyophilized to obtain a white powder, which was added to the Alg-*g*-CD solutions at Pluronic® F108:β-CD ratios of 1:4 and 1:2, respectively. Hydrogels and single host and guest polymer solutions were injected into glass vials; the glass vials were stored at either 25 or 37 ˚C. Optical images were taken at each time point after the injection to analyze hydrogel stability. To qualitatively analyze hydrolytic erosion of the hydrogels, images were taken of the hydrogels after adding a known amount of PBS on top of each hydrogel to qualitatively visualize hydrogel surface erosion over a period of 14 days at 37 ˚C under gentle agitation in a shaking incubator (see additional Supplemental Materials). Samples were sealed with parafilm to eliminate water evaporation.

Rheological Characterization: All experiments were performed using an AR2000 stress-controlled rheometer (TA Instruments) fitted with a 40 mm diameter 1°59’47’’ steel cone geometry and 27 μm gap at 37 °C, however, the temperature sweep study included a temperature range. Oscillatory time sweeps for single polymer

constituents (e.g., 4% (w/v) Alg-*g*-CD, 10% Pluronic® F108) and hydrogels were deformed at 1% strain and 10 Hz over 250 s. Oscillatory frequency sweeps were performed at 0.5% strain with increasing frequency from 0.1 to 100 Hz. Continuous flow experiments used a shear rate linearly ramped from 0 to 1 s^{-1}. Oscillatory strain sweeps were performed at 10 Hz with increasing radial strain from 0.01 to 500%. Dynamic shear strain tests were performed at high (250%) and low (0.5%) strains at 1 Hz and 37 °C for certain lengths of time and the cycles were repeated three times to test the self-healing and recovery properties of the hydrogels. Temperature sweeps were performed at 1 Hz and 1% strain, with a heating rate of 0.5 °C*min^{-1} from 25 to 37 °C.

In Vitro Cytotoxicity Assay: Materials for the *in vitro* cell study were lyophilized and exposed to UV light overnight. The hydrogels and polymer solutions were prepared with sterile PBS using similar protocols stated above. Primary human mesenchymal stem cells (MSCs) were purchased from Rooster Bio. MSCs (passage 4) were seeded in 48-well tissue culture polystyrene (TCPS) plates at a density of 20,000 cells/well in 500 μL/well of standard MSC growth medium (α-MEM, 10% FBS, 100 U mL^{-1} penicillin, 100 μg mL^{-1} streptomycin) and allowed to adhere for 24 h. Cells were incubated in the presence of Alg-C6 hydrogels with ratios of 1:4 and 1:2 and Alg-C2 hydrogels with ratios of 1:4 and 1:2. In addition, cells were incubated without hydrogels under the same culture conditions as control group. After 24 h of incubation, media containing the hydrogel and polymer solutions was removed, and cells were rinsed two times in sterile PBS then analyzed using a MTT-based *In Vitro* Toxicology

Assay Kit following the manufacturer's protocol. The optical density was measured at 570 nm using a BioTek plate reader. Background absorbance at 690 nm was subtracted from the measured absorbance. Absorbance values for the experimental and control samples were normalized to non-modified TCPS controls.[66]

In Vitro BSA Release: BSA (10 mg) was added to 1 mL of different hydrogel solutions (prepared as stated above) and injected into 24-well plates. The plates were incubated at 37 ºC overnight to ensure gelation complete. One mL of PBS was added to each well and the plate was gently agitated at 37 ºC in a shaker incubator. At each time point, 100 µL sample aliquots were removed and replaced with 100 µL fresh PBS. The protein concentration was determined using a BCA Protein Assay Kit according to the manufacture's protocol. The optical density was measured at 562 nm using a BioTek plate reader. Background absorbance of non-modified TCPS controls was subtracted from the measured absorbance; absorbance values for the experimental, blank (i.e., containing no BSA), and control samples were reported.

Statistical Methods: All experiments were performed in triplicate; results are reported as mean ± standard deviation. Statistical analysis was performed on the storage moduli for 25 and 37 °C between each of the treatment groups and *in vitro* cytotoxicity data respectively, using one-way ANOVA with Tukey multiple comparisons ($\alpha = 0.05$) via the SAS statistics program in the GLM procedure as the post-test to compare all of the groups. $P < 0.05$ was considered significantly different.

6.3. Results and Discussion

6.3.1. Dual Strategies for Synthesizing Alginate-*graft* Cyclodextrin (Alg-*g*-CD)

Two strategies were employed to synthesize Alg-*g*-CD (i.e., host macromolecules) using a short-chain methylene group to conjugate β-CD onto the alginate backbone, providing mobility and thus crosslinking efficiency. While one reaction was performed in an organic solvent with six methylene groups (-CH_2-) connecting the alginate backbone to β-CD (Alg-C6),[12] the other reaction was performed in aqueous solution with two methylene groups (-CH_2-) connecting the alginate backbone to β-CD (Alg-C2).[65] The detailed chemical synthesis for both reactions are presented in **Figure 6-1 A**. Briefly, β-CD was first reacted with TosCl to obtain β-CD-TosCl. In one reaction scheme, β-CD-TosCl was reacted with HDA in DMF at 80 °C for 18 h. Amine groups reacted with carboxyl groups (pre-neutralized with TBA salt) on alginate in DMSO in the presence of BOP. Alternatively, in the aqueous solution method, β-CD-TosCl was reacted with EDA at 60 °C for 12 h to obtain β-CD-EDA. The standard ^{1}H-NMR spectra for the final products, Alg-C6 and Alg-C2, are provided in **6.7 supplemental materials** (chapter 6.5).

In addition to standard ^{1}H-NMR, solvent suppression (water) ^{1}H-NMR as well as diffusion edited ^{1}H-NMR at 95% strength for alginate, Alg-C2 and Alg-C6, were performed to confirm the covalent conjugation of β-CD onto alginate. The detailed ^{1}H-NMR spectra are provided in the supplemental data. The spectra indicated that β-CD was covalently conjugated onto alginate in both Alg-C2 and Alg-C6. By comparing

alginate, Alg-C2 and Alg-C6 spectra, peaks between 1 – 3 ppm were only presented in the final product of Alg-C2 and Alg-C6 rather than alginate, suggesting the covalent conjugation of methylene groups, as linker between β-CD and alginate. The degree of β-CD modification, i.e., β-CD density, may generate an effect on the hydrogel physical and mechanical properties.[12] The theoretical reaction ratio of β-CD to alginate repeat units $(C_6H_7NaO_6)_n$ was 50%. However, by calculating the ratio of hydrogen integration of sugar units (both on alginate backbone repeat units and on β-CD repeat units), and hydrogen integration of the methylene groups on the linker between the backbone and β-CD,[65] the actual β-CD modification for both reaction methods was 28% and 30%, respectively for Alg-C2 and Alg-C6, indicating no significant differences in alginate modification for the different Alg-*g*-CD reaction schemes. There are limitations with using ^{1}H-NMR to calculate the β-CD degree of modification due to the high molecular weight and polydispersity of the alginate (M_v 67-142 kg/mol) starting material; however, using either standard ^{1}H-NMR or diffusion edited ^{1}H-NMR is common in this type of polymer chemistry characterization.[5, 12, 48]

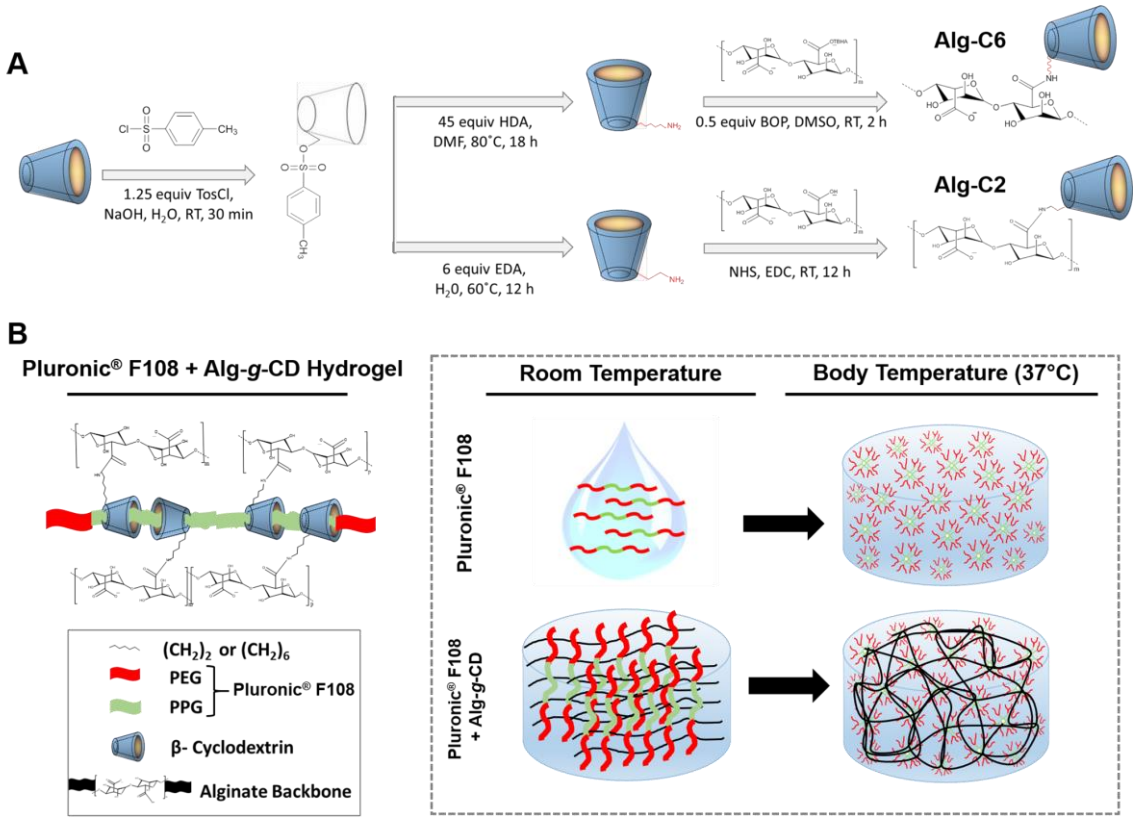

Figure 6-1 A) Schematic of Alg-g-CD synthesis using organic solvents or aqueous-based solutions. Alg-C6 was the product of the organic synthesis (top), and Alg-C2 was the product of the aqueous synthesis (bottom). B) Schematic of physical crosslinking between Alg-g-CD macromolecules and Pluronic® F108, and the effect of Pluronic® F108 on the thermo-response of hydrogel network; Pluronic® F108 forms micelles and self-crosslinks at body temperature due to the triblock structure of PEG-b-PPG-b-PEG. β-CD conjugated onto the alginate backbone served as the host (Alg-g-CD), which formed a physically-crosslinked supramolecular inclusion complex with the guest, the PPG component (green) of Pluronic® F108.

.

6.3.2. Hydrogel Formation and Rheological Analysis

A self-assembled hydrogel network formed almost immediately upon mixing Alg-*g*-CD and Pluronic® F108 solutions (quantity based on constituent molar ratios). The formation of a pseudo-plastic hydrogel occurred through the complexation of host-guest moieties, i.e., β-CD conjugated alginate (Alg-*g*-CD) and PPG, as part of the Pluronic® F108 structure. In addition to the supramolecular inclusion complex formation between Alg-*g*-CD and Pluronic® F108, a dual-crosslinked hydrogel was created via the innate thermo-response of Pluronic® F108. Such dual-crosslinking capabilities significantly increased the storage moduli compared to a single physical crosslinking technique based on host-guest chemistry alone (**Figure 6-1 B**).

The formation and physical integrity of the supramolecular inclusion complex hydrogels were quantified using rheometry. Hydrogels and their pre-curser solutions were exposed to varying shear forces to examine steady-state shear moduli with time, the effect of frequency on shear moduli, and the effect of shear rate on the shear stress and viscosity of hydrogel pre-curser solutions. To examine the hydrogels in their least compliant states, experiments were performed at 37 °C. In **Figure 6-2 A**, the shear rate was linearly ramped from 0 to 1 s^{-1} to investigate the effect of shear rate on viscosity and resultant shear stress; the Alg-C2 group generated an increase in shear stress from approximately 40 Pa to 400 Pa while shear rates increased from 0 to 0.3 s^{-1} and then plateaued until 1 s^{-1}. The viscosity decreased from near 3500 to 300 Pa*s while shear rates increased from 0 to 0.7 s^{-1}. For the Alg-C6 hydrogels (**Figure 6-2 B**), the shear

stress increased from approximately 5 to 50 Pa for 4% (w/v) Alg-C6 hydrogels and from 100 to 400 Pa for 6% and 8% Alg-C6 hydrogels. While maintaining the same molar ratio between Alg-*g*-CD and Pluronic® F108, a more distinct concentration-dependent behavior was seen in the Alg-C6 groups compared to the Alg-C2 groups. This may be due to the self-crosslinking of the Alg-C2 polymers, as the material properties were less dependent on polymer concentration, as the β-CD conjugation for both materials was ~30%.[65]

Shear storage and loss moduli were measured to both verify and quantify the formation of the supramolecular inclusion complex hydrogel from independent measurements of pre-curser solutions. Oscillatory rheology confirmed that the individual Pluronic® F108 and Alg-*g*-CD pre-cursers were solutions at high frequencies and that an increase in moduli of several orders of magnitude occurred immediately upon mixing of the two components. While the individual polymer solutions (i.e., hydrogel constituents) displayed viscous behaviors associated with intermolecular entanglement in solution, the formed supramolecular inclusion complex hydrogel was stable during a qualitative inversion test. Pluronic® F108 remained unstable and free flowing at room temperature and formed small micelles (size ~20nm) at body temperature.[67, 68] The micelles were inter-connected with each other and therefore, higher concentrations of Pluronic® F108 formed a soft network in solution, also shown by the slight increase in viscosity. For the Alg-C2, the G′ increased from 300 Pa to 12 kPa (**Figure 2C).** The multi-arm structure of EDA on β-CD may also react with various

carboxyl groups on neighboring alginate molecules, to create an intramolecular-crosslinked network beyond the host-guest interaction. Previous literature has shown the concept that such crosslinking will increase the stiffness of the hydrogel, although only slightly.[32] For Alg-C6, the G′ increased from 300 Pa for the polymer solution, to near 10 kPa for the Pluronic® F108:Alg-*g*-CD hydrogel (1:2), and G″ increased from 50 Pa for the polymer solution to 10 kPa for the Pluronic® F108:Alg-*g*-CD hydrogel. The large increase in shear moduli that occurred after mixing the two polymer constituents verified that an interaction took place to form a more permanent network, compared to polymer solutions alone; the formation of the supramolecular inclusion complex resulted in the 100-fold increase in shear moduli (**Figure 6-2 C,D**). Thus, the bulk material response indicated that the chemical modification of alginate was successful, through the formation of a stiff hydrogel network upon mixing with Pluronic® F108.

Shear storage and loss moduli were also measured to determine effect of frequency during dynamic shear application. Oscillatory frequency sweeps were performed on 4% Alg-C6 and Alg-C2 hydrogels with a ratio Pluronic® F108:Alg-*g*-CD 1:4 at 0.5% radial strain and 37 °C. The hydrogel exhibited steady-state behavior up to 10 Hz, after which the moduli increased in response to the increasing shear rate. The effect followed an exponential trend for frequencies greater than 10 Hz for the Alg-C2 hydrogels (**Figure 6-2 E**). In addition, the hydrogels were considered to be stable at lower frequencies and not responsive to frequency as an input parameter. The Alg-C6 hydrogels displayed noisy data, which suggested a less stable network, especially at

increasing frequencies (**Figure 2F**).

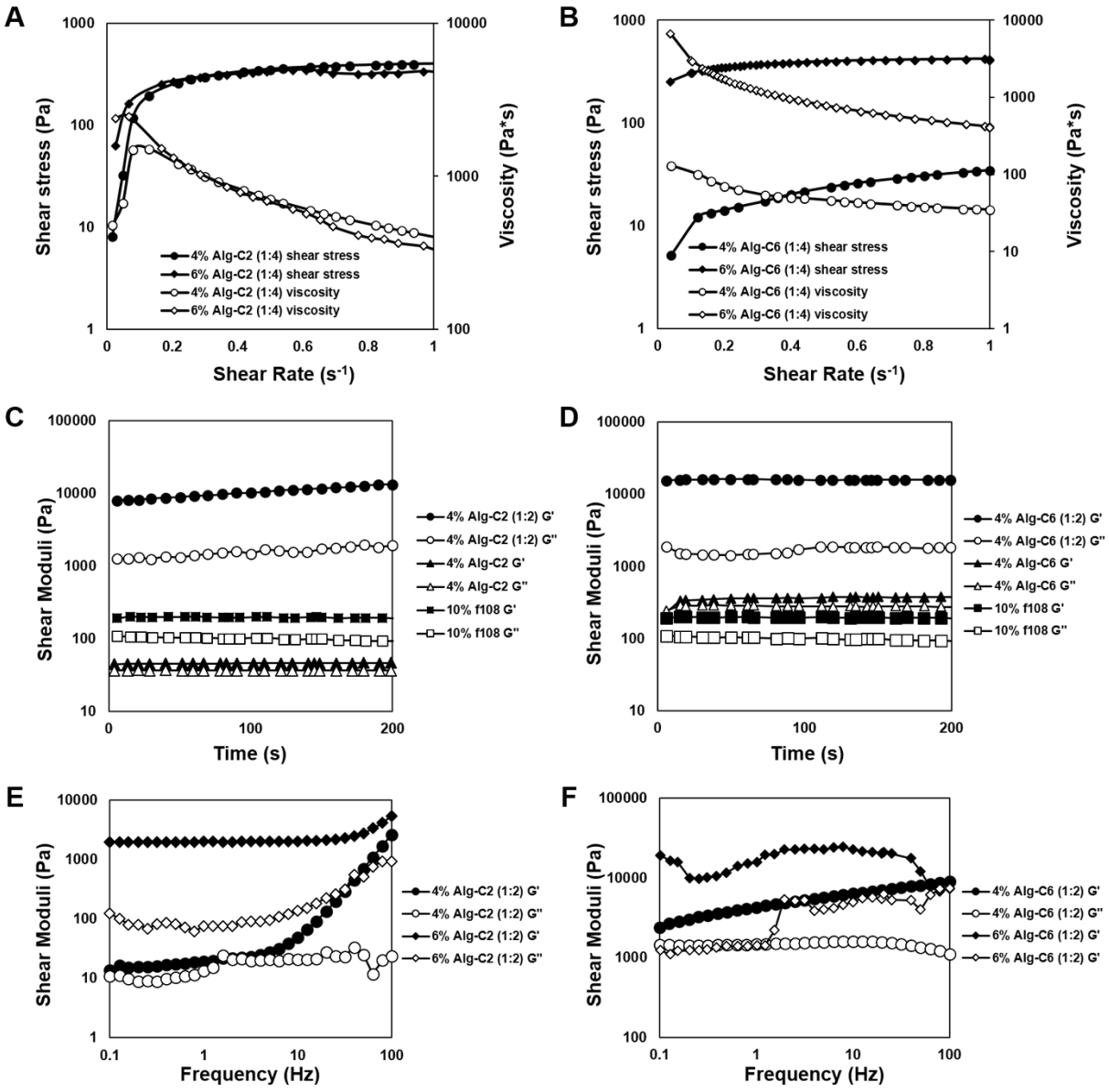

Figure 6-2. Rheological experiments were performed at 37 °C to verify formation and physical integrity of the supramolecular alginate network. (A, B) Continuous, increasing shear rates allowed for the determination of viscosity and shear stress of formed

.

hydrogels; A) Alg-C2 and B) Alg-C6. The shear stress increased with an increase in shear rate from 0 to 1 s^{-1}, demonstrating viscoelastic behavior. (C, D) Oscillatory time sweep experiments for hydrogel pre-curser solutions, Alg-g-CD and Pluronic® F108, and formed hydrogels at 1% strain, 10 Hz, 37 °C; C) Alg-C2 and D) Alg-C6. The storage moduli increased from 100 Pa for single polymer constituents to 10 kPa for 4% (w/v) Pluronic® F108:Alg-g-CD hydrogels. (E, F) Oscillatory frequency sweeps were performed at 0.5% radial strain; E) Alg-C2 and F) Alg-C6.

6.3.3. Strain Responsive Properties and Self-Healing

Multi-chain entanglements of macromolecular guest polymers create a unique structure upon crosslinking which affords a high modulus hydrogel with shear-thinning behaviors. Reversible, dynamic physical crosslinks allow supramolecular inclusion complex hydrogels to exhibit flow and recovery characteristics under mechanical radial strain. To validate and optimize the shear-shinning properties of the injectable delivery systems, hydrogels were tested using oscillatory strain sweeps from 0.01% to 500% radial strain at a frequency of 10 Hz. Both Alg-C2 and Alg-C6 (**Figure 6-3 A,B**) groups were more elastic at low strains, with storage moduli (G') greater than the loss moduli (G"). At 1% strain, the G' and G" curves for Alg-C2 began to cross over, indicating a transition from an elastic solid material to a compliant, viscous liquid. The crossover of G' and G" for Alg-C6 hydrogels occurred near 10% strain, suggesting that the inter-molecular crosslinking density for Alg-C6 was higher compared to Alg-C2;

.

this may be attributed to a longer amine chain, which may have provided more mobility to allow Pluronic® F108 to enter the β-CD cavity. The shear-thinning characteristics were also dependent on the de-association of host-guest polymers. Alg-C2 hydrogel networks were more easily strained to failure compared to Alg-C6 hydrogels, and the Alg-C2 hydrogels exhibited a lower transition strain (%) compared to Alg-C6 hydrogels.

The reversibility and repeatability of the self-healing properties of the hydrogels were independent of host:guest ratios or polymer concentration. To assess material recovery, hydrogels were subjected to cycles of high amplitude oscillatory strain (250%) followed by low amplitude oscillatory strain (0.5%) at 1 Hz. Storage moduli (G') decreased 1/100 fold with a change from low to high amplitude strain (i.e., each time step with strain variation). A decline in moduli was concurrent with the presence of solid-liquid transitions during the application of high strain. During transitions from high to low strains, the initial mechanical properties were recovered in a short time period of 10 s. These results indicate that the novel hydrogels exhibit shear-shinning behavior, recovering mechanical properties immediately upon un-loading. Various hydrogel formulations demonstrated a variety of strain-induced shear moduli values: D) Alg-C6 (1:2) (**Figure 6-3 D**) and Alg-C2 (1:4) (**Figure 6-3 E**) hydrogels exhibited a change in G' over 3 orders of magnitude, whereas the Alg-C2 (1:2) (**Figure 6-3 C**) and Alg-C6 (1:4) (**Figure 6-3 F)** exhibited a change in G' by 2 orders of magnitude. Despite that the crossover transient points for both Alg-C2 and Alg-C6 upon strain changes in

strain were relatively low, the mechanical properties were as high as 10 kPa, indicating a dynamic material with a range of achievable moduli.

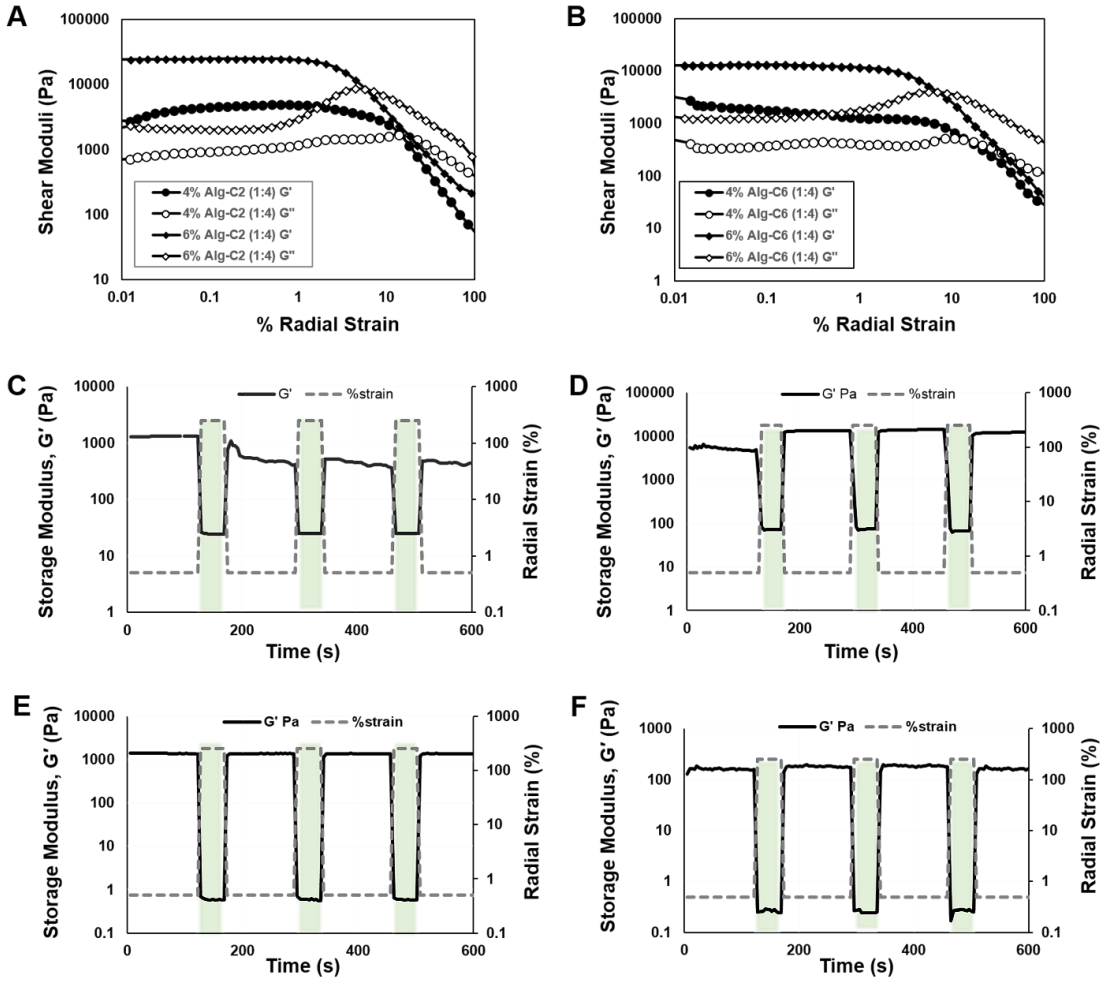

Figure 6-3 (A, B) Oscillatory strain sweeps were performed at 10 Hz and 37 °C using a 40 mm 1°59'47" steel cone geometry on F108:Alg-g-CD hydrogels: A) Alg-C2 and B) Alg-C6 hydrogels. The storage moduli (G') and loss moduli (G") of the hydrogels crossed at higher strains, demonstrating a solid-liquid transition. (C – F) Dynamic shear strain testing of hydrogels was performed to demonstrate a self-healing, physically crosslinked

.

network. Dashed gray lines represent the radial strain (%) input parameters and the solid black lines represent shear storage moduli (G') results. All of the groups tested demonstrated a repeatable ability to deform and re-assemble upon loading and un-loading, resulting in radial shear deformations. Hydrogels consisting of 4% (w/v) Alg-g-CD were analyzed at various ratios of Pluronic® F108:Alg-g-CD; C) Alg-C2 (1:2), D) Alg-C6 (1:2), E) Alg-C2 (1:4), F) Alg-C6 (1:4). The hydrogels exhibited higher storage moduli values at 0.5% strain while exhibiting lower G' values at 250% strain. Compared to alginate supramolecular inclusion complexes formed with β-CD, the novel Pluronic® F108:Alg-g-CD hydrogels presented here are shear-thinning, and amendable to injectable biomaterials applications[25].

6.3.4. Thermo-Responsive Properties

The alginate-based supramolecular inclusion complex hydrogels are thermo-responsive and exhibit secondary crosslinking effects with increasing temperature, due to the incorporation of Pluronic® F108. To demonstrate the thermo-responsive properties of the Alg-*g*-CD and Pluronic® F108 hydrogels, temperature sweeps were performed from 25 to 37 °C at a heating rate of 0.5 °C min^{-1} (1% strain; 1 Hz). The significant transition temperatures occurred near 30 °C. For all hydrogel groups tested, the storage moduli (G') increased with increasing temperature (**Figure 6-4**). The shear moduli for all hydrogel samples were statistically different between 25 and 37 °C for all samples within the same group (**Figure 6-4**), with G' values significantly higher at

.

body temperature compared to room temperature. Independent of polymer concentration, hydrogels fabricated using Pluronic® F108:Alg-*g*-CD ratios of 1:2 were significantly stiffer compared to ratios of 1:4 at both 25 and 37 °C. The differences in G' within the same group at the different temperatures were elevated due to the addition of Pluronic® F108 in the hydrogel system, indicating that Pluronic® F108 played a significant role in the thermo-response of the host-guest hydrogels. Furthermore, considering only hydrogels with a Pluronic® F108:Alg-*g*-CD ratio of 1:4, 6% (w/v) Alg-*g*-CD hydrogels were significant higher compared to 4% hydrogels, for both Alg-C2 and Alg-C6 formulations. Alg-C6 (1:2) hydrogels exhibited G' values of near 30 kPa at 37 °C, which corresponded to a ~3% increase in stiffness compared to hydrogels at 25 °C (< 10 kPa). The thermo-transition from room temperature to body temperature was markedly higher compared to existing literature,[69] suggesting potential *in vivo* applications of the thermal-responsive hydrogel in drug delivery and tissue engineering. The novel Pluronic® F108:Alg-*g*-CD hydrogels were strain-responsive, i.e., shear-thinning, in addition to exhibiting thermo-responsive behavior, exhibiting mechanical and temperature responsive properties. Strain-responsive alginate-based supramolecular inclusion complexes presented in the literature do not exhibit thermo-responsive behavior.[70] Likewise, thermo-responsive alginate hydrogels do not exhibit shear-thinning and self-healing behavior.[71-73]

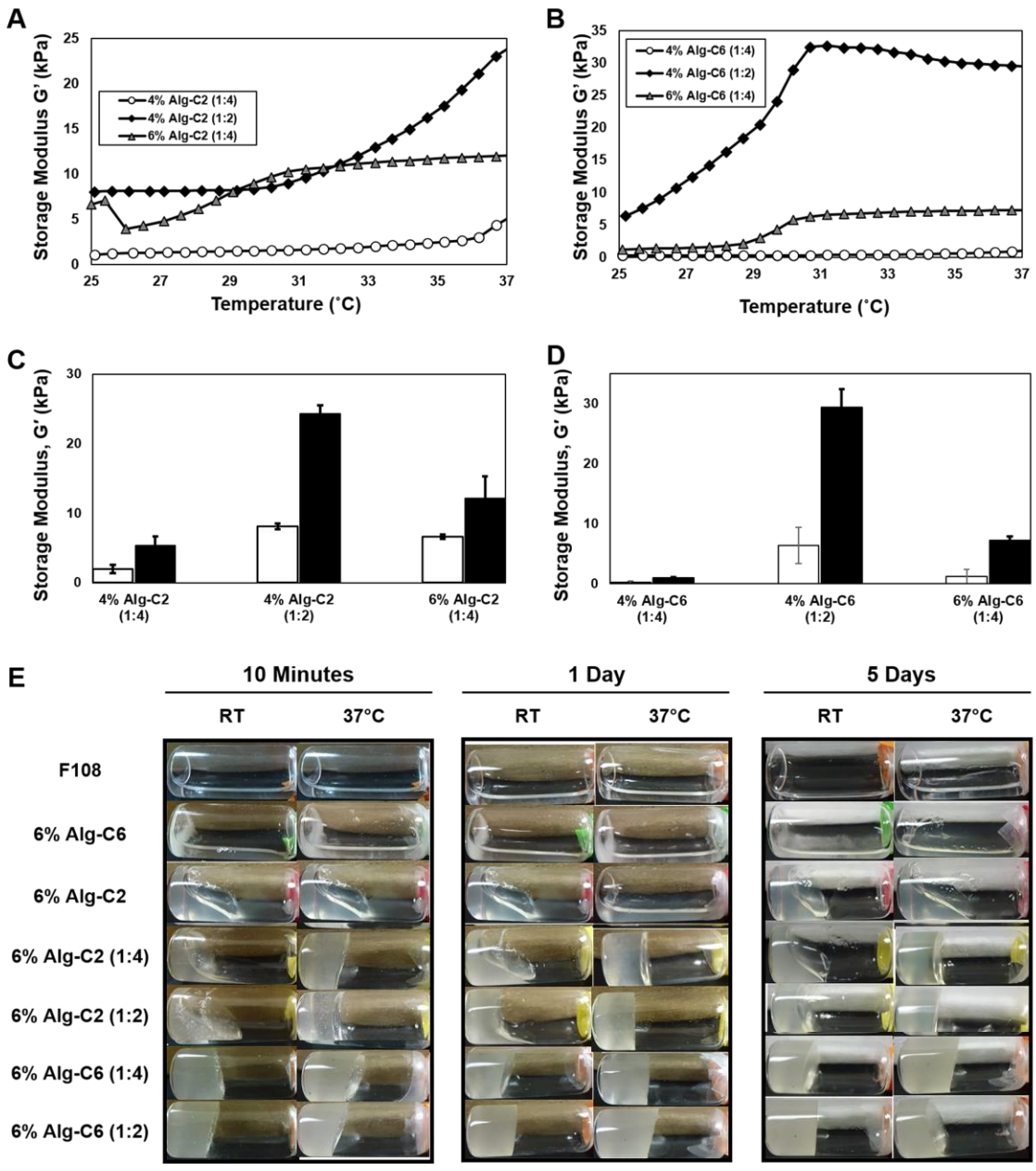

Figure 6-4 (A, B) Oscillatory temperature sweeps were performed at 1 Hz and 1% radial strain on Alg-g-CD hydrogels: A) Alg-C2 and B) Alg-C6. (C, D) Shear storage moduli (G') for Alg-g-CD hydrogels at 25 °C (white bars) and 37 °C (black bars) (n = 3, average ± standard deviation), specifically C) Alg-C2 and D) Alg-C6. The ratio of Alg-g-CD to

.

Pluronic® F108 was critical to the magnitude of the thermo-responsive properties. The greater the ratio of Pluronic® F108, the stiffer the hydrogel and more responsive the thermal behavior. Significant differences, of the same hydrogel sample between 25 and 37 °C, were observed in both Alg-g-CD hydrogel formulations. E) Images of Alg-g-CD and Pluronic® F108 solutions, and Alg-g-CD hydrogels formed after mixing the two pre-cursers and waiting 10 min, 1 day, and 5 days. Images were taken of hydrogels incubated at room temperature (RT) and 37 °C, respectively.

6.3.5. Hydrogel Stability

The physical integrity of the hydrogel network (i.e., supramolecular inclusion complex) was visually analyzed by examining hydrogel stability over 5 days at both room temperature and 37 °C. The 4% (w/v) Alg-*g*-CD hydrogels, with Pluronic® F108:Alg-*g*-CD ratios of 1:4 and 1:2, solidified (i.e., physically crosslinked) quicker when exposed to 37 °C compared to those hydrogels exposed to room temperature. For 4% Alg-C2 (1:4 and 1:2) and 4% Alg-when C6 (1:4) formulations, a solid hydrogel was only formed at 37 °C rather than at room temperature, indicating the significant impact of the secondary physical crosslinking arising from the micelle formation of Pluronic® F108. This effect was evident for hydrogels formed from lower concentration solutions (**supplemental materials 6.5**). For higher concentration solutions, the hydrogel formed upon mixing of the pre-curser solutions at room temperature (**Figure 6-4**). In summary, hydrogels remained stable for up to 5 days after initial formation of the supramolecular inclusion complex, in a non-disturbed, static state. Further

.

observation was performed of Alg-C2 and Alg-C6 hydrogels (see supplemental material) at room temperature for over 6 months (sealed with parafilm to eliminate water evaporation); optical photographs are shown in supplemental information 9 under "day 0". They remained solid and crosslinked, demonstrating the stability of the hydrogels in air. However, in order to assess the stability of the hydrogels under physiological conditions, a degradation or erosion experiment must also be performed.

6.3.6. Hydrogel Erosion

To visualize hydrolytic erosion of Alg-C2 and Alg-C6 supramolecular inclusion complex hydrogels, a qualitative surface erosion was performed. Freshly prepared hydrogels were injected into glass vials, flowed to take the shape of the container before completion of crosslinked, and solidified at 37 ˚C. PBS was added to the vials, and the vials were inverted each day 1 – 7, followed by static incubation for an additional 7 days. After day 3, the Alg-C2 hydrogels appeared to reach a swollen equilibrium state and remained at the bottom of the vial until day 14 (supplemental information 9 under newly injected from day 0 with PBS to day 14). The surface erosion of 4% and 6% Alg-C6 (1:4) hydrogels was observed as the height of the solidified hydrogels getting shorter until day 14, which was different compared to the response of the Alg-C2 hydrogels. The 4% (w/v) Alg-C2 hydrogels exhibited decreased stability and less resistance to flow after 3 days of culture in PBS during physical inversion; however, when the vials were returned to a static state, the hydrogels

solidified. Over time hydrogels appeared to continue to crosslink, indicative of self-healing characteristics, quantified above. Interestingly, the 6% Alg-C6 (1:2) hydrogel network swelled and incorporated the PBS into the network, and solidified the solution. This was likely due to surface erosion releasing Alg-C6 and Pluronic® F108 polymers into the PBS. In addition, the Alg-C6 hydrogels may inherently enabled more flexibility to the CD functional group compared to the Alg-C2 due to the longer methylene group. This recovery and stability of the Alg-C6 hydrogels was more evident compared to the Alg-C2 over the 14-day period.

6.3.7. *In Vitro* BSA Release

The inner cavity of β-CD undergoes hydrophobic interactions, not only with PPG but with other organic molecules, and such interactions have been extensively employed as drug carriers. Specifically, drug release profiles for supramolecular inclusion network hydrogels utilizing β-CD as a physical crosslinker are of recent interest.[5] For this study, BSA, a moderately sized biomolecule (66.5 kDa) with a globular structure, was encapsulated and released from Alg-*g*-CD hydrogels. BSA release was quantified for up to 14 days for both 4% (w/v) and 6% Alg-C6 and Alg-C2 hydrogels with ratios of 1:2 and 1:4. For each sample, BSA exhibited a sustained release over 14 days to afford a release amount of 40% of the encapsulated drug (**Figure 6-5**). A lower amount of BSA was released from hydrogels formulated with a Pluronic® F108:Alg-*g*-CD ratio of 1:4, suggesting that the reduction in Pluronic® F108

content created a moderately crosslinked hydrogel, resulting in a greater release of BSA. Alg-C2 hydrogels **(Figure 6-A**) released less BSA compared to Alg-C6 hydrogels (**Figure 6-5**) over a period of 14 days, due to a swollen host-guest intermolecular network observed in the qualitative surface erosion study (supplemental information). As stated above, Alg-C2 hydrogels swelled after the addition of PBS. Thus, the hydrogel structure was weakened and compromised, resulting an enhanced released compared to Alg-C6 gels, who was degraded gradually from the top surface to the bottom of glass vials.

6.3.8. *In Vitro* Cytotoxicity

The safety and efficacy of the alginate-based hydrogels for biomedical applications was tested using a 24 h mitochondrial activity (i.e., MTT content) based assay. 4% (w/v) and 6% Alg-*g*-CD hydrogels, with Pluronic® F108:Alg-*g*-CD ratios 1:2 and 1:4, were co-cultured with primary human MSCs for 24 h. An *in vitro* cytotoxicity assay showed no toxic effects related to the presence of the hydrogels. Alg-C2 hydrogels were slightly less cytotoxic compared to Alg-C6 hydrogels; however, there were no significant differences between experimental groups (**Figure 6-5**) and the control group (non-modified TCPS).

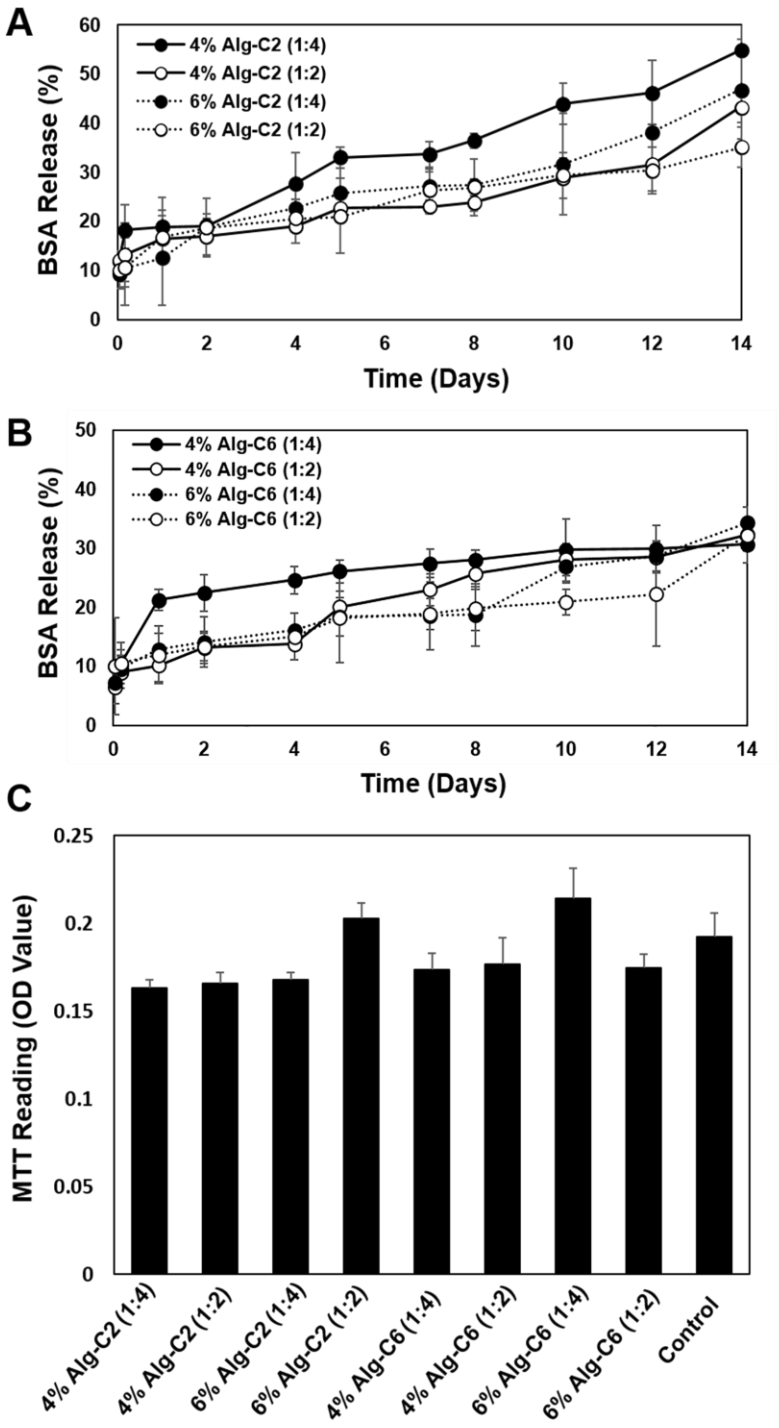
A
4% Alg-C2 (1:4)
4% Alg-C2 (1:2)
6% Alg-C2 (1:4)
6% Alg-C2 (1:2)
BSA Release (%)
Time (Days)
B
4% Alg-C6 (1:4)
4% Alg-C6 (1:2)
6% Alg-C6 (1:4)
6% Alg-C6 (1:2)
BSA Release (%)
Time (Days)
C
MTT Reading (OD Value)
4% Alg-C2 (1:4)
4% Alg-C2 (1:2)
6% Alg-C2 (1:4)
6% Alg-C2 (1:2)
4% Alg-C6 (1:4)
4% Alg-C6 (1:2)
6% Alg-C6 (1:4)
6% Alg-C6 (1:2)
Control

Figure 6-5. (A,B) In vitro BSA release from Pluronic® F108:Alg-g-CD hydrogels. Experiments were performed at 37 °C under mild agitation in PBS, pH 7.4, investigating A) Alg-C2 and B) Alg-C6 hydrogels. Black circles represent 6% (w/v) Alg-g-CD solutions, open circles represent 4% Alg-g-CD solutions. Solid lines represent Pluronic® F108:Alg-g-CD hydrogels with ratios of 1:2; dashed lines represent hydrogels with ratios of 1:4. C) In vitro MTT-based assay results of hydrogels cultured with primary human MSCs indicated no toxic effect for the various hydrogels analyzed along with the non-material treated control group. There were no significant differences between each group.

6.4. Conclusions

In summary, we have developed the first dual-crosslinked, self-healing, and strain and thermo-responsive alginate-based hydrogels with moderate mechanical properties, based on the supramolecular inclusion complex formation between Pluronic® F108 and Alg-*g*-CD. The intermolecular entanglement of guest polymers (e.g., PPG) creates a unique structure upon crosslinking which affords shear-thinning behavior. Furthermore, Pluronic® F108 affords a thermo-responsive behavior of the injectable hydrogel, generating a dual-crosslinked hydrogel upon increase to body temperature. Upon mixing host and guest polymers, the shear storage moduli of the hydrogel reached as high as 30 kPa at body temperature, exhibiting biologically-relevant mechanical properties for biomedical applications.

.

6.5. Supplemental Materials

1. ^{1}H-NMR spectrum of β-CD-TsCl

^{1}H-NMR (DMSO-d6) δ = 2.42 (s, 3H), , 4.12−4.40 (m, 6H), 4.77 (s, 2H), 4.83 (s, 5H), 5.60−6.05 (br s, 14H), 7.43 (d, 2H), 7.75 (d, 2H).

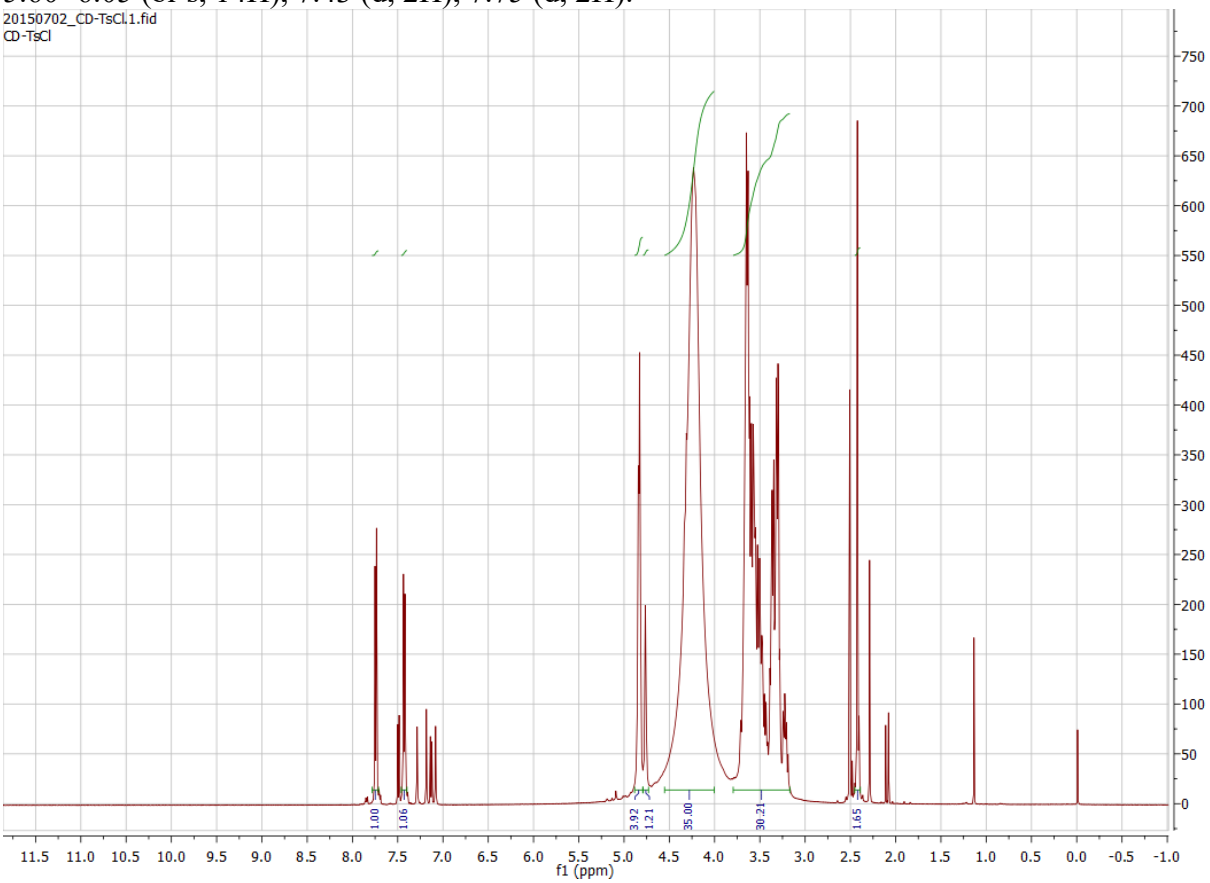

Figure 6-6. ^{1}H-NMR spectrum of β-CD-TsCl in DMSO-d_6. The peaks corresponding to δ = 7.43 ppm (2H) and δ = 7.75 ppm (2H) identify the hydrogens on the benzene ring of the toluenesulfonyl group. The remaining peaks between δ = 7 and 8 ppm refer to non-purified p-tuluenesulfonyl chloride. The peak corresponding to δ = 2.42 ppm (3H) refers to the hydrogens of the methylene group of the toluenesulfonyl group. Peaks between δ = 4.0 and 5.0 ppm refer to the hydrogens on the β-CD ring.[5] [12]

.

2. ^{1}H-NMR spectrum of β-CD-HAD

H NMR (DMSO-d6) δ = 1.14−1.61 (m, 12H), 3.48−3.78 (m, 28H), 4.28−4.56 (br s, 6H), 4.83 (s, 7H), 5.59−5.88 (br s, 14H).

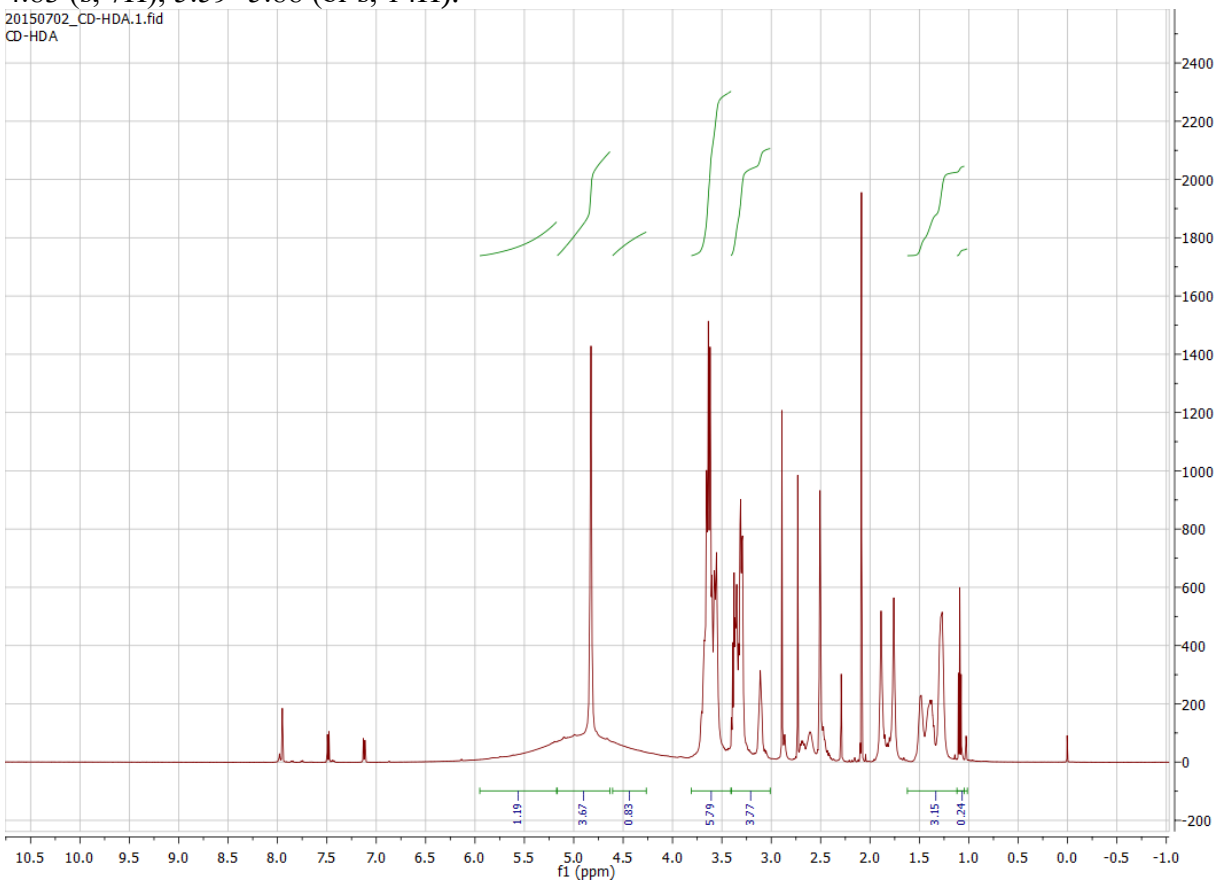

Figure 6-7. ^{1}H-NMR spectrum of β-CD-HDA. The disappearance of peaks between δ = 7 and 8 ppm indicates that the toluenesulfonyl group was replaced with hexanediamine. The peaks corresponding to δ = 1.14-1.16 ppm (12H) refer to hydrogens on the hexanediamine group. Peaks between δ = 3 and 5 ppm represent hydrogens on the β-CD ring. Peaks between δ = 1.00 and 1.10 ppm (2H) represent hydrogens on the amine group. [5, 12]

.

3. ^{1}H-NMR spectrum of β-CD-EDA

^{1}H NMR (300 MHz, D2O, DSS) δ = 2.61 (2H, -NHCH$_2$-), 2.73 (3H, -CH$_2$CH$_2$NH$_2$, -CH$_2$(H-6')-N), 2.92 (d, 1H, -CH$_2$(H-6')-), 3.33 (t, 1H, -CH(H-4')-), 3.36-3.51 (m, 14H, -CH(H-2,H-2')-, -CH(H-5')-, -CH(H-4)-), 3.73-3.84 (m, 25H, -CH(H-3,H-3')-, -CH(H-5)-, -CH$_2$(H-6)-), 4.92 (d, 7H, -CH(H-1, H-1')-) ppm.

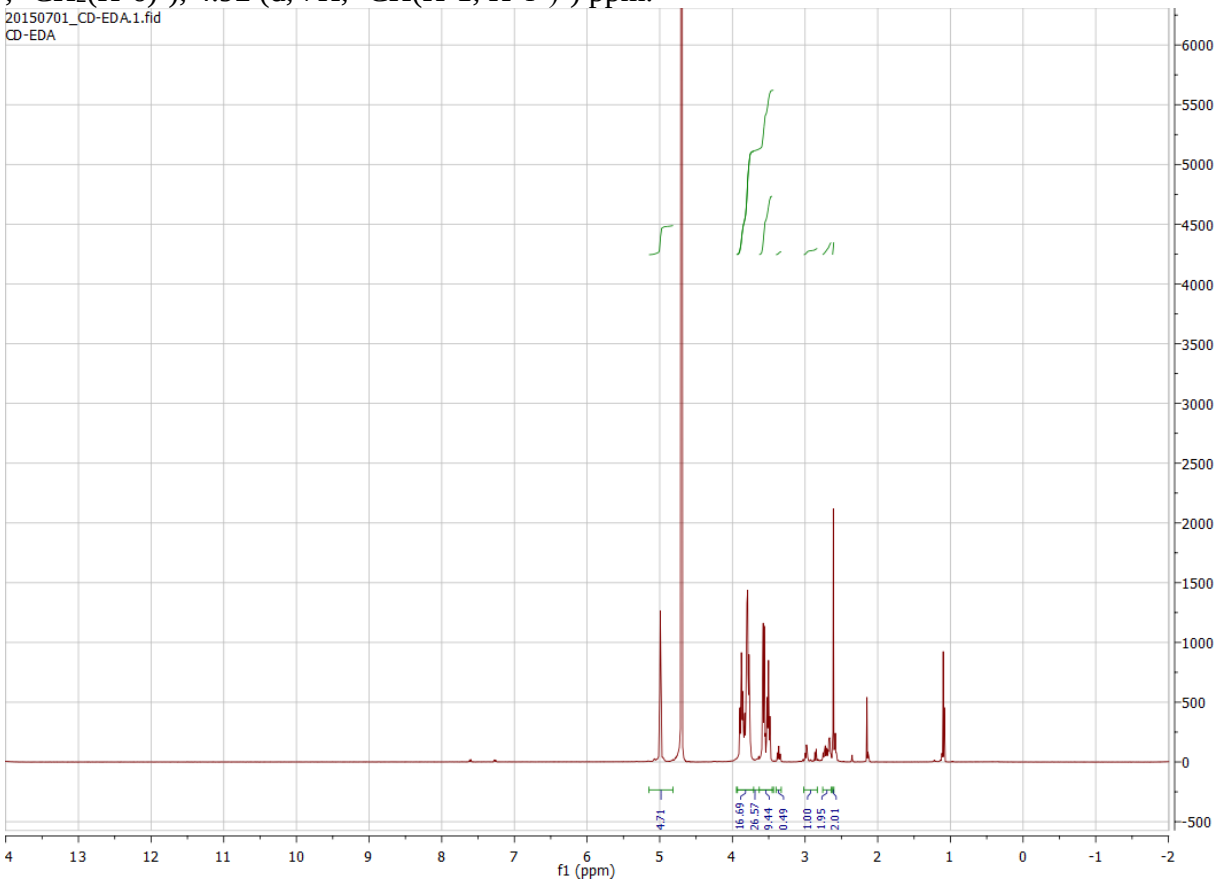

Figure 6-8. ^{1}H-NMR spectrum of β-CD-EDA. The disappearance of peaks between δ = 7 and 8 ppm indicate that the toluenesulfonyl group was replaced with ethylenediamine. The peak at δ = 2.61 ppm (2H) refers to hydrogens on the amine group. The peak at δ = 2.73 ppm (3H) refers to hydrogens on the methylene chain. Peaks between δ = 3.73 and 3.84 ppm represent hydrogens on the β-CD ring.[65]

.

4.

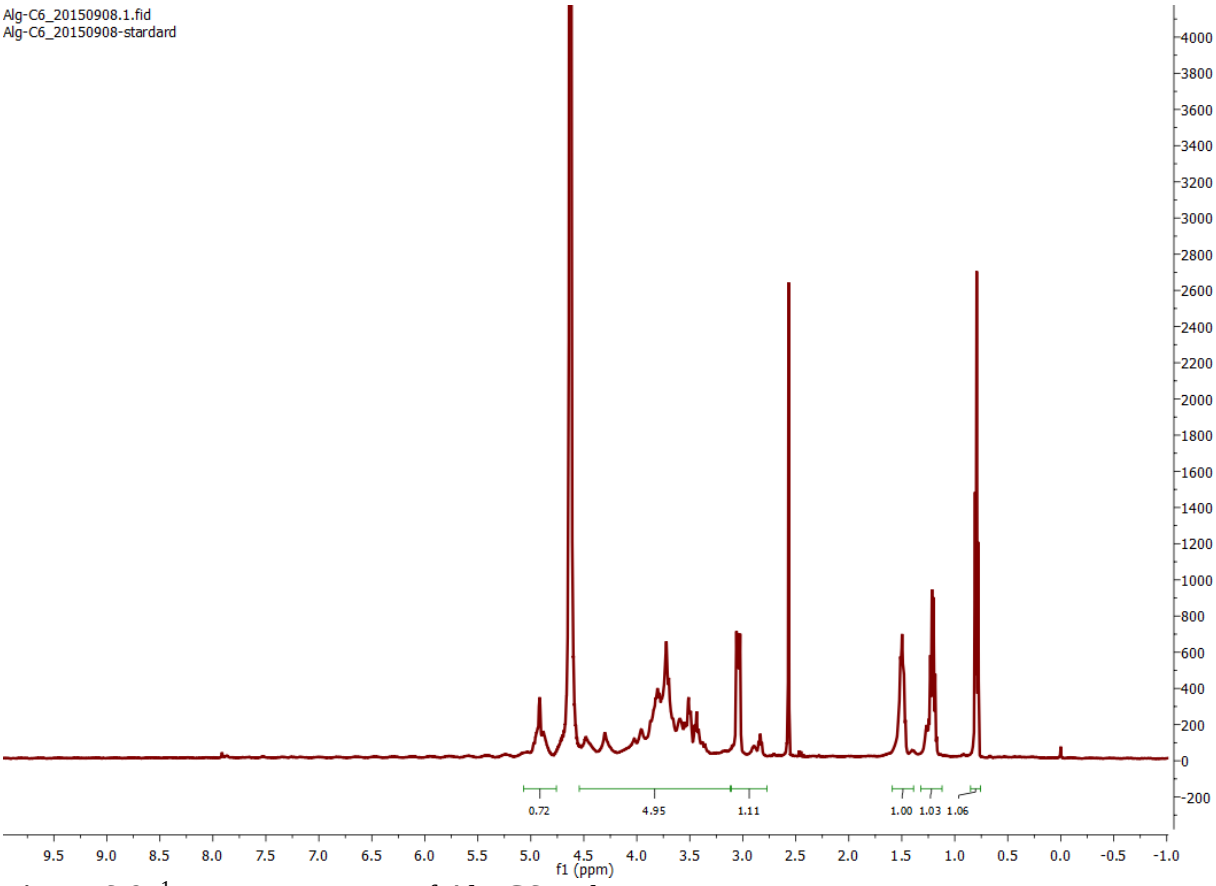

Figure 6-9. ^{1}H-NMR spectrum of Alg-C6 with integration

.

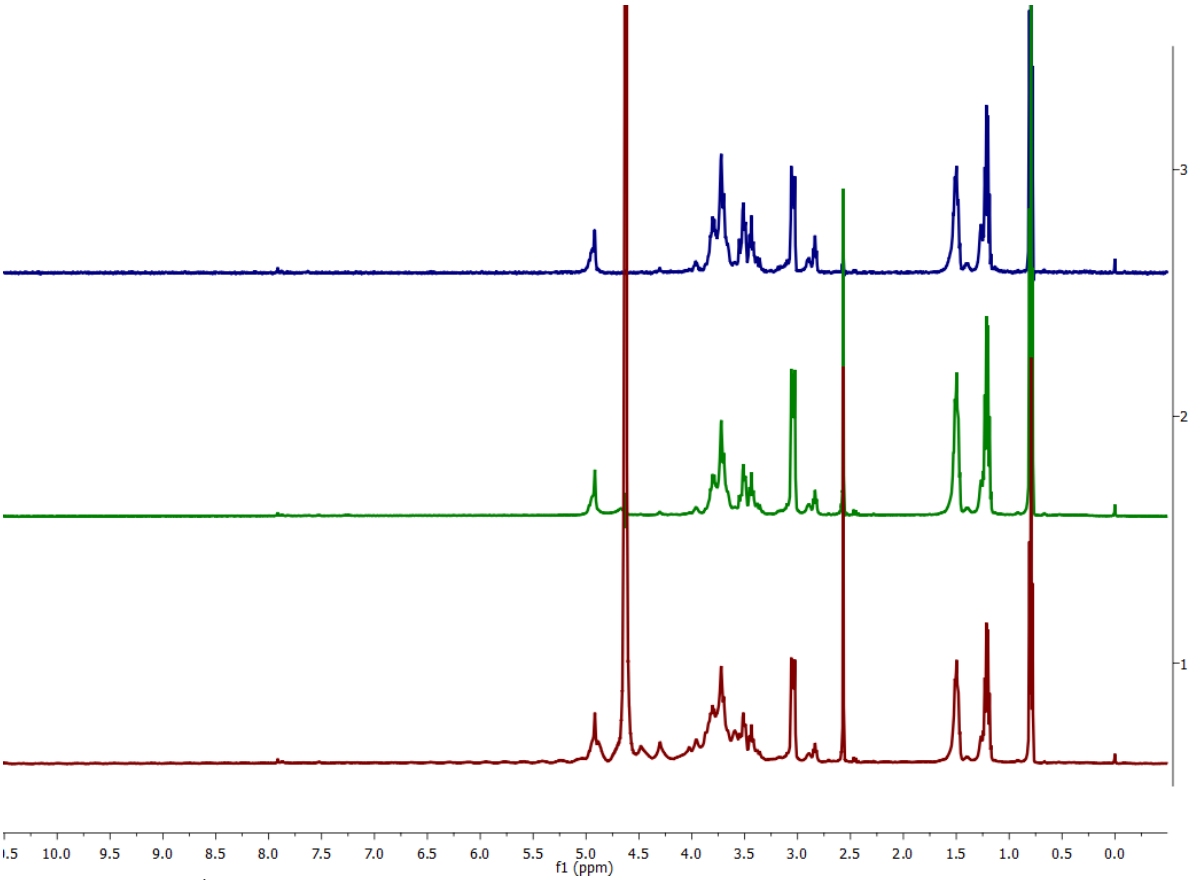

Figure 6-10. ^{1}H-NMR spectra of Alg-C6 with standard procedure (brown), water suppression procedure (green), and diffusion edit procedure at 95% strength (blue).

.

5.

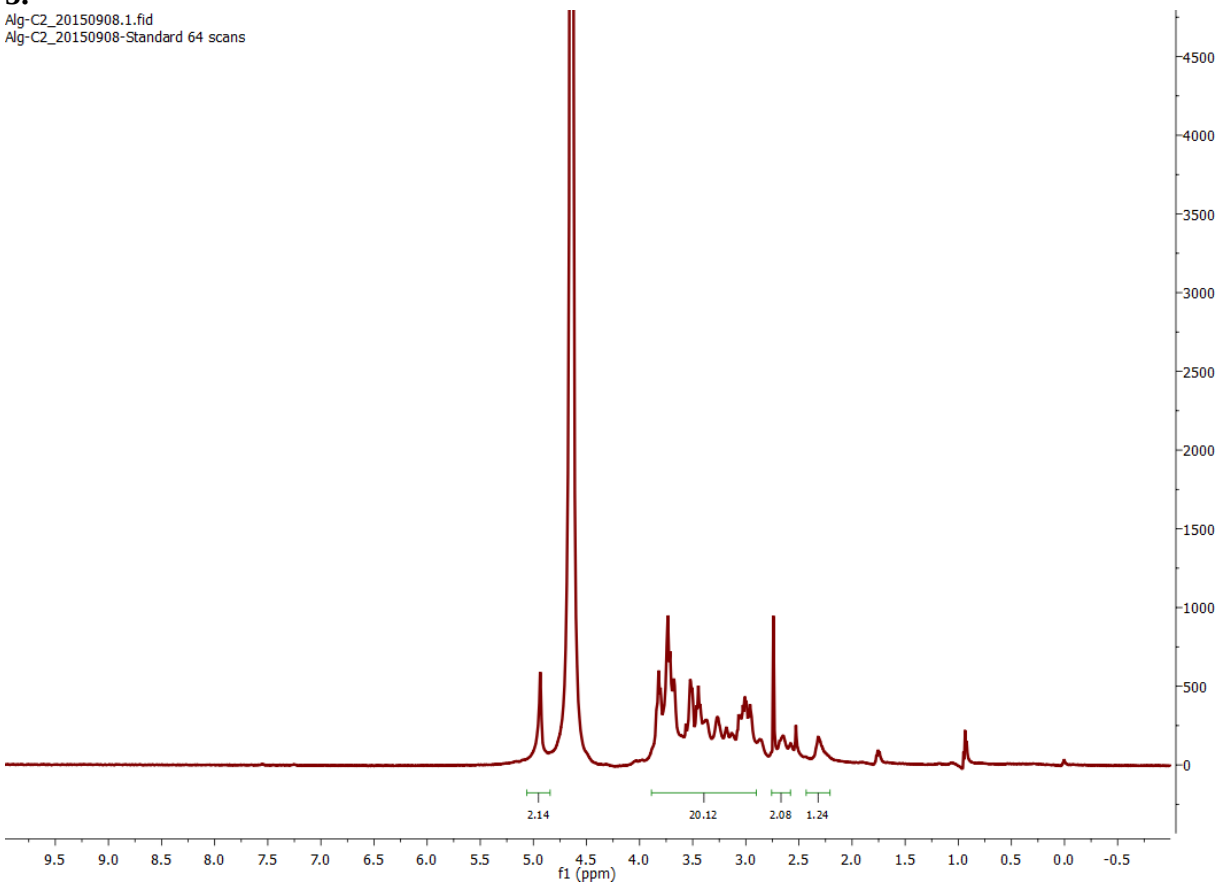

Figure 6-11. ^{1}H-NMR spectrum of Alg-C2 with integration.

.

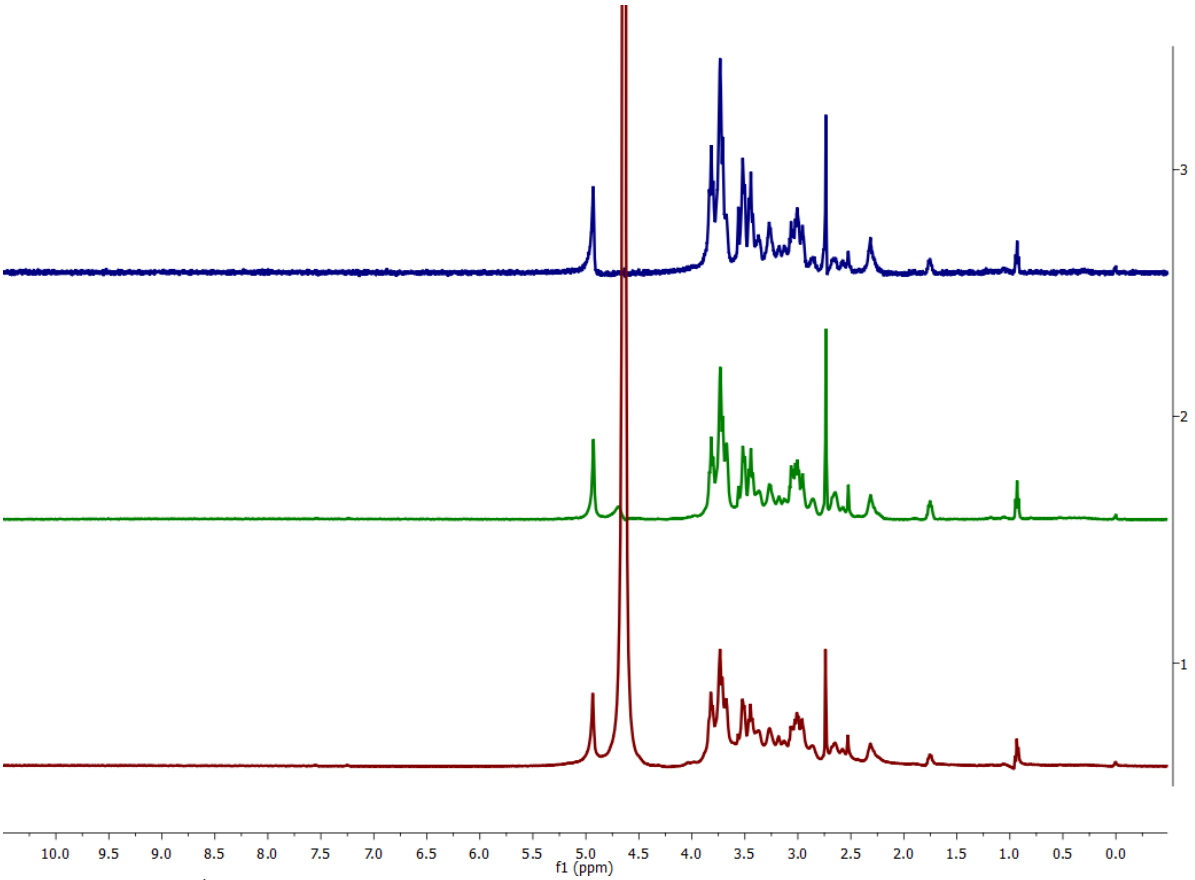

Figure 6-12. ^{1}H-NMR spectra of Alg-C6 with standard procedure (brown), water suppression procedure (green), and diffusion edit procedure at 95% strength (blue).

.

6.

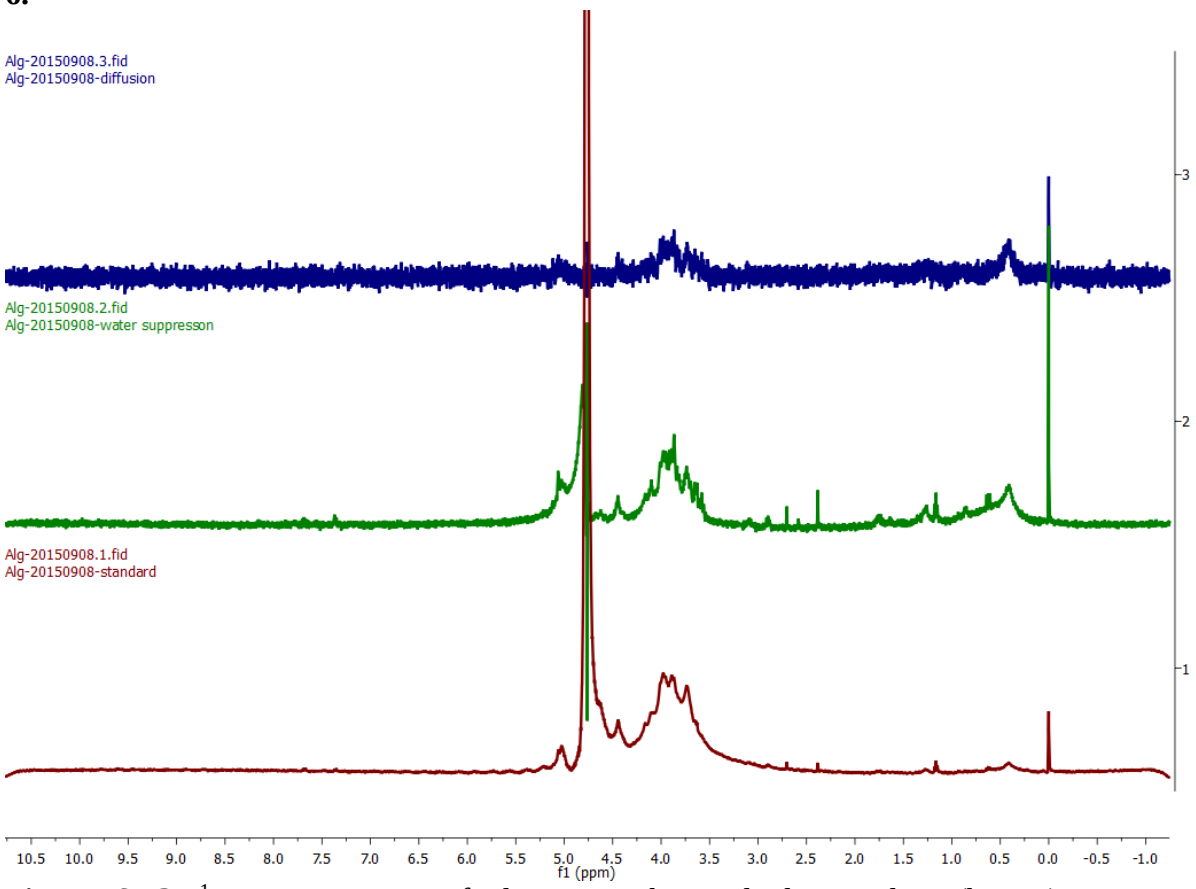

Figure 6-13. ^{1}H-NMR spectra of alginate with standard procedure (brown), water suppression procedure (green), and diffusion edit procedure at 95% strength (blue).

.

7. Stacked ^{1}H-NMR spectra of alginate (brown), Alg-C2 (green and Alg-C6 (brown).

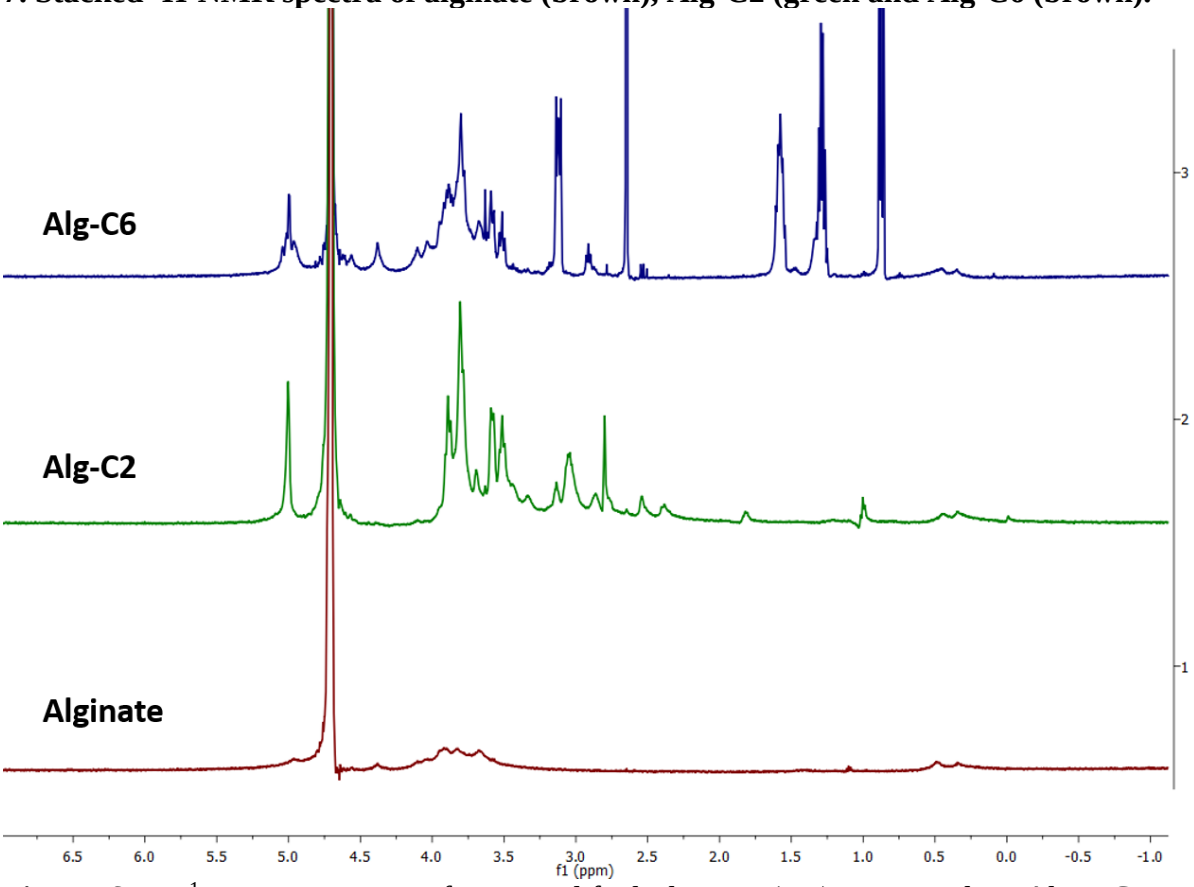

Figure 6-14. ^{1}H-NMR spectra of non-modified alginate (top) compared to Alg-*g*-CD (middle, bottom). Peaks between δ = 7 and 8 ppm represent the hydrogens on the amine group. Peaks between δ = 1 and 2 ppm refer to hydrogens on the methylene chain.

.

8.

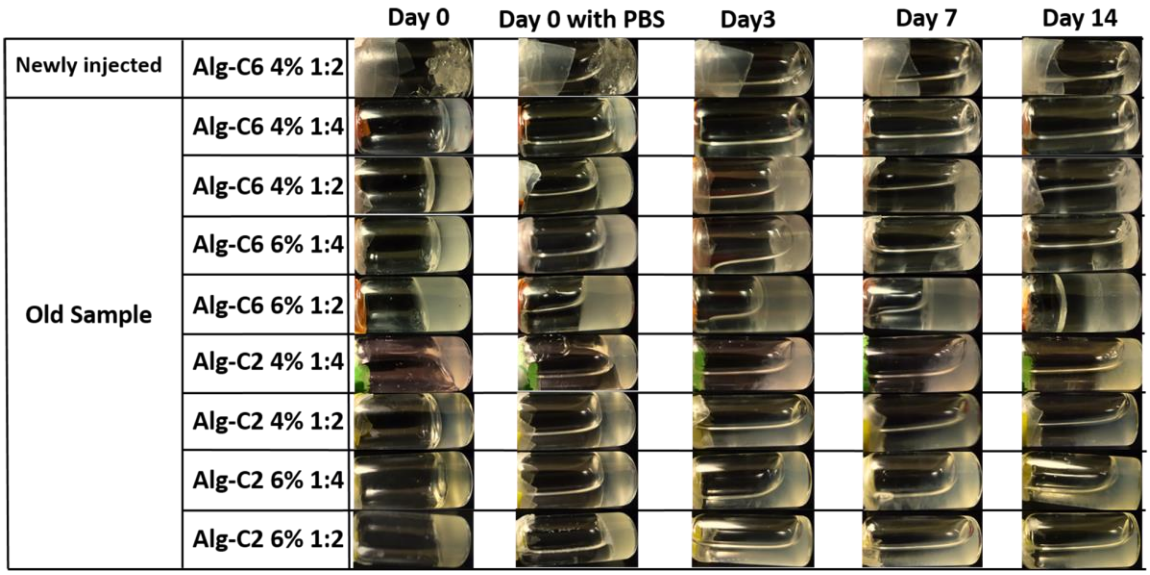

Figure 6-15. Optical photographs of hydrogel surface erosion in PBS at 37 ˚C over 14 days. Day 0 images demonstrate that the hydrogels crosslinked in the bottles, taking the shape of the container; hydrogels were not exposed to PBS. Day 0 with PBS images demonstrate how the hydrogels behaved after the addition of PBS. Day 3, 7 and 14 are series photos taken of the same sample at a specific time point. During the 14 day study, hydrogels were incubated at 37 ˚C under gentle agitation.

.

The Alg-C2 hydrogel can be conjugate with cell instructive peptide such as RGD. The hydrogel containing A549 cells were injected out and cultured for 24h before staining with live/dead stain and imaged under CLS.

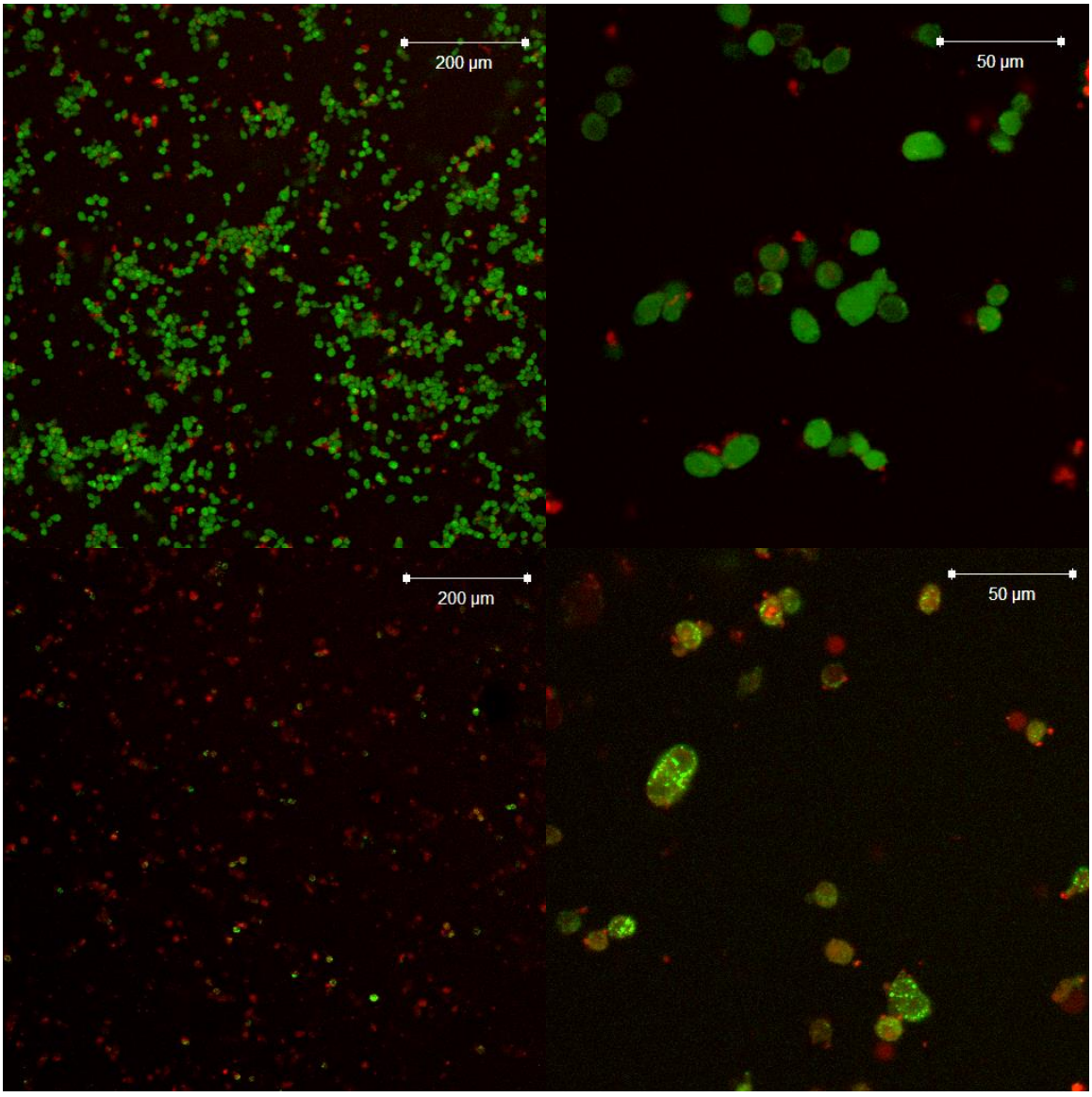

.

References

[1] Appel EA, del Barrio J, Loh XJ, Scherman OA. Supramolecular polymeric hydrogels. Chemical Society Reviews 2012;41:6195-214.
[2] Bae KH, Wang L-S, Kurisawa M. Injectable biodegradable hydrogels: progress and challenges. Journal of Materials Chemistry B 2013;1:5371-88.
[3] Burdick JA, Murphy WL. Moving from static to dynamic complexity in hydrogel design. Nat Commun 2012;3:1269.
[4] Yang J-A, Yeom J, Hwang BW, Hoffman AS, Hahn SK. In situ-forming injectable hydrogels for regenerative medicine. Progress in Polymer Science 2014;39:1973-86.
[5] Rodell CB, Kaminski AL, Burdick JA. Rational Design of Network Properties in Guest–Host Assembled and Shear-Thinning Hyaluronic Acid Hydrogels. Biomacromolecules 2013;14:4125-34.
[6] Williams CG, Malik AN, Kim TK, Manson PN, Elisseeff JH. Variable cytocompatibility of six cell lines with photoinitiators used for polymerizing hydrogels and cell encapsulation. Biomaterials 2005;26:1211-8.
[7] McCall JD, Anseth KS. Thiol–Ene Photopolymerizations Provide a Facile Method To Encapsulate Proteins and Maintain Their Bioactivity. Biomacromolecules 2012;13:2410-7.
[8] Berger J, Reist M, Mayer JM, Felt O, Peppas NA, Gurny R. Structure and interactions in covalently and ionically crosslinked chitosan hydrogels for biomedical applications. European Journal of Pharmaceutics and Biopharmaceutics 2004;57:19-34.
[9] Yan X, Wang F, Zheng B, Huang F. Stimuli-responsive supramolecular polymeric materials. Chemical Society Reviews 2012;41:6042-65.
[10] Chen Q, Zhu L, Chen H, Yan H, Huang L, Yang J, et al. A Novel Design Strategy for Fully Physically Linked Double Network Hydrogels with Tough, Fatigue Resistant, and Self-Healing Properties. Advanced Functional Materials 2015;25:1598-607.
[11] Appel EA, Tibbitt MW, Webber MJ, Mattix BA, Veiseh O, Langer R. Self-assembled hydrogels utilizing polymer-nanoparticle interactions. Nat Commun 2015;6:6295.
[12] Rodell CB, MacArthur JW, Dorsey SM, Wade RJ, Wang LL, Woo YJ, et al. Shear-Thinning Supramolecular Hydrogels with Secondary Autonomous Covalent Crosslinking to Modulate Viscoelastic Properties In Vivo. Advanced Functional Materials 2015;25:636-44.
[13] Rodell CB, Rai R, Faubel S, Burdick JA, Soranno DE. Local immunotherapy via delivery of interleukin-10 and transforming growth factor β antagonist for treatment of chronic kidney disease. Journal of Controlled Release 2015;206:131-9.
[14] Blaiszik B, Kramer S, Olugebefola S, Moore JS, Sottos NR, White SR. Self-healing polymers and composites. Annual Review of Materials Research 2010;40:179-211.
[15] Harada A, Takashima Y, Yamaguchi H. Cyclodextrin-based supramolecular polymers. Chemical Society Reviews 2009;38:875-82.
[16] Cai L, Dewi RE, Heilshorn SC. Injectable Hydrogels with In Situ Double Network Formation Enhance Retention of Transplanted Stem Cells. Advanced Functional Materials 2015;25:1344-51.
[17] Chiang C-Y, Chu C-C. Synthesis of photoresponsive hybrid alginate hydrogel with photo-controlled release behavior. Carbohydrate Polymers 2015;119:18-25.
[18] Huang F, Scherman OA. Supramolecular polymers. Chemical Society Reviews 2012;41:5879-80.
[19] Guvendiren M, Lu HD, Burdick JA. Shear-thinning hydrogels for biomedical applications. Soft Matter 2012;8:260-72.

.

[20] Wei Z, Yang JH, Liu ZQ, Xu F, Zhou JX, Zrínyi M, et al. Self-Healing Materials: Novel Biocompatible Polysaccharide-Based Self-Healing Hydrogel (Adv. Funct. Mater. 9/2015). Advanced Functional Materials 2015;25:1471-.
[21] Kuhl E. Growing matter: a review of growth in living systems. J Mech Behav Biomed Mater 2014;29:529-43.
[22] Del Valle EMM. Cyclodextrins and their uses: a review. Process Biochemistry 2004;39:1033-46.
[23] Boekhoven J, Rubert Pérez CM, Sur S, Worthy A, Stupp SI. Dynamic Display of Bioactivity through Host–Guest Chemistry. Angewandte Chemie International Edition 2013;52:12077-80.
[24] Fernandes Fraceto L, Grillo R, Sobarzo-Sanchez E. Cyclodextrin inclusion complexes loaded in particles as drug carrier systems. Current topics in medicinal chemistry 2014;14:518-25.
[25] Tan L, Liu Y, Ha W, Ding L-S, Peng S-L, Zhang S, et al. Stimuli-induced gel-sol transition of multi-sensitive supramolecular [small beta]-cyclodextrin grafted alginate/ferrocene modified pluronic hydrogel. Soft Matter 2012;8:5746-9.
[26] Ciofani G, Raffa V, Menciassi A, Dario P. Alginate and chitosan particles are drug delivery system for cell therapy. Biomed Microdevices 2008;10:597-600.
[27] Jay SM, Saltzman WM. Controlled delivery of VEGF via modulation of alginate microparticle ionic crosslinking. Journal of Controlled Release 2009;134:26-34.
[28] Jay SM, Shepherd BR, Bertram JP, Pober JS, Saltzman WM. Engineering of multifunctional gels integrating highly efficient growth factor delivery with endothelial cell transplantation. FASEB J 2008;22:2949-56.
[29] Lemoine D, Wauters F, Bouchend'homme S, Préat V. Preparation and characterization of alginate microspheres containing a model antigen. International Journal of Pharmaceutics 1998;176:9-19.
[30] Augst AD, Kong HJ, Mooney DJ. Alginate hydrogels as biomaterials. Macromolecular bioscience 2006;6:623-33.
[31] Lee KY, Mooney DJ. Alginate: properties and biomedical applications. Progress in polymer science 2012;37:106-26.
[32] Brewster ME, Loftsson T. Cyclodextrins as pharmaceutical solubilizers. Advanced Drug Delivery Reviews 2007;59:645-66.
[33] Paolino M, Ennen F, Lamponi S, Cernescu M, Voit B, Cappelli A, et al. Cyclodextrin-Adamantane Host–Guest Interactions on the Surface of Biocompatible Adamantyl-Modified Glycodendrimers. Macromolecules 2013;46:3215-27.
[34] Granadero D, Bordello J, Pérez-Alvite MJ, Novo M, Al-Soufi W. Host-Guest Complexation Studied by Fluorescence Correlation Spectroscopy: Adamantane–Cyclodextrin Inclusion. International Journal of Molecular Sciences 2010;11:173-88.
[35] van de Manakker F, Braeckmans K, Morabit Ne, De Smedt SC, van Nostrum CF, Hennink WE. Protein-Release Behavior of Self-Assembled PEG–β-Cyclodextrin/PEG–Cholesterol Hydrogels. Advanced Functional Materials 2009;19:2992-3001.
[36] Yamaguchi H, Kobayashi Y, Kobayashi R, Takashima Y, Hashidzume A, Harada A. Photoswitchable gel assembly based on molecular recognition. Nat Commun 2012;3:603.
[37] Pozuelo J, Mendicuti F, Mattice WL. Inclusion Complexes of Chain Molecules with Cycloamyloses III. Molecular Dynamics Simulations of Polyrotaxanes Formed by Poly(propylene glycol) and [beta]-Cyclodextrins. Polym J 1998;30:479-84.
[38] Qin J, Meng X, Li B, Ha W, Yu X, Zhang S. Self-assembly of β-cyclodextrin and pluronic into

.

hollow nanospheres in aqueous solution. Journal of colloid and interface science 2010;350:447-52.
[39] Okada M, Kamachi M, Harada A. Preparation and Characterization of Inclusion Complexes of Poly(propylene glycol) with Methylated Cyclodextrins. The Journal of Physical Chemistry B 1999;103:2607-13.
[40] Harada A, Okada M, Li J, Kamachi M. Preparation and Characterization of Inclusion Complexes of Poly(propylene glycol) with Cyclodextrins. Macromolecules 1995;28:8406-11.
[41] Corey JM, Gertz CC, Sutton TJ, Chen Q, Mycek KB, Wang B-S, et al. Patterning N-type and S-type neuroblastoma cells with Pluronic F108 and ECM proteins. Journal of Biomedical Materials Research Part A 2010;93A:673-86.
[42] Tharmalingam T, Goudar CT. Evaluating the impact of high Pluronic® F68 concentrations on antibody producing CHO cell lines. Biotechnology and Bioengineering 2015;112:832-7.
[43] Loh XJ, Goh SH, Li J. Hydrolytic degradation and protein release studies of thermogelling polyurethane copolymers consisting of poly[(R)-3-hydroxybutyrate], poly(ethylene glycol), and poly(propylene glycol). Biomaterials 2007;28:4113-23.
[44] Loh XJ, Peh P, Liao S, Sng C, Li J. Controlled drug release from biodegradable thermoresponsive physical hydrogel nanofibers. Journal of Controlled Release 2010;143:175-82.
[45] Loh XJ, Colin Sng KB, Li J. Synthesis and water-swelling of thermo-responsive poly(ester urethane)s containing poly(ε-caprolactone), poly(ethylene glycol) and poly(propylene glycol). Biomaterials 2008;29:3185-94.
[46] Loh XJ, Tan YX, Li Z, Teo LS, Goh SH, Li J. Biodegradable thermogelling poly(ester urethane)s consisting of poly(lactic acid) – Thermodynamics of micellization and hydrolytic degradation. Biomaterials 2008;29:2164-72.
[47] Pradal C, Jack KS, Grøndahl L, Cooper-White JJ. Gelation Kinetics and Viscoelastic Properties of Pluronic and α-Cyclodextrin-Based Pseudopolyrotaxane Hydrogels. Biomacromolecules 2013;14:3780-92.
[48] Pradal C, Grondahl L, Cooper-White JJ. Hydrolytically degradable polyrotaxane hydrogels for drug and cell delivery applications. Biomacromolecules 2015;16:389-403.
[49] Lin N, Dufresne A. Supramolecular hydrogels from in situ host-guest inclusion between chemically modified cellulose nanocrystals and cyclodextrin. Biomacromolecules 2013;14:871-80.
[50] Matthew JE, Nazario YL, Roberts SC, Bhatia SR. Effect of mammalian cell culture medium on the gelation properties of Pluronic® F127. Biomaterials 2002;23:4615-9.
[51] Khattak SF, Bhatia SR, Roberts SC. Pluronic F127 as a cell encapsulation material: utilization of membrane-stabilizing agents. Tissue engineering 2005;11:974-83.
[52] Hofig I, Atkinson MJ, Mall S, Krackhardt AM, Thirion C, Anastasov N. Poloxamer synperonic F108 improves cellular transduction with lentiviral vectors. The journal of gene medicine 2012;14:549-60.
[53] Badi N, Lutz J-F. PEG-based thermogels: Applicability in physiological media. Journal of Controlled Release 2009;140:224-9.
[54] Fujita H, Ooya T, Yui N. Thermally-Responsive Properties of a Polyrotaxane Consisting of [beta]-Cyclodextrins and a Poly(ethylene glycol)-Poly(propylene glycol) Triblock-Copolymer. Polym J 1999;31:1099-104.
[55] Guan Y, Zhang Y. PNIPAM microgels for biomedical applications: from dispersed particles to 3D assemblies. Soft Matter 2011;7:6375-84.

.

[56] Klouda L, Mikos AG. Thermoresponsive hydrogels in biomedical applications - a review. European journal of pharmaceutics and biopharmaceutics : official journal of Arbeitsgemeinschaft fur Pharmazeutische Verfahrenstechnik eV 2008;68:34-45.
[57] Babak VG, Skotnikova EA, Lukina IG, Pelletier S, Hubert P, Dellacherie E. Hydrophobically Associating Alginate Derivatives: Surface Tension Properties of Their Mixed Aqueous Solutions with Oppositely Charged Surfactants. Journal of colloid and interface science 2000;225:505-10.
[58] Pawar SN, Edgar KJ. Chemical Modification of Alginates in Organic Solvent Systems. Biomacromolecules 2011;12:4095-103.
[59] Pawar SN, Edgar KJ. Alginate esters via chemoselective carboxyl group modification. Carbohydrate Polymers 2013;98:1288-96.
[60] Schleeh T, Madau M, Roessner D. Synthesis enhancements for generating highly soluble tetrabutylammonium alginates in organic solvents. Carbohydr Polym 2014;114:493-9.
[61] Daemi H, Barikani M. Molecular engineering of manipulated alginate-based polyurethanes. Carbohydr Polym 2014;112:638-47.
[62] Petter RC, Salek JS, Sikorski CT, Kumaravel G, Lin FT. Cooperative binding by aggregated mono-6-(alkylamino)-.beta.-cyclodextrins. Journal of the American Chemical Society 1990;112:3860-8.
[63] McNaughton M, Engman L, Birmingham A, Powis G, Cotgreave IA. Cyclodextrin-Derived Diorganyl Tellurides as Glutathione Peroxidase Mimics and Inhibitors of Thioredoxin Reductase and Cancer Cell Growth. Journal of Medicinal Chemistry 2004;47:233-9.
[64] Kaya E, Mathias LJ. Synthesis and characterization of physical crosslinking systems based on cyclodextrin inclusion/host-guest complexation. Journal of Polymer Science Part A: Polymer Chemistry 2010;48:581-92.
[65] Izawa H, Kawakami K, Sumita M, Tateyama Y, Hill JP, Ariga K. [small beta]-Cyclodextrin-crosslinked alginate gel for patient-controlled drug delivery systems: regulation of host-guest interactions with mechanical stimuli. Journal of Materials Chemistry B 2013;1:2155-61.
[66] Miao T, Rao KS, Spees JL, Oldinski RA. Osteogenic differentiation of human mesenchymal stem cells through alginate-graft-poly(ethylene glycol) microsphere-mediated intracellular growth factor delivery. Journal of Controlled Release 2014;192:57-66.
[67] Cohn D, Sagiv H, Benyamin A, Lando G. Engineering thermoresponsive polymeric nanoshells. Biomaterials 2009;30:3289-96.
[68] Huang H-Y, Hu S-H, Chian C-S, Chen S-Y, Lai H-Y, Chen Y-Y. Self-assembling PVA-F127 thermosensitive nanocarriers with highly sensitive magnetically-triggered drug release for epilepsy therapy in vivo. Journal of Materials Chemistry 2012;22:8566-73.
[69] Sinha MK, Gao J, Stowell CET, Wang Y. Synthesis and biocompatibility of a biodegradable and functionalizable thermo-sensitive hydrogel. Regenerative Biomaterials 2015.
[70] Tan L, Li J, Liu Y, Zhou H, Zhang Z, Deng L. Synthesis and characterization of β-cyclodextrin-conjugated alginate hydrogel for controlled release of hydrocortisone acetate in response to mechanical stimulation. Journal of Bioactive and Compatible Polymers: Biomedical Applications 2015.
[71] Vasile C, Nita LE. Novel multi-stimuli responsive sodium alginate-grafted-poly(N-isopropylacrylamide) copolymers: II. Dilute solution properties. Carbohydrate Polymers 2011;86:77-84.
[72] Soledad Lencina MM, Iatridi Z, Villar MA, Tsitsilianis C. Thermoresponsive hydrogels from alginate-based graft copolymers. European Polymer Journal 2014;61:33-44.

.

[73] Teodorescu M, Andrei M, Turturică G, Stănescu PO, Zaharia A, Sârbu A. Novel Thermoreversible Injectable Hydrogel Formulations Based on Sodium Alginate and Poly(N-Isopropylacrylamide). International Journal of Polymeric Materials and Polymeric Biomaterials 2015;64:763-71.

.

CHAPTER 7 CONCLUSIONS AND FUTURE DIRECTIONS

The present dissertation has attempted to design and fabricate alginate based biomaterials for biomedical applications. Starting with commercially available polysaccharide material alginate, I have designed four generations of alginate based nanoparticles with different types of polymer chemistry reactions. The first generation is basic alginate nanoparticles fabricated through benchtop water/oil emulsion. With the addition of poly (ethylene glycol) onto alginate, I was able to create particles with a more neutral surface charge, which are favorable for cell uptake compared to cationic alginates. This is the second generation of alginate-based nanoparticles. The third generation of nanoparticles was created through disulfide bond chemistry, where I conjugated short cell signal peptides for targeting delivery. However, the targeting efficacy was not as specific compared to full antibody. Therefore, in the latest (forth) generation of nanoparticle, I designed the streptavidin coated alginate nanoparticles, which can conjugate to commercially available biotinylated antibodies to target cell types.

All four generations of alginate nanoparticles can be readily internalized by human mesenchymal stem cells, human cancer cells (A549), human epithelial cells (HBE), mice macrophages, T cells and B cells. The application of alginate nanoparticles ranges from tissue engineering to promote bone regeneration for treating osteoporosis to cancer therapy for deliver chemotherapeutics to lung cancers. With the powerful delivery alginate particles, I have been able to elucidate the intracrine

mechanism underlying human mesenchymal stem cells and cancer cells, and modulate the cell behavior based on the need for different therapies for different diseases.

However, particulate based drug delivery was just the first goal of this thesis. A novel multi-stimuli hydrogel based drug delivery system was also design based on the supramolecular interactions between β-cyclodextrin and pluronic®F108. β-cyclodextrin (β-CD), with a lipophilic inner cavity and hydrophilic outer surface, interacts with a large variety of non-polar guest molecules to form non-covalent inclusion complexes. Conjugation of β-CD onto alginates can form physically-crosslinked hydrogel networks upon mixing with a guest molecule. I have developed and characterized self-healing, thermo-responsive hydrogels based on host-guest inclusion complexes between alginate-graft-β-CD and Pluronic® F108 (poly(ethylene glycol)-b-poly(propylene glycol)-b-poly(ethylene glycol)). The mechanics, flow characteristics, and thermal response were contingent on the polymer concentration and the host-guest molar ratio. Transient and reversible physical crosslinking between host and guest polymers governed self-assembly, allowing flow under shear stress, and facilitating complete recovery of the material properties within a few seconds of unloading. The mechanical properties of the dual-crosslinked, multi-stimuli responsive hydrogels were tuned as high as 30 kPa at body temperature, which make them potential candidates for biomedical applications such as drug delivery and cell transplantation.

In additional to the alginate-based materials discussed in this thesis, I also developed theta-gel networks for promoting chondrogenic differentiation. Theta-gels

are hydrogels that form during the solidification and phase separation of two dislike polymers, in which a low molecular weight polymer behaves as a porogen and is removed through dialysis. Interpenetrating polymer network (IPN) hydrogels were formed between polyvinyl alcohol (PVA) and gelatin using theta-gel fabrication techniques, i.e., in the presence of a porogen. The addition of gelatin to a PVA theta-gel, formed with a porogen, polyethylene glycol (PEG), created macro-porous hydrogels, and increased shear storage moduli and elastic moduli, compared to PVA–gelatin scaffold controls. A reduction in PVA crystallinity was verified by Fourier transform infrared (FTIR) spectroscopy in hydrogels fabricated using a porogen, i.e., PVA–PEG–gelatin, compared to PVA, PVA–PEG, or PVA–gelatin hydrogels alone. Van Geison staining confirmed the retention of gelatin after dialysis. A range of hydrogel moduli was achieved by optimizing PVA concentration, molecular weight, and gelatin concentration. PVA–gelatin hydrogels maintained primary human mesenchymal stem cell (MSC) viability. Soft (~10 kPa) and stiff (~100 kPa) PVA–gelatin hydrogels containing type II collagen significantly increased glycosaminoglycan (GAG) production compared to controls. PVA–gelatin hydrogels, formed using theta-gel techniques, warrant further investigation as articular cartilage tissue engineering scaffolds.

Alginates have become an important polymer of polysaccharides because of their utility in preparing hydrogels at mild pH and temperature conditions, suitable for sensitive biomolecules like proteins and nucleic acids, and even for living cells such as

islets of Langerhans[1]. These polysaccharides-based biomaterials have been designed and modified to meet the different needs of drug delivery and form particulates and scaffolds, which may have great potential for various biomedical application.

.

Reference

[1] Pawar SN, Edgar KJ. Alginate derivatization: A review of chemistry, properties and applications. Biomaterials 2012;33:3279-305.

.

.

APPENDIX: PHYSICALLY CROSSLINKED POLYVINYL ALCOHOL AND GELATIN INTERPENETRATING POLYMER NETWORK THETA-GELS FOR CARTILAGE REGENERATION

Theta-gels are hydrogels that form during the solidification and phase separation of two dislike polymers, in which a low molecular weight polymer behaves as a porogen and is removed through dialysis. For this study, interpenetrating polymer network (IPN) hydrogels were formed between polyvinyl alcohol (PVA) and gelatin using theta-gel fabrication techniques, i.e., in the presence of a porogen. The addition of gelatin to a PVA theta-gel, formed with a porogen, polyethylene glycol (PEG), created macro-porous hydrogels, and increased shear storage moduli and elastic moduli, compared to PVA-gelatin scaffold controls. A reduction in PVA crystallinity was verified by Fourier transform infrared (FTIR) spectroscopy in hydrogels fabricated using a porogen, i.e., PVA-PEG-gelatin, compared to PVA, PVA-PEG, or PVA-gelatin hydrogels alone. Van Geison staining confirmed the retention of gelatin after dialysis. A range of hydrogel moduli was achieved by optimizing PVA concentration, molecular weight, and gelatin concentration. PVA-gelatin hydrogels maintained primary human mesenchymal stem cell (MSC) viability. Soft (~10 kPa) and stiff (~ 100 kPa) PVA-gelatin hydrogels containing type II collagen significantly increased glycosaminoglycan (GAG) production compared to controls. PVA-gelatin hydrogels, formed using theta-gel techniques, warrant further investigation as articular cartilage tissue engineering scaffolds.

1. Introduction

Osteoarthritis is a degenerative inflammatory disease that results in irreversible degradation of osteochondral tissue, which consists of surface articular cartilage and underlying subchondral bone.[1] Recent tissue engineering approaches show promise; however, innovative strategies are needed to recapitulate the mechanotransduction pathways found in osteochondral tissue for tissue regeneration, and to maintain tissue homeostasis.[2] The mechanisms by which cells receive signals from their environment can be examined through the manipulation of the structure (e.g., topography and porosity), level of bioactivity (e.g., cell adhesion, stem cell differentiation), and the dynamic mechanical properties (e.g., stiffness, elasticity, toughness, etc.) of the material systems.[3-5] Therefore, it is critical to define each parameter – structure, bioactivity, and mechanical properties – independently and collectively to define the critical parameters required to regenerate tissue, or treat a disease.[6-9]

Tissue engineering relies on synthetic or natural-based material systems to interact with cells in order to enhance tissue regeneration. Material stiffness,[10] porosity,[11] and bioactivity parameters influence the cellular response, in particular, cell transcription and stem cell differentiation.[5] Thus, various mechanotransduction pathways can be activated to direct stem cell differentiation for specific applications.[12-18] Indeed, mesenchymal stem cells (MSCs) cultured on stiff substrates favor an osteogenic differentiation pathway,[19, 20] while MSCs cultured on soft substrates favor a chondrogenic differentiation pathway.[4] In addition to

mechanical cues, MSCs are responsive to biological signals from their physical environment. Collagen is an amino acid based protein that is found in the fibrous tissues of the human body, including bone and cartilage.[21] Collagen increases cell adhesion, migration, and proliferation.[22] Specifically, type II collagen, a component of articular cartilage extracellular matrix (ECM), is known to significantly influence chondrogenic differentiation and the maintenance of chondrocyte phenotype *in vitro* and *in vivo*.[23]

Polyvinyl alcohol (PVA) is a synthetic, biocompatible polymer utilized for soft tissue replacements and tissue regeneration.[24-26] PVA hydrogels are formed by the crystallization of polymer chains through non-covalent linkages, i.e., physical crosslinks.[27],[28, 29] Specifically, the formation of theta-gels incorporates the use of a small molecular weight hydrophilic polymer, such as polyethylene glycol (PEG) as a porogen during cooling, or solidification of a PVA solution.[30, 31] During a thermal transition, PEG porogens phase separate from PVA, increasing the density of PVA-rich regions, thus inducing crystallization. The PVA hydrogel network forms during a large thermal transition and the creation of intermolecular hydrogen bonds.[32, 33] PEG is removed through dialysis after the thermal transition, which results in large pores in a rigid hydrogel network.

PVA hydrogels lack cell adhesion functionalities, and investigators have incorporated biomolecules into the hydrogel network to enhance hydrogel mechanical properties and bioactivity.[34] To enhance bioactivity of PVA hydrogels,

polysaccharides and proteins have been added during hydrogel crosslinking. Gelatin, a non-specific derivative of the protein collagen, contains cell adhesion ligands, which provide cell adhesion sites to PVA hydrogels when blended together. While cryo-gels of PVA and gelatin blends have been studied, the effect of adding gelatin to PVA theta-gels, in the presence of PEG, has not been investigated.

The aim of this study was to develop and characterize PVA-gelatin hydrogels with improved mechanical properties, through the incorporation of PEG porogens. We hypothesized that the addition of a porogen would increase the density and interactions of PVA and gelation, compared to the solidification of PVA and gelatin alone, to result in macro-porous hydrogels with increased shear and compressive moduli. We evaluated the potential of PVA-gelatin hydrogels to support chondrogenic MSC differentiation, and varied hydrogel stiffness and the addition of type II collagen.

2. Experimental Section

2.1. Fabrication of PVA-Gelatin Theta-Gels

PVA-gelatin theta-gels, i.e., hydrogels, were prepared using different molecular weights and concentrations of PVA, PEG, and gelatin. PVA (Mw = 145 kg/mol (H) and 95 kg/mol (L), Sigma Aldrich) was combined with 20% (w/v) PEG (Mw = 400 g/mol, Sigma Aldrich) in DI water. PVA concentrations, for both molecular weights, were 18 and 36% (w/v). Experimental groups contained gelatin (Sigma Aldrich) at 1, 5, and

.

18% (w/v). The control and experimental polymer blend solutions were autoclaved for 1 hour and the warm, homogenous solutions were transferred to curing molds consisting of glass slides and 3.2 mm thick Teflon spacers, preheated to 90 °C. The molds containing the polymer solutions were cooled to room temperature and cured for 24 hours. The hydrogel sheets were removed from the molds and dialyzed in DI water for 5 days to remove PEG porogens; dialysis water was changed every 12 hours.

2.2. Fourier-Transform Infrared (FTIR) Spectroscopy

All sample hydrogels were prepared prior to performing spectroscopy: 18% (w/v) PVA, high molecular weight, and 1% (w/v) gelatin solutions were prepared and used as controls, 20% (w/v) PEG was used for all theta-gels. The hydrogels were dialyzed for 5 days, to ensure removal of the porogen and air-dried after dialysis and cut into small pieces. Then they were tested using Thermo-Nicolet IR200 FTIR spectrometer with an attenuated total reflectance (ATR) head for 32 scans.

2.3. Rheological Characterization

All experiments were performed using an AR2000 stress-controlled rheometer (TA Instruments) fitted with a 20 mm diameter steel cone geometry at 25 °C, however, the temperature sweep study included a temperature range. All sample solutions were prepared prior to performing the temperature sweep: 18% (w/v) PVA, high molecular weight, and 1% (w/v) gelatin solutions were prepared and used as controls, 20% (w/v) PEG was used for all theta-gels. Temperature sweeps were performed at 1 Hz and 1%

strain, with a cooling rate of -5 °C*min^{-1} from 60 to 20 °C. Oscillatory time sweeps for experimental (PVA-PEG-1Gel) and control hydrogels (gelatin, PVA, PVA-1Gel) were tested directly after hydrolysis, and were deformed at 1% radial strain and 10 Hz over 100 s. Oscillatory frequency sweeps were performed at 0.5% radialstrain with increasing frequency from 0.1 to 100 Hz.

2.4. Scanning Electron Microscopy

Hydrogel samples, containing PVA and PEG, with and without gelatin, were flash frozen in liquid nitrogen after dialysis in DI water, cryo-fractured, lyophilized, and characterized by scanning electronic microscopy (SEM, JEOL 600). Samples were sputter coated with 10 nm of Au-Pd prior to imaging. SEM was used to quantify pore diameters and characterize the inner structure of PVA-PEG-Gel hydrogel cross-sections compared to PVA-PEG controls。

2.5. Van Geison Staining

To characterize the retention of gelation, hydrated hydrogels were placed in Van Geison staining solution (ThermoFisher) for 2 minutes and rinsed in DI water several times until the water remained clear. PVA-PEG-Gel hydrogels consisting of 18 and 36% (w/v) PVA, using low (L, 95 kDa) or high (H, 145 kDa) molecular weight PVA, and 18% (w/v) PEG, were fabricated. Hydrogels also varied in gelatin content: 1, 5, and 18% (w/v). Control groups included PVA-PEG hydrogels with no gelatin content.

Samples were dried at room temperature, and color images were taken using a digital camera.

2.6. Equilibrium Water Content and Weight Loss

Cylindrical hydrogel specimens (6 mm x 3 mm) were lyophilized to ensure all moisture was alleviated in preparation for equilibrium water content measurements and weight loss values. The dehydrated specimens were weighed, then placed in 5 mL PBS, pH 7.4, to rehydrate the scaffolds for 48 hours at 37 °C. Each specimen was weighed, and the wet weight was recorded. Equilibrium water content was calculated as the percentage of wet weight divided by initial dry weight. After each specimen's wet weight was recorded, each specimen was again froze to prepare for lyophilization. Each specimen was then lyophilized for 24 hours. A second dry weight was then recorded to test for how much weight was lost through the dehydration process. The weight loss was calculated as final mass subtracted from the initial mass, divided by the initial mass. Dry scaffolds were weight to determine the initial amount of polymer. To determine the amount of non-crosslinked polymer, scaffolds were hydrated for 24 hours in order to dissociate non-crosslinked PVA and gelatin. Scaffolds were then lyophilized and massed. To determine the polymer loss due to hydration and diffusion of non-crosslinked molecules, the mass of a dry sample after the crosslinking process was performed was measured.

2.7. Unconfined Compression Testing

The unconfined compressive moduli of various hydrogel groups were determined directly after dialysis. Cylindrical hydrogel specimens (6 mm x 3 mm) were tested at 25 ˚C using an AR2000 rheometer (TA Instruments) equipped with a Peltier plate and normal force transducer. Specimens were placed on the rheometer and the geometry was lowered until a force of 0.01 N was measured, and the force was normalized. The gap height was recorded as the original gage length for the modulus calculation. A 20% uni-axial compressive strain was applied at a rate of 10 μm/s. Force (N) and changes in gap height (μm) were obtained using analytical software (TA Universal Analysis) and were subsequently used to calculate elastic strain (ε, %) and stress (σ, kPa). The elastic modulus (E) was calculated as the slope of a linear fit between 5 and 15% compressive strain within the linear-elastic region. A minimum of four replicates from each group were tested.

2.8. Cytotoxicity Assay

The cytotoxicity of PVA-gelatin hydrogels to primary bone-marrow derived human MSCs was assessed as a function of mitochondrial activity in living cells. MSCs were seeded in treated 48-well tissue culture polystyrene (TCPS) plates at a density of 20,000 cells/well in 100 μL/well of standard MSC growth media (alpha minimum essential medium (MEM), 10% fetal bovine serum (FBS), 100 U/mL penicillin, 100 μg/mL streptomycin) and allowed to adhere for 24 hours. MSCs were incubated in the

presence of various PVA-gelatin hydrogels (n = 4) at 37 °C and 5% CO_2. Spherical hydrogel specimens were 4 mm wide and 2 mm tall. After 24 hours of incubation, media was removed and cells were rinsed two times in sterile PBS. Mitochondrial activity was analyzed using a 3-[4,5-dimethylthiazol-2-yl]-2,5-diphenyl tetrazolium bromide (MTT) based *In Vitro* Toxicology Assay Kit (Sigma Aldrich) following the manufacturer's protocol with a plate reader (H1 Synergy, BioTek). Absorbance values were recorded at 570 nm with background absorbance at 690 nm deducted. Average absorbance values for the experimental samples were compared to positive cell control values recorded for wells containing media and cells alone.

2.9. Chondrogenic Differentiation

PVA-gelatin hydrogels selected for cell-seeding were coated with type II collagen using the following protocol. After fabrication and dialysis, PVA-gelatin hydrogels were formed into cylinders, 3 mm x 2 mm, using a 4mm biopsy punch. The hydrogels (soft and stiff scaffold groups) were immersed in type II rat collagen (50 mg/mL, Sigma-Aldrich) in phosphate buffered saline (PBS), which was pre-filtered to obtain cell culture sterile solution, for 1 hour at room temperature.[35] The hydrogel samples were removed from the collagen solution, rinsed in sterile PBS, and prepared for cell culture.

Primary bone-marrow derived human MSCs (Lonza), passage 4, were seeded onto PVA-gelatin hydrogels with or without type II collagen. 38 µL of 700,000 cells

suspended in standard MSC culture media were placed onto cylindrical hydrogel scaffolds (3 mm x 2 mm), and the scaffolds were placed in 96-well TCPS plates. Cell-seeded scaffolds were incubated at 37 ˚C, 5% CO_2 for 30 minutes, and then the wells were supplemented with 150 µL of chondrogenic media (standard MSC growth media supplemented with 10 ng/mL of human transforming growth factor beta one (TGF-β1, Peprotech)).[11]

2.10. Dimethylmethylene Blue (DMMB) Assay

Intracellular sulfated GAG content was quantified using a DMMB assay.[11] Cell lysate was collected after 4, 7, and 14 days of culture. Scaffolds were removed from tissue culture plates, trypsin-EDTA was added, and the scaffolds were incubated for 5 minutes. Equal volumes of standard MSC culture media were added to the cell suspensions, cell suspensions were placed in micro-centrifuge tubes, and centrifuged at 4000 rpm for 2 minutes. The supernatant was collected and 150 µL of cell lytic solution was added. Standard chondroitin sulfate solutions with concentrations ranging from 0 to 30 µg/mL were used to form the standard curve. Using a 96-well plate, 25 µL of cell lysate sample or standard was added to each well. Next, 150 µL of DMMB solution was added to each well. The absorbance at 525 nm was measured. Controls were MSCs cultured in chondrogenic media in 96-well tissue culture treated polystyrene plates.

GAG production was normalized to the cell population per sample using intracellular protein and the Pierce™ Protein Assay Kit (ThermoFisher). Briefly,

standard bovine serum albumin (BSA) solutions with concentrations ranging from 20 to 2000 µg/mL were used to form the standard curve. Using a 96-well plate, 25 µL of cell lysate sample or standard was added to each well. Next, 175 µL of working solution was added to each well. The absorbance at 562 nm was measured. Controls were MSCs cultured in chondrogenic media in 96-well tissue culture treated polystyrene plates.

2.11. In Vitro Mechanical Testing

MSC-seeded scaffolds were tested in unconfined compression using the same methods detailed above. Briefly, cylindrical scaffolds (3 mm x 2 mm) were subjected to uni-axial unconfined compressive strain at 10 µm/s to a final strain of 20%. Samples were tested after 4, 7, and 14 days of culture with MSCs in chondrogenic media. At day 14, non-seeded PVA-gelatin hydrogel controls were mechanically tested as degradation controls.

2.12. Statistical Analysis

All experiments were performed in triplicate with results reported as mean ± standard deviation. Statistical analysis was performed with a GLM procedure using Statistical Analysis System software. A fixed effect multi-factorial (concentration, molecular weight, and gelatin concentration, eliminated inside the model if one of the factor is not significant relevant) model was generated to study the contribution of each factor to PVA-gelatin hydrogels with a range of compressive elastic moduli, swell ratio

and weight loss based on ANOVA analysis. The multiple comparisons were performed with Tukey adjustment. For analyzing cytotoxicity, similar GLM procedures were preformed to obtain one-way ANOVA results. A $p < 0.05$ was considered significantly different for all analysis. GAG assay results were analyzed using a standard student t-test.

3. Results and Discussion

3.1. PVA-Gelatin Theta-Gel Formation

Bio-synthetic hydrogels were obtained from the physical crosslinking of PVA and gelatin, and the diffusion of PEG for pore formation (**Figure 8-1**). The thermal gelation of both PVA and gelatin in the presence of PEG created a macro-porous IPN. The short-chain, hydrophilic PEG molecules behaved as porogens, aggregating into large domains. After cooling, the PVA-gelatin hydrogel was dialyzed for 5 days, allowing the soluble, nucleated PEG molecules to escape the hydrogels, creating a large interconnected porous structure.

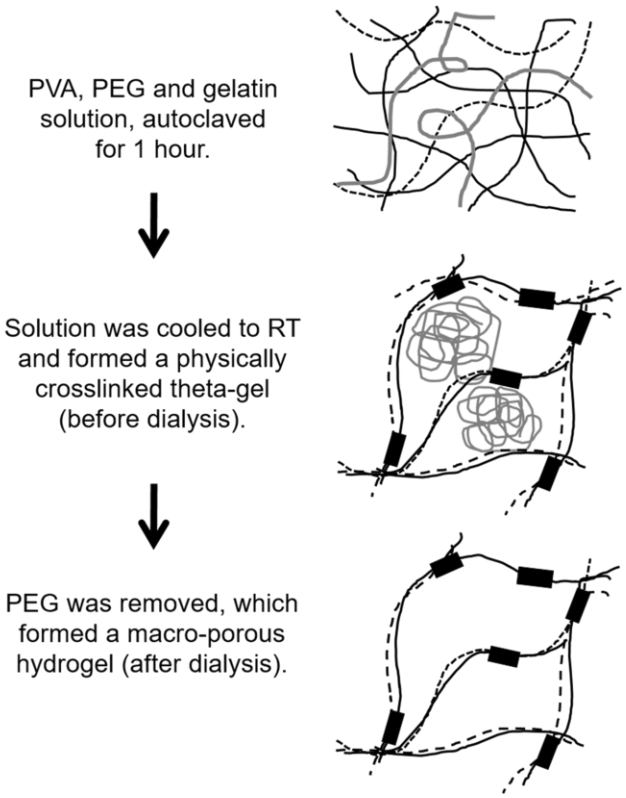

Figure 8-1. Schematic illustrating the formation of a PVA and gelatin theta-gel, through the physical crosslinking of PVA (solid black lines) and gelatin (dashed black lines), respectively, in the presence and subsequent removal of PEG. Areas of hydrogen bonding (i.e., physical crosslinks) between gelatin and PVA are represented by black rectangles. Nucleation of PEG porogens (gray lines) during solidification and subsequent removal through dialysis resulted in a macro-porous network.

To demonstrate the formation of an IPN, soft hydrogels with 18% PVA (high molecular weight), 1% gelatin and 20% PEG (PVA-PEG-1Gel) were synthesized, in addition to control samples including 18% PVA (PVA), 1% gelatin (Gelatin), 18% PVA-1% gelatin (PVA-1Gel) and 18% PVA-20% PEG (PVA-PEG). These samples were tested under

.

attenuated total reflectance (ATR) Fourier transform infrared (FTIR) spectroscopy. The physical crosslinking of PVA and PVA-1Gel controls occurred due to numerous inter-chain hydrogen bonds between OH groups, formed during crystallization of the polymer and identified as a peak in the FTIR spectra at 1141 cm^{-1} (**Figure 8-2 C,D**).[36, 37] The intensity of this peak is related to the C-O stretching vibrations of an intramolecular hydrogen bond was formed between two neighboring OH groups. The C-O peak had a lower intensity for PVA and gelatin hydrogels, which were solidified in the presence of PEG porogens – the experimental group PVA-PEG-1Gel (**Figure 8-2 B**). The control groups also formed peaks within 1090 – 1150 cm^{-1}, associated with C-O-C stretching vibrations; these peaks also appeared in the PVA-PEG-1Gel spectrum with lower intensities. It was hypothesized that crosslinking also occurred due to the increased polymer concentration at the solidifying regions containing PVA and gelatin, and the subsequent generation of van der Waals interactions between hydrocarbon polymer backbones between gelatin and PVA. As a result of introducing PEG into the solidification process, the PVA and gelatin interacted with each other differently than simply mixing the two polymers together, illustrated in **Figure 8-2**.

.

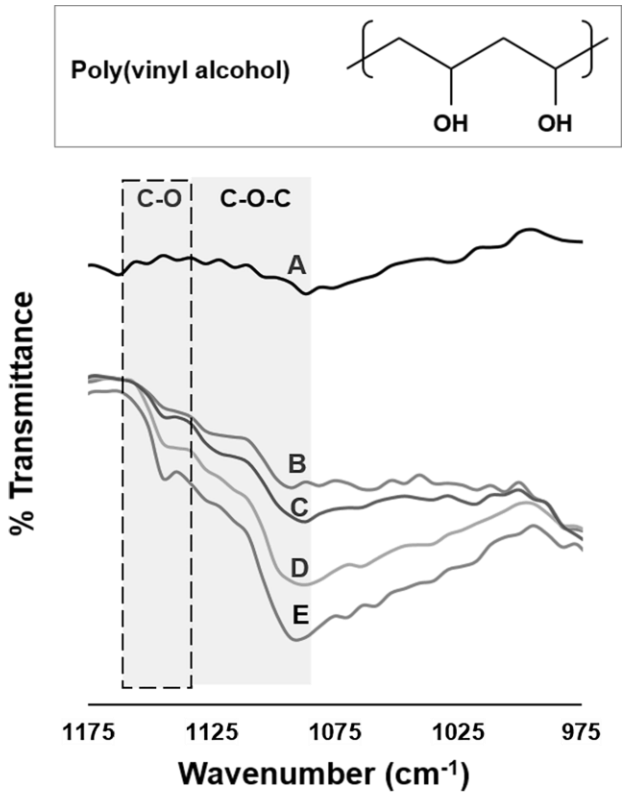

Figure 8-2. Top: Chemical structure of PVA; physical crosslinking takes place at OH groups between PVA molecules. Bottom: fourier transform infrared spectroscopy (FTIR) spectra of (A) gelatin, (B) PVA-PEG-1Gel, (C) PVA-PEG, (D) PVA-1Gel and (E) PVA hydrogel films, stretching vibrational bands associated with PVA physical crosslinking include C-O and C-O-C.

The pore diameters of PVA-gelatin hydrogels (**Figure 8-3 D**) were approximately ten times larger than the control PVA hydrogels (**Figure 8-3 B**), confirmed through scanning electron micrographs. Large pores may also have been the result of non-crosslinked gelatin leaving during dialysis, which may result from interference of PVA in the formation of intra-molecular crosslinks. Van Geison staining qualitatively verified that

.

gelatin was retained in the hydrogels after dialysis (gelatin samples stained red, PVA controls did not; **Figure 8-3 E**). Qualitatively no differences were seen between groups in the stained images.

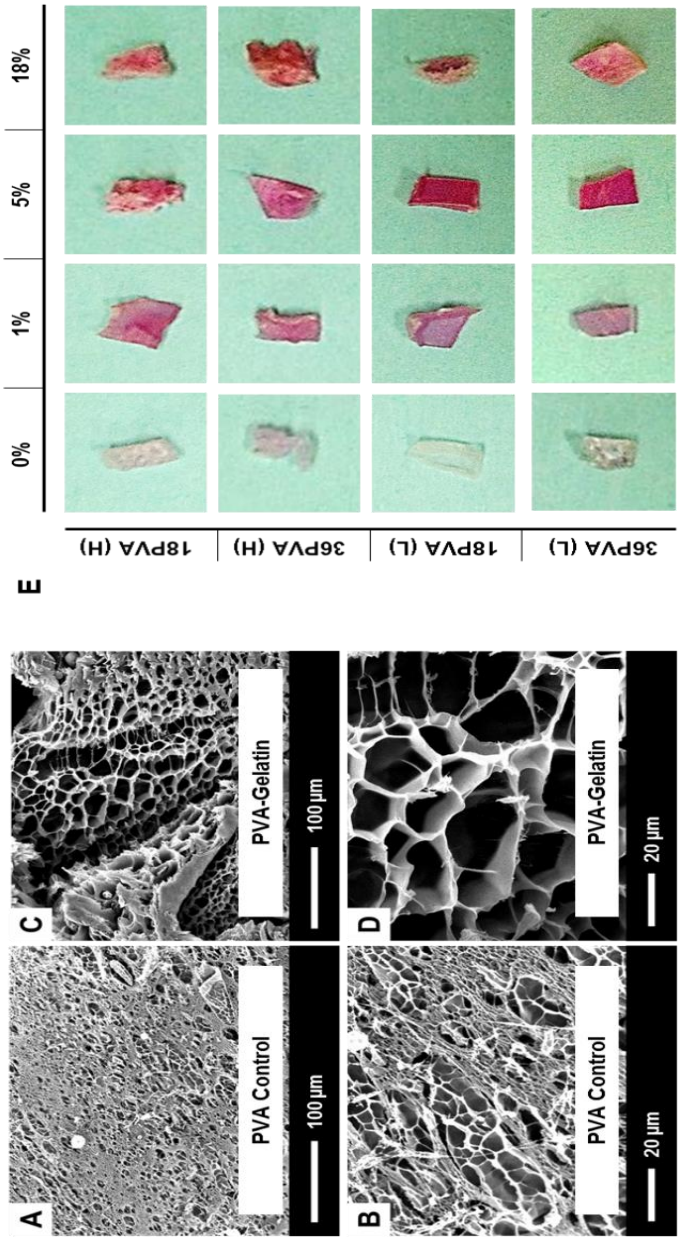

Figure 8-3. SEM images of lyophilized and cryo-fractured surfaces of 18% PVA

.

hydrogel samples, fabricated in the presence of PEG alone (A, B) or with the addition of 5% gelatin (C, D). Magnifications at 250x, scale bar = 100 μm (A, C) and 800x, scale bar = 20 μm (B, D). (E) Van Geison staining qualitatively verified gelatin retention in the hydrogels, which were fabricated using theta-gel techniques. PVA-gelatin hydrogels consisting of 18 and 36% PVA, using low or high molecular weight PVA, were fabricated. Hydrogels also varied in gelatin content; top numbers represent weight percent of gelatin. Samples containing gelatin displayed a higher intensity of the red stain.

3.2. Physical Characterization and Mechanical Properties

To demonstrate the formation of an IPN, soft hydrogels with. Rheological experiments were performed on experimental samples, 18% PVA (high molecular weight), 1% gelatin and 20% PEG (PVA-PEG-1Gel), in addition to control samples including 18% PVA (PVA), 1% gelatin (Gelatin), 18% PVA-1% gelatin (PVA-1Gel) and 18% PVA-20% PEG (PVA-PEG) to examine the effect of PEG porogens on the mechanical response of PVA-gelatin hydrogels. Polymer hydrogel pre-curser solutions were autoclaved to dissolve in water and then immediately transferred to a AR2000 stress-controlled rheometer (TA Instrument). A temperature sweep was performed from 60 ºC to 20 ºC. For all samples except 1% gelatin, storage modulus increased as temperature goes down; the gelatin control remains similar level for the whole tested time period. With the addition of gelatin in the PVA hydrogel, storage moduli increased from 24 Pa to 71 Pa. However, storage moduli jumped to 1863 Pa after introducing

.

PEG into the PVA hydrogel without gelatin. By having all three components in the system, the storage modulus increased to 5266 Pa, indicating the positive effect of PEG porogens on the mechanical response of PVA-gelatin hydrogels (**Figure 8-4 A**).

After all sample hydrogels were dialyzed against water for one week (the gelatin control remained in liquid form and was tested directly without dialyzing), oscillatory time sweeps were performed to examine the mechanical properties of the hydrogels. PVA and PVA-1Gel exhibited similar mechanical properties overtime around 500 Pa. However, those hydrogels fabricated in the presence of PEG had a much higher storage modulus around 4000 Pa. Same as the previous temperate sweep result, PVA-PEG-1Gel had the highest storage modulus around 6000 Pa. Therefore, after dialysis, PEG porogens resulted in large porous structures and stiffer scaffolds (**Figure 8-4 B**).

Shear storage moduli were also measured to determine the effect of frequency during dynamic shear application for various different monomers and hydrogels after dialyzing. Oscillatory frequency sweeps were performed at 1% radial strain and 25 ºC. The hydrogel exhibited steady-state behavior up to 10 Hz, after which the moduli increased in response to the increasing shear rate. PVA and PVA-1Gel control groups exhibited similar storage moduli. Similar with the previous two experiments, the PVA-PEG-1Gel revealed the highest storage modulus compared to all of the other groups (**Figure 8-4 C**).

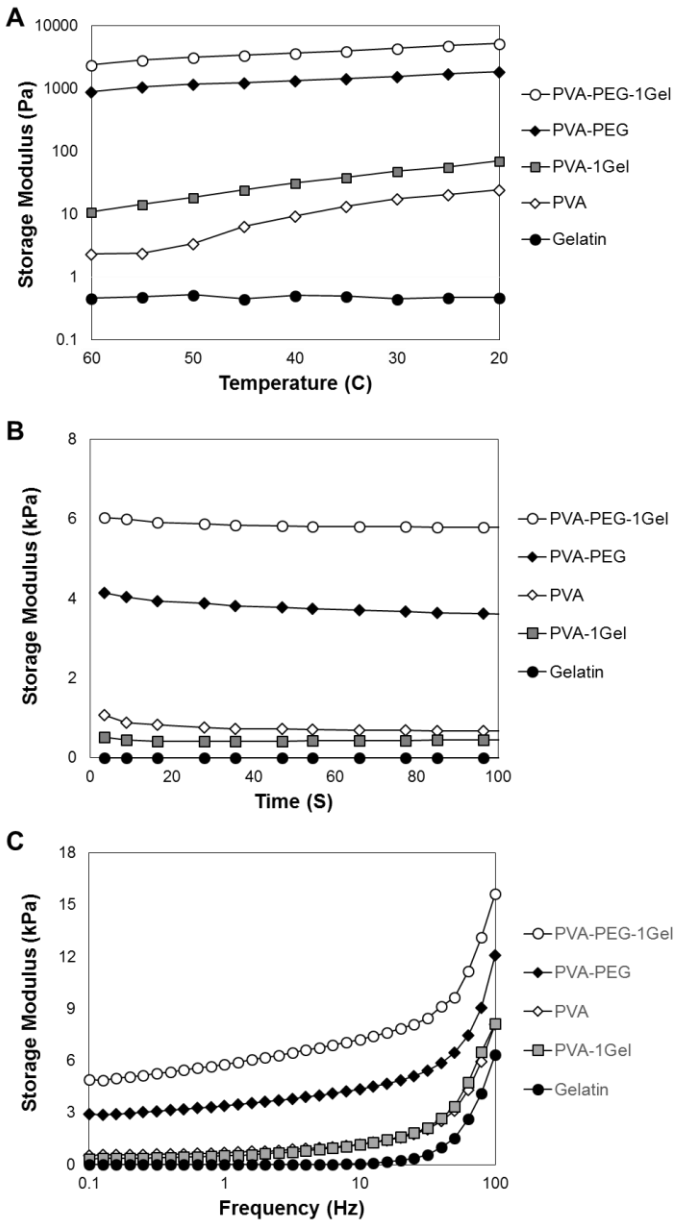

Figure 8-4. Rheological experiments were performed to examine the effect of PEG porogens on the mechanical response of PVA-gelatin hydrogels. A) Temperature sweep of single macromers, control solutions (PVA-1Gel, PVA-PEG), experimental solutions

.

(PVA-PEG-1Gel); solution from the autoclave was tested from 60 ˚C to 20 ˚C to show the gelation process of each sample. B) Oscillatory time sweep experiments for control hydrogels (gelatin, PVA, PVA-1Gel, PVA-PEG), and experimental hydrogels (PVA-PEG-1Gel) were tested after dialysis at 25 ˚C. C) Oscillatory frequency sweeps were performed on hydrogels at 1% radial strain from 0.1 to 100 Hz at 25 ˚C.

PVA hydrogels with and without gelatin swelled > 100% after hydration (**Figure 8-3 A**). The PVA molecular weight influenced water content; lower molecular weight PVA-gelatin hydrogels swelled less compared to higher molecular weight PVA-gelatin hydrogels, likely due to an increase in physical crosslinking. A fixed-effect tri-factorial model (e.g., PVA concentration, PVA molecular weight, and gelatin concentration) was generated to study the contribution of each factor to the hydrogel material properties. All three factors contributed significantly to the equilibrium water content of the hydrogel. The addition of gelatin increased the overall water content.

Weight loss was calculated to determine polymer mass lost due to hydrolysis. While some material was lost due to non-crosslinked PVA chains and degraded polymer during physical crosslinking (< 10%), indicated by the white bars in **Figure 8-3 B**, the PVA-gelatin hydrogels, specifically the 18% gelatin samples, black bars in **Figure 8-3 B**, lost more weight (2 – 31%). These results correlate with the FTIR data, which indicated that gelatin interrupted PVA crystallization during cooling, thus allowing more amorphous species to be lost during hydration (**Figure 8-2**).

Unconfined compression tests were performed on hydrogels directly after

.

dialysis. Increasing the gelatin concentration created a stiffer hydrogel up to 5% (w/v); concentrations greater than 5% interfered with the formation of a network, resulting in a more compliant hydrogel (**Figure 8-3 C**); PVA control hydrogels, fabricated with PEG, without gelatin, were too compliant to collect compressive moduli values thus data is not shown. A fixed effect tri-factorial model (e.g., PVA concentration, PVA molecular weight, and gelatin concentration) was generated to study the contribution of each factor to the IPN hydrogels with a range of compressive elastic moduli. All three factors had significant contributions to the resulting moduli, among which PVA concentration interacted with PVA molecular weight, and PVA molecular weight interacted with gelation concentration: 18%PVA(H) ranged from 17 to 95 kPa, 36%PVA(H) ranged from 116 to 193 kPa, 18PVA(H) ranged from 26 to 92 kPa, and 36PVA(L) ranged from 189 to 351 kPa. The three factors were also interacting with each other, and contributing of the compressive moduli of the hydrogels. Overall, the formation of a crosslinked network of PVA and gelatin, to form a swollen, stiff hydrogel, was dependent on the PVA concentration and molecular weight, and the concentration of gelatin.

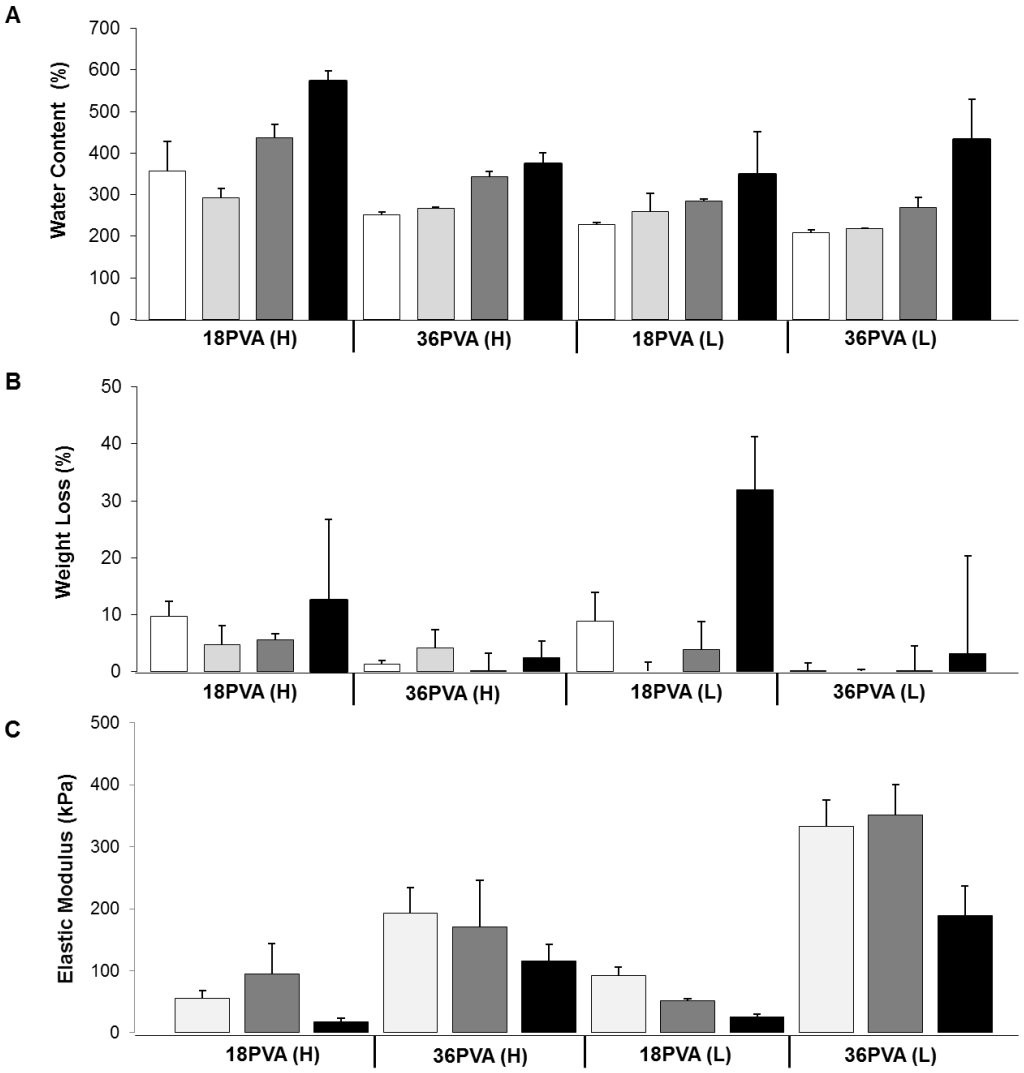

Figure 8-5. The physical and mechanical properties of PVA-gelatin hydrogels, developed using theta-gel techniques, are reported. PVA-gelatin hydrogels consisting of 18 and 36% (w/v) PVA, using low (L, 95 kDa) or high (H, 145 kDa) molecular weight PVA, were fabricated. Hydrogels also varied in gelatin content; white = no gelatin, light gray = 1% gelatin, dark gray = 5% gelatin, black = 18% gelatin. (A) To evaluate hydration, the equilibrium water content of PVA-gelatin hydrogels and PVA controls was

.

calculated; lyophilized hydrogel samples were hydrated in phosphate buffered saline (PBS), pH 7.4, for 24 hours at room temperature. (B) Weight loss values were calculated after removal of the hydrogel samples from solution. Measurements were used to determine the loss of soluble low molecular species and hydrolytic degradation. (C) Unconfined compression tests were performed and elastic moduli of PVA-gelatin hydrogels were calculated using a linear regression of the stress-strain curve between 5 – 15% axial compressive strain; average ± standard deviation are reported (n = 4). PVA samples were left out of the study due to high compliance.

3.3. In Vitro Chondrogenic Differentiation

The bioactive properties of the PVA-gelatin hydrogels were investigated for cartilage tissue engineering applications. Two different PVA-gelatin hydrogel formulations were selected for *in vitro* cell culture based on the physical characterization and mechanical analysis. Hydrogel formulations were chosen to reflect differences in elastic moduli, and with or without the addition of a cell-signaling molecule, type II collagen. Prior to chondrogenic differentiation, an *in vitro* MTT-based cytotoxicity assay was used to measure the mitochondrial activity of human MSCs after 24 hours of culture in the presence of PVA-based hydrogels in standard MSC culture media. All of the PVA-gelatin groups displayed non-cytotoxic effects and maintained mitochondrial activity levels > 75%. There were no significant results among the groups; however, the cytotoxicity assay results indicate a dependence on gelatin content.

.

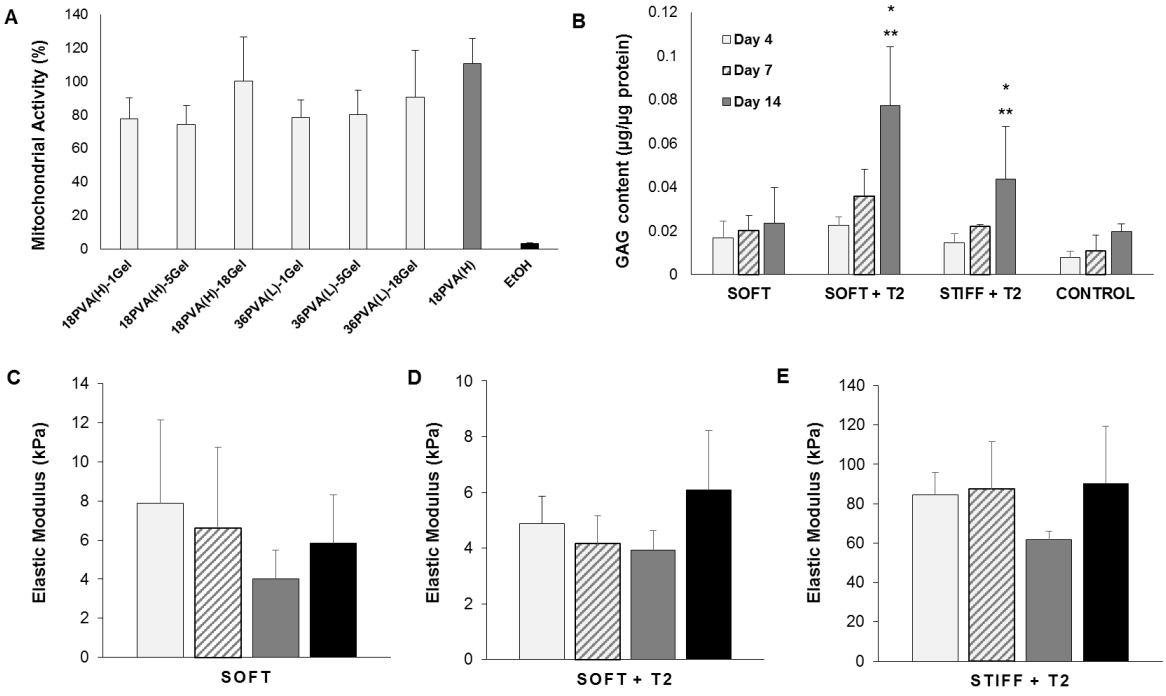

Figure 8-6. (A) Mitochondrial activity was determined using an MTT-based cytotoxicity assay. The absorbance values for PVA-gelatin and PVA hydrogels were normalized to non-modified cell controls cultured on tissue culture polystyrene; ethanol (EtOH) was used as a negative control. Confluent human MSCs were cultured with PVA-based hydrogels for 24 hours in standard MSC culture medium at 37 ˚C and 5% $C0_2$ (n = 4). (B) Sulfated GAG production was quantified for MSCs cultured in PVA-gelatin scaffolds and in non-modified treated polystyrene culture plates in chondrogenic media. Hydrogel experimental groups consisted of: 18PVA(H)-1Gel (soft), 18PVA(H)-1Gel + type II collagen (soft + T2), and 36PVA(L)-5Gel + type II collagen (stiff +T2); results are reported as average ± standard deviation (n = 4). (* = $p < 0.005$ compared to control

.

samples at day 14; ** = $p < 0.03$ compared to day 4 results within the same sample group.) Unconfined compression tests were performed and the elastic moduli of human MSC-seeded hydrogels and non-seeded hydrogel controls were calculated using a linear regression of the stress-strain curve from 5 – 15% axial compressive strain. Hydrogel experimental groups consisted of: 18PVA(H)-1Gel (soft), 18PVA(H)-1Gel + type II collagen (soft + T2), and 36PVA(L)-5Gel + type II collagen (stiff +T2); results are reported as average ± standard deviation (n = 4).

The efficacy of using PVA-gelatin hydrogels, formed using theta-gels techniques, to support chondrogenic differentiation was evaluated by measuring initial matrix content production. The chondrogenic differentiation of the MSCs was measured using a dimethylmethylene blue (DMMB) assay 4, 7, and 14 days post-seeding onto PVA-gelatin hydrogels. PVA-gelatin hydrogel groups were selected according to elastic moduli values and two groups were chosen to reflect high and low moduli (soft ~ 10 kPa, stiff ~ 100 kPa). The presence of a cartilage matrix protein, type II collagen, was investigated; hydrogel groups varied in bioactivity (with or without type II collagen). Reports from the literature suggest that compliant hydrogels promote and/or enhance chondrogenic differentiation. Therefore, the effect of the bioactive molecule was investigated in the soft hydrogel groups.

The intracellular sulfated glycosaminoglycan (GAG) content was measured in primary human MSCs cultured on PVA-gelatin hydrogel scaffolds in chondrogenic media over a period of 14 days. Soft PVA-gelatin hydrogels, without the addition of

.

type II collagen, did not show any significant differences compared to non-modified cell controls at all three time points (**Figure 8-6 B**). However, both soft and stiff hydrogels containing type II collagen significantly increased intracellular GAG content compared to the controls after 14 days of culture ($p < 0.005$). In addition, both the soft+ T2 and stiff+ T2 hydrogel groups significantly increased intracellular GAG content after 14 days compared to 4 days of culture ($p < 0.03$). The results also suggest that the soft + T2 hydrogel samples had a greater influence on intracellular GAG production compared to the stiff + T2 hydrogels. Thus, the combination of both a selective moduli value and the presence of a bioactive molecule will significantly enhance the ability for PVA-gelatin hydrogels to support chondrogenic differentiation, and potentially tissue regeneration. While the two-week duration of the *in vitro* is a limitation of the study, the efficacy of using PVA-gelatin hydrogels, which incorporate type II collagen, for cartilage tissue engineering applications is supported.

Unconfined compression tests were conducted on cell-seeded hydrogels to determine what effect the cells may have on the mechanical properties of their physical environment, i.e., the hydrogel scaffold. PVA-gelatin hydrogel controls were incubated in standard MSC culture media until testing. At day 4, 7, and 14 the elastic moduli of the MSC-seeded experimental groups were not significantly different compared to the controls (**Figure 8-5**, day 4 = light gray bars, day 7 = striped gray bars, day 14 = dark gray bars, hydrogel controls = black bars). However, a trend showing the decrease in elastic moduli of cell-seeded hydrogels with time may reflect the cells remodeling the

hydrogel scaffold during differentiation. Longer time points may reveal significant data, and future work will examine degradation and the dynamic mechanical properties of cell-seeded hydrogels.

4. Conclusions

Cell-instructive PVA-gelatin hydrogels were fabricated in the presence of a PEG porogen to enhance network integrity. Theta-gels with macro-porous structures formed through the physical interactions of PVA and gelatin, and supported chondrogenic differentiation and cartilage matrix deposition. Adding gelatin to PVA hydrogels formed in the presence of PEG porogensw significantly increased the hydrogel stiffness and pore size.[34] Bio-synthetic IPN hydrogels were formed using theta-gel techniques and are promising candidates for cartilage regeneration scaffolds due to their large pore diameters (10 – 50 μm), moderately high compressive elastic moduli (20 – 400 kPa), and ability to significantly increase chondrogenesis. Future work will investigate the role of the gelatin during cell culture and longer *in vitro* culture time points. In addition, the effect of dynamic culture will be investigated.

.

References

[1] Luyten FP, Denti M, Filardo G, Kon E, Engebretsen L. Definition and classification of early osteoarthritis of the knee. Knee Surg Sports Traumatol Arthrosc 2012;20:401-6.
[2] Grassel S, Lorenz J. Tissue-engineering strategies to repair chondral and osteochondral tissue in osteoarthritis: use of mesenchymal stem cells. Curr Rheumatol Rep 2014;16:452.
[3] Autissier A, Le Visage C, Pouzet C, Chaubet F, Letourneur D. Fabrication of porous polysaccharide-based scaffolds using a combined freeze-drying/cross-linking process. Acta Biomaterialia 2010;6:3640-8.
[4] Wang T, Lai JH, Han LH, Tong X, Yang F. Chondrogenic differentiation of adipose-derived stromal cells in combinatorial hydrogels containing cartilage matrix proteins with decoupled mechanical stiffness. Tissue Eng Part A 2014;20:2131-9.
[5] Murphy CM, Matsiko A, Haugh MG, Gleeson JP, O'Brien FJ. Mesenchymal stem cell fate is regulated by the composition and mechanical properties of collagen-glycosaminoglycan scaffolds. J Mech Behav Biomed Mater 2012;11:53-62.
[6] Morrone G, Guzzardella GA, Torricelli P, Rocca M, Tigani D, Brodano GB, et al. Osteochondral lesion repair of the knee in the rabbit after low-power diode Ga-Al-As laser biostimulation: an experimental study. Artificial cells, blood substitutes, and immobilization biotechnology 2000;28:321-36.
[7] O'Driscoll SW. The healing and regeneration of articular cartilage. The Journal of bone and joint surgery American volume 1998;80:1795-812.
[8] Duda GN, Maldonado ZM, Klein P, Heller MO, Burns J, Bail H. On the influence of mechanical conditions in osteochondral defect healing. J Biomech 2005;38:843-51.
[9] Rodrigues MT, Gomes ME, Reis RL. Current strategies for osteochondral regeneration: from stem cells to pre-clinical approaches. Current Opinion in Biotechnology 2011;22:726-33.
[10] Lv HW, Li LS, Sun MY, Zhang Y, Chen L, Rong Y, et al. Mechanism of regulation of stem cell differentiation by matrix stiffness. Stem Cell Res Ther 2015;6.
[11] Galperin A, Oldinski RA, Florczyk SJ, Bryers JD, Zhang M, Ratner BD. Integrated bi-layered scaffold for osteochondral tissue engineering. Adv Healthc Mater 2013;2:872-83.
[12] Zouani OF, Kalisky J, Ibarboure E, Durrieu MC. Effect of BMP-2 from matrices of different stiffnesses for the modulation of stem cell fate. Biomaterials 2013;34:2157-66.
[13] Huebsch N, Arany PR, Mao AS, Shvartsman D, Ali OA, Bencherif SA, et al. Harnessing traction-mediated manipulation of the cell/matrix interface to control stem-cell fate. Nature materials 2010;9:518-26.
[14] Engler AJ, Sen S, Sweeney HL, Discher DE. Matrix elasticity directs stem cell lineage specification. Cell 2006;126:677-89.
[15] Williams CG, Kim TK, Taboas A, Malik A, Manson P, Elisseeff J. In vitro chondrogenesis of bone marrow-derived mesenchymal stem cells in a photopolymerizing hydrogel. Tissue engineering 2003;9:679-88.
[16] Kelly DJ, Jacobs CR. The role of mechanical signals in regulating chondrogenesis and osteogenesis of mesenchymal stem cells. Birth defects research Part C, Embryo today : reviews 2010;90:75-85.
[17] Angele P, Schumann D, Angele M, Kinner B, Englert C, Hente R, et al. Cyclic, mechanical compression enhances chondrogenesis of mesenchymal progenitor cells in tissue engineering scaffolds. Biorheology 2004;41:335-46.

.

[18] Pelaez D, Huang CY, Cheung HS. Cyclic compression maintains viability and induces chondrogenesis of human mesenchymal stem cells in fibrin gel scaffolds. Stem cells and development 2009;18:93-102.
[19] Tan S, Fang JY, Yang Z, Nimni ME, Han B. The synergetic effect of hydrogel stiffness and growth factor on osteogenic differentiation. Biomaterials 2014;35:5294-306.
[20] Oldinski RA, Ruckh TT, Staiger MP, Popat KC, James SP. Dynamic mechanical analysis and biomineralization of hyaluronan-polyethylene copolymers for potential use in osteochondral defect repair. Acta Biomater 2011;7:1184-91.
[21] Diamant J, Keller A, Baer E, Litt M, Arridge RGC. Collagen; Ultrastructure and Its Relation to Mechanical Properties as a Function of Ageing1972.
[22] Ruoslahti E, Pierschbacher MD. New perspectives in cell adhesion: RGD and integrins. Science 1987;238:491-7.
[23] Bosnakovski D, Mizuno M, Kim G, Takagi S, Okumura M, Fujinaga T. Chondrogenic differentiation of bovine bone marrow mesenchymal stem cells (MSCs) in different hydrogels: influence of collagen type II extracellular matrix on MSC chondrogenesis. Biotechnol Bioeng 2006;93:1152-63.
[24] Nuttelman CR, Henry SM, Anseth KS. Synthesis and characterization of photocrosslinkable, degradable poly(vinyl alcohol)-based tissue engineering scaffolds. Biomaterials 2002;23:3617-26.
[25] Martens PJ, Bryant SJ, Anseth KS. Tailoring the degradation of hydrogels formed from multivinyl poly(ethylene glycol) and poly(vinyl alcohol) macromers for cartilage tissue engineering. Biomacromolecules 2003;4:283-92.
[26] Bryant SJ, Nuttelman CR, Anseth KS. The effects of crosslinking density on cartilage formation in photocrosslinkable hydrogels. Biomedical sciences instrumentation 1999;35:309-14.
[27] Stammen JA, Williams S, Ku DN, Guldberg RE. Mechanical properties of a novel PVA hydrogel in shear and unconfined compression. Biomaterials 2001;22:799-806.
[28] Gutierrez M, Garcia-Carvajal Z, Jobbagy M, Rubio F, Yuste L, Rogo F, et al. Poly(vinyl alcohol) scaffolds with tailored morphologies for drug delivery and controlled release. Advanced Functional Materials 2007;17:3505-13.
[29] Alves MH, Jensen BE, Smith AA, Zelikin AN. Poly(vinyl alcohol) physical hydrogels: new vista on a long serving biomaterial. Macromolecular bioscience 2011;11:1293-313.
[30] Bichara DA, Zhao X, Bodugoz-Senturk H, Ballyns FP, Oral E, Randolph MA, et al. Porous poly(vinyl alcohol)-hydrogel matrix-engineered biosynthetic cartilage. Tissue Eng Part A 2011;17:301-9.
[31] Bodugoz-Senturk H, Choi J, Oral E, Kung JH, Macias CE, Braithwaite G, et al. The effect of polyethylene glycol on the stability of pores in polyvinyl alcohol hydrogels during annealing. Biomaterials 2008;29:141-9.
[32] Lee SY, Wee AS, Lim CK, Abbas AA, Selvaratnam L, Merican AM, et al. Supermacroporous poly(vinyl alcohol)-carboxylmethyl chitosan-poly(ethylene glycol) scaffold: an in vitro and in vivo pre-assessments for cartilage tissue engineering. Journal of materials science Materials in medicine 2013;24:1561-70.
[33] Bodugoz-Senturk H, Oral E, Choi J, Macias C, Muratoglu OK. Molecular weight effect on theta-gel formation in poly(vinyl alcohol)-poly(ethylene glycol) mixtures. Journal of Applied Polymer Science 2012;125:2890-5.
[34] Lim KS, Alves MH, Poole-Warren LA, Martens PJ. Covalent incorporation of non-chemically modified gelatin into degradable PVA-tyramine hydrogels. Biomaterials 2013;34:7097-105.

.

[35] Wang T, Yang X, Qi X, Jiang C. Osteoinduction and proliferation of bone-marrow stromal cells in three-dimensional poly (epsilon-caprolactone)/ hydroxyapatite/collagen scaffolds. J Transl Med 2015;13:152.
[36] Peppas NA, Wright SL. Solute Diffusion in Poly(vinyl alcohol)/Poly(acrylic acid) Interpenetrating Networks. Macromolecules 1996;29:8798-804.
[37] Mallapragada SK, Peppas NA. Dissolution mechanism of semicrystalline poly(vinyl alcohol) in water. Journal of Polymer Science Part B: Polymer Physics 1996;34:1339-46.

.

BIBLIOGRAPHY

Ahn, D. G., Lee, J., Park, S. Y., Kwark, Y. J., & Lee, K. Y. (2014). Doxorubicin-loaded alginate-g-poly(N-isopropylacrylamide) micelles for cancer imaging and therapy. *ACS Appl Mater Interfaces, 6*(24), 22069-22077. doi:10.1021/am505444c

Akinc, A., Thomas, M., Klibanov, A. M., & Langer, R. (2005). Exploring polyethylenimine-mediated DNA transfection and the proton sponge hypothesis. *The Journal of Gene Medicine, 7*(5), 657-663.

Aldridge, A., Kouroupis, D., Churchman, S., English, A., Ingham, E., & Jones, E. (2013). Assay validation for the assessment of adipogenesis of multipotential stromal cells—a direct comparison of four different methods. *Cytotherapy, 15*(1), 89-101. doi:http://dx.doi.org/10.1016/j.jcyt.2012.07.001

Almubarak, S., Nethercott, H., Freeberg, M., Beaudon, C., Jha, A., Jackson, W., . . . Bahney, C. (2016). Tissue engineering strategies for promoting vascularized bone regeneration. *Bone, 83*, 197-209. doi:http://dx.doi.org/10.1016/j.bone.2015.11.011

Alrifaiy, A., Lindahl, O. A., & Ramser, K. (2012). Polymer-based microfluidic devices for pharmacy, biology and tissue engineering. *Polymers, 4*(3), 1349-1398.

Alves, M. H., Jensen, B. E., Smith, A. A., & Zelikin, A. N. (2011). Poly(vinyl alcohol) physical hydrogels: new vista on a long serving biomaterial. *Macromol Biosci, 11*(10), 1293-1313. doi:10.1002/mabi.201100145

Angele, P., Schumann, D., Angele, M., Kinner, B., Englert, C., Hente, R., . . . Kujat, R. (2004). Cyclic, mechanical compression enhances chondrogenesis of mesenchymal progenitor cells in tissue engineering scaffolds. *Biorheology, 41*(3-4), 335-346. Retrieved from http://www.ncbi.nlm.nih.gov/pubmed/15299266

Appel, E. A., del Barrio, J., Loh, X. J., & Scherman, O. A. (2012). Supramolecular polymeric hydrogels. *Chemical Society Reviews, 41*(18), 6195-6214. doi:10.1039/C2CS35264H

Appel, E. A., Tibbitt, M. W., Webber, M. J., Mattix, B. A., Veiseh, O., & Langer, R. (2015). Self-assembled hydrogels utilizing polymer-nanoparticle interactions. *Nat Commun, 6*, 6295. doi:10.1038/ncomms7295

Aubel-Sadron, G., & Londos-Gagliardi, D. (1984). Daunorubicin and doxorubicin, anthracycline antibiotics, a physicochemical and biological review. *Biochimie,*

.

66(5), 333-352. doi:http://dx.doi.org/10.1016/0300-9084(84)90018-X

Augst, A. D., Kong, H. J., & Mooney, D. J. (2006). Alginate hydrogels as biomaterials. *Macromol Biosci, 6*(8), 623-633. doi:10.1002/mabi.200600069

Autissier, A., Le Visage, C., Pouzet, C., Chaubet, F., & Letourneur, D. (2010). Fabrication of porous polysaccharide-based scaffolds using a combined freeze-drying/cross-linking process. *Acta Biomaterialia, 6*, 3640-3648.

Babak, V. G., Skotnikova, E. A., Lukina, I. G., Pelletier, S., Hubert, P., & Dellacherie, E. (2000). Hydrophobically Associating Alginate Derivatives: Surface Tension Properties of Their Mixed Aqueous Solutions with Oppositely Charged Surfactants. *J Colloid Interface Sci, 225*(2), 505-510. doi:10.1006/jcis.2000.6788

Badi, N., & Lutz, J.-F. (2009). PEG-based thermogels: Applicability in physiological media. *Journal of Controlled Release, 140*(3), 224-229. doi:http://dx.doi.org/10.1016/j.jconrel.2009.04.012

Bae, K. H., Wang, L.-S., & Kurisawa, M. (2013). Injectable biodegradable hydrogels: progress and challenges. *Journal of Materials Chemistry B, 1*(40), 5371-5388. doi:10.1039/C3TB20940G

Baimark, Y., & Srisuwan, Y. (2014). Preparation of alginate microspheres by water-in-oil emulsion method for drug delivery: Effect of Ca2+ post-cross-linking. *Advanced Powder Technology, 25*(5), 1541-1546. doi:http://dx.doi.org/10.1016/j.apt.2014.05.001

Balakrishnan, B., Joshi, N., Jayakrishnan, A., & Banerjee, R. (2014). Self-crosslinked oxidized alginate/gelatin hydrogel as injectable, adhesive biomimetic scaffolds for cartilage regeneration. *Acta Biomater, 10*(8), 3650-3663. doi:10.1016/j.actbio.2014.04.031

Bandak, S., Ramu, A., Barenholz, Y., & Gabizon, A. (1999). Reduced UV-induced degradation of doxorubicin encapsulated in polyethyleneglycol-coated liposomes. *Pharm Res, 16*(6), 841-846.

Bassyouni, F., ElHalwany, N., Abdel Rehim, M., & Neyfeh, M. (2013). Advances and new technologies applied in controlled drug delivery system. *Research on Chemical Intermediates*, 1-36. doi:10.1007/s11164-013-1338-2

Bayes, M., Rabasseda, X., & Prous, J. (2007). Gateways to clinical trials. *Methods and findings in experimental and clinical pharmacology, 29*(10), 697-735.

.

Berger, J., Reist, M., Mayer, J. M., Felt, O., Peppas, N. A., & Gurny, R. (2004). Structure and interactions in covalently and ionically crosslinked chitosan hydrogels for biomedical applications. *European Journal of Pharmaceutics and Biopharmaceutics, 57*(1), 19-34. doi:http://dx.doi.org/10.1016/S0939-6411(03)00161-9

Bernkop-Schnürch, A., & Dünnhaupt, S. (2012). Chitosan-based drug delivery systems. *European Journal of Pharmaceutics and Biopharmaceutics, 81*(3), 463-469. doi:http://dx.doi.org/10.1016/j.ejpb.2012.04.007

Bian, L., Zhai, D. Y., Tous, E., Rai, R., Mauck, R. L., & Burdick, J. A. (2011). Enhanced MSC chondrogenesis following delivery of TGF-beta3 from alginate microspheres within hyaluronic acid hydrogels in vitro and in vivo. *Biomaterials, 32*(27), 6425-6434. doi:10.1016/j.biomaterials.2011.05.033

Bichara, D. A., Zhao, X., Bodugoz-Senturk, H., Ballyns, F. P., Oral, E., Randolph, M. A., . . . Muratoglu, O. K. (2011). Porous poly(vinyl alcohol)-hydrogel matrix-engineered biosynthetic cartilage. *Tissue Eng Part A, 17*(3-4), 301-309. doi:10.1089/ten.TEA.2010.0322

Bilak, M. M., Hossain, W. A., & Morest, D. K. (2003). Intracellular fibroblast growth factor produces effects different from those of extracellular application on development of avian cochleovestibular ganglion cells in vitro. *J Neurosci Res, 71*(5), 629-647. doi:10.1002/jnr.10498

Bisht, S., & Maitra, A. (2009). Dextran-doxorubicin/chitosan nanoparticles for solid tumor therapy. *Wiley Interdiscip Rev Nanomed Nanobiotechnol, 1*(4), 415-425. doi:10.1002/wnan.43

Blaiszik, B., Kramer, S., Olugebefola, S., Moore, J. S., Sottos, N. R., & White, S. R. (2010). Self-healing polymers and composites. *Annual Review of Materials Research, 40*, 179-211.

Bodugoz-Senturk, H., Choi, J., Oral, E., Kung, J. H., Macias, C. E., Braithwaite, G., & Muratoglu, O. K. (2008). The effect of polyethylene glycol on the stability of pores in polyvinyl alcohol hydrogels during annealing. *Biomaterials, 29*(2), 141-149. doi:10.1016/j.biomaterials.2007.09.015

Bodugoz-Senturk, H., Oral, E., Choi, J., Macias, C., & Muratoglu, O. K. (2012). Molecular weight effect on theta-gel formation in poly(vinyl alcohol)-poly(ethylene glycol) mixtures. *Journal of Applied Polymer Science, 125*, 2890-2895.

.

Boekhoven, J., Rubert Pérez, C. M., Sur, S., Worthy, A., & Stupp, S. I. (2013). Dynamic Display of Bioactivity through Host–Guest Chemistry. *Angewandte Chemie International Edition, 52*(46), 12077-12080. doi:10.1002/anie.201306278

Bonadonna, G., Monfardini, S., De Lena, M., Fossati-Bellani, F., & Beretta, G. (1970). Phase I and preliminary phase II evaluation of adriamycin (NSC 123127). *Cancer Research, 30*(10), 2572-2582.

Bosnakovski, D., Mizuno, M., Kim, G., Takagi, S., Okumura, M., & Fujinaga, T. (2006). Chondrogenic differentiation of bovine bone marrow mesenchymal stem cells (MSCs) in different hydrogels: influence of collagen type II extracellular matrix on MSC chondrogenesis. *Biotechnol Bioeng, 93*(6), 1152-1163. doi:10.1002/bit.20828

Bouhadir, K. H., Lee, K. Y., Alsberg, E., Damm, K. L., Anderson, K. W., & Mooney, D. J. (2001). Degradation of partially oxidized alginate and its potential application for tissue engineering. *Biotechnol Prog, 17*(5), 945-950. doi:10.1021/bp010070p

Brewster, M. E., & Loftsson, T. (2007). Cyclodextrins as pharmaceutical solubilizers. *Advanced Drug Delivery Reviews, 59*(7), 645-666. doi:http://dx.doi.org/10.1016/j.addr.2007.05.012

Bryant, S. J., Nuttelman, C. R., & Anseth, K. S. (1999). The effects of crosslinking density on cartilage formation in photocrosslinkable hydrogels. *Biomed Sci Instrum, 35*, 309-314. Retrieved from http://www.ncbi.nlm.nih.gov/pubmed/11143369

Burdick, J. A., & Murphy, W. L. (2012). Moving from static to dynamic complexity in hydrogel design. *Nat Commun, 3*, 1269. Retrieved from http://dx.doi.org/10.1038/ncomms2271

Cafaggi, S., Russo, E., Stefani, R., Leardi, R., Caviglioli, G., Parodi, B., . . . Viale, M. (2007). Preparation and evaluation of nanoparticles made of chitosan or N-trimethyl chitosan and a cisplatin–alginate complex. *Journal of Controlled Release, 121*(1–2), 110-123. doi:http://dx.doi.org/10.1016/j.jconrel.2007.05.037

Cai, L., Dewi, R. E., & Heilshorn, S. C. (2015). Injectable Hydrogels with In Situ Double Network Formation Enhance Retention of Transplanted Stem Cells. *Advanced Functional Materials, 25*(9), 1344-1351. doi:10.1002/adfm.201403631

Carter, P. J. (2006). Potent antibody therapeutics by design. *Nat Rev Immunol, 6*(5), 343-357. doi:http://www.nature.com/nri/journal/v6/n5/suppinfo/nri1837_S1.html

Carvalho, F. S., Burgeiro, A., Garcia, R., Moreno, A. J., Carvalho, R. A., & Oliveira, P. J.

.

(2014). Doxorubicin-induced cardiotoxicity: from bioenergetic failure and cell death to cardiomyopathy. *Med Res Rev, 34*(1), 106-135. doi:10.1002/med.21280

Chan, M., Lux, J., Nishimura, T., Akiyoshi, K., & Almutairi, A. (2015). Long-Lasting and Efficient Tumor Imaging Using a High Relaxivity Polysaccharide Nanogel Magnetic Resonance Imaging Contrast Agent. *Biomacromolecules, 16*(9), 2964-2971. doi:10.1021/acs.biomac.5b00867

Chang, S. J., Lee, C. H., Hsu, C. Y., & Wang, Y. J. (2002). Biocompatible microcapsules with enhanced mechanical strength. *Journal of Biomedical Materials Research, 59*, 118-126.

Charron, P. N., Fenn, S. L., Poniz, A., & Oldinski, R. A. (2016). Mechanical properties and failure analysis of visible light crosslinked alginate-based tissue sealants. *J Mech Behav Biomed Mater, 59*, 314-321. doi:10.1016/j.jmbbm.2016.02.003

Chen, B., Miller, R. J., & Dhal, P. K. (2014). Hyaluronic Acid-Based Drug Conjugates: State-of-the-Art and Perspectives. *Journal of Biomedical Nanotechnology, 10*(1), 4-16. doi:10.1166/jbn.2014.1781

Chen, F.-m., Ma, Z.-w., Dong, G.-y., & Wu, Z.-f. (2009). Composite glycidyl methacrylated dextran (Dex-GMA)/gelatin nanoparticles for localized protein delivery. *Acta Pharmacologica Sinica, 30*(4), 485-493. doi:10.1038/aps.2009.15

Chen, Q., Zhu, L., Chen, H., Yan, H., Huang, L., Yang, J., & Zheng, J. (2015). A Novel Design Strategy for Fully Physically Linked Double Network Hydrogels with Tough, Fatigue Resistant, and Self-Healing Properties. *Advanced Functional Materials, 25*(10), 1598-1607. doi:10.1002/adfm.201404357

Chen, W., Kim, J. H., Zhang, D., Lee, K. H., Cangelosi, G. A., Soelberg, S. D., . . . Shen, A. Q. (2013). Microfluidic one-step synthesis of alginate microspheres immobilized with antibodies. *J R Soc Interface, 10*(88), 20130566. doi:10.1098/rsif.2013.0566

Chen, Z., Fillmore, C. M., Hammerman, P. S., Kim, C. F., & Wong, K.-K. (2014). Non-small-cell lung cancers: a heterogeneous set of diseases. *Nat Rev Cancer, 14*(8), 535-546. doi:10.1038/nrc3775

Chiang, C.-Y., & Chu, C.-C. (2015). Synthesis of photoresponsive hybrid alginate hydrogel with photo-controlled release behavior. *Carbohydrate Polymers, 119*(0), 18-25. doi:http://dx.doi.org/10.1016/j.carbpol.2014.11.043

Chivers, Claire E., Koner, Apurba L., Lowe, Edward D., & Howarth, M. (2011). How the biotin–streptavidin interaction was made even stronger: investigation via

.

crystallography and a chimaeric tetramer. *Biochemical Journal, 435*(Pt 1), 55-63. doi:10.1042/BJ20101593

Chlebova, K., Bryja, V., Dvorak, P., Kozubik, A., Wilcox, W. R., & Krejci, P. (2009). High molecular weight FGF2: the biology of a nuclear growth factor. *Cellular and molecular life sciences : CMLS, 66*(2), 225-235. doi:10.1007/s00018-008-8440-4

Choi, G. H., Lee, H. J., & Lee, S. C. (2014). Titanium-adhesive polymer nanoparticles as a surface-releasing system of dual osteogenic growth factors. *Macromol Biosci, 14*(4), 496-507. doi:10.1002/mabi.201300368

Choi, K. Y., Chung, H., Min, K. H., Yoon, H. Y., Kim, K., Park, J. H., . . . Jeong, S. Y. (2010). Self-assembled hyaluronic acid nanoparticles for active tumor targeting. *Biomaterials, 31*(1), 106-114. doi:http://dx.doi.org/10.1016/j.biomaterials.2009.09.030

Chou, A. I., Akintoye, S. O., & Nicoll, S. B. (2009). Photo-crosslinked Alginate Hydrogels Support Enhanced Matrix Accumulation by Nucleus Pulposus Cells In Vivo. *Osteoarthritis and cartilage / OARS, Osteoarthritis Research Society, 17*(10), 1377-1384. doi:10.1016/j.joca.2009.04.012

Chung, H. J., & Park, T. G. (2007). Surface engineered and drug releasing pre-fabricated scaffolds for tissue engineering. *Advanced Drug Delivery Reviews, 59*(4-5), 249-262. doi:10.1016/j.addr.2007.03.015

Ciofani, G., Raffa, V., Menciassi, A., & Dario, P. (2008a). Alginate and chitosan particles are drug delivery system for cell therapy. *Biomedical Microdevices, 10*(4), 597-600. doi:10.1007/s10544-008-9191-6

Ciofani, G., Raffa, V., Menciassi, A., & Dario, P. (2008b). Alginate and chitosan particles as drug delivery system for cell therapy. *Biomedical Microdevices, 10*, 131-140.

Clark, A. R., & Dean, J. L. (2012). The p38 MAPK Pathway in Rheumatoid Arthritis: A Sideways Look. *Open Rheumatol J, 6*, 209-219. doi:10.2174/1874312901206010209

Clark, A. R., Dean, J. L., & Saklatvala, J. (2009). The p38 MAPK pathway mediates both antiinflammatory and proinflammatory processes: comment on the article by Damjanov and the editorial by Genovese. *Arthritis Rheum, 60*(11), 3513-3514. doi:10.1002/art.24919

Cohn, D., Sagiv, H., Benyamin, A., & Lando, G. (2009). Engineering thermoresponsive polymeric nanoshells. *Biomaterials, 30*(19), 3289-3296.

.

doi:http://dx.doi.org/10.1016/j.biomaterials.2009.02.026

Collins, M. N., & Birkinshaw, C. (2013). Hyaluronic acid based scaffolds for tissue engineering—A review. *Carbohydrate Polymers, 92*(2), 1262-1279. doi:http://dx.doi.org/10.1016/j.carbpol.2012.10.028

Colombo, R., Mingozzi, M., Belvisi, L., Arosio, D., Piarulli, U., Carenini, N., . . . Gennari, C. (2012). Synthesis and Biological Evaluation (in Vitro and in Vivo) of Cyclic Arginine-Glycine-Aspartate (RGD) Peptidomimetic-Paclitaxel Conjugates Targeting lntegrin alpha(v)beta(3). *Journal of Medicinal Chemistry, 55*(23), 10460-10474. doi:Doi 10.1021/Jm301058f

Corey, J. M., Gertz, C. C., Sutton, T. J., Chen, Q., Mycek, K. B., Wang, B.-S., . . . Feldman, E. L. (2010). Patterning N-type and S-type neuroblastoma cells with Pluronic F108 and ECM proteins. *Journal of Biomedical Materials Research Part A, 93A*(2), 673-686. doi:10.1002/jbm.a.32485

Couvreur, P., Roblot-Treupel, L., Poupon, M. F., Brasseur, F., & Puisieux, F. (1990). Nanoparticulate Systems for Drug Delivery Nanoparticles as microcarriers for anticancer drugs. *Advanced Drug Delivery Reviews, 5*(3), 209-230. doi:http://dx.doi.org/10.1016/0169-409X(90)90017-M

Crini, G. (2014). Review: A History of Cyclodextrins. *Chemical Reviews, 114*(21), 10940-10975. doi:10.1021/cr500081p

Cumpstey, I. (2013). Chemical Modification of Polysaccharides. *ISRN Organic Chemistry, 2013*, 27. doi:10.1155/2013/417672

Daemi, H., & Barikani, M. (2014). Molecular engineering of manipulated alginate-based polyurethanes. *Carbohydr Polym, 112*, 638-647. doi:10.1016/j.carbpol.2014.06.023

Dambach, D. M. (2005). Potential adverse effects associated with inhibition of p38alpha/beta MAP kinases. *Curr Top Med Chem, 5*(10), 929-939. Retrieved from http://www.ncbi.nlm.nih.gov/pubmed/16178738

Davidovich-Pinhas, M., & Bianco-Peled, H. (2011a). Alginate-PEGAc: A new mucoadhesive polymer. *Acta Biomaterialia, 7*, 625-633.

Davidovich-Pinhas, M., & Bianco-Peled, H. (2011b). Physical and structural characteristics of acrylated poly(ethylene glycol)-alginate conjugates. *Acta Biomaterialia, 7*, 2817-2825.

.

De Cicco, F., Russo, P., Reverchon, E., García-González, C. A., Aquino, R. P., & Del Gaudio, P. Prilling and Supercritical Drying: a Successful Duo to Produce Core-Shell Polysaccharide Aerogel Beads for wound healing. *Carbohydrate Polymers*. doi:http://dx.doi.org/10.1016/j.carbpol.2016.04.031

Del Valle, E. M. M. (2004). Cyclodextrins and their uses: a review. *Process Biochemistry, 39*(9), 1033-1046. doi:http://dx.doi.org/10.1016/S0032-9592(03)00258-9

Delrieu, I. (2000). The high molecular weight isoforms of basic fibroblast growth factor (FGF-2): an insight into an intracrine mechanism. *FEBS Letters, 468*(1), 6-10. doi:http://dx.doi.org/10.1016/S0014-5793(00)01189-3

Deonarain, M. P. (2008). Recombinant antibodies for cancer therapy. *Expert Opin Biol Ther, 8*(8), 1123-1141. doi:10.1517/14712598.8.8.1123

Deonarain, M. P., Kousparou, C. A., & Epenetos, A. A. (2009). Antibodies targeting cancer stem cells: A new paradigm in immunotherapy? *mAbs, 1*(1), 12-25. Retrieved from http://www.ncbi.nlm.nih.gov/pmc/articles/PMC2715180/

Devi, D. A., Smitha, B., Sridhar, S., Jawalkar, S. S., & Aminabhavi, T. M. (2007). Novel sodium alginate/polyethyleneimine polyion complex membranes for pervaporation dehydration at the azeotropic composition of various alcohols. *Journal of Chemical Technology & Biotechnology, 82*(11), 993-1003. doi:10.1002/jctb.1735

Dhaneshwar, S. S., Kandpal, M., Gairola, N., & Kadam, S. (2006). Dextran: A promising macromolecular drug carrier. *Indian journal of pharmaceutical sciences, 68*(6), 705.

Diamant, J., Keller, A., Baer, E., Litt, M., & Arridge, R. G. C. (1972). *Collagen; Ultrastructure and Its Relation to Mechanical Properties as a Function of Ageing* (Vol. 180).

Diolosà, M., Donati, I., Turco, G., Cadenaro, M., Di Lenarda, R., Breschi, L., & Paoletti, S. (2014). Use of Methacrylate-Modified Chitosan to Increase the Durability of Dentine Bonding Systems. *Biomacromolecules, 15*(12), 4606-4613. doi:10.1021/bm5014124

Dong, R., Pang, Y., Su, Y., & Zhu, X. (2015). Supramolecular hydrogels: synthesis, properties and their biomedical applications. *Biomaterials Science, 3*(7), 937-954. doi:10.1039/C4BM00448E

Duda, G. N., Maldonado, Z. M., Klein, P., Heller, M. O., Burns, J., & Bail, H. (2005). On the

.

influence of mechanical conditions in osteochondral defect healing. *J Biomech, 38*(4), 843-851. doi:10.1016/j.jbiomech.2004.04.034

Engler, A. J., Sen, S., Sweeney, H. L., & Discher, D. E. (2006). Matrix elasticity directs stem cell lineage specification. *Cell, 126*(4), 677-689. doi:10.1016/j.cell.2006.06.044

Fahmy, T. M., Fong, P. M., Goyal, A., & Saltzman, W. M. (2005). Targeted for drug delivery. *Materials Today, 8*(8, Supplement), 18-26. doi:http://dx.doi.org/10.1016/S1369-7021(05)71033-6

Fenn, S. L., & Oldinski, R. A. (2015). Visible light crosslinking of methacrylated hyaluronan hydrogels for injectable tissue repair. *J Biomed Mater Res B Appl Biomater*. doi:10.1002/jbm.b.33476

Fernandes Fraceto, L., Grillo, R., & Sobarzo-Sanchez, E. (2014). Cyclodextrin inclusion complexes loaded in particles as drug carrier systems. *Current topics in medicinal chemistry, 14*(4), 518-525.

Ferrara, N., Gerber, H. P., & LeCouter, J. (2003). The biology of VEGF and its receptors. *Nat Med, 9*(6), 669-676. doi:10.1038/nm0603-669

Freemantle, M. (1999). DOWNSIZING CHEMISTRY. *Chemical & Engineering News Archive, 77*(8), 27-36. doi:10.1021/cen-v077n008.p027

Frey, N., Linke, A., Suselbeck, T., Muller-Ehmsen, J., Vermeersch, P., Schoors, D., . . . Leor, J. (2014). Intracoronary delivery of injectable bioabsorbable scaffold (IK-5001) to treat left ventricular remodeling after ST-elevation myocardial infarction: a first-in-man study. *Circ Cardiovasc Interv, 7*(6), 806-812. doi:10.1161/circinterventions.114.001478

Frohman, E. M., Racke, M. K., & Raine, C. S. (2006). Multiple sclerosis--the plaque and its pathogenesis. *N Engl J Med, 354*(9), 942-955. doi:354/9/942

Fujita, H., Ooya, T., & Yui, N. (1999). Thermally-Responsive Properties of a Polyrotaxane Consisting of [beta]-Cyclodextrins and a Poly(ethylene glycol)-Poly(propylene glycol) Triblock-Copolymer. *Polym J, 31*(11_2), 1099-1104. doi:10.1295/polymj.31.1099

Galperin, A., Oldinski, R. A., Florczyk, S. J., Bryers, J. D., Zhang, M., & Ratner, B. D. (2013). Integrated bi-layered scaffold for osteochondral tissue engineering. *Adv Healthc Mater, 2*(6), 872-883. doi:10.1002/adhm.201200345

Ganesh, S., Iyer, A. K., Gattacceca, F., Morrissey, D. V., & Amiji, M. M. (2013). In vivo

.

biodistribution of siRNA and cisplatin administered using CD44-targeted hyaluronic acid nanoparticles. *Journal of Controlled Release, 172*(3), 699-706. doi:http://dx.doi.org/10.1016/j.jconrel.2013.10.016

Garcia, A. J., & Reyes, C. D. (2005). Bio-adhesive surfaces to promote osteoblast differentiation and bone formation. *J Dent Res, 84*(5), 407-413.

Gåserød, O., Sannes, A., & Skjåk-Bræk, G. (1999). Microcapsules of alginate–chitosan. II. A study of capsule stability and permeability. *Biomaterials, 20*(8), 773-783. doi:http://dx.doi.org/10.1016/S0142-9612(98)00230-0

Gaubert, F., Escaffit, F., Bertrand, C., Korc, M., Pradayrol, L., Clemente, F., & Estival, A. (2001). Expression of the high molecular weight fibroblast growth factor-2 isoform of 210 amino acids is associated with modulation of protein kinases C delta and epsilon and ERK activation. *J Biol Chem, 276*(2), 1545-1554. doi:10.1074/jbc.M001184200

Genovese, M. C. (2009). Inhibition of p38: has the fat lady sung? *Arthritis Rheum, 60*(2), 317-320. doi:10.1002/art.24264

Gomes, B., Moreira, I., Rocha, S., Coelho, M., & Pereira, M. d. C. (2013). Polysaccharide-Based Nanoparticles for Cancer Therapy. *Journal of Nanopharmaceutics and Drug Delivery, 1*(4), 335-354. doi:10.1166/jnd.2013.1039

Grabovac, V., Guggi, D., & Bernkop-Schnurch, A. (2005). Comparison of the mucoadhesive properties of various polymers. *Adv Drug Deliv Rev, 57*(11), 1713-1723. doi:10.1016/j.addr.2005.07.006

Granadero, D., Bordello, J., Pérez-Alvite, M. J., Novo, M., & Al-Soufi, W. (2010). Host-Guest Complexation Studied by Fluorescence Correlation Spectroscopy: Adamantane–Cyclodextrin Inclusion. *International Journal of Molecular Sciences, 11*(1), 173-188. doi:10.3390/ijms11010173

Grassel, S., & Lorenz, J. (2014). Tissue-engineering strategies to repair chondral and osteochondral tissue in osteoarthritis: use of mesenchymal stem cells. *Curr Rheumatol Rep, 16*(10), 452. doi:10.1007/s11926-014-0452-5

Greenstein, J. I. (2007). Current concepts of the cellular and molecular pathophysiology of multiple sclerosis. *Dev Neurobiol, 67*(9), 1248-1265. doi:10.1002/dneu.20387

Greenwood-Goodwin, M., Teasley, E. S., & Heilshorn, S. C. (2014). Dual-stage growth factor release within 3D protein-engineered hydrogel niches promotes

.

adipogenesis. *Biomaterials Science, 2*(11), 1627-1639. doi:10.1039/C4BM00142G

Gregory, C. A., Gunn, W. G., Peister, A., & Prockop, D. J. (2004). An Alizarin red-based assay of mineralization by adherent cells in culture: comparison with cetylpyridinium chloride extraction. *Analytical Biochemistry, 329*(1), 77-84. doi:Doi 10.1016/J.Ab.2004.02.002

Guan, Y., & Zhang, Y. (2011). PNIPAM microgels for biomedical applications: from dispersed particles to 3D assemblies. *Soft Matter, 7*(14), 6375-6384. doi:10.1039/C0SM01541E

Guma, M., Hammaker, D., Topolewski, K., Corr, M., Boyle, D. L., Karin, M., & Firestein, G. S. (2012). Antiinflammatory functions of p38 in mouse models of rheumatoid arthritis: advantages of targeting upstream kinases MKK-3 or MKK-6. *Arthritis Rheum, 64*(9), 2887-2895. doi:10.1002/art.34489

Guo, H., Lai, Q., Wang, W., Wu, Y., Zhang, C., Liu, Y., & Yuan, Z. (2013). Functional alginate nanoparticles for efficient intracellular release of doxorubicin and hepatoma carcinoma cell targeting therapy. *Int J Pharm, 451*(1-2), 1-11. doi:10.1016/j.ijpharm.2013.04.025

Gutierrez, M., Garcia-Carvajal, Z., Jobbagy, M., Rubio, F., Yuste, L., Rogo, F., . . . del Monte, F. (2007). Poly(vinyl alcohol) scaffolds with tailored morphologies for drug delivery and controlled release. *Advanced Functional Materials, 17*, 3505-3513.

Guvendiren, M., Lu, H. D., & Burdick, J. A. (2012). Shear-thinning hydrogels for biomedical applications. *Soft Matter, 8*(2), 260-272. doi:10.1039/C1SM06513K

Hamidi, M., Azadi, A., & Rafiei, P. (2008). Hydrogel nanoparticles in drug delivery. *Adv Drug Deliv Rev, 60*(15), 1638-1649. doi:10.1016/j.addr.2008.08.002

Hammaker, D., & Firestein, G. S. (2010). "Go upstream, young man": lessons learned from the p38 saga. *Ann Rheum Dis, 69 Suppl 1*, i77-82. doi:10.1136/ard.2009.119479

Han, H. S., Thambi, T., Choi, K. Y., Son, S., Ko, H., Lee, M. C., . . . Park, J. H. (2015). Bioreducible Shell-Cross-Linked Hyaluronic Acid Nanoparticles for Tumor-Targeted Drug Delivery. *Biomacromolecules, 16*(2), 447-456. doi:10.1021/bm5017755

Harada, A., Okada, M., Li, J., & Kamachi, M. (1995). Preparation and Characterization of Inclusion Complexes of Poly(propylene glycol) with Cyclodextrins.

.

Macromolecules, 28(24), 8406-8411. doi:10.1021/ma00128a060

Harada, A., Takashima, Y., & Yamaguchi, H. (2009). Cyclodextrin-based supramolecular polymers. *Chemical Society Reviews, 38*(4), 875-882. doi:10.1039/B705458K

Harvey, N., Dennison, E., & Cooper, C. (2010). Osteoporosis: impact on health and economics. *Nat Rev Rheumatol, 6*(2), 99-105. Retrieved from http://dx.doi.org/10.1038/nrrheum.2009.260

Hauser, S. L., Chan, J. R., & Oksenberg, J. R. (2013). Multiple sclerosis: Prospects and promise. *Ann Neurol*. doi:10.1002/ana.24009

Hennink, W. E., & van Nostrum, C. F. (2012). Novel crosslinking methods to design hydrogels. *Advanced Drug Delivery Reviews, 64, Supplement*, 223-236. doi:http://dx.doi.org/10.1016/j.addr.2012.09.009

Hersel, U., Dahmen, C., & Kessler, H. (2003). RGD modified polymers: biomaterials for stimulated cell adhesion and beyond. *Biomaterials, 24*(24), 4385-4415. doi:http://dx.doi.org/10.1016/S0142-9612(03)00343-0

Hofig, I., Atkinson, M. J., Mall, S., Krackhardt, A. M., Thirion, C., & Anastasov, N. (2012). Poloxamer synperonic F108 improves cellular transduction with lentiviral vectors. *J Gene Med, 14*(8), 549-560. doi:10.1002/jgm.2653

Hortobagyi, G. N. (1997). Anthracyclines in the treatment of cancer. An overview. *Drugs, 54 Suppl 4*, 1-7.

Hotaling, S. O. (2015). *Design and Fabrication of Flow-Focusing Devices for Tissue Engineering Applications.* (Undergraduate Honor Degree Honors College Thesis), University of Vermont, UVM Honors College Senior Theses. Retrieved from http://scholarworks.uvm.edu/hcoltheses/54 Available from UVM Honors College Senior Theses.

Hou, X., Lewis, K. T., Wu, Q., Wang, S., Chen, X., Flack, A., . . . Jena, B. P. (2014). Proteome of the porosome complex in human airway epithelia: Interaction with the cystic fibrosis transmembrane conductance regulator (CFTR). *Journal of Proteomics, 96*, 82-91. doi:http://dx.doi.org/10.1016/j.jprot.2013.10.041

Hristova, M., Habibovic, A., Veith, C., Janssen-Heininger, Y. M. W., Dixon, A. E., Geiszt, M., & van der Vliet, A. Airway epithelial dual oxidase 1 mediates allergen-induced IL-33 secretion and activation of type 2 immune responses. *Journal of Allergy and Clinical Immunology*.

.

doi:http://dx.doi.org/10.1016/j.jaci.2015.10.003

Hrubý, M., Koňák, Č., & Ulbrich, K. (2005). Polymeric micellar pH-sensitive drug delivery system for doxorubicin. *Journal of Controlled Release, 103*(1), 137-148. doi:http://dx.doi.org/10.1016/j.jconrel.2004.11.017

Huang, F., & Scherman, O. A. (2012). Supramolecular polymers. *Chemical Society Reviews, 41*(18), 5879-5880. doi:10.1039/C2CS90071H

Huang, H.-Y., Hu, S.-H., Chian, C.-S., Chen, S.-Y., Lai, H.-Y., & Chen, Y.-Y. (2012). Self-assembling PVA-F127 thermosensitive nanocarriers with highly sensitive magnetically-triggered drug release for epilepsy therapy in vivo. *Journal of Materials Chemistry, 22*(17), 8566-8573. doi:10.1039/C2JM00032F

Huang, R., Ke, W., Han, L., Liu, Y., Shao, K., Ye, L., . . . Pei, Y. (2009). Brain-targeting mechanisms of lactoferrin-modified DNA-loaded nanoparticles. *Journal of Cerebral Blood Flow & Metabolism, 29*(12), 1914-1923.

Huang, S.-Y., Pooyan, S., Wang, J., Choudhury, I., Leibowitz, M. J., & Stein, S. (1998). A Polyethylene Glycol Copolymer for Carrying and Releasing Multiple Copies of Cysteine-Containing Peptides. *Bioconjugate Chem., 9*(5), 612-617. doi:10.1021/BC980038P

Huebsch, N., Arany, P. R., Mao, A. S., Shvartsman, D., Ali, O. A., Bencherif, S. A., . . . Mooney, D. J. (2010). Harnessing traction-mediated manipulation of the cell/matrix interface to control stem-cell fate. *Nat Mater, 9*(6), 518-526. doi:10.1038/nmat2732

Hung, L.-H., & Lee, A. P. (2007). Microfluidic devices for the synthesis of nanoparticles and biomaterials. *Journal of Medical and Biological Engineering, 27*(1), 1.

Iliescu, C., Taylor, H., Avram, M., Miao, J., & Franssila, S. (2012). A practical guide for the fabrication of microfluidic devices using glass and silicon. *Biomicrofluidics, 6*(1), 016505-016505-016516. doi:10.1063/1.3689939

Iso, Y., Rao, K. S., Poole, C. N., Zaman, A. K., Curril, I., Sobel, B. E., . . . Spees, J. L. (2014). Priming with ligands secreted by human stromal progenitor cells promotes grafts of cardiac stem/progenitor cells after myocardial infarction. *Stem Cells, 32*(3), 674-683. doi:10.1002/stem.1546

Izawa, H., Kawakami, K., Sumita, M., Tateyama, Y., Hill, J. P., & Ariga, K. (2013). [small beta]-Cyclodextrin-crosslinked alginate gel for patient-controlled drug delivery systems: regulation of host-guest interactions with mechanical stimuli. *Journal of*

.

Materials Chemistry B, 1(16), 2155-2161. doi:10.1039/C3TB00503H

Jain, S., & Amiji, M. (2012a). Tuftsin-Modified Alginate Nanoparticles as a Noncondensing Macrophage-Targeted DNA Delivery System. *Biomacromolecules, 13*(4), 1074-1085. doi:10.1021/bm2017993

Jain, S., & Amiji, M. (2012b). Tuftsin-modified alginate nanoparticles as a noncondensing macrophage-targeted DNA delivery system. *Biomacromolecules, 13*, 1074-1085.

Janes, K. A., Fresneau, M. P., Marazuela, A., Fabra, A., & Alonso, M. a. J. (2001). Chitosan nanoparticles as delivery systems for doxorubicin. *Journal of Controlled Release, 73*(2–3), 255-267. doi:http://dx.doi.org/10.1016/S0168-3659(01)00294-2

Jay, S. M., & Saltzman, W. M. (2009a). Controlled delivery of VEGF via modulation of alginate microparticle ionic crosslinking. *J Control Release, 134*(1), 26-34. doi:10.1016/j.jconrel.2008.10.019

Jay, S. M., & Saltzman, W. M. (2009b). Controlled delivery of VEGF via modulation of alginate microparticle ionic crosslinking. *Journal of Controlled Release, 134*(1), 26-34. doi:http://dx.doi.org/10.1016/j.jconrel.2008.10.019

Jay, S. M., Shepherd, B. R., Bertram, J. P., Pober, J. S., & Saltzman, W. M. (2008). Engineering of multifunctional gels integrating highly efficient growth factor delivery with endothelial cell transplantation. *FASEB J, 22*(8), 2949-2956. doi:10.1096/fj.08-108803

Jemal, A., Bray, F., Center, M. M., Ferlay, J., Ward, E., & Forman, D. (2011). Global cancer statistics. *CA Cancer J Clin, 61*(2), 69-90. doi:10.3322/caac.20107

Jeon, O., Alt, D. S., Ahmed, S. M., & Alsberg, E. (2012). The effect of oxidation on the degradation of photocrosslinkable alginate hydrogels. *Biomaterials, 33*(13), 3503-3514. doi:http://dx.doi.org/10.1016/j.biomaterials.2012.01.041

Jeon, O., Bouhadir, K. H., Mansour, J. M., & Alsberg, E. (2009). Photocrosslinked alginate hydrogels with tunable biodegradation rates and mechanical properties. *Biomaterials, 30*(14), 2724-2734. doi:10.1016/j.biomaterials.2009.01.034

Jeong, Y. I., Kim, S. T., Jin, S. G., Ryu, H. H., Jin, Y. H., Jung, T. Y., . . . Jung, S. (2008). Cisplatin-incorporated hyaluronic acid nanoparticles based on ion-complex formation. *J Pharm Sci, 97*(3), 1268-1276. doi:10.1002/jps.21103

Jiang, T., Kim, Y. K., Singh, B., Kang, S. K., Choi, Y. J., & Cho, C. S. (2013). Effect of microencapsulation of Lactobacillus plantarum 25 into

.

alginate/chitosan/alginate microcapsules on viability and cytokine induction. *J Nanosci Nanotechnol, 13*(8), 5291-5295.

Kang, S.-W., Cha, B.-H., Park, H., Park, K.-S., Lee, K. Y., & Lee, S.-H. (2011). The Effect of Conjugating RGD into 3D Alginate Hydrogels on Adipogenic Differentiation of Human Adipose-Derived Stromal Cells. *Macromolecular Bioscience, 11*(5), 673-679. doi:10.1002/mabi.201000479

Kaya, E., & Mathias, L. J. (2010). Synthesis and characterization of physical crosslinking systems based on cyclodextrin inclusion/host-guest complexation. *Journal of Polymer Science Part A: Polymer Chemistry, 48*(3), 581-592. doi:10.1002/pola.23771

Kelly, D. J., & Jacobs, C. R. (2010). The role of mechanical signals in regulating chondrogenesis and osteogenesis of mesenchymal stem cells. *Birth Defects Res C Embryo Today, 90*(1), 75-85. doi:10.1002/bdrc.20173

Khalil, I. A., Kogure, K., Akita, H., & Harashima, H. (2006). Uptake pathways and subsequent intracellular trafficking in nonviral gene delivery. *Pharmacological Reviews, 58*(1), 32-45.

Khattak, S. F., Bhatia, S. R., & Roberts, S. C. (2005). Pluronic F127 as a cell encapsulation material: utilization of membrane-stabilizing agents. *Tissue Eng, 11*(5-6), 974-983. doi:10.1089/ten.2005.11.974

Khetan, S., Guvendiren, M., Legant, W. R., Cohen, D. M., Chen, C. S., & Burdick, J. A. (2013). Degradation-mediated cellular traction directs stem cell fate in covalently crosslinked three-dimensional hydrogels. *Nature materials, 12*(5), 458-465. doi:10.1038/nmat3586

Kim, C., Sano, Y., Todorova, K., Carlson, B. A., Arpa, L., Celada, A., . . . Park, J. M. (2008). The kinase p38 alpha serves cell type-specific inflammatory functions in skin injury and coordinates pro- and anti-inflammatory gene expression. *Nat Immunol, 9*(9), 1019-1027. doi:10.1038/ni.1640ni.1640 [pii]

Kim, S., Kim, J.-H., Jeon, O., Kwon, I. C., & Park, K. (2009). Engineered polymers for advanced drug delivery. *European Journal of Pharmaceutics and Biopharmaceutics, 71*(3), 420-430.

Kirchhausen, T., Macia, E., & Pelish, H. E. (2008). Use of dynasore, the small molecule inhibitor of dynamin, in the regulation of endocytosis. *Methods Enzymol, 438*, 77-93. doi:10.1016/s0076-6879(07)38006-3

.

Klouda, L., & Mikos, A. G. (2008). Thermoresponsive hydrogels in biomedical applications - a review. *European journal of pharmaceutics and biopharmaceutics : official journal of Arbeitsgemeinschaft fur Pharmazeutische Verfahrenstechnik e.V, 68*(1), 34-45. doi:10.1016/j.ejpb.2007.02.025

Knop, K., Hoogenboom, R., Fischer, D., & Schubert, U. S. (2010). Poly(ethylene glycol) in Drug Delivery: Pros and Cons as Well as Potential Alternatives. *Angewandte Chemie International Edition, 49*(36), 6288-6308. doi:10.1002/anie.200902672

Kou, L., Sun, J., Zhai, Y., & He, Z. (2013). The endocytosis and intracellular fate of nanomedicines: Implication for rational design. *Asian Journal of Pharmaceutical Sciences, 8*(1), 1-10. doi:http://dx.doi.org/10.1016/j.ajps.2013.07.001

Krebs, M. D., Jeon, O., & Alsberg, E. (2009). Localized and sustained delivery of silencing RNA from macroscopic biopolymer hydrogels. *J Am Chem Soc, 131*(26), 9204-9206. doi:10.1021/ja9037615

Kuhl, E. (2014). Growing matter: a review of growth in living systems. *J Mech Behav Biomed Mater, 29*, 529-543. doi:10.1016/j.jmbbm.2013.10.009

Kuraitis, D., Arzhangi, Z., Hyatt, A., Vulesevica, B., Merrett, K., & Zhang, J. (2012). Tertiary biomaterial encapsulation controls the release of FGF-2 without impacting bioactivity. *Open Tissue Eng Regen Med J, 5*, 4.

Lao, L. L., Peppas, N. A., Boey, F. Y. C., & Venkatraman, S. S. (2011). Modeling of drug release from bulk-degrading polymers. *International Journal of Pharmaceutics, 418*(1), 28-41. doi:http://dx.doi.org/10.1016/j.ijpharm.2010.12.020

Lao, L. L., Venkatraman, S. S., & Peppas, N. A. (2008). Modeling of drug release from biodegradable polymer blends. *European Journal of Pharmaceutics and Biopharmaceutics, 70*(3), 796-803. doi:http://dx.doi.org/10.1016/j.ejpb.2008.05.024

Leahy, D. J., Aukhil, I., & Erickson, H. P. (1996). 2.0 $\approx$ Crystal Structure of a Four-Domain Segment of Human Fibronectin Encompassing the RGD Loop and Synergy Region. *Cell, 84*(1), 155-164. Retrieved from http://linkinghub.elsevier.com/retrieve/pii/S0092867400810028

Lee, G. Y., Kim, J.-H., Choi, K. Y., Yoon, H. Y., Kim, K., Kwon, I. C., . . . Kim, I.-S. (2015). Hyaluronic acid nanoparticles for active targeting atherosclerosis. *Biomaterials, 53*, 341-348. doi:http://dx.doi.org/10.1016/j.biomaterials.2015.02.089

Lee, J. C., Laydon, J. T., McDonnell, P. C., Gallagher, T. F., Kumar, S., Green, D., . . . et al.

.

(1994). A protein kinase involved in the regulation of inflammatory cytokine biosynthesis. *Nature, 372*(6508), 739-746. doi:10.1038/372739a0

Lee, K. Y., Alsberg, E., Hsiong, S., Comisar, W., Linderman, J., Ziff, R., & Mooney, D. (2004). Nanoscale Adhesion Ligand Organization Regulates Osteoblast Proliferation and Differentiation. *Nano Lett, 4*(8), 1501-1506. doi:10.1021/nl0493592

Lee, K. Y., & Mooney, D. J. (2012a). Alginate: Properties and biomedical applications. *Progress in Polymer Science, 37*, 106-126.

Lee, K. Y., & Mooney, D. J. (2012b). Alginate: properties and biomedical applications. *Progress in polymer science, 37*(1), 106-126. doi:10.1016/j.progpolymsci.2011.06.003

Lee, R. J., Wang, S., & Low, P. S. (1996). Measurement of endosome pH following folate receptor-mediated endocytosis. *Biochimica et Biophysica Acta (BBA)-Molecular Cell Research, 1312*(3), 237-242.

Lee, S. Y., Wee, A. S., Lim, C. K., Abbas, A. A., Selvaratnam, L., Merican, A. M., . . . Kamarul, T. (2013). Supermacroporous poly(vinyl alcohol)-carboxylmethyl chitosan-poly(ethylene glycol) scaffold: an in vitro and in vivo pre-assessments for cartilage tissue engineering. *J Mater Sci Mater Med, 24*(6), 1561-1570. doi:10.1007/s10856-013-4907-4

Lee, W. L., Guo, W. M., Ho, V. H. B., Saha, A., Chong, H. C., Tan, N. S., . . . Loo, S. C. J. (2015). Delivery of doxorubicin and paclitaxel from double-layered microparticles: The effects of layer thickness and dual-drug vs. single-drug loading. *Acta Biomaterialia, 27*, 53-65. doi:http://dx.doi.org/10.1016/j.actbio.2015.08.051

Lemiere, S., Azar, R., Belloc, F., Gursel, D., Pyronnet, S., Bikfalvi, A., & Auguste, P. (2008). Overexpression of high molecular weight FGF-2 forms inhibits glioma growth by acting on cell-cycle progression and protein translation. *Exp Cell Res, 314*(20), 3701-3711. doi:10.1016/j.yexcr.2008.09.022

Lemoine, D., Wauters, F., Bouchend'homme, S., & Prεατ, ς. (1998). Preparation and characterization of alginate microspheres containing a model antigen. *International Journal of Pharmaceutics, 176*, 9-19.

Lesley, J., He, Q., Miyake, K., Hamann, A., Hyman, R., & Kincade, P. W. (1992). Requirements for hyaluronic acid binding by CD44: a role for the cytoplasmic domain and activation by antibody. *J Exp Med, 175*(1), 257-266.

.

Leung, K. (2004a). Ferumoxides *Molecular Imaging and Contrast Agent Database (MICAD)*. Bethesda (MD): National Center for Biotechnology Information (US).

Leung, K. (2004b). Ferumoxtran *Molecular Imaging and Contrast Agent Database (MICAD)*. Bethesda (MD): National Center for Biotechnology Information (US).

Levy, M. C., & Edwards-Levy, F. (1996). Coating alginate beads with cross-linked biopolymers: a novel method based on a transacylation reaction. *J Microencapsul, 13*(2), 169-183. doi:10.3109/02652049609052905

Li, G., Parmar, M., & Lee, D.-W. (2015). An oxidized liquid metal-based microfluidic platform for tunable electronic device applications. *Lab on a Chip, 15*(3), 766-775. doi:10.1039/C4LC01013B

Li, T., Shi, X. W., Du, Y. M., & Tang, Y. F. (2007). Quaternized chitosan/alginate nanoparticles for protein delivery. *Journal of Biomedical Materials Research Part A, 83*(2), 383-390.

Li, W., Guan, T., Zhang, X., Wang, Z., Wang, M., Zhong, W., . . . Kong, J. (2015). The Effect of Layer-by-Layer Assembly Coating on the Proliferation and Differentiation of Neural Stem Cells. *ACS Applied Materials & Interfaces, 7*(5), 3018-3029. doi:10.1021/am504456t

Li, X., Ding, L., Xu, Y., Wang, Y., & Ping, Q. (2009). Targeted delivery of doxorubicin using stealth liposomes modified with transferrin. *International Journal of Pharmaceutics, 373*(1–2), 116-123. doi:http://dx.doi.org/10.1016/j.ijpharm.2009.01.023

Liao, S., Bodmer, J., Pietras, D., Azhar, M., Doetschman, T., & Schultz, J. E. J. (2009). Biological Functions of the Low and High Molecular Weight Protein Isoforms of Fibroblast Growth Factor-2 in Cardiovascular Development and Disease. *Developmental dynamics : an official publication of the American Association of Anatomists, 238*(2), 249-264. doi:10.1002/dvdy.21677

Lim, K. S., Alves, M. H., Poole-Warren, L. A., & Martens, P. J. (2013). Covalent incorporation of non-chemically modified gelatin into degradable PVA-tyramine hydrogels. *Biomaterials, 34*(29), 7097-7105. doi:10.1016/j.biomaterials.2013.06.005

Lin, N., & Dufresne, A. (2013). Supramolecular hydrogels from in situ host-guest inclusion between chemically modified cellulose nanocrystals and cyclodextrin. *Biomacromolecules, 14*(3), 871-880. doi:10.1021/bm301955k

.

Lin, N., Huang, J., Chang, P. R., Feng, L., & Yu, J. (2011). Effect of polysaccharide nanocrystals on structure, properties, and drug release kinetics of alginate-based microspheres. *Colloids and Surfaces B: Biointerfaces, 85*(2), 270-279.

Lin, N., Huang, J., & Dufresne, A. (2012). Preparation, properties and applications of polysaccharide nanocrystals in advanced functional nanomaterials: a review. *Nanoscale, 4*(11), 3274-3294. doi:10.1039/c2nr30260h

Liu, G., Swierczewska, M., Lee, S., & Chen, X. (2010). FUNCTIONAL NANOPARTICLES FOR MOLECULAR IMAGING GUIDED GENE DELIVERY. *Nano Today, 5*(6), 524-539. doi:10.1016/j.nantod.2010.10.005

Liu, H., Zhang, J., Chen, X., Du, X.-S., Zhang, J.-L., Liu, G., & Zhang, W.-G. (2016). Application of iron oxide nanoparticles in glioma imaging and therapy: from bench to bedside. *Nanoscale, 8*(15), 7808-7826. doi:10.1039/C6NR00147E

Liu, J., Willför, S., & Xu, C. (2015). A review of bioactive plant polysaccharides: Biological activities, functionalization, and biomedical applications. *Bioactive Carbohydrates and Dietary Fibre, 5*(1), 31-61. doi:http://dx.doi.org/10.1016/j.bcdf.2014.12.001

Liu, J., Zhou, H. Z., Weir, M. D., Xu, H. H. K., Chen, Q. M., & Trotman, C. A. (2012). Fast-Degradable Microbeads Encapsulating Human Umbilical Cord Stem Cells in Alginate for Muscle Tissue Engineering. *Tissue Engineering Part A, 18*(21-22), 2303-2314. doi:DOI 10.1089/ten.tea.2011.0658

Liu, Y., Berendsen, A. D., Jia, S., Lotinun, S., Baron, R., Ferrara, N., & Olsen, B. R. (2012). Intracellular VEGF regulates the balance between osteoblast and adipocyte differentiation. *J Clin Invest, 122*(9), 3101-3113. doi:10.1172/jci61209

Liu, Z., Jiao, Y., Wang, Y., Zhou, C., & Zhang, Z. (2008). Polysaccharides-based nanoparticles as drug delivery systems. *Advanced Drug Delivery Reviews, 60*(15), 1650-1662. doi:http://dx.doi.org/10.1016/j.addr.2008.09.001

Loh, X. J., Colin Sng, K. B., & Li, J. (2008). Synthesis and water-swelling of thermo-responsive poly(ester urethane)s containing poly(ε-caprolactone), poly(ethylene glycol) and poly(propylene glycol). *Biomaterials, 29*(22), 3185-3194. doi:http://dx.doi.org/10.1016/j.biomaterials.2008.04.015

Loh, X. J., Goh, S. H., & Li, J. (2007). Hydrolytic degradation and protein release studies of thermogelling polyurethane copolymers consisting of poly[(R)-3-hydroxybutyrate], poly(ethylene glycol), and poly(propylene glycol). *Biomaterials,*

.

28(28), 4113-4123. doi:http://dx.doi.org/10.1016/j.biomaterials.2007.05.016

Loh, X. J., Peh, P., Liao, S., Sng, C., & Li, J. (2010). Controlled drug release from biodegradable thermoresponsive physical hydrogel nanofibers. *Journal of Controlled Release, 143*(2), 175-182. doi:http://dx.doi.org/10.1016/j.jconrel.2009.12.030

Loh, X. J., Tan, Y. X., Li, Z., Teo, L. S., Goh, S. H., & Li, J. (2008). Biodegradable thermogelling poly(ester urethane)s consisting of poly(lactic acid) – Thermodynamics of micellization and hydrolytic degradation. *Biomaterials, 29*(14), 2164-2172. doi:http://dx.doi.org/10.1016/j.biomaterials.2008.01.016

Lovelyn, C., & Attama, A. A. (2011). Current state of nanoemulsions in drug delivery. *Journal of Biomaterials and Nanobiotechnology, 2*(05), 626.

Lu, H., Lv, L., Dai, Y., Wu, G., Zhao, H., & Zhang, F. (2013). Porous Chitosan Scaffolds with Embedded Hyaluronic Acid/Chitosan/Plasmid-DNA Nanoparticles Encoding TGF-β1 Induce DNA Controlled Release, Transfected Chondrocytes, and Promoted Cell Proliferation. *PLoS ONE, 8*(7), e69950. doi:10.1371/journal.pone.0069950

Luo, K., Tian, J., Liu, G., Sun, J., Xia, C., Tang, H., . . . Gu, Z. (2010). Self-assembly of SiO2/Gd-DTPA-polyethylenimine nanocomposites as magnetic resonance imaging probes. *J Nanosci Nanotechnol, 10*(1), 540-548.

Luyten, F. P., Denti, M., Filardo, G., Kon, E., & Engebretsen, L. (2012). Definition and classification of early osteoarthritis of the knee. *Knee Surg Sports Traumatol Arthrosc, 20*(3), 401-406. doi:10.1007/s00167-011-1743-2

Lv, H. W., Li, L. S., Sun, M. Y., Zhang, Y., Chen, L., Rong, Y., & Li, Y. L. (2015). Mechanism of regulation of stem cell differentiation by matrix stiffness. *Stem Cell Research & Therapy, 6*. doi:ARTN 10310.1186/s13287-015-0083-4

Ma, X., Dang, X., Claus, P., Hirst, C., Fandrich, R. R., Jin, Y., . . . Kardami, E. (2007). Chromatin compaction and cell death by high molecular weight FGF-2 depend on its nuclear localization, intracrine ERK activation, and engagement of mitochondria. *J Cell Physiol, 213*(3), 690-698. doi:10.1002/jcp.21139

Machado, A. H. E., Lundberg, D., Ribeiro, A. J., Veiga, F. J., Lindman, B., Miguel, M. G., & Olsson, U. (2012). Preparation of Calcium Alginate Nanoparticles Using Water-in-Oil (W/O) Nanoemulsions. *Langmuir, 28*(9), 4131-4141. doi:10.1021/la204944j

Mahou, R., Tran, N. M., Dufresne, M., Legallais, C., & Wandrey, C. (2012). Encapsulation of Huh-7 cells within alginate-poly(ethylene glycol) hybrid microspheres. *Journal*

.

of Materials Science-Materials in Medicine, 23(1), 171-179. doi:DOI 10.1007/s10856-011-4512-3

Mahou, R., & Wandrey, C. (2010). Alginate-Poly(ethylene glycol) Hybrid Microspheres with Adjustable Physical Properties. *Macromolecules (Washington, DC, U. S.), 43*(3), 1371-1378. doi:10.1021/ma902469f

Maia, J., Carvalho, R. A., Coelho, J. F. J., Simões, P. N., & Gil, M. H. (2011). Insight on the periodate oxidation of dextran and its structural vicissitudes. *Polymer, 52*(2), 258-265. doi:http://dx.doi.org/10.1016/j.polymer.2010.11.058

Majzoub, R. N., Chan, C.-L., Ewert, K. K., Silva, B. F. B., Liang, K. S., Jacovetty, E. L., . . . Safinya, C. R. Uptake and transfection efficiency of PEGylated cationic liposome–DNA complexes with and without RGD-tagging. *Biomaterials*(0). doi:http://dx.doi.org/10.1016/j.biomaterials.2014.03.007

Mallapragada, S. K., & Peppas, N. A. (1996). Dissolution mechanism of semicrystalline poly(vinyl alcohol) in water. *Journal of Polymer Science Part B: Polymer Physics, 34*(7), 1339-1346. doi:10.1002/(SICI)1099-0488(199605)34:7<1339::AID-POLB15>3.0.CO;2-B

Manegold, C. (2001). Chemotherapy for advanced non-small cell lung cancer: standards. *Lung Cancer, 34 Suppl 2*, S165-170.

Marchal, S., Hor, A. E., Millard, M., Gillon, V., & Bezdetnaya, L. (2015). Anticancer Drug Delivery: An Update on Clinically Applied Nanotherapeutics. *Drugs, 75*(14), 1601-1611. doi:10.1007/s40265-015-0453-3

Martens, P. J., Bryant, S. J., & Anseth, K. S. (2003). Tailoring the degradation of hydrogels formed from multivinyl poly(ethylene glycol) and poly(vinyl alcohol) macromers for cartilage tissue engineering. *Biomacromolecules, 4*(2), 283-292. doi:10.1021/bm025666v

Matthew, J. E., Nazario, Y. L., Roberts, S. C., & Bhatia, S. R. (2002). Effect of mammalian cell culture medium on the gelation properties of Pluronic® F127. *Biomaterials, 23*(23), 4615-4619.

McCall, J. D., & Anseth, K. S. (2012). Thiol–Ene Photopolymerizations Provide a Facile Method To Encapsulate Proteins and Maintain Their Bioactivity. *Biomacromolecules, 13*(8), 2410-2417. doi:10.1021/bm300671s

McNaughton, M., Engman, L., Birmingham, A., Powis, G., & Cotgreave, I. A. (2004). Cyclodextrin-Derived Diorganyl Tellurides as Glutathione Peroxidase Mimics and

.

Inhibitors of Thioredoxin Reductase and Cancer Cell Growth. *Journal of Medicinal Chemistry, 47*(1), 233-239. doi:10.1021/jm030916r

McQuilling, J. P., Arenas-Herrera, J., Childers, C., Pareta, R. A., Khanna, O., Jiang, B., . . . Opara, E. C. (2011). New alginate microcapsule system for angiogenic protein delivery and immunoisolation of islets for transplantation in the rat omentum pouch. *Transplant Proc, 43*(9), 3262-3264. doi:10.1016/j.transproceed.2011.10.030

Meng, X.-W., Ha, W., Cheng, C., Dong, Z.-Q., Ding, L.-S., Li, B.-J., & Zhang, S. (2011). Hollow nanospheres based on the self-assembly of alginate-graft-poly(ethylene glycol) and α-cyclodextrin. *Langmuir, 27*, 14401-14407.

Meng, X.-W., Qin, J., Liu, Y., Fan, M.-M., Li, B.-J., Zhang, S., & Yu, X.-Q. (2010). Degradable hollow spheres based on self-assembly inclusion. *Chemical Communications, 46*, 643-645.

Mero, A., & Campisi, M. (2014). Hyaluronic Acid Bioconjugates for the Delivery of Bioactive Molecules. *Polymers, 6*(2), 346. Retrieved from http://www.mdpi.com/2073-4360/6/2/346

Mettlen, M., Pucadyil, T., Ramachandran, R., & Schmid, S. L. (2009). Dissecting dynamin's role in clathrin-mediated endocytosis. *Biochemical Society transactions, 37*(Pt 5), 1022-1026. doi:10.1042/BST0371022

Meyer, K., & Palmer, J. W. (1934). THE POLYSACCHARIDE OF THE VITREOUS HUMOR. *Journal of Biological Chemistry, 107*(3), 629-634. Retrieved from http://www.jbc.org/content/107/3/629.short

Miao, T., Fenn, S. L., Charron, P. N., & Oldinski, R. A. (2015). Self-Healing and Thermoresponsive Dual-Cross-Linked Alginate Hydrogels Based on Supramolecular Inclusion Complexes. *Biomacromolecules, 16*(12), 3740-3750. doi:10.1021/acs.biomac.5b00940

Miao, T., Rao, K. S., Spees, J. L., & Oldinski, R. A. (2014). Osteogenic differentiation of human mesenchymal stem cells through alginate-graft-poly(ethylene glycol) microsphere-mediated intracellular growth factor delivery. *Journal of Controlled Release, 192*, 57-66. doi:http://dx.doi.org/10.1016/j.jconrel.2014.06.029

Miao, T., Zhang, Y., Zeng, Y., Tian, R., & Liu, G. (2016). Functional Nanoparticles for Molecular Imaging-Guided Gene Delivery and Therapy. In Z. Dai (Ed.), *Advances in Nanotheranostics II: Cancer Theranostic Nanomedicine* (pp. 273-305).

.

Singapore: Springer Singapore.

Midoux, P., Breuzard, G., Gomez, J. P., & Pichon, C. (2008). Polymer-based gene delivery: A current review on the uptake and intracellular trafficking of polyplexes. *Current Gene Therapy, 8*(5), 335-352.

Mierisch, C. M., Cohen, S. B., Jordan, L. C., Robertson, P. G., Balian, G., & Diduch, D. R. (2002). Transforming growth factor-beta in calcium alginate beads for the treatment of articular cartilage defects in the rabbit. *Arthroscopy, 18*(8), 892-900.

Mittal, S. K., Aggarwal, N., Sailaja, G., van Olphen, A., HogenEsch, H., North, A., . . . Moffatt, S. (2000). Immunization with DNA, adenovirus or both in biodegradable alginate microspheres: effect of route of inoculation on immune response. *Vaccine, 19*(2-3), 253-263.

Moffett, J., Kratz, E., Myers, J., Stachowiak, E. K., Florkiewicz, R. Z., & Stachowiak, M. K. (1998). Transcriptional regulation of fibroblast growth factor-2 expression in human astrocytes: implications for cell plasticity. *Molecular Biology of the Cell, 9*(8), 2269-2285. Retrieved from http://www.ncbi.nlm.nih.gov/pubmed/9693381

Mohandas, A., Anisha, B. S., Chennazhi, K. P., & Jayakumar, R. (2015). Chitosan–hyaluronic acid/VEGF loaded fibrin nanoparticles composite sponges for enhancing angiogenesis in wounds. *Colloids and Surfaces B: Biointerfaces, 127*, 105-113. doi:http://dx.doi.org/10.1016/j.colsurfb.2015.01.024

Mokhtarzadeh, A., Alibakhshi, A., Yaghoobi, H., Hashemi, M., Hejazi, M., & Ramezani, M. (2016). Recent advances on biocompatible and biodegradable nanoparticles as gene carriers. *Expert Opinion on Biological Therapy*(just-accepted).

Monteiro, N., Martins, A., Reis, R. L., & Neves, N. M. (2015). Nanoparticle-based bioactive agent release systems for bone and cartilage tissue engineering. *Regenerative Therapy, 1*, 109-118. doi:http://dx.doi.org/10.1016/j.reth.2015.05.004

Morrone, G., Guzzardella, G. A., Torricelli, P., Rocca, M., Tigani, D., Brodano, G. B., . . . Giardino, R. (2000). Osteochondral lesion repair of the knee in the rabbit after low-power diode Ga-Al-As laser biostimulation: an experimental study. *Artif Cells Blood Substit Immobil Biotechnol, 28*(4), 321-336. Retrieved from http://www.ncbi.nlm.nih.gov/pubmed/10928702

Moshaverinia, A., Chen, C., Xu, X., Akiyama, K., Ansari, S., Zadeh, H. H., & Shi, S. (2013).

.

Bone Regeneration Potential of Stem Cells Derived from Periodontal Ligament or Gingival Tissue Sources Encapsulated in RGD-Modified Alginate Scaffold. *Tissue Eng Part A*. doi:10.1089/ten.TEA.2013.0229

Mosmann, T. (1983). Rapid colorimetric assay for cellular growth and survival: Application to proliferation and cytotoxicity assays. *Journal of Immunological Methods, 65*(1), 55-63. doi:http://dx.doi.org/10.1016/0022-1759(83)90303-4

Murphy, C. M., Matsiko, A., Haugh, M. G., Gleeson, J. P., & O'Brien, F. J. (2012). Mesenchymal stem cell fate is regulated by the composition and mechanical properties of collagen-glycosaminoglycan scaffolds. *J Mech Behav Biomed Mater, 11*, 53-62. doi:10.1016/j.jmbbm.2011.11.009

Nam, H. Y., Kwon, S. M., Chung, H., Lee, S.-Y., Kwon, S.-H., Jeon, H., . . . Jeong, S. Y. (2009). Cellular uptake mechanism and intracellular fate of hydrophobically modified glycol chitosan nanoparticles. *Journal of Controlled Release, 135*(3), 259-267. doi:http://dx.doi.org/10.1016/j.jconrel.2009.01.018

Nuttelman, C. R., Henry, S. M., & Anseth, K. S. (2002). Synthesis and characterization of photocrosslinkable, degradable poly(vinyl alcohol)-based tissue engineering scaffolds. *Biomaterials, 23*, 3617-3626.

O'Driscoll, S. W. (1998). The healing and regeneration of articular cartilage. *J Bone Joint Surg Am, 80*(12), 1795-1812. Retrieved from http://www.ncbi.nlm.nih.gov/pubmed/9875939

Oda, K., Matsuoka, Y., Funahashi, A., & Kitano, H. (2005). A comprehensive pathway map of epidermal growth factor receptor signaling. *Molecular Systems Biology, 1*, 2005.0010-2005.0010. doi:10.1038/msb4100014

Oerther, S., Maurin, A. C., Payan, E., Hubert, P., Lapicque, F., Presle, N., . . . Lapicque, F. (2000). High interaction alginate-hyaluronate associations by hyaluronate deacetylation for the preparation of efficient biomaterials. *Biopolymers, 54*(4), 273-281. doi:10.1002/1097-0282(20001005)54:4<273::aid-bip40>3.0.co;2-i

Okada, M., Kamachi, M., & Harada, A. (1999). Preparation and Characterization of Inclusion Complexes of Poly(propylene glycol) with Methylated Cyclodextrins. *The Journal of Physical Chemistry B, 103*(14), 2607-2613. doi:10.1021/jp9823852

Oldinski, R. A., Ruckh, T. T., Staiger, M. P., Popat, K. C., & James, S. P. (2011). Dynamic mechanical analysis and biomineralization of hyaluronan-polyethylene copolymers for potential use in osteochondral defect repair. *Acta Biomater, 7*(3),

.

1184-1191. doi:10.1016/j.actbio.2010.11.019

Otsuka, M., Kang, Y. J., Ren, J., Jiang, H., Wang, Y., Omata, M., & Han, J. (2010). Distinct effects of p38alpha deletion in myeloid lineage and gut epithelia in mouse models of inflammatory bowel disease. *Gastroenterology, 138*(4), 1255-1265, 1265 e1251-1259. doi:10.1053/j.gastro.2010.01.005S0016-5085(10)00022-3 [pii]

Paolino, M., Ennen, F., Lamponi, S., Cernescu, M., Voit, B., Cappelli, A., . . . Komber, H. (2013). Cyclodextrin-Adamantane Host–Guest Interactions on the Surface of Biocompatible Adamantyl-Modified Glycodendrimers. *Macromolecules, 46*(9), 3215-3227. doi:10.1021/ma400352m

Paques, J. P., van der Linden, E., van Rijn, C. J. M., & Sagis, L. M. C. (2014). Preparation methods of alginate nanoparticles. *Advances in Colloid and Interface Science, 209*, 163-171. doi:http://dx.doi.org/10.1016/j.cis.2014.03.009

Parajó, Y., d'Angelo, I., Welle, A., Garcia-Fuentes, M., & Alonso, M. J. (2010). Hyaluronic acid/Chitosan nanoparticles as delivery vehicles for VEGF and PDGF-BB. *Drug Delivery, 17*(8), 596-604. doi:10.3109/10717544.2010.509357

Park, J. S., Yang, H. N., Jeon, S. Y., Woo, D. G., Na, K., & Park, K.-H. (2010). Osteogenic differentiation of human mesenchymal stem cells using RGD-modified BMP-2 coated microspheres. *Biomaterials, 31*(24), 6239-6248. doi:http://dx.doi.org/10.1016/j.biomaterials.2010.05.002

Pawar, S. N., & Edgar, K. J. (2011). Chemical Modification of Alginates in Organic Solvent Systems. *Biomacromolecules, 12*(11), 4095-4103. doi:10.1021/bm201152a

Pawar, S. N., & Edgar, K. J. (2012). Alginate derivatization: A review of chemistry, properties and applications. *Biomaterials, 33*, 3279-3305.

Pawar, S. N., & Edgar, K. J. (2013). Alginate esters via chemoselective carboxyl group modification. *Carbohydrate Polymers, 98*(2), 1288-1296. doi:http://dx.doi.org/10.1016/j.carbpol.2013.08.014

Peach, R. J., Hollenbaugh, D., Stamenkovic, I., & Aruffo, A. (1993). Identification of hyaluronic acid binding sites in the extracellular domain of CD44. *J Cell Biol, 122*(1), 257-264.

Pelaez, D., Huang, C. Y., & Cheung, H. S. (2009). Cyclic compression maintains viability and induces chondrogenesis of human mesenchymal stem cells in fibrin gel scaffolds. *Stem Cells Dev, 18*(1), 93-102. doi:10.1089/scd.2008.0030

.

Peppas, N. A., & Wright, S. L. (1996). Solute Diffusion in Poly(vinyl alcohol)/Poly(acrylic acid) Interpenetrating Networks. *Macromolecules, 29*(27), 8798-8804. doi:10.1021/ma9613392

Petrie, T. A., Raynor, J. E., Reyes, C. D., Burns, K. L., Collard, D. M., & García, A. J. (2008). The effect of integrin-specific bioactive coatings on tissue healing and implant osseointegration. *Biomaterials, 29*(19), 2849-2857. doi:http://dx.doi.org/10.1016/j.biomaterials.2008.03.036

Petter, R. C., Salek, J. S., Sikorski, C. T., Kumaravel, G., & Lin, F. T. (1990). Cooperative binding by aggregated mono-6-(alkylamino)-.beta.-cyclodextrins. *Journal of the American Chemical Society, 112*(10), 3860-3868. doi:10.1021/ja00166a021

Pinnix, C., Perkins, G. H., Strom, E. A., Tereffe, W., Woodward, W., Oh, J. L., . . . Yu, T. K. (2012). Topical Hyaluronic acid vs. Standard of Care for the Prevention of Radiation Dermatitis after Adjuvant Radiotherapy for Breast Cancer: Single-Blind Randomized Phase III Clinical Trial. *International journal of radiation oncology, biology, physics, 83*(4), 1089-1094. doi:10.1016/j.ijrobp.2011.09.021

Pinto Reis, C., Neufeld, R. J., Ribeiro, A. J., & Veiga, F. (2006). Nanoencapsulation I. Methods for preparation of drug-loaded polymeric nanoparticles. *Nanomedicine, 2*(1), 8-21. doi:10.1016/j.nano.2005.12.003

Pluemsab, W., Sakairi, N., & Furuike, T. (2005). Synthesis and inclusion property of α-cyclodextrin-linked alginate. *Polymer, 46*(23), 9778-9783. doi:http://dx.doi.org/10.1016/j.polymer.2005.08.005

Polyak, B., Geresh, S., & Marks, R. S. (2004). Synthesis and Characterization of a Biotin-Alginate Conjugate and Its Application in a Biosensor Construction. *Biomacromolecules, 5*(2), 389-396. doi:10.1021/bm034454a

Pozuelo, J., Mendicuti, F., & Mattice, W. L. (1998). Inclusion Complexes of Chain Molecules with Cycloamyloses III. Molecular Dynamics Simulations of Polyrotaxanes Formed by Poly(propylene glycol) and [beta]-Cyclodextrins. *Polym J, 30*(6), 479-484. doi:10.1295/polymj.30.479

Pradal, C., Grondahl, L., & Cooper-White, J. J. (2015). Hydrolytically degradable polyrotaxane hydrogels for drug and cell delivery applications. *Biomacromolecules, 16*(1), 389-403. doi:10.1021/bm501615p

Pradal, C., Jack, K. S., Grøndahl, L., & Cooper-White, J. J. (2013). Gelation Kinetics and Viscoelastic Properties of Pluronic and α-Cyclodextrin-Based

.

Pseudopolyrotaxane Hydrogels. *Biomacromolecules, 14*(10), 3780-3792. doi:10.1021/bm401168h

Preta, G., Cronin, J. G., & Sheldon, I. M. (2015). Dynasore - not just a dynamin inhibitor. *Cell Communication and Signaling : CCS, 13*, 24. doi:10.1186/s12964-015-0102-1

Priddy, L. B., Chaudhuri, O., Stevens, H. Y., Krishnan, L., Uhrig, B. A., Willett, N. J., & Guldberg, R. E. (2014). Oxidized alginate hydrogels for bone morphogenetic protein-2 delivery in long bone defects. *Acta Biomater, 10*(10), 4390-4399. doi:10.1016/j.actbio.2014.06.015

Pritchard, M. F., Powell, L. C., Menzies, G. E., Lewis, P. D., Hawkins, K., Wright, C., . . . Thomas, D. W. (2016). A New Class of Safe Oligosaccharide Polymer Therapy To Modify the Mucus Barrier of Chronic Respiratory Disease. *Molecular Pharmaceutics, 13*(3), 863-872. doi:10.1021/acs.molpharmaceut.5b00794

Prockop, D. J. (1997). Marrow Stromal Cells as Stem Cells for Nonhematopoietic Tissues. *Science, 276*(5309), 71-74. doi:10.1126/science.276.5309.71

Qin, J., Meng, X., Li, B., Ha, W., Yu, X., & Zhang, S. (2010). Self-assembly of β-cyclodextrin and pluronic into hollow nanospheres in aqueous solution. *J Colloid Interface Sci, 350*(2), 447-452. doi:http://dx.doi.org/10.1016/j.jcis.2010.07.019

Rafat, M., Li, F., Fagerholm, P., Lagali, N. S., Watsky, M. A., Munger, R., . . . Griffith, M. (2008). PEG-stabilized carbodiimide crosslinked collagen–chitosan hydrogels for corneal tissue engineering. *Biomaterials, 29*(29), 3960-3972. doi:http://dx.doi.org/10.1016/j.biomaterials.2008.06.017

Ravi Kumar, M. N. V. (2000). A review of chitin and chitosan applications. *Reactive and Functional Polymers, 46*(1), 1-27. doi:http://dx.doi.org/10.1016/S1381-5148(00)00038-9

Reck, M., Heigener, D. F., Mok, T., Soria, J.-C., & Rabe, K. F. Management of non-small-cell lung cancer: recent developments. *The Lancet, 382*(9893), 709-719. doi:10.1016/S0140-6736(13)61502-0

Rincon, M., & Davis, R. J. (2009). Regulation of the immune response by stress-activated protein kinases. *Immunol Rev, 228*(1), 212-224. doi:IMR744 [pii] 0.1111/j.1600-065X.2008.00744.x

Ritprajak, P., Hayakawa, M., Sano, Y., Otsu, K., & Park, J. M. (2012). Cell type-specific targeting dissociates the therapeutic from the adverse effects of protein kinase inhibition in allergic skin disease. *Proc Natl Acad Sci U S A, 109*(23), 9089-9094.

.

doi:10.1073/pnas.12029841091202984109 [pii]

Riva, R., Ragelle, H., Rieux, A., Duhem, N., Jérôme, C., & Préat, V. (2011). Chitosan and Chitosan Derivatives in Drug Delivery and Tissue Engineering. In R. Jayakumar, M. Prabaharan, & A. R. A. Muzzarelli (Eds.), *Chitosan for Biomaterials II* (pp. 19-44). Berlin, Heidelberg: Springer Berlin Heidelberg.

Rochette, L., Guenancia, C., Gudjoncik, A., Hachet, O., Zeller, M., Cottin, Y., & Vergely, C. (2015). Anthracyclines/trastuzumab: new aspects of cardiotoxicity and molecular mechanisms. *Trends in Pharmacological Sciences, 36*(6), 326-348. doi:http://dx.doi.org/10.1016/j.tips.2015.03.005

Rodell, C. B., Kaminski, A. L., & Burdick, J. A. (2013). Rational Design of Network Properties in Guest–Host Assembled and Shear-Thinning Hyaluronic Acid Hydrogels. *Biomacromolecules, 14*(11), 4125-4134. doi:10.1021/bm401280z

Rodell, C. B., MacArthur, J. W., Dorsey, S. M., Wade, R. J., Wang, L. L., Woo, Y. J., & Burdick, J. A. (2015). Shear-Thinning Supramolecular Hydrogels with Secondary Autonomous Covalent Crosslinking to Modulate Viscoelastic Properties In Vivo. *Advanced Functional Materials, 25*(4), 636-644. doi:10.1002/adfm.201403550

Rodell, C. B., Rai, R., Faubel, S., Burdick, J. A., & Soranno, D. E. (2015). Local immunotherapy via delivery of interleukin-10 and transforming growth factor β antagonist for treatment of chronic kidney disease. *Journal of Controlled Release, 206*(0), 131-139. doi:http://dx.doi.org/10.1016/j.jconrel.2015.03.025

Rodrigues, M., Griffith, L. G., & Wells, A. (2010). Growth factor regulation of proliferation and survival of multipotential stromal cells. *Stem Cell Research & Therapy, 1*(4), 1-12. doi:10.1186/scrt32

Rodrigues, M. T., Gomes, M. E., & Reis, R. L. (2011). Current strategies for osteochondral regeneration: from stem cells to pre-clinical approaches. *Current Opinion in Biotechnology, 22*, 726-733.

Rodriguez, J. P., Montecinos, L., Rios, S., Reyes, P., & Martinez, J. (2000). Mesenchymal stem cells from osteoporotic patients produce a type I collagen-deficient extracellular matrix favoring adipogenic differentiation. *Journal of Cellular Biochemistry, 79*(4), 557-565. doi:Doi 10.1002/1097-4644(20001215)79:4<557::Aid-Jcb40>3.0.Co;2-H

Rowley, J. A., Madlambayan, G., & Mooney, D. J. (1999). Alginate hydrogels as synthetic extracellular matrix materials. *Biomaterials, 20*(1), 45-53.

.

doi:http://dx.doi.org/10.1016/S0142-9612(98)00107-0

Ruoslahti, E. (1996). RGD and Other Reconition Sequencies for Intrgrins. *Annual Review of Cell and Developmental Biology, 12*(1), 697-715. doi:doi:10.1146/annurev.cellbio.12.1.697

Ruoslahti, E., & Pierschbacher, M. D. (1987). New perspectives in cell adhesion: RGD and integrins. *Science, 238*(4826), 491-497. Retrieved from http://www.ncbi.nlm.nih.gov/pubmed/2821619

Salinas, C. N., & Anseth, K. S. (2008). The enhancement of chondrogenic differentiation of human mesenchymal stem cells by enzymatically regulated RGD functionalities. *Biomaterials, 29*(15), 2370-2377. doi:Doi 10.1016/J.Biomaterials.2008.01.035

Salva, E., Kabasakal, L., Eren, F., Ozkan, N., Cakalagaoglu, F., & Akbuga, J. (2012). Local delivery of chitosan/VEGF siRNA nanoplexes reduces angiogenesis and growth of breast cancer in vivo. *Nucleic Acid Ther, 22*(1), 40-48. doi:10.1089/nat.2011.0312

Sarmento, B., Ribeiro, A., Veiga, F., Sampaio, P., Neufeld, R., & Ferreira, D. (2007). Alginate/chitosan nanoparticles are effective for oral insulin delivery. *Pharmaceutical research, 24*(12), 2198-2206.

Schindler, J. F., Monahan, J. B., & Smith, W. G. (2007). p38 pathway kinases as anti-inflammatory drug targets. *J Dent Res, 86*(9), 800-811. doi:86/9/800 [pii]

Schleeh, T., Madau, M., & Roessner, D. (2014). Synthesis enhancements for generating highly soluble tetrabutylammonium alginates in organic solvents. *Carbohydr Polym, 114*, 493-499. doi:10.1016/j.carbpol.2014.07.079

Serra, L., Doménech, J., & Peppas, N. A. (2006). Drug transport mechanisms and release kinetics from molecularly designed poly (acrylic acid-g-ethylene glycol) hydrogels. *Biomaterials, 27*(31), 5440-5451.

Shachar, M., Tsur-Gang, O., Dvir, T., Leor, J., & Cohen, S. (2011). The effect of immobilized RGD peptide in alginate scaffolds on cardiac tissue engineering. *Acta Biomaterialia, 7*(1), 152-162. doi:http://dx.doi.org/10.1016/j.actbio.2010.07.034

Sham, D., Wesley, U. V., Hristova, M., & van der Vliet, A. (2013). ATP-mediated transactivation of the epidermal growth factor receptor in airway epithelial cells involves DUOX1-dependent oxidation of Src and ADAM17. *PLoS One, 8*(1), e54391. doi:10.1371/journal.pone.0054391

.

Shazly, T. M., Baker, A. B., Naber, J. R., Bon, A., Van Vliet, K. J., & Edelman, E. R. (2010). Augmentation of postswelling surgical sealant potential of adhesive hydrogels. *J Biomed Mater Res A, 95*(4), 1159-1169. doi:10.1002/jbm.a.32942

Shelke, N. B., James, R., Laurencin, C. T., & Kumbar, S. G. (2014). Polysaccharide biomaterials for drug delivery and regenerative engineering. *Polymers for Advanced Technologies, 25*(5), 448-460. doi:10.1002/pat.3266

Shimoda, A., Sawada, S. i., & Akiyoshi, K. (2011). Cell Specific Peptide‐Conjugated Polysaccharide Nanogels for Protein Delivery. *Macromolecular bioscience, 11*(7), 882-888.

Siegel, R. L., Miller, K. D., & Jemal, A. (2015). Cancer statistics, 2015. *CA: A Cancer Journal for Clinicians, 65*(1), 5-29. doi:10.3322/caac.21254

Siegel, R. L., Miller, K. D., & Jemal, A. (2016). Cancer statistics, 2016. *CA: A Cancer Journal for Clinicians, 66*(1), 7-30. doi:10.3322/caac.21332

Sigsgaard, T., Thorne, P. S., Schlünssen, V., Bønløkke, J., Riddervold, I. S., Hoppe, K. A., . . . Mackenzie, N. M. (2015). The change in nasal inflammatory markers after intranasal challenges with particulate chitin and lipopolysaccharide: a randomized, double-blind, placebo-controlled, crossover study with a positive control. *International Forum of Allergy & Rhinology, 5*(8), 716-723. doi:10.1002/alr.21534

Singh, M. N., Hemant, K. S. Y., Ram, M., & Shivakumar, H. G. (2010). Microencapsulation: A promising technique for controlled drug delivery. *Research in Pharmaceutical Sciences, 5*(2), 65-77. Retrieved from http://www.ncbi.nlm.nih.gov/pmc/articles/PMC3093624/

Sinha, M. K., Gao, J., Stowell, C. E. T., & Wang, Y. (2015). Synthesis and biocompatibility of a biodegradable and functionalizable thermo-sensitive hydrogel. *Regenerative Biomaterials*. doi:10.1093/rb/rbv009

Sinha, V. R., & Trehan, A. (2003). Biodegradable microspheres for protein delivery. *Journal of Controlled Release, 90*(3), 261-280. doi:Doi 10.1016/S0168-3659(03)00194-9

Sogias, I. A., Williams, A. C., & Khutoryanskiy, V. V. (2008). Why is chitosan mucoadhesive? *Biomacromolecules, 9*(7), 1837-1842. doi:10.1021/bm800276d

Soledad Lencina, M. M., Iatridi, Z., Villar, M. A., & Tsitsilianis, C. (2014). Thermoresponsive hydrogels from alginate-based graft copolymers. *European*

.

Polymer Journal, 61, 33-44. doi:http://dx.doi.org/10.1016/j.eurpolymj.2014.09.011

Sosnik, A. (2014). Alginate Particles as Platform for Drug Delivery by the Oral Route: State-of-the-Art. *ISRN Pharmaceutics, 2014*, 17. doi:10.1155/2014/926157

Stachowiak, E. K., Maher, P. A., Tucholski, J., Mordechai, E., Joy, A., Moffett, J., . . . Stachowiak, M. K. (1997). Nuclear accumulation of fibroblast growth factor receptors in human glial cells--association with cell proliferation. *Oncogene, 14*(18), 2201-2211. doi:10.1038/sj.onc.1201057

Stammen, J. A., Williams, S., Ku, D. N., & Guldberg, R. E. (2001). Mechanical properties of a novel PVA hydrogel in shear and unconfined compression. *Biomaterials, 22*(8), 799-806. Retrieved from http://www.ncbi.nlm.nih.gov/pubmed/11246948

Steinman, L., & Zamvil, S. S. (2006). How to successfully apply animal studies in experimental allergic encephalomyelitis to research on multiple sclerosis. *Ann Neurol, 60*(1), 12-21. doi:10.1002/ana.20913

Su, H., Wu, C., Zhu, J., Miao, T., Wang, D., Xia, C., . . . Ai, H. (2012). Rigid Mn(ii) chelate as efficient MRI contrast agent for vascular imaging. *Dalton Transactions, 41*(48), 14480-14483. doi:10.1039/C2DT31696J

Suarez, S., Grover, G. N., Braden, R. L., Christman, K. L., & Almutairi, A. (2013). Tunable Protein Release from Acetalated Dextran Microparticles: A Platform for Delivery of Protein Therapeutics to the Heart Post-MI. *Biomacromolecules, 14*(11), 3927-3935. doi:10.1021/bm401050j

Swierczewska, M., Han, H. S., Kim, K., Park, J. H., & Lee, S. (2016). Polysaccharide-based nanoparticles for theranostic nanomedicine. *Advanced Drug Delivery Reviews, 99, Part A*, 70-84. doi:http://dx.doi.org/10.1016/j.addr.2015.11.015

Tabata, Y. (2003). Tissue regeneration based on growth factor release. *Tissue Engineering, 9*(4, Supplement 1), 5-15.

Tan, L., Li, J., Liu, Y., Zhou, H., Zhang, Z., & Deng, L. (2015). Synthesis and characterization of β-cyclodextrin-conjugated alginate hydrogel for controlled release of hydrocortisone acetate in response to mechanical stimulation. *Journal of Bioactive and Compatible Polymers: Biomedical Applications*. doi:10.1177/0883911515590494

Tan, L., Liu, Y., Ha, W., Ding, L.-S., Peng, S.-L., Zhang, S., & Li, B.-J. (2012). Stimuli-induced

.

gel-sol transition of multi-sensitive supramolecular [small beta]-cyclodextrin grafted alginate/ferrocene modified pluronic hydrogel. *Soft Matter, 8*(21), 5746-5749. doi:10.1039/C2SM25084E

Tan, S., Fang, J. Y., Yang, Z., Nimni, M. E., & Han, B. (2014). The synergetic effect of hydrogel stiffness and growth factor on osteogenic differentiation. *Biomaterials, 35*(20), 5294-5306. doi:10.1016/j.biomaterials.2014.02.040

Temming, K., Schiffelers, R. M., Molema, G., & Kok, R. J. (2005). RGD-based strategies for selective delivery of therapeutics and imaging agents to the tumour vasculature. *Drug Resistance Updates, 8*(6), 381-402. doi:DOI 10.1016/j.drup.2005.10.002

Teodorescu, M., Andrei, M., Turturică, G., Stănescu, P. O., Zaharia, A., & Sârbu, A. (2015). Novel Thermoreversible Injectable Hydrogel Formulations Based on Sodium Alginate and Poly(N-Isopropylacrylamide). *International Journal of Polymeric Materials and Polymeric Biomaterials, 64*(15), 763-771. doi:10.1080/00914037.2015.1030646

Tharmalingam, T., & Goudar, C. T. (2015). Evaluating the impact of high Pluronic® F68 concentrations on antibody producing CHO cell lines. *Biotechnology and Bioengineering, 112*(4), 832-837. doi:10.1002/bit.25491

Thomas, R. G., Moon, M. J., Lee, H., Sasikala, A. R. K., Kim, C. S., Park, I.-K., & Jeong, Y. Y. (2015). Hyaluronic acid conjugated superparamagnetic iron oxide nanoparticle for cancer diagnosis and hyperthermia therapy. *Carbohydrate Polymers, 131*, 439-446. doi:http://dx.doi.org/10.1016/j.carbpol.2015.06.010

Tiwari, G., Tiwari, R., & Rai, A. K. (2010). Cyclodextrins in delivery systems: Applications. *Journal of Pharmacy and Bioallied Sciences, 2*(2), 72-79. doi:10.4103/0975-7406.67003

Tonnesen, H. H., & Karlsen, J. (2002). Alginate in drug delivery systems. *Drug Development and Industrial Pharmacy, 28*(6), 621-630.

Tonnesen, H. H., & Karlsen, J. (2002). Alginate in drug delivery systems. *Drug Dev Ind Pharm, 28*(6), 621-630. doi:10.1081/DDC-120003853

Topazio, L., Miano, R., Maurelli, V., Gaziev, G., Gacci, M., Iacovelli, V., & Finazzi-Agro, E. (2014). Could hyaluronic acid (HA) reduce Bacillus Calmette-Guerin (BCG) local side effects? Results of a pilot study. *BMC Urol, 14*, 64. doi:10.1186/1471-2490-14-64

Torre, L. A., Bray, F., Siegel, R. L., Ferlay, J., Lortet-Tieulent, J., & Jemal, A. (2015). Global

.

cancer statistics, 2012. *CA: A Cancer Journal for Clinicians, 65*(2), 87-108. doi:10.3322/caac.21262

van de Manakker, F., Braeckmans, K., Morabit, N. e., De Smedt, S. C., van Nostrum, C. F., & Hennink, W. E. (2009). Protein-Release Behavior of Self-Assembled PEG–β-Cyclodextrin/PEG–Cholesterol Hydrogels. *Advanced Functional Materials, 19*(18), 2992-3001. doi:10.1002/adfm.200900603

Varela, G., & Thomas, P. A. (2014). Surgical management of advanced non-small cell lung cancer. *Journal of Thoracic Disease, 6*(Suppl 2), S217-S223. doi:10.3978/j.issn.2072-1439.2014.04.34

Varshosaz, J. (2012). Dextran conjugates in drug delivery. *Expert Opin Drug Deliv, 9*(5), 509-523. doi:10.1517/17425247.2012.673580

Vasile, C., & Nita, L. E. (2011). Novel multi-stimuli responsive sodium alginate-grafted-poly(N-isopropylacrylamide) copolymers: II. Dilute solution properties. *Carbohydrate Polymers, 86*(1), 77-84. doi:http://dx.doi.org/10.1016/j.carbpol.2011.04.012

Wagner, D. E., Fenn, S. L., Bonenfant, N. R., Marks, E. R., Borg, Z., Saunders, P., . . . Weiss, D. J. (2014). Design and Synthesis of an Artificial Pulmonary Pleura for High Throughput Studies in Acellular Human Lungs. *Cell Mol Bioeng, 7*(2), 184-195. doi:10.1007/s12195-014-0323-1

Wagner, E. R., Luther, G., Zhu, G., Luo, Q., Shi, Q., Kim, S. H., . . . Yang, K. (2011). Defective osteogenic differentiation in the development of osteosarcoma. *Sarcoma, 2011*.

Wan, J. (2012). Microfluidic-Based Synthesis of Hydrogel Particles for Cell Microencapsulation and Cell-Based Drug Delivery. *Polymers, 4*(2), 1084. Retrieved from http://www.mdpi.com/2073-4360/4/2/1084

Wang, J., Mi, P., Lin, G., Wang, Y. X., Liu, G., & Chen, X. (2016). Imaging-guided delivery of RNAi for anticancer treatment. *Adv Drug Deliv Rev*. doi:10.1016/j.addr.2016.01.008

Wang, S., Lee, J. S., Bishop, N., Jeremic, A., Cho, W. J., Chen, X., . . . Jena, B. P. (2012). 3D organization and function of the cell: Golgi budding and vesicle biogenesis to docking at the porosome complex. *Histochem Cell Biol, 137*(6), 703-718. doi:10.1007/s00418-012-0948-x

Wang, T., Lai, J. H., Han, L. H., Tong, X., & Yang, F. (2014). Chondrogenic differentiation

.

of adipose-derived stromal cells in combinatorial hydrogels containing cartilage matrix proteins with decoupled mechanical stiffness. *Tissue Eng Part A, 20*(15-16), 2131-2139. doi:10.1089/ten.tea.2013.0531

Wang, T., Yang, X., Qi, X., & Jiang, C. (2015). Osteoinduction and proliferation of bone-marrow stromal cells in three-dimensional poly (epsilon-caprolactone)/ hydroxyapatite/collagen scaffolds. *J Transl Med, 13*, 152. doi:10.1186/s12967-015-0499-8

Wang, Y., & Irvine, D. J. (2011). Engineering chemoattractant gradients using chemokine-releasing polysaccharide microspheres. *Biomaterials, 32*(21), 4903-4913.

Wang, Y., Zhou, J., Qiu, L., Wang, X., Chen, L., Liu, T., & Di, W. (2014). Cisplatin–alginate conjugate liposomes for targeted delivery to EGFR-positive ovarian cancer cells. *Biomaterials, 35*(14), 4297-4309. doi:http://dx.doi.org/10.1016/j.biomaterials.2014.01.035

Wawer, A. A., Harvey, L. J., Dainty, J. R., Perez-Moral, N., Sharp, P., & Fairweather-Tait, S. J. (2014). Alginate inhibits iron absorption from ferrous gluconate in a randomized controlled trial and reduces iron uptake into Caco-2 cells. *PLoS ONE, 9*(11), e112144. doi:10.1371/journal.pone.0112144

Weber, P., Ohlendorf, D., Wendoloski, J., & Salemme, F. (1989). Structural origins of high-affinity biotin binding to streptavidin. *Science, 243*(4887), 85-88. doi:10.1126/science.2911722

Wei, Z., Yang, J. H., Liu, Z. Q., Xu, F., Zhou, J. X., Zrínyi, M., . . . Chen, Y. M. (2015). Self-Healing Materials: Novel Biocompatible Polysaccharide-Based Self-Healing Hydrogel (Adv. Funct. Mater. 9/2015). *Advanced Functional Materials, 25*(9), 1471-1471. doi:10.1002/adfm.201570065

Weiner, H. L. (2009). The challenge of multiple sclerosis: how do we cure a chronic heterogeneous disease? *Ann Neurol, 65*(3), 239-248. doi:10.1002/ana.21640

Wheatley, M. A., Chang, M., Park, E., & Langer, R. (1991). Coated alginate microspheres: factors influencing the controlled delivery of macromolecules. *Journal of Applied Polymer Science, 43*, 2123-2135.

Williams, C. G., Kim, T. K., Taboas, A., Malik, A., Manson, P., & Elisseeff, J. (2003). In vitro chondrogenesis of bone marrow-derived mesenchymal stem cells in a photopolymerizing hydrogel. *Tissue Eng, 9*(4), 679-688.

.

doi:10.1089/107632703768247377

Williams, C. G., Malik, A. N., Kim, T. K., Manson, P. N., & Elisseeff, J. H. (2005). Variable cytocompatibility of six cell lines with photoinitiators used for polymerizing hydrogels and cell encapsulation. *Biomaterials, 26*(11), 1211-1218. doi:10.1016/j.biomaterials.2004.04.024

Wong, H. L., Bendayan, R., Rauth, A. M., Li, Y., & Wu, X. Y. (2007). Chemotherapy with anticancer drugs encapsulated in solid lipid nanoparticles. *Advanced Drug Delivery Reviews, 59*(6), 491-504. doi:http://dx.doi.org/10.1016/j.addr.2007.04.008

Wu, H., Liao, C., Jiao, Q., Wang, Z., Cheng, W., & Wan, Y. (2012). Fabrication of core–shell microspheres using alginate and chitosan–polycaprolactone for controlled release of vascular endothelial growth factor. *Reactive and Functional Polymers, 72*(7), 427-437. doi:http://dx.doi.org/10.1016/j.reactfunctpolym.2012.04.007

Wu, J. L., Wang, C. Q., Zhuo, R. X., & Cheng, S. X. (2014). Multi-drug delivery system based on alginate/calcium carbonate hybrid nanoparticles for combination chemotherapy. *Colloids Surf B Biointerfaces, 123*, 498-505. doi:10.1016/j.colsurfb.2014.09.047

Wu, Y. Q., MacKay, J. A., McDaniel, J. R., Chilkoti, A., & Clark, R. L. (2009). Fabrication of Elastin-Like polypeptide Nanoparticles for Drug Delivery by Electrospraying. *Biomacromolecules, 10*(1), 19-24. doi:Doi 10.1021/Bm801033f

Xie, J., Wang, H., Wang, Y., Ren, F., Yi, W., Zhao, K., . . . Yi, D. (2013). Induction of Angiogenesis by Controlled Delivery of Vascular Endothelial Growth Factor Using Nanoparticles. *Cardiovascular Therapeutics, 31*(3), e12-e18. doi:10.1111/j.1755-5922.2012.00317.x

Xu, Z., Wang, Y., Zhang, L., & Huang, L. (2014). Nanoparticle-delivered transforming growth factor-beta siRNA enhances vaccination against advanced melanoma by modifying tumor microenvironment. *ACS Nano, 8*(4), 3636-3645. doi:10.1021/nn500216y

Yamaguchi, H., Kobayashi, Y., Kobayashi, R., Takashima, Y., Hashidzume, A., & Harada, A. (2012). Photoswitchable gel assembly based on molecular recognition. *Nat Commun, 3*, 603. doi:http://www.nature.com/ncomms/journal/v3/n1/suppinfo/ncomms1617_S1.html

.

Yan, X., Wang, F., Zheng, B., & Huang, F. (2012). Stimuli-responsive supramolecular polymeric materials. *Chemical Society Reviews, 41*(18), 6042-6065. doi:10.1039/C2CS35091B

Yang, J.-A., Yeom, J., Hwang, B. W., Hoffman, A. S., & Hahn, S. K. (2014). In situ-forming injectable hydrogels for regenerative medicine. *Progress in polymer science, 39*(12), 1973-1986. doi:http://dx.doi.org/10.1016/j.progpolymsci.2014.07.006

Yang, J.-S., Xie, Y.-J., & He, W. (2011). Research progress on chemical modification of alginate: A review. *Carbohydrate Polymers, 84*(1), 33-39. doi:http://dx.doi.org/10.1016/j.carbpol.2010.11.048

Yeo, L. Y., Chang, H. C., Chan, P. P., & Friend, J. R. (2011). Microfluidic devices for bioapplications. *Small, 7*(1), 12-48. doi:10.1002/smll.201000946

Yin, S., Huai, J., Chen, X., Yang, Y., Zhang, X., Gan, Y., . . . Li, J. (2015). Intracellular delivery and antitumor effects of a redox-responsive polymeric paclitaxel conjugate based on hyaluronic acid. *Acta Biomater, 26*, 274-285. doi:10.1016/j.actbio.2015.08.029

Yoon, H. Y., Kim, H. R., Saravanakumar, G., Heo, R., Chae, S. Y., Um, W., . . . Park, J. H. (2013). Bioreducible hyaluronic acid conjugates as siRNA carrier for tumor targeting. *Journal of Controlled Release, 172*(3), 653-661. doi:http://dx.doi.org/10.1016/j.jconrel.2013.09.008

Yoon, H. Y., Koo, H., Choi, K. Y., Chan Kwon, I., Choi, K., Park, J. H., & Kim, K. (2013). Photo-crosslinked hyaluronic acid nanoparticles with improved stability for in vivo tumor-targeted drug delivery. *Biomaterials, 34*(21), 5273-5280. doi:http://dx.doi.org/10.1016/j.biomaterials.2013.03.050

Yu, M. K., Park, J., & Jon, S. (2012). Targeting Strategies for Multifunctional Nanoparticles in Cancer Imaging and Therapy. *Theranostics, 2*(1), 3-44. doi:10.7150/thno.3463

Zhang, C., Wang, W., Liu, T., Wu, Y., Guo, H., Wang, P., . . . Yuan, Z. (2012). Doxorubicin-loaded glycyrrhetinic acid-modified alginate nanoparticles for liver tumor chemotherapy. *Biomaterials, 33*(7), 2187-2196. doi:http://dx.doi.org/10.1016/j.biomaterials.2011.11.045

Zhang, C., Wang, W., Liu, T., Wu, Y., Guo, H., Wang, P., . . . Yuan, Z. (2012). Doxorubicin-loaded glycyrrhetinic acid-modified alginate nanoparticles for liver tumor chemotherapy. *Biomaterials, 33*(7), 2187-2196.

.

doi:10.1016/j.biomaterials.2011.11.045

Zhang, N., Wardwell, P. R., & Bader, R. A. (2013). Polysaccharide-Based Micelles for Drug Delivery. *Pharmaceutics, 5*(2), 329-352. doi:10.3390/pharmaceutics5020329

Zhao, L., Zhang, K., Bu, W., Xu, X., Jin, H., Chang, B., . . . Sun, H. (2016). Effective delivery of bone morphogenetic protein 2 gene using chitosan-polyethylenimine nanoparticle to promote bone formation. *RSC Advances, 6*(41), 34081-34089. doi:10.1039/C5RA24891D

Zhao, Q., Han, B., Wang, Z., Gao, C., Peng, C., & Shen, J. (2007). Hollow chitosan-alginate multilayer microcapsules as drug delivery vehicle: doxorubicin loading and in vitro and in vivo studies. *Nanomedicine: Nanotechnology, Biology and Medicine, 3*(1), 63-74. doi:http://dx.doi.org/10.1016/j.nano.2006.11.007

Zheng, J., Lin, Z., Zhang, L., & Yang, H. (2015). Polydopamine-mediated immobilization of phenylboronic acid on magnetic microspheres for selective enrichment of glycoproteins and glycopeptides. *Science China Chemistry, 58*(6), 1056-1064. doi:10.1007/s11426-014-5286-5

Zouani, O. F., Kalisky, J., Ibarboure, E., & Durrieu, M. C. (2013). Effect of BMP-2 from matrices of different stiffnesses for the modulation of stem cell fate. *Biomaterials, 34*(9), 2157-2166. doi:10.1016/j.biomaterials.2012.12.007

.